Functional characterization of clade-I HIPP proteins from *Arabidopsis thaliana* interacting with cytokinin-catabolizing CKX enzymes

Inaugural-Dissertation

to obtain the academic degree

Doctor rerum naturalium (Dr. rer. nat.)

submitted to the Department of Biology, Chemistry and Pharmacy

of Freien Universität Berlin

by

Tianqi Guo

Berlin 2018

The investigations described in the following thesis were performed from October 2011 to November 2018 under supervision of Prof. Dr. Tomáš Werner at the Institute of Biology, Department of Applied Genetics of the Freien Universität Berlin.

1st Reviewer: Prof. Dr. Tomáš Werner (University of Graz)

2nd Reviewer: Prof. Dr. Thomas Schmülling (FU Berlin)

Date of defense: 26.02.2019

Table of contents

List of figures

List of tables

List of abbreviations

3-AT	3-amino-1,2,4-triazole
A	Absorbance
ABA	Abscisic acid
ACT7	*ACTIN7*
AHK	*ARABIDOPSIS HISTIDINE KINASE*
AHP	*ARABIDOPSIS HISTIDINE PHOSPHOTRANSFER PROTEIN*
ALG	asparagine-linked glycosylation
amiRNA	Artificial micro RNA
APS	Ammonium persulfate
Arg	Arginine
ARR	*ARABIDOPSIS RESPONSE REGULATOR*
Asn	Asparagine
ATP	Adenosine triphosphate
BA	N^6-Benzyladenine
bHLH	Basic helix-loop-helix
BiFC	Bimolecular fluorescence complementation
bp	Base pair(s)
BSA	Bovine serum albumin
°C	Degree Celsius
Ca^{2+}	Calcium ion
CaMV	Cauliflower mosaic virus
cDNA	Complementary deoxyribonucleic acid
ChIP	Chromatin immunoprecipitation
CKX	*CYTOKININ OXIDASE/DEHYDROGENASE*
CNX	Calnexin
Co-IP	Co-immunoprecipitation
Col-0	Ecotype/accession Columbia-0
CRE1	*CYTOKININ RESPONSE 1* (=*AHK4*)
CRF	*CYTOKININ RESPONSE FACTOR*
CRISPR/CAS	Clustered regularly interspaced short palindromic repeats/CRISPR-associated protein
CRT	Calreticulin
Ct	Threshold cycle
cZ	*cis*-zeatin
ddH2O	Double deionized water
DMSO	Dimethyl sulfoxide
DNA	Deoxyribonucleic acid
DNase	Deoxyribonuclease
dNTP	Deoxyribonucleoside triphosphate
DolPP	Dolichol pyrophosphate
DTT	Dithiothreitol
DZ	Dihydrozeation
e.g.	*exempli gratia* (Latin: for example)
EDTA	Ethylenediaminetetraacetic acid
EMS	Ethyl methanesulfonate
ER	Endoplasmic reticulum
ERAD	ER-associated degradation

ERQC	ER-mediated protein quality control
et al.	*et alii* (Latin: and others)
F	Forward
F1, F2, F3…	First, second, third… filial generation after a cross
Fe	Iron
Fig./Figs.	Figure/figures
FW	Fresh weight
g	Gram
GA	Gibberellin
GA20OX	Gibberellin 20-oxidase
GA2OX	Gibberellin 2-oxidase
GA3OX	Gibberellin 3 beta-hydroxylase
GFP	Green fluorescent protein
Glc	Glucose
Glu	Glutamine
GOI	Gene of interest
GUS	β-glucuronidase
h	Hour
HEPES	4-(2-Hydroxyethyl)piperazineethanesulfonic acid
HMA	Heavy metal-associated domain
HIPP	Heavy metal-associated isoprenylated plant protein
His	Histidine
Hrd	HMG-CoA reductase degradation
Htm1	Homologous to mannosidase 1
i.e.	*id est* (Latin: that is)
iP	Isopentenyl adenine
IPT	Isopentenyltransferase
kb	Kilobase pair(s)
KMD	*KISS ME DEADLY*
LB	Luria and Broth
LD	Long-day (light/dark: 16 h/8 h)
Leu	Leucine
m	Meter
Man	Mannose
MES	2-(*N*-morpholino)ethanesulfonic acid
min	Minute
mRNA	Messenger RNA
MS	Murashige and Skoog
NAD(P)H	Reduced nicotinamide adenine dinucleotide (phosphate)
NCBI	National Center for Biotechnology Information
NLS	Nuclear localization signal
OD	Optical density
p	Probability
PCR	Polymerase chain reaction
PD	Plasmodesmata
PIN	*PIN-FORMED*
PP2AA2	*PROTEIN PHOSPHATASE 2A SUBUNIT A2*
PR	*PATHOGENESIS-RELATED*
QC	Quiescent center
qRT-PCR	Quantitative real-time polymerase chain reaction

R	Reverse
Raf	Raffinose
RAM	Root apical meristem
RbcL	Large subunit of ribulose-1,5-bisphosphate carboxylase/oxygenase (RuBisCO)
RNA	Ribonucleic acid
RNAi	Ribonucleic acid interference
RNase	Ribonuclease
ROCK	*REPRESSOR OF CYTOKININ DEFICIENCY*
rpm	Rounds per minute
RT	Room temperature
RT-PCR	Reverse transcription polymerase chain reaction
sec	second
SA	Salicylic acid
SAM	Shoot apical meristem
SCF	SKP1/Cullin/F-box
SD	Short-day (light/dark: 8 h/16 h)
SDS	Sodium dodecyl sulfate
SHR	*SHORT ROOT*
SIGnAL	Salk Institute Genomic Analysis Laboratory
T1, T2, T3	First, second, third generation after a transformation
Tab.	Table
TAE	Tris acetate ethylenediaminetetraacetic acid
TAIR	The Arabidopsis Information Resource
TCS	Two-component signaling
TCP	TEOSINT BRANCED1/CYCLOIDEA/PROLIFERATING CELL FACTOR1
T-DNA	Transfer DNA
TEMED	*N*,*N*,*N'*,*N'*-Tetramethylethane-1,2-diamine
Tris	tris(hydroxymethyl)aminomethane
tRNA	Transfer RNA
Trp	Tryptophane
tZ	*trans*-zeatin
U	Unit
UBC10	*UBIQUITIN-CONJUGATING ENZYME 10*
UGT	UDP-glycosyltransferase
Ura	Uracil
WMD3	Web MicroRNA Designer 3
WT	Wild type (if not stated otherwise, Col-0)
WUS	WUSCHEL
X-Gluc	5-Bromo-4-chloro-1H-indol-3-yl β-D-glucopyranosiduronic acid
Y2H	Yeast two-hybrid
Zm	*Zea mays*

1 Introduction

As the title of my thesis reveals, the function of novel proteins interacting with cytokinin-catabolizing enzymes have been investigated. In contrast to cytokinin, which is a well-characterized phytohormone, the molecular and cellular properties of the cytokinin oxidase/dehydrogenase (CKX) enzymes are largely unknown. Recent studies have suggested that CKX proteins are relevant for regulating cytokinin concentration in the endoplasmic reticulum (ER), which is the major site of cytokinin signal perception, and that their levels are controlled by a proteasome-dependent ER-associated degradation (ERAD) mechanism. In this work, several plant-specific proteins, called heavy metal-associated isoprenylated plant protein (HIPP), were found to interact with CKXs and influence their activity. The following chapters will cover several different topics, including cytokinin and their role in plant development, the basic biochemical properties of CKXs, protein ERAD as well as the current knowledge about HIPP proteins.

1.1 Cytokinin

1.1.1 Cytokinin structural variation, biosynthesis, and metabolism

The plant hormone cytokinin plays diverse roles in plant development, morphogenesis, and many other physiological processes (Werner and Schmülling, 2009; Perilli et al., 2010; Kieber and Schaller, 2018). Cytokinins are adenine derivatives carrying either an isoprene-derived or an aromatic side chain at the N^6 terminus, whereby the nature of the chain can markedly influence the biological activity of the cytokinin (Mok and Mok, 2001). Cytokinin was first discovered by Skoog, Miller, and associates in 1955 due to its cell division-promoting effect (Miller et al., 1955; Mok and Mok, 2001). Nowadays, the definition of cytokinins has grown to include a wide variety of natural and synthetic compounds. The main naturally occurring cytokinins are *trans*-zeatin (tZ), *cis*-zeatin (cZ), isopentenyladenine (iP) and dihydrozeatin (DZ) (Fig. 1) (Sakakibara, 2006). Among them, tZ and iP as well as their sugar conjugates are the major cytokinin forms and tZ and iP exhibit higher activity in *Arabidopsis thaliana* (Arabidopsis) (Spíchal et al., 2004; Romanov et al., 2005), whereas cZ is generally considered as the weakly active or inactive isoform and no specific function has been reported in Arabidopsis (Gajdošová et al., 2011).

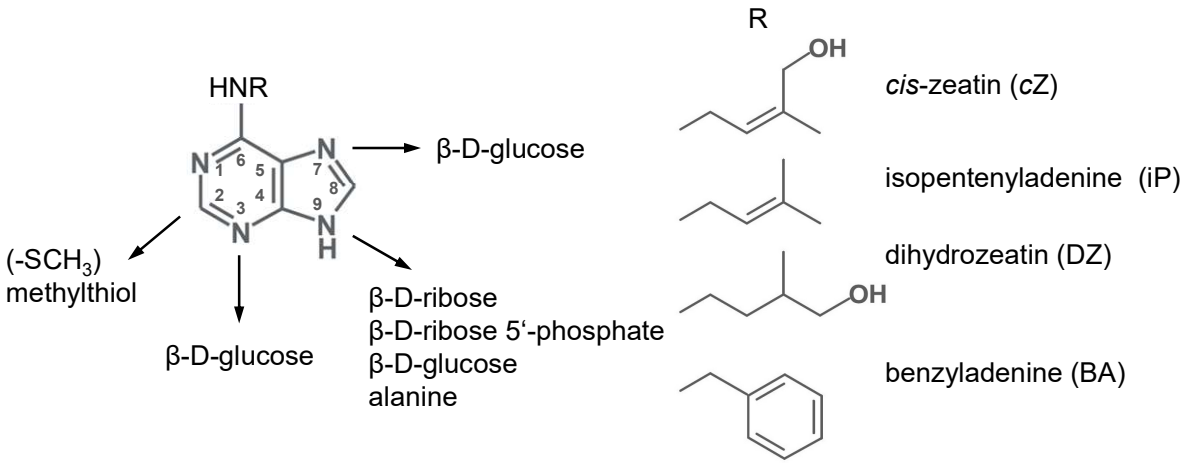

Figure 1. Structures of representative cytokinin species and their conjugates (modified from Sakakibara, 2006).

The first step in the biosynthesis of cytokinin is the addition of a prenyl side chain derived from dimethylallyl diphosphate to the N^6 position of ADP or ATP by isopentenyltransferase (IPT) enzymes (Sakakibara, 2006). IPTs are encoded by a multigene family in most plants, e.g. Arabidopsis genome encodes seven IPTs and two tRNA-IPTs which use tRNA as substrate and produce cZ (Sakakibara et al., 2005). The resulting cytokinin nucleotides can be *trans*-hydroxylated to form tZ nucleotides by the cytochrome P450 enzyme CYP735A1 and CYP735A2 (Takei et al., 2004). The release of the active, free-base, cytokinin forms from their nucleotide precursors are catalyzed by LONELY GUY (LOG) family of cytokinin riboside 5'-monophosphate phosphoribohydrolases in a single step (Kurakawa et al., 2007; Kuroha et al., 2009).

The levels of cytokinin in individual tissues, cells, and organelles are also depended on cytokinin conjugation or degradation. The most common conjugation of cytokinin involves *N*-glycosylation, which occurs on the *N3*-, *N7*- or *N9*-position of the adenine ring, and *O*-glycosylation, which occurs at the hydroxyl group of the side chains of cytokinins. Cytokinin *N7*- and *N9*-glucosides are usually inactive because the conjugation is thought to be irreversible (Bajguz and Piotrowska, 2009). In contrast, *O*-glucosylated cytokinins can be converted into active cytokinins and are considered important for storage, transport and protection against degradation (Bajguz and Piotrowska, 2009). Cytokinin degradation is catalyzed by cytokinin oxidases (CKXs) encoded by seven genes in Arabidopsis (Schmülling et al., 2003). CKXs irreversibly cleave unsaturated N^6-isoprenoid side chains from the free-base and riboside forms of cytokinins, converting active cytokinins to adenine (Werner et al., 2006).

The maintenance of cytokinin homeostasis is regulated by multiple inputs, including interchanges between bases, nucleosides and nucleotides and external factors as biotic or

abiotic cues (Sakakibara et al., 2005; Werner et al., 2006; Kieber and Schaller, 2018). For example, in Arabidopsis cytokinin accumulation is closely correlated with *IPT* genes expression and the *ipt* loss-of-function mutants have lower cytokinin levels and exhibit retarded shoot growth and enhanced root growth (Miyawaki et al., 2006). Furthermore, the expression of these *IPT* genes is downregulated by cytokinin, indicating a feedback mechanism (Miyawaki et al., 2004). Cytokinin levels are also regulated by diverse environmental factors (Bielach et al., 2017). For instance, nitrate as well as phosphate induce the expression of *IPT* genes (Argueso et al., 2009), and high concentrations of heavy metals increase the ratio of cytokinin conjugation (Atanasova et al., 2004). Moreover, it has been shown that numerous microbes, including pathogenic or symbiotic bacteria and fungi, can modulate cytokinin levels in the host plants (Joshi and Loria, 2007; Pertry et al., 2009; Siddique et al., 2015).

1.1.2 Cytokinin transport

Cytokinin biosynthesis was originally thought to take place exclusively in the roots, and then transported in the xylem from the roots to the shoots (Beck and Wagner, 1994; Beveridge et al., 1997), but more recent work has shown that cytokinin could be synthesized also in shoots and be transported to the roots through the phloem (Miyawaki et al., 2004; Hirose et al., 2008; Kamada-Nobusada and Sakakibara, 2009). tZ-type cytokinins are produced primarily in roots, where the *CYP735A2* gene is predominantly expressed (Takei et al., 2004) and tZ riboside is the major cytokinin translocated in the xylem (Hirose et al., 2008). By contrast, iP- and cZ-type cytokinins are predominantly in the phloem sap. Cytokinin acts as long-distance signal to coordinate root and shoot development, but also can be synthesized in numerous cell types and function as local signals (Kieber and Schaller, 2014). For example, conditional induction of *IPT* gene expression in a single shoot lateral bud promotes the outgrowth of single bud, but not adjacent buds (Faiss et al., 1997).

Based on the structural similarity between cytokinins and purines, two membrane-located cytokinin transporters, purine permeases (PUPs) and equilibrative nucleoside transporters (ENTs), have been identified (Durán-Medina et al., 2017; Kang et al., 2017). Complementation assays using adenine uptake deficient yeast mutant revealed that PUP1 and PUP2 mediated the import of nucleobase cytokinins (Gillissen et al., 2000; Bürkle et al., 2003). Interestingly, Zürcher et al. recently reported that the cytokinin uptake transporter PUP14 regulates cellular cytokinin signaling by depleting the pool of active cytokinins from the apoplast, which makes them unavailable to be perceived by plasma membrane-localized receptors (Zürcher et al., 2016). Unlike PUP, ENTs carry the nonspecific translocation of cytokinin ribosides (Hirose et al., 2008). In Arabidopsis, the ATP-binding cassette (ABC)

transporter ABCG14 is the sole transporter that has been shown to export cytokinins across the plasma membrane (Ko et al., 2014; Zhang et al., 2014). ABCG14 loads cytokinins from their biosynthetic site into the xylem in the roots and transports them to the shoots. Disruption of ABCG14 results in defects in the long-distance translocation and distribution of cytokinins and retardation of shoot growth (Ko et al., 2014; Zhang et al., 2014).

1.1.3 Cytokinin perception and signaling

Cytokinin signaling involves a His-Asp phosphorelay system, which is similar to the bacterial two-component signaling (TCS) systems for sensing environmental stimuli (Hwang and Sheen, 2001). Typically, the TCS consist of two conserved proteins, one of which is a membrane-located receptor kinase with an extracellular sensing domain and a cytoplasmic His kinase (HK) domain (Hwang et al., 2002). Upon binding a ligand, the kinase domain is activated and autophosphorylates a conserved His residue. Without any additional ATP requirement, the phosphoryl group is transferred to an Asp residue on the receiver domain of the second protein component, the response regulator, which activates downstream responses (Mizuno, 1997; Imamura et al., 1998; Imamura et al., 1999). Among the multicellular eukaryotes, the TCS is unique to higher plants, utilizing an extended version of the basic TCS where the phosphoryl residue transfer from the sensor HK to the response regulator via a multistep phosphorylation events alternating between His and Asp residues (To and Kieber, 2008; Argueso et al., 2010). In the model plant Arabidopsis, cytokinin signaling cascade involves various elements that are encoded by multigene families, including ARABIDOPSIS HISTIDINE KINASE (AHK) receptors, histidine-containing phosphotransfer proteins (AHPs) and response regulators (ARRs) (Fig. 2) (Werner and Schmülling, 2009).

The first cytokinin receptor AHK4/CRE1/WOL was independently identified by three groups in 2001 (Mähönen et al., 2000; Inoue et al., 2001; Suzuki et al., 2001; Ueguchi et al., 2001). AHK cytokinin receptors (Fig. 2) have a conserved extracellular CHASE (cyclases/histidine kinases-associated sensory extracellular) domain, which was shown to be sufficient for cytokinin binding (Heyl et al., 2007), at least two transmembrane domains, and cytoplasmic HK domain and receiver domains (Heyl and Schmülling, 2003). AHK4/CRE1/WOL but not AHK2, nor AHK3 can mediate cytokinin signaling via bidirectional phosphorelay (Fig. 2): it phosphorylates AHPs in the presence of cytokinin and acts as a phosphatase in the absence of cytokinin (Mähönen et al., 2006a). AHK proteins were reported to predominantly localize to the endoplasmic reticulum (ER), with the CHASE domain localized into the lumen of the ER and the C-terminal kinase domain and receiver domain exposed to the cytoplasm, suggesting that the cytokinin signaling is predominantly initiated in the ER (Caesar et al., 2011; Lomin et

al., 2011; Wulfetange et al., 2011). Smaller fraction of AHK proteins localizes to the plasma membrane. The functional relevance of the differential localization of AHK receptors is currently unclear (Zürcher et al., 2016; Romanov et al., 2018). Upon cytokinin binding, the cytosolic HK domain is activated and autophosphorylation occurs on the conserved His residue (Inoue et al., 2001) followed by a transfer of a phosphoryl group to a conserved Asp within the receiver domain (Suzuki et al., 2001; Ueguchi et al., 2001; Yamada et al., 2001; Hwang et al., 2002).

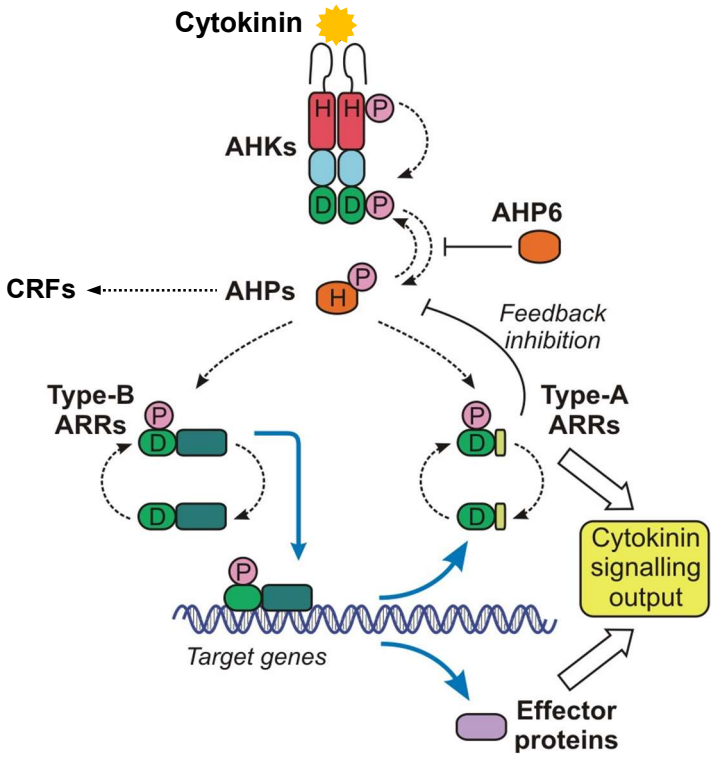

Figure 2. Schematic model of core steps of the cytokinin signaling pathway.
The binding of bioactive cytokinins to the CHASE domain of histidine kinase receptors (AHKs) results in the autophosphorylation of a histidine (H) residue in the protein kinase domain (red). The phosphoryl group is transferred intramolecularly to an Asp-residue (D) of the receptor receiver domain (green) and then to a conserved His-residue of the histidine phosphotransfer proteins (AHPs). In the absence of cytokinin, AHK4/CRE1 acts as a phosphatase that dephosphorylates AHPs. AHP proteins transfer the phosphoryl group to type-B or type-A response regulators (ARRs). AHP6, a pseudo-phosphotransfer protein that lacks the conserved His-residue, inhibits the phosphorelay. Type-B ARRs, which contain a C-terminal DNA-binding domain (turquoise), act as transcription factors that bind to the promoter regions of their target genes including type-A *ARRs* and other cytokinin-related genes. One function of the type-A ARRs is to repress signaling in a negative feedback loop. CRFs overlapping with type-B ARRs modulate the expression of many cytokinin target genes (Rashotte et al., 2006). These effector proteins together determine the signaling output of the pathway. The figure has been adapted from Werner and Schmülling (2009).

The AHPs, which shuttle between the cytosol and the nucleus, transfer the phosphoryl group from the receiver domain of an activated AHK to the receiver domain of an ARR in the nucleus (Fig. 2) (Punwani et al., 2010). In Arabidopsis, AHPs are encoded by five genes and all of them contain a highly conserved XHQXKGSSXS motif which is responsible for the His-Asp phosphor-transfer (Hwang et al., 2002), and a cysteine residue that can be S-nitrosylated by

nitric oxide to attenuate cytokinin signaling (Feng et al., 2013). AHP proteins play largely redundant role in positive regulating cytokinin signaling (Hutchison et al., 2006). AHP6 is a pseudo AHP, which lacks the conserved His residue, and repress cytokinin signaling by inhibiting the phosphotransfer reaction (Fig. 2) (Mähönen et al., 2006b). Interestingly, the expression of *AHP6* is downregulated by cytokinin indicating that it may have a role in generating a shaper signaling boundaries during a certain development stage or within a specific tissue (Mähönen et al., 2006b; Moreira et al., 2013; Besnard et al., 2014).

There are mainly two types of ARRs that modulate cytokinin signaling in Arabidopsis: type-A and -B ARRs (Fig. 2) (Imamura et al., 1998; D'Agostino et al., 2000; Zürcher and Müller, 2016). They have a conserved N-terminal receiver domain but differ in their C-terminal domains (Heyl and Schmülling, 2003; To and Kieber, 2008). The 11 type-B ARRs can be activated by phosphorylation of the Asp residue in their receiver domain and act as transcriptional activators with C-terminal extension containing a Myb-like DNA-binding domain (Kieber and Schaller, 2014). Higher-order loss-of-function mutations of the type-B *ARR*s display almost complete cytokinin insensitivity and inherently exhibit reduced cytokinin responses (Argyros et al., 2008; Ishida et al., 2008). By contrast, the 10 type-A ARRs are shorter proteins that contain only the receiver domain but lack the DNA-binding domain. The type-A *ARRs* are primary target genes of the type-B ARRs and their expression is used to monitor transcriptional activity in response to cytokinin (D'Agostino et al., 2000; Hwang and Sheen, 2001). Type-A *ARR*s function as negative-feedback regulators of cytokinin signaling (To et al., 2007; Lee et al., 2008).

Several studies has shown that there are additional factors that can modulate the TCS pathway and link it to the other pathways (El-Showk et al., 2013). For example, 160 proteins have been identified to interact with 17 different proteins of the TCS in a yeast two-hybrid screen. Among them, several cytokinin receptor-interacting proteins, such as ADL1A and GNOM, are involved in membrane trafficking, indicating that the subcellular localization of AHK receptors might be dynamic (Dortay et al., 2008). The KISS ME DEADLY (KMD) F-box proteins from the E3-ubiquitin ligase complex have been found to interact directly with type-B ARRs to regulate their rate of turnover (Kim et al., 2013). The CYTOKININ RESPONSE FACTORS (CRFs), belonging to a subset of Arabidopsis AP2 transcription factors, are transcriptionally upregulated in response to cytokinin and act in parallel to the type-B ARRs (Fig. 2) (Rashotte et al., 2006).

1.1.4 Cytokinin crosstalk

For over half a century, the antagonism between cytokinin and auxin has been known (Skoog and Miller, 1957), and recently studies have begun to unravel the molecular and mechanistic

bases for the antagonism (Moubayidin et al., 2009). For example, the expression of the *IPT* genes has been shown to respond to exogenous auxin application (Miyawaki et al., 2004). Similarly, the expression of another cytokinin biosynthesis gene *CYP735A* is significantly decreased by exogenous auxin (Takei et al., 2004) and this hormone also differently regulates the expression of the *CKX* genes (Werner et al., 2006). More recently, studies have shown that cytokinin also interact with other phytohormones to coordinate plant growth and development.

1.1.4.1 Cytokinin-gibberellin crosstalk

Gibberellin (GA) is phytonormone that control diverse aspects of plant growth and development, from seed germination and stem elongation to leaf expansion and flower development (Sun, 2008). GA inhibits various cytokinin responses during plant growth and development (El-Showk et al., 2013). For example, exogenous GA application promoted root elongation by repressing the expression of *ARR1* via the DELLA protein RGA during root meristem growth (Greenboim-Wainberg et al., 2005; Moubayidin et al., 2010). Marín-de la Rosa et al. (2015) further demonstrated that DELLA proteins interact with several type-B ARRs (ARR1, ARR2 and ARR14) and act as transcriptional co-activators of these ARRs to promote the expression of cytokinin-regulated genes (Marín-de la Rosa et al., 2015). In addition, mutation of the single *DELLA* gene in tomato did not repress cytokinin responses, while exogenous GA application suppressed the effect of *IPT7* overexpression on leaf complexity, indicating that GA could affect cytokinin responses via a DELLA-independent pathway (Fleishon et al., 2011). Furthermore, recent studies in *Medicago truncatula* have revealed that GAs induce the expression of the *CKX3* gene via a DELLA1-dependent way to regulate cytokinin metabolism whereas cytokinin regulates the expression of key GA biosynthesis genes in a AHK-dependent manner (Fonouni-Farde et al., 2018).

1.1.4.2 Crosstalk with abscisic acid

Abscisic acid is considered to be the main stress plant hormone, because of its rapid response and prominent role in plant adaptation to an adverse environment (Vishwakarma et al., 2017). Modified cytokinin levels or signaling could alter plant sensitivity to ABA, indicating a crosstalk between these two hormones (Tran et al., 2007a; Werner et al., 2010; Nishiyama et al., 2011; Nishiyama et al., 2013; Nguyen et al., 2016). Indeed, several type-A ARRs (ARR4, ARR5 and ARR6) have been reported to directly interact with ABSCISIC ACID INSENSITIVE5 (ABI5), which is a basic leucine zipper transcription factor regulating the ABA-mediated inhibitory of seed germination (Wang et al., 2011). Furthermore, Guan et al.

(2014) have shown that cytokinin promotes the proteasomal degradation of ABI5 requiring a functional cytokinin signaling pathway. Moreover, functional analysis of ABI4, which is an APETALA2 (AP2)-type transcription factor mediating the ABA signaling, has demonstrated that ABI4 negatively regulates the expression of several type-A *ARRs* (*ARR6*, *ARR7* and *ARR15*) by directly binding to their promoters (Huang et al., 2017).

1.1.4.3 Cytokinin and its crosstalk with salicylic acid

The plant hormone salicylic acid (SA) has long been implicated as a key signaling component involved in defense responses (Durner et al., 1997). Studies have also uncovered a role of cytokinin in plant immunity (Albrecht and Argueso, 2017), and the cytokinin-induced immunity is at least partially dependent on the crosstalk with SA (Choi et al., 2010; Argueso et al., 2012; Jiang et al., 2013). One indication of the crosstalk between cytokinin and SA has emerged from the analysis of a resistance (R) protein, the coiled-coil nucleotide-binding leucine-rich-repeat protein (CC-NB-LRR). A semi-dominant gain-of-function mutation of this gene (*uni-1D*) results in the constitutive upregulation of the *pathogenesis-related* (*PR*) *protein* genes and several type-A *ARR* genes (*ARR4*, *ARR5* and *ARR6*) (Igari et al., 2008). PRs have been used in numerous studies to elucidate transcriptional control mechanisms regulating plant immune responses, and the expression of *PR* genes is induced by SA (Carr et al., 2010). Introducing *CKX1* genes in *uni-1D* plants not only suppressed the upregulation of *ARR5* gene, but also repressed the activation of *PR-1* gene, suggesting that cytokinin levels could mediate the expression of SA immune genes (Igari et al., 2008). This crosstalk between cytokinin and SA pathways has been further demonstrated by Naseem et al. (2012) showing that exogenous cytokinin application protects Arabidopsis plants against infection by *Pseudomonas syringae* pv. *tomato* DC3000 via the activation of the PR-1.

1.1.5 Cytokinin functions in plant developmental processes

Cytokinin is an essential phytohormone that is involved in numerous plant growth and developmental processes. These include the effects on seed germination (Khan, 1971; Wang et al., 2011), the role in promoting apical and axillary meristems activity (Leibfried et al., 2005; Barton, 2010; Wang et al., 2017), the leaf senescence (Gan and Amasino, 1995), the development of the female gametophyte (Hejátko et al., 2003; Deng et al., 2010; Kinoshita-Tsujimura and Kakimoto, 2011; Bencivenga et al., 2012; Cheng et al., 2013), the size of the flower organs (Bartrina et al., 2011), the seed size (Riefler et al., 2006), the regulation of cell proliferation and differentiation in root apical meristem (Werner et al., 2003; Dello Ioio et al., 2007; Zhang et al., 2013), the root nodule organogenesis (Tirichine et al.,

2007), the root vascular differentiation (Mähönen et al., 2006b; Hejátko et al., 2009), the development of the lateral root (Chang et al., 2013), and the responses to biotic and abiotic stress (Frugier et al., 2008; Werner et al., 2010). Cytokinin regulates many of these processes in a crosstalk with other phytohormones (Zhao et al., 2010; Wang et al., 2011; A Seif El-Yazal et al., 2015; Schaller et al., 2015). Molecular mechanisms involved in the cytokinin-mediated control of four developmental programs will be discussed.

1.1.5.1 Cytokinin function in the shoot apical meristem

In Arabidopsis, the shoot apical meristem (SAM) forms during embryogenesis between the two cotyledons. The dome-shaped SAM contains distinct zones determined by master regulatory gene expression. The homeodomain transcription factor WUSCHEL (WUS) specifically expresses in the organizing center (OC), and then moves from OC to stem cells in the overlaying central zone (CZ), which is defined by the specific expression of the *CLAVATA3* (*CLV3*) (Barton, 2010). WUS promotes the stem cell activity and *CLV3* expression, while CLV3 in turn suppresses stem cell activity and restricts the *WUS* expression domain via the CLAVATA1,2 (CLV1/2) receptor signaling pathway (Soyars et al., 2016). The WUS-CLV3 feedback loop is necessary for the maintenance of cell populations in both the OC and CZ (Truskina and Vernoux, 2018). Cytokinin has long been known to play a crucial role in regulating SAM (Werner et al., 2001). Plants treated with exogenous cytokinin or the *ckx3,5* mutants, which contains increase cytokinin levels, show increased *WUS* expression and form larger SAM (Gordon et al., 2009; Bartrina et al., 2011). This cytokinin-induced *WUS* expression requires cytokinin receptor AHK2 and AHK4 (Gordon et al., 2009). In turn, the accumulation of the WUS leads to the repression of type-A *ARRs* and promotes further the cytokinin signaling (Leibfried et al., 2005). Moreover, the expression of *CLV1* is suppressed in response to cytokinin treatment, causing further increase in *WUS* transcription (Gordon et al., 2009).

1.1.5.2 Cytokinin regulates leaf development

The final size and shape of leaves are determined by a tight control of cell division and cell expansion (Gonzalez et al., 2012). The Arabidopsis *cyclin D3* (*CYCD3*) genes are expressed in lateral organs and play key roles in promoting cell division (Gaudin et al., 2000; Dewitte et al., 2007). The CYCD3-containing cyclin-dependent kinase complexes promote cell entry into S-phase by phosphorylating retinoblastoma-related protein (RBP) and hence relieving its inhibition of the E2F transcription factors (Dewitte et al., 2003). Ectopic expression of *CYCD3* in plants accelerates the progression from G1 to S phase, resulting in the accumulation of

cells in G2 and promoting mitotic cycles (Menges et al., 2006). Cytokinin promotes cell division in Arabidopsis through inducing the expression of these *CYCD3* genes (Riou-Khamlichi et al., 1999). Constitutive *CYCD3*-expression induced the formation of green calli from callus cells regardless of the presence of exogenous cytokinin (Riou-Khamlichi et al., 1999). In contrary, the *cycd3;1-3* triple mutant calli did not develop shoots even in the presence of high cytokinin (Dewitte et al., 2007).

In addition to the regulation of cell division, cytokinin also modulates the process of cell expansion (Holst et al., 2011; Li et al., 2013a). Holst et al. (2011) have shown that ectopic expression of *CKX3* under the control of the *ANT* promoter causes a specific cytokinin deficiency in young leaves. The epidermal cell size in *ANT:CKX3* leaves was on average 2.5 times increased compared to the wild type (WT), but the leaf blade was much smaller due to the early ceased cell proliferation. Interestingly, *ANT:CKX3* cells were about 60% larger than those of *35S:CKX3* leaves, which display constitutive cytokinin deficiency during the whole lifespan, suggesting that cell expansion was restrained by cytokinin deficiency during the differentiation phase (Holst et al., 2011). The interdigitated pattern of Arabidopsis leaf pavement cell (PC) is determined by a series of local expansions towards multi polar site (Yang, 2008). Li et al. (2013a) has shown that cytokinin signaling is involved in the regulation of the PC morphogenesis. In the *ahk3/cre1* cytokinin receptor mutant, the PC interdigitation pattern is enhanced, whereas in plants over-producing cytokinin or overexpressing a B-type *ARR*, *ARR20*, the PC lobes are reduced, demonstrating a role of cytokinin in controlling the local expansion of PCs.

The leaf margin architecture is mainly controlled by the CUP-SHAPED COTYLENDON (CUC) transcription factors, encoded by three genes in Arabidopsis (Bilsborough et al., 2011). *CUC2* and *CUC3* are specifically expressed in leaf primordia and are required for leaf serration (Hasson et al., 2011). Plants expressing a *miRNA164*-resistant *CUC2* gene form deeper serrations, whereas the *cuc2* and *cuc3* loss-of-function mutants showed reduced serrations (Nikovics et al., 2006; Hasson et al., 2011). Cytokinin controls this process partially through the induction of *CUC* genes. It has been reported that ectopic expression of *IPT4* elevates the expression of both *CUC2* and *CUC3* genes in Arabidopsis (Li et al., 2010).

Additionally, other transcription factor families have been reported to regulate leaf size and shape via modulating cytokinin signaling pathway (Bar et al., 2016). One of them is the TEOSINTE BRANCHED1/CYCLOIDEA/PROLIFERATING CELL FACTOR1 (TCP) family (Efroni et al., 2013). TCPs can be subdivided into two types, based on differences within their TCP domains (Martin-Trillo and Cubas, 2010), that antagonistically mediate the cytokinin signaling pathway to control the growth of leaves. For example, overexpression of one of the class I type *TCPs*, *TCP14*, produced plants hypersensitive to cytokinin, whereas the *tcp14tcp15* double mutants were hyposensitive to the hormone (Steiner et al., 2012).

Conversely, the reduction in expression of *CIN-TCPs*, which contains 8 genes belonging to class II *TCP*, increased plants sensitivity to cytokinin and produced crinkly leaves (Palatnik et al., 2003; Efroni et al., 2013).

1.1.5.3 The role of cytokinin in regulating root growth and development

The Arabidopsis primary root is initiated during embryogenesis and is maintained via the activity of the root apical meristem (RAM) (Tian et al., 2014). Cells in the meristematic zone (MZ) divide several times before entering the transition zone (TZ) in which they stop dividing, and undergo rapid elongation and differentiation in the elongation zone (EZ). Cell division coordinated with cell elongation and differentiation contributes to the continuous growth and development of the primary root (Moubayidin et al., 2013). Cytokinin and auxin antagonistically control the cells division and cell elongation in the root apex (Kong et al., 2018). Auxin promotes cell division in the proximal meristem, whereas cytokinin inhibits the root growth by dampening auxin output and redistribution via SHY2 to promote cell differentiation in the TZ (Dello Ioio et al., 2007; Dello Ioio et al., 2012). Application of exogenous cytokinin or overexpression of a gain-of-function *ARR1* gene cause a decrease in root meristem size, resulting in a short primary root; cytokinin-deficient plants or signaling mutants display a larger root owing to an accumulation of meristematic cells (Werner et al., 2003; Dello Ioio et al., 2007; Kurepa et al., 2014). Cytokinin also inhibits lateral root initiation, acting as a positional cue to regulate lateral root spacing in Arabidopsis (Laplaze et al., 2007; Chang et al., 2013, 2015).

1.1.5.4 Cytokinin signaling mediates drought stress responses

Water deficit is a major environmental factor that limits plant productivity worldwide (Bray, 1997). As sessile organisms, plants have to develop elaborate and sensitive protection systems to protect them from dehydration (Tran et al., 2007b). Cytokinin signaling components have been reported to have both positive and negative effects on plant drought tolerance (Li et al., 2016). Regarding the positive effect of cytokinin on drought tolerance, studies of transgenic plants with higher endogenous cytokinin levels revealed enhanced drought tolerance through delaying premature plant senescence (Rivero et al., 2007; Golan et al., 2016). The negative effect of cytokinin on drought tolerance is evidenced in studying the cytokinin deficient plants, such as *CKX* overexpression lines and *ipt1,3,5,7* quadruple mutants, or cytokinin-signaling mutants, such as *ahk2,3*, *ahp2,3,5*, and *arr1,10,12* multiple mutants, that have improved drought tolerance through elevating abscisic acid (ABA) hypersensitivity (Werner et al., 2010; Nishiyama et al., 2011; Nishiyama et al., 2013; Nguyen et al., 2016).

Interestingly, although cytokinin deficiency increased plants ABA hypersensitivity, the plants had a significant reduction in endogenous ABA contents which is due to a downregulation of key ABA biosynthetic genes (Nishiyama et al., 2011). Huang et al., (2018) has recently reported that the Sucrose nonfermenting1-related kinases (SnRKs) of the ABA signaling pathway directly phosphorylate Ser residues of ARR5, resulting in the enhancement of the ARR5 protein stability, and that *ARR5* overexpression increases ABA sensitivity and drought tolerance. Several B-type ARRs physically interact with SnRKs and repress the kinase activity, suggesting an integrated cytokinin-ABA crosstalk mediating plant growth under drought stress (Huang et al., 2018).

1.2 Cytokinin oxidase/dehydrogenase

Cytokinin degradation is irreversibly catalyzed by cytokinin oxidase/dehydrogenase (CKX) enzymes encoded by seven genes in Arabidopsis (Schmülling et al., 2003). The study of transgenic plants overexpressing *CKX* genes, which cause CKs deficiency, has provided us with knowledge of cytokinin functions during plant growth and development. However, individual CKX proteins differ in their basic biochemical properties and subcellular localization (Werner et al., 2003; Köllmer et al., 2014). For instance, comparing with other CKX proteins, CKX2 and CKX4 displayed higher enzymatic activity when tested with isoprenoid CK substrates (Werner et al., 2003). Whereas CKX1 has been shown to act as cytokinin dehydrogenase with low activity in *in vitro* assays (Galuszka et al., 2007). Therefore, it's necessary to learn the molecular features of different *CKX* genes and proteins, including their structure and catalytic properties, their expression patterns, subcellular localizations, and factors that could regulate CKX activity.

1.2.1 Structure and catalytic properties of CKX

Despite the low overall sequence homology between the different Arabidopsis CKX proteins, about one-third of all amino acid positions are highly conserved (Schmülling et al., 2003). The three-dimensional structure of *Zea mays* ZmCKX1 protein displays that a large part of these conserved regions are domains for FAD and substrate binding (Malito et al., 2004). CKXs belong to the group of flavoproteins with the FAD co-factor covalently linked to the apoprotein (Bilyeu et al., 2001; Malito et al., 2004). The covalent FAD linkage has been shown to be important for maintaining the enzyme's structural integrity, stability and high rates with electron acceptors (Kopečný et al., 2016). Additionally, short highly conserved motifs are also found at the N- and C- termini of CKX proteins. For instance, a GlWeVPHPWLNL motif is found around position 390 and a PGQxIF signature is at the C-terminal ends of the proteins

(Schmülling et al., 2003). These conserved domains may function in electron transport, substrate recognition or other aspects of molecular activity of CKX.

CKX was originally thought to serve as an oxidase, which utilizes molecular oxygen as an electron acceptor (Armstrong, 1994), but the reaction efficiency is generally low. Detailed kinetic study on recombinant ZmCKX1 demonstrated that the enzyme acted preferentially in the dehydrogenase mode and its activity was dramatically enhanced in the presence of a suitable organic electron acceptor (Frébortová et al., 2004). Although, a possible natural electron acceptor has been proposed in maize (Frébortová et al., 2010), the identity of the CKX electron acceptor(s) in Arabidopsis is unclear. Individual CKX proteins display maximum activities at different pH (Bilyeu et al., 2001; Galuszka et al., 2001; Frébort et al., 2002; Galuszka et al., 2004; Galuszka et al., 2007), which may reflect differential pH optima for the different electron acceptors.

The elucidation of the crystal structure of maize ZmCKX1 revealed the mechanisms of cytokinin degradation by the CKX enzyme. Taking the breakdown of iP as an example (Fig. 3), the N10 atom of the isoprenoid side chain is bound with Asp169 residue inside the CKX protein and the adenine ring is bound in a funnel-shaped site on the protein surface (Malito et al., 2004). The C11 carbon atom is in contact with the flavin N5 atom facilitating thus probably a direct transfer of the electrons and the proton to the flavin (Malito et al., 2004). Subtle variation in the amino acid composition in the binding funnel of different CKX enzymes is considered part of the causal mechanism for the enzyme specificity towards different cytokinin substrates (Galuszka et al., 2007; Kopečný et al., 2016).

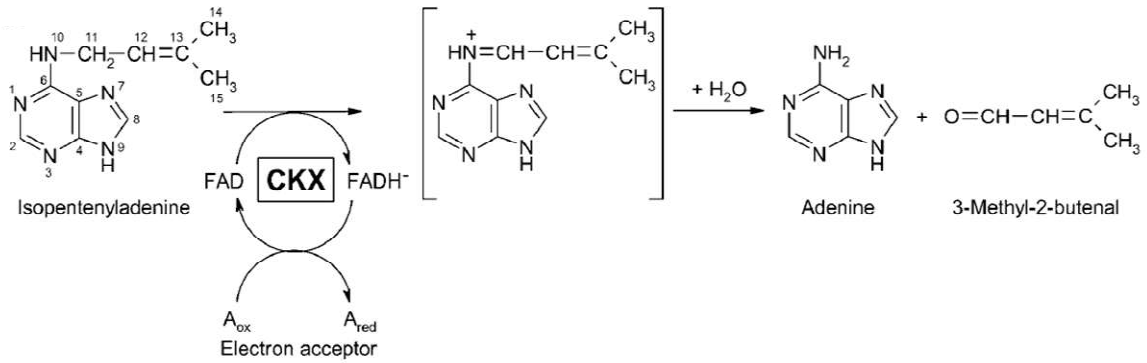

Figure 3. Scheme of the reaction catalyzed by the CKX enzyme with isopentenyladenine. (Figure from Werner et al., 2006).

Galuszka et al. (2007) have demonstrated that the secreted Arabidopsis CKX enzymes, CKX2 and CKX4, have the overall highest activity, especially against free cytokinin bases, whereas CKX1 and CKX3 show preference for the nucleotides as substrates. Moreover, CKX1 also shows a high affinity for the glycosylated cytokinin iP9G. Similar preference has

been also observed for CKX7 (Galuszka et al., 2007). Based on the specific binding of the CKX enzymes towards their substrates, new synthetic cytokinin derivatives have been developed to function as CKX inhibitors. For example, INCYDE (2-chloro-6-(3-methoxyphenyl) aminopurine), which strongly binds into the CKX enzyme active site, but is weakly sensed by the cytokinin receptors, competitively blocks the CKX activity (Zatloukal et al., 2008). This inhibitor has been used to probe the function of cytokinin during environmental stress repsonses. It has shown positive effects on seedling growth under heavy metal stress (Gemrotová et al., 2013) and protected tomato plants against sodium chloride (NaCl)-stress (Aremu et al. 2014).

1.2.2 Expression pattern and subcellular localization of CKX

In higher plant species, CKX proteins are encoded by multigene families. Whereas there are seven distinct *CKX* genes (*CKX1-CKX7*) encoding the enzymes in Arabidopsis, eleven and thirteen *CKX* homologues are, for instance, identified in the rice and maize genome, respectively (Gu et al., 2010). The seven *CKX* genes in Arabidopsis have shown distinct expression patterns, while the overall expression levels of all *CKX* genes are very low, and specifically restricted to small distinct expression domains (Werner et al., 2003). For example, most of the *CKX* genes are expressed in zones of cell division, like the shoot apex (*CKX1-CKX3, CKX5*), stomatal meristemoids (*CKX4*), the developing petiole of the youngest leaves (*CKX5*), and the procambial region of the root meristem (*CKX5*), whereas *CKX6* and *CKX7* are expressed in the vascular tissue (Werner et al., 2003; Bartrina et al., 2011; Pillitteri et al., 2011; Köllmer et al., 2014). Interestingly, Miyawaki et al. (2004) have shown that the expression domains of some cytokinin-biosynthesis *IPT* genes partially overlap with the expression domains of the *CKX* genes, suggesting that the steady state cytokinin concentration in a certain tissue is strictly controlled by the cytokinin biosynthesis and degradation process.

The expression of *CKX* genes is induced by the exogenous application of cytokinin, functioning as a negative feedback loop to maintain cytokinin homeostasis (Brugière et al., 2003; Motyka et al., 2003; Werner et al., 2006; Bhargava et al., 2013). Moreover, *CKX* genes are also found to be regulated by other phytohormones (Werner et al., 2006). For example, *CKX4* has been identified as auxin-repressed gene (Goda et al., 2004; Rashotte et al., 2005). Several *CKX* genes (*CKX1, CKX3, CKX4, and CKX6*) have been shown are down-regulated by ABA (Werner et al., 2006). The effects of other hormones on the expression of these *CKX* genes indicate a potential role of CKX in the crosstalk between cytokinin with other hormones.

Furthermore, the expression of *CKX* genes is also found to response to a numerous biotic and abiotic cues (Uhde-Stone et al., 2003; Zimmermann et al., 2004; Werner et al., 2006). For instance, the expression of a putative *CKX* homologous gene is increased in response to drought stress in leaves of pea (*Pisum sativum*) (Vaseva-Gemisheva et al., 2005). White lupin (*Lupinus albus*) and other plant species could adapt to phosphate deficiency by differentially regulating *CKX* genes expression to promote the development of the specialized short, densely spaced lateral roots (called proteoid root or cluster root) (Neumann et al., 1999; Watt and Evans, 1999; Uhde-Stone et al., 2003). Canopy shade significantly increases the expression of *CKX6*, which causes a rapid and transient arrest in leaf development (Carabelli et al., 2007).

Several previous analyses have shown that individual CKX proteins from Arabidopsis are targeted to different subcellular compartments. Sequence analyses predict that most of the CKX proteins (CKX1-CKX6) have a signal peptide or a signal anchor at their N-termini (Niemann et al., 2018). CKX2, CKX4, CKX5 and CKX6 are thought to be targeted to the ER by the cleavable signal peptide at their N-termini and subsequently transported through the secretory pathway to the apoplast (Werner et al., 2003; Niemann et al., 2018). CKX1 and CKX3 have been shown to localize in the ER, endomembrane system and vacuole (Werner et al., 2003; Niemann et al., 2018). Intriguingly, the vacuolar localization of CKX1 was detected mainly in smaller root cells but not in leaf epidermal cells (Werner et al. 2003). Recently, Niemann et al., (2018) have shown that CKX1 is a type II integral membrane protein with a short N-terminal cytoplasmic tail, a single TM domain, and a luminally oriented catalytic domain and that the protein localizes predominantly in the ER. The authors have shown that the GFP-fused CKX1 proteins could not be detected in the vacuole and pointed out that the vacuolar targeting observed previously might be an overexpression artefact. Interestingly, it has been demonstrated that the CKX1 TM helix mediates largely the protein homodimerization as well as its retention in the ER. It has been proposed that oligomerization is an important parameter regulating CKX1 biological activity and the cytokinin concentration in the ER (Niemann et al., 2018). In contrast to CKX1-CKX6, CKX7 does not have a signal peptide and is localized in the cytosol (Köllmer et al., 2014). Different subcellular localization of the individual CKX isoforms is an important feature of the proteins and might be relevant to define their specific functions, extracellularly or in different subcellular compartments. For example, the AHK cytokinin receptors in Arabidopsis have been shown to be predominantly localized in the ER (Caesar et al., 2011; Wulfetange et al., 2011), suggesting that the ER-resident CKX1 might play an important role in controlling cytokinin concentrations, which are directly perceived by the cytokinin receptor AHK, in the ER compartment. On the other hand, a physiologically relevant function of the apoplastic cytokinin has been recently

proposed as well (Zürcher et al. 2016), suggesting that the secreted CKX isoforms may participate in controlling cytokinin concentrations in this compartment.

1.2.3 Regulation of CKX activity

Previous works have reported discrepancy between the calculated and apparent molecular masses of the CKX proteins, indicating that the proteins might undergo posttranslational modifications. Indeed, CKX proteins isolated from different plant species have been reported to be glycoproteins (Armstrong, 1994; Morris et al., 1999; Schmülling et al., 2003; Niemann et al., 2015) and all Arabidopsis CKX proteins are predicted to have several *N*-glycosylation sites (Schmülling et al., 2003). Glycosylation sites could be found in the identified maize ZmCKX1 crystal structure (Malito et al., 2004). Deglycosylation of the recombinant ZmCKX1 enzyme produced heterologously in yeast (*Yarrowia lipolytica*) decreased its activity and thermostability, suggesting the functional importance of ZmCKX1 glycosylation (Kopečný et al., 2005; Franc et al., 2012). Similarly, Motyka et al. (1996) have shown that both glycosylated and nonglycosylated CKX isoforms exist in cultured tobacco callus cells. After cytokinin induction, the CKX activity is enhanced predominantly with the secreted glycosylated enzyme isoform, indicating a possible function of *N*-glycosylation in the regulation of CKX activity (Motyka et al., 2003).

Recently, Niemann et al., (2015) have shown that Arabidopsis CKX1 is an *N*-glycoprotein and contains mainly high-mannose *N*-glycans. They also reported that mutation of an ER-resident protein REPRESSOR OF CYTOKININ DEFICIENCY 1 (ROCK1), which functions as a nucleotide sugar transporter transporting UDP-*N*-acetylglucosamine (UDP-GlcNAc) and UDP-*N*-acetylgalactosamine (UDP-GalNAc) as main substrates, could suppress phenotypes caused by overexpression of the ER-resident CKX1 as well as other secretory CKX proteins, but not the cytosolic CKX7 (Niemann et al., 2015). Intriguingly, it has been shown that ROCK1 is apparently not involved in CKX1 *N*-glycosylation as the protein was still glycosylated in the *rock1* mutant (Niemann et al., 2015). Rather, it has been proposed that ROCK1 regulates the ER-mediated protein quality control (ERQC) system (Niemann et al., 2015; Strasser, 2018). The abundance of CKX proteins could be controlled by ERQC and the terminally misfolded CKX proteins are removed from the ER and degraded by the proteasome-dependent ER-associated degradation (ERAD) mechanism (Niemann et al., 2015; Berner et al., 2018; Wu and Rapoport, 2018).

1.2.4 ER-mediated protein quality control (ERQC) and ER-associated degradation (ERAD)

The endoplasmic reticulum (ER) is the entry gate to the secretory pathway and serves as a dynamic protein-folding organelle where the ER-resident molecular chaperones and folding catalysts promote newly synthesized proteins to attain their native conformations (Strasser, 2018). Misfolded proteins not only lead to dysfunction but also induce cellular toxicity effects. Therefore, ER evolves a highly efficient ER-mediated protein quality control (ERQC) system to monitor an efficient and accurate folding process, recognize non-native protein conformations for additional rounds of chaperone-assisted folding, and target terminally misfolded proteins and unassembled proteins for ER-associated degradation (ERAD) (Berner et al., 2018).

1.2.4.1 *N*-linked glycosylation-regulated protein folding and quality control in the ER

The promotion of protein folding in the ERQC system is controlled by protein *N*-linked glycosylation (Ferris et al., 2014). The majority of proteins produced in the ER are co-translationally glycosylated with an oligosaccharide attaching to the asparagines (Asn) in the Asn-X-Ser/Thr sequons (X can be any amino acid except proline while Ser/Thr denote serine/threonine residue) when entering the ER (Aebi, 2013). These oligosaccharides, termed *N*-linked glycans or simply *N*-glycans, play an important role in the protein folding and quality control (Schwarz and Aebi, 2011). The current model for protein *N*-glycosylation, which is mainly based on the studies in yeast and animals, includes two parts: the first part is the assembly of a glycan molecule and the second part is the transferring of the glycan to an Asn residue on a nascent protein. In the first part, multiple glycosyltransferases, including a series of highly specific asparagines-linked glycosylation (ALG) proteins, sequentially add a monosaccharide onto an ER-membrane-anchored lipid called dolichol-pyrophosphate (Dol-PP) to assemble a oligosaccharide consisting of three glucose, nine mannose and two N-acetylglucosamine residues ($Glc_3Man_9GlcNAc_2$) (Fig. 4) (Strasser, 2016). In the second part of *N*-glycosylation, this 14-sugar oligosaccharide is transferred to the Asn residues within the sequon of a nascent polypeptide catalyzed by a membrane-bound multi-subunit complex oligosaccharyltransferase (OST) associating with the translocon pore on the ER membrane (Fig. 4) (Hong et al., 2009; Mohorko et al., 2011). For ERQC, sequential cleavage of the terminal and middle Glc residues from the *N*-glycans is a major factor in determining the fate of ER glycoproteins (Fig. 4) (Strasser, 2016). The outermost Glc residue is removed almost immediately by the membrane-bound enzyme glucosidase I (GI) (Hubbard and Robbins, 1979) and the middle Glc residue is sequentially removed by glucosidase II (GII), generating a

monoglucosylated *N*-glycan, $GlcMan_9GlcNAc_2$, which is recognized by the ER membrane-anchored lectin-like chaperone calnexin (CNX) and its ER luminal homolog calreticulin (CRT) (Rutkevich and Williams, 2011; Wijeyesakere et al., 2013).

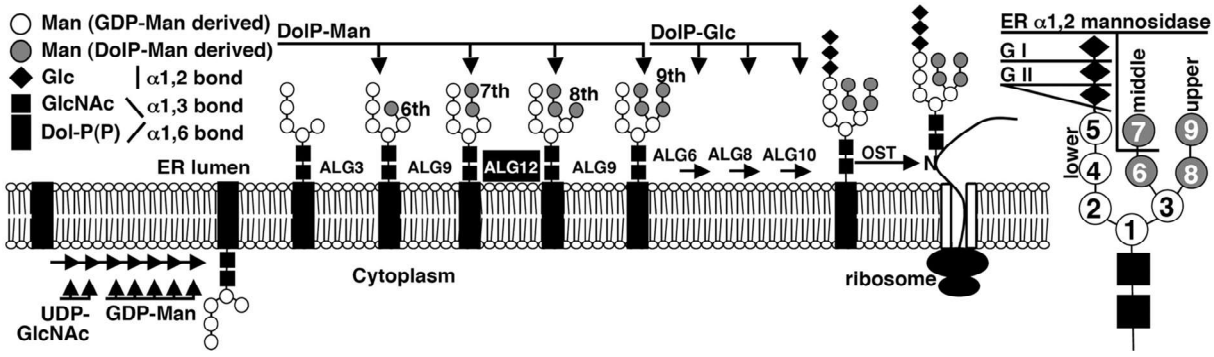

Figure 4. Scheme of assembly of *N*-glycan precursor $Glc_3Man_9GlcNAc_2$.
The assembly of the *N*-glycan precursor initiates at the cytoplasmic surface of the ER by adding two cytoplasmic UDP-GlcNAc and five GDP-Man residues to the membrane-anchored dolichol-pyrophosphate (Dol-PP) linker and the resulting Dol-PP-$Man_5GlcNAc_2$ is flipped over into the ER lumen. Four Man and three Glc residues are sequentially added to the flipped Dol-PP-$Man_5GlcNAc_2$ by mannosyltransferases ALGs to form the 14-sugar precursor, Dol-PP-$Glc_3Man_9GlcNAc_2$, that is transferred to nascent proteins by OST. The added glycoresidues, the corresponding glycosyltransferases, and three types of mannosyl bonds are shown. The enlarged $Glc_3Man_9GlcNAc_2$ structure is shown with circled numbers representing the order of each Man residues addition. The enzymes that remove the three Glc residues and Man residues (GI, GII, and α-1, 2-mannosidase) are indicated, respectively. Figure from Hong et al., (2009).

Glycoprotein association with CNX/CRT is crucial for folding of nascent polypeptides because CNX/CRT can recruit other ER-chaperones and folding enzymes which assist the nascent polypeptides in achieving a native conformation and correct disulfide bonds (Caramelo and Parodi, 2008). A second deglucosylation by GII releases the glycoprotein from the CNX/CRT (D'Alessio et al., 2010). If the protein has achieved the native conformation, it will be transported to its final destination. In contrast, protein with non-native folds will be recognized by an ER-resident folding sensor UDP-glucose:glycoprotein glucosyltransferase (UGGT), and undergo reglucosylation. As a result, a Glc residue is added back to the glycoprotein, that permits it once again entering the CNX/CRT cycle for folding assistance (D'Alessio et al., 2010). However, if glycoprotein fails to achieve its native conformation within a given time window, it will be eliminated by ERAD (Vembar and Brodsky, 2008).

1.2.4.2 ER-associated degradation (ERAD)

ERAD is a conserved, multistep process involving the recognition of terminally misfolded proteins from folding intermediates and reparable misfolded proteins, retrotranslocation from the ER to cytosol, polyubiquitination, and degradation by the ubiquitin-proteasome system (Strasser, 2018). The ERAD signal for misfolded glycoproteins is generated by the removal of the terminal α-1,2-Man residues from the *N*-glycan, catalyzed by homologous of yeast

mannosidase 1 (Htm1) (MNS4 and MNS5 in Arabidopsis) (Quan et al., 2008; Clerc et al., 2009; Liebminger et al., 2009; Hüttner et al., 2014). The ERAD signal sensor, ER-luminal lectin osteosarcoma9 (Yos9 in yeast; Os9/EBS6 in Arabidopsis), specially recognizes terminal misfolded proteins in the ER (Yoshida and Tanaka, 2010). In yeast, an ER-resident protein, HMG-CoA reductase degradation 3 (Hrd3; HRD3A/EBS5 in Arabidopsis), which is a type I transmembrane protein, is also required for the selection of ERAD clients (Hirsch et al., 2009; Liu et al., 2011). Once the ERAD clients were chosen by the Yos9 and Hrd3, the ERAD substrates will be brought to the membrane-anchored ERAD complexes for retrotranslocation and ubiquitination (Fig. 5). In yeast, there are at least two such ERAD complexes differing in their core component, which is a membrane-embedded protein with a RING finger-type ubiquitin ligase (E3) activity exposed to the cytosolic surface of the ER membrane, including Hrd1 and Degradation of alpha2 (Doa10) (Fig. 5) (Strasser, 2018). Based on the studies from mammals and yeast, three different ER-associated degradation pathways have been identified, depending on the location of folding lesions. ERAD-L substrates, having a lesion in the ER luminal area, can be soluble or membrane-anchored proteins. ERAD-M substrates are membrane proteins, which have a lesion in the transmembrane segment. ERAD-C substrates are membrane-bound proteins that expose a defect in the cytosolic domain (Vembar and Brodsky, 2008). In the most cases, ERAD-L/M substrates are eliminated by Hdr1 complexes and ERAD-C substrates are degraded by the Doa10 complexes (Liu and Li, 2014). Because the catalytic domains of these E3 ligases expose to the cytosolic surface of the ER membrane, ERAD clients need to undergo retrotranslocation for ubiquitination. However, the molecular mechanism underlying this retrotranslocation is largely unknown (Hampton and Sommer, 2012). Studies suggested that the Sec61 channel, which is responsible for the importing of nascent polypeptides into the ER lumen, also serves as retrograde protein exporting ERAD substrates from the ER into the cytosol (Römisch, 2017). However, a recent study has shown that the E3 ligase Hrd1 itself can form a ubiquitin-gated protein-conducting channel for the retrotranslocation of ERAD clients (Baldridge and Rapoport, 2016). The retrotranslocation by the Hrd1 complex is in cooperation with Ui-Snp1 associating-1 (Usa1) and Degradation in the ER (Der1) (Fig. 5). Usa1 is an ER membrane protein that is important for the stability and oligomerization of Hrd1, while the integral ER membrane protein Der1 might function as an alternative retrotranslocation channel (Wu and Rapoport, 2018).

Once the ERAD clients expose to the catalytic domains of the E3 ligase, ubiquitin is attached to the substrates through a three-step process, including activation, conjugation and ligation catalyzed by ubiquitin-activating enzyme (E1), ubiquitin-conjugating enzyme (E2), and E3 ligase, respectively (Pickart, 2004). The ubiquitinated proteins are sequentially extracted from the ligase complex by the Cdc48 ATPase complex (Fig. 5) (Wolf and Stolz, 2012). An ER membrane protein Ubx2 is responsible for recruiting Cdc48 to the E3 complex (Neuber et al.,

2005). The transfer of ERAD substrates from Cdc48 to the 26S proteasome is not well understood. Recent studies showed that the extracted ERAD substrates are further processed by deubiquitinating enzymes (DUBs) to trim the polyubiquitin chain, which triggers the release of the substrates from the Cdc48 complex (Bodnar and Rapoport, 2017). The released ERAD substrates are delivered to the cytosolic proteasome with the help of two ubiquitin receptors, Rad23 and Dsk2, and degraded (Medicherla et al., 2004).

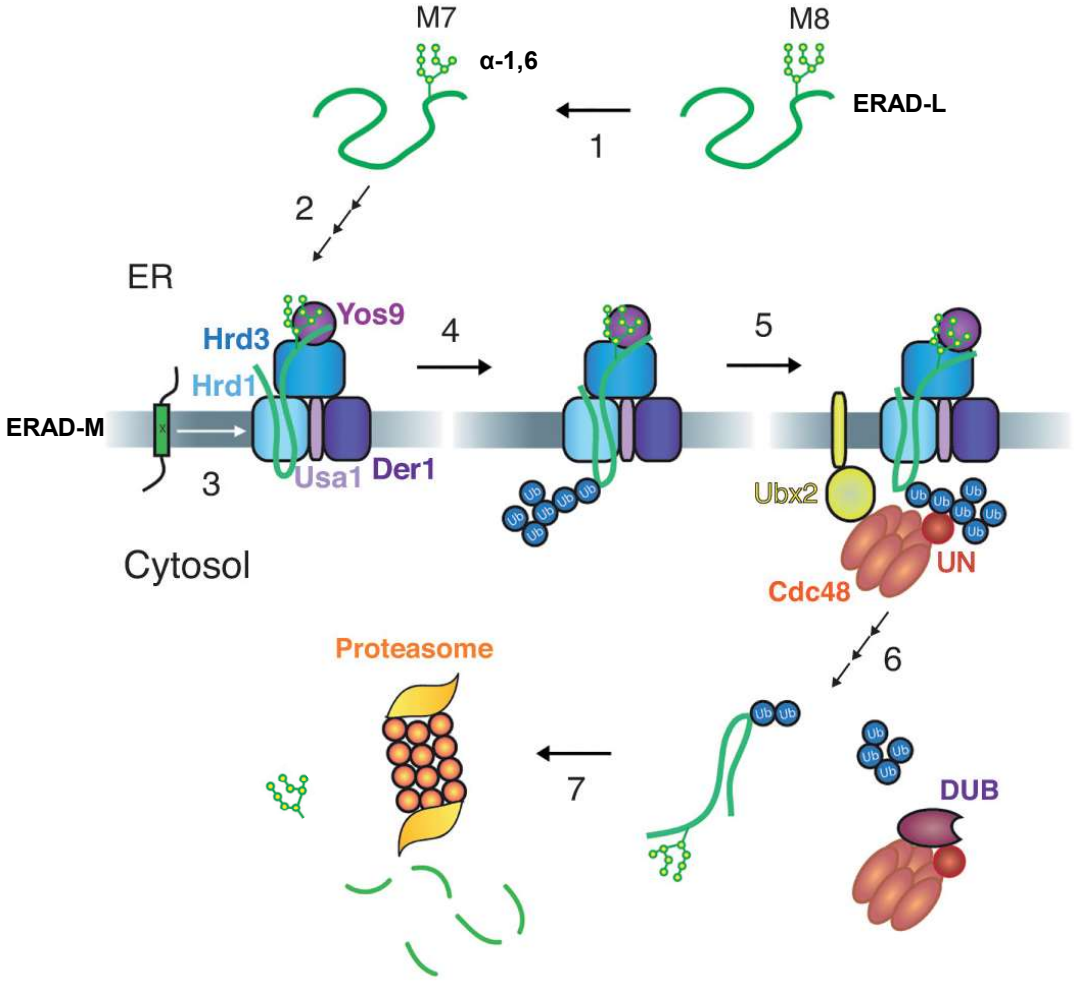

Figure 5. Schematic model of core steps of the ERAD.
Stepwise degradation of ERAD-L and -M substrates is shown. **1.** The terminally misfolded luminal glycoprotein is removed from the folding cycle by trimming of the terminal α-1,2-Man residues from the *N*-glycan. **2.** The generated terminal α1,6-linked mannose residue is recognized by the ERAD sensor Yos9 and an ER membrane-anchored protein Hrd3. The ERAD clients insert into the Hrd1 retrotranslocation channel with the help of Usa1 and Der1. **3.** ERAD-M clients, having folding lesion in the transmembrane segment (indicated by an 'x'), enter Hrd1 sideways. **4.** Both ERAD-L and ERAD-M clients are polyubiquitinated by Hrd1 ligase at the cytosolic surface of the ER membrane. **5.** The Cdc48 ATPase complex is recruited to the ER membrane by binding to the ER membrane protein Ubx2 and by binding to the ubiquitin chain of the ERAD clients. **6.** Cdc48 pulls the polypeptide substrate out of the membrane using the energy from ATP hydrolysis. The extracted ERAD substarte is processed by a series of enzymes, including a DUB to trim the ubiquitin chain. **7.** The substrate is delivered to the 26S proteasome with the help of ubiquitin receptors and degraded. The figure was adapted from Wu and Rapoport (2018).

1.3 Heavy metal-associated isoprenylated plant proteins

Based on a genome-wide yeast two-hybrid (Y2H) screen with the CKX1 protein as bait, which has previously been performed in the Dr. Werner's group, a group of positive CKX-interacting proteins, which belongs to the plant-unique heavy metal associated isoprenylated plant protein (HIPP) family, were identified. HIPP proteins are characterized by the presence of one or two heavy metal binding (HMA) domains and a lipid modification site, isoprenylation motif, at the protein C terminus. In addition, most HIPPs contain glycine- and proline-rich regions between these domains (Barth et al., 2009; Tehseen et al., 2010; de Abreu-Neto et al., 2013). 45 HIPPs and additional 22 HMA-containing proteins (HPP) lacking the isoprenylation site have been identified in Arabidopsis (Fig. 6) (Barth et al., 2009; Tehseen et al., 2010; de Abreu-Neto et al., 2013). Based on the sequence homologies all HIPP and HPP proteins are divided into seven distinct phylogenetic clusters (I-VII) (Tehseen et al., 2010). HIPP proteins of cluster I are the only members containing two conserved HMA domains.

Limited experimental data to deduce the biological function of HIPP proteins are currently available. Because of the occurrence of HMA domain, HIPPs have been previously discussed as metallochaperones that act mainly in heavy metal homeostasis and detoxification (Suzuki et al., 2002; Chandran et al., 2008; Gao et al., 2009; Tehseen et al., 2010). Recent studies have shown that HIPPs may interacting with other proteins and facilitate thereby, for example, transcriptional responses to biotic and abiotic stresses (Barth et al., 2009; Cowan et al., 2018).

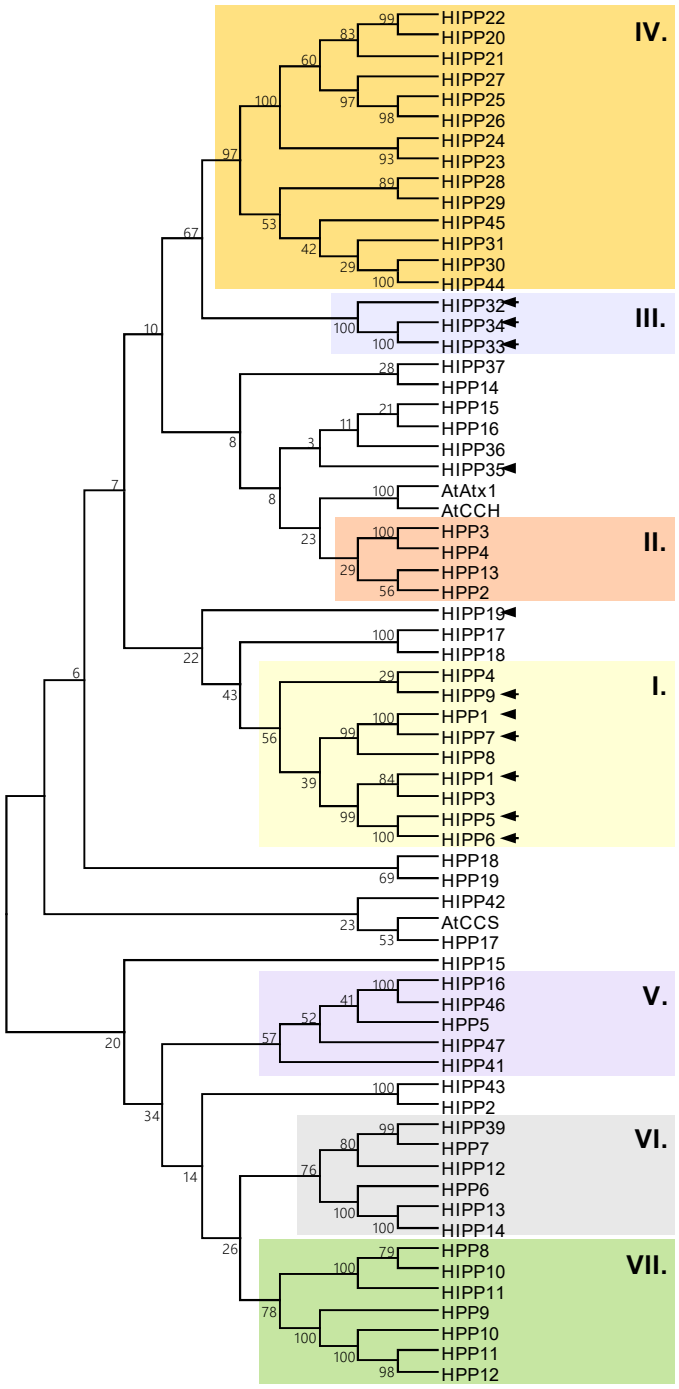

Figure 6. Phylogenetic tree of HIPP and HPP proteins in Arabidopsis. (Figure from Dr. Werner's group unpublished data).

The nomenclature of HIPP and HPP proteins and the numbering of phylogenetic groups was adopted from Tehseen et al., (2010). Full-length amino acid sequences were retrieved from The Arabidopsis Information Resource (TAIR; http://www.arabidopsis.org/). HIPP41 corresponds to AT1G55790.2 according to the TAIR10 genome annotation. A neighbor-joining tree was constructed using MEGA4 (Tamura et al., 2007) with 1000 bootstrap replicates. Arrows and arrowheads indicate proteins interacting and noninteracting with CKX1 in Y2H assays, respectively.

1.3.1 Function of HMA domain

Intensive studies on heavy metal-associated (HMA) domain containing proteins had previously mainly focused on the copper-binding capacity of the HMA domain, suggesting a function of these protein in heavy metal transport and heavy metal homeostasis (Huffman and O'Halloran, 2001). HMA domains are found in bacteria, yeast, animal and plants, and are characterized by a ferredoxin-like structural fold containing the conserved M/LXCXXC heavy metal binding sequence. Several well characterized HMA-containing proteins play an important role in regulating cellular heavy metal homeostasis. They function as metallochaperones, which tightly bind metallic ions (including copper, nickel and zinc), to prevent their toxic effect and transport them to specific cellular sites for sequestration or to target proteins requiring metal ions either as a structural component or as a catalytic factor (Wernimont et al., 2000; Rubino and Franz, 2012). It has been shown that HMA domains often mediate the protein-protein interactions between metallochaperone and the cognate target protein. For instance, the interaction between the copper chaperone Atx1 and the Ccc2 ATPase are mediated by the transition of copper. And the Cys residues of the HMA domain are essential for the transfer of copper (Arnesano et al., 2001; Banci et al., 2006). In plants, a HMA domain-containing protein NaKR1 (HPP2) has been shown to interact with FLOWERING LOCUT T (FT) *in vitro* and *in vivo*. Interestingly, a truncated protein containing only the HMA domain of NaKR1 was sufficient for interacting with FT, implying that HMA domain mediates the interaction (Zhu et al., 2016). Similarly, the interaction of HIPP26 with the zinc finger homeodomain transcription factor ATHB29 was abolished by mutation of Cys residues in the HMA domain of HIPP26 (Barth et al. 2009). In contrast, the recently reported interaction between HIPP26 homologue from *Nicotiana benthamiana* and the potato mop-top virus movement protein TGB1 was not mediated by the HMA domain (Cowan et al. 2018).

1.3.2 Protein prenylation

Protein isoprenylation (prenylation) is one of the post-translational lipid modifications, which are required for regulatory molecules to directly interact with the hydrophobic core of membranes or with other proteins (Hemsley, 2015). Protein prenylation is conserved among eukaryotes and involves the process by which proteins bearing a C-terminal CaaX motif (where C = Cys, a = aliphatic amino acid reside, and X = Met, Ala, Gln, Ser, or Cys) are posttranslationally modified by the covalent attachment of either a 15-carbon farnesyl or a 20-carbon geranylgeranyl isoprenoid via a thioether bond (Fig. 7) (Galichet and Gruissem, 2003; Crowell and Huizinga, 2009). Three distinct heterodimeric protein isoprenyltransferases mediate protein prenylation in fungi, animals and plants (Casey and Seabra, 1996;

Maurer-Stroh et al., 2003; McTaggart, 2006). Protein farnesyltransferase (PFT) and protein geranylgeranyltransferase type I (PGGTI) are soluble enzymes that are localized in the cytoplasm. They share a common α-subunit but have distantly related β-subunits. PFT transfers a farnesyl group from farnesyl diphosphate (FPP) to the cysteine residue of a carboxyl terminal CaaX motif, whereas PGGT I usually transfers a geranylgeranyl group to the cysteine residue of a similar CaaX motif (where 'X' is leucine or isoleucine). Protein geranylgeranyltransferase type II (PGGT II, also called RAB geranylgeranyltransferase) transfers two geranylgeranyl groups to the cysteine residues of XCCXX, XXCXC, XXCCX, XXXCC, XCXXX, or CCXXX motifs at the carboxyl terminus of RAB proteins bound to the RAB Escort Protein (REP) (Casey and Seabra, 1996; Maurer-Stroh et al., 2003; McTaggart, 2006).

Prenylated proteins undergo two additional posttranslational modifications collectively referred to as CaaX processing (Young et al., 2001). This involves cleavage of the carboxy-terminal three amino acids 'aaX' catalyzed by STE24 and RCE1 endoproteases (Boyartchuk et al., 1997; Young et al., 2001), and methylation of the free carboxyl group of the isoprenyl cysteine by an isoprenylcysteine methyltransferase (ICMT) (Fig. 7) (Young et al., 2001). Arabidopsis contains single STE24 and RCE1 and two ICMT homologs, which are localized in the endoplasmic reticulum membranes (Bracha-Drori et al., 2008). The CaaX processing not only increase the affinity of the prenylation protein for membranes, but also protect them from degradation, and facilitate their functional interactions with other proteins (Hancock et al., 1991; Michaelson et al., 2005). The fully processed prenylated proteins are then trafficked to their appropriate cellular location, which is often the endomembrane system, through mechanisms that are still poorly understood (Winter-Vann and Casey, 2005).

Protein prenylation appears to serve as a membrane anchor and, in some cases, mediate protein-protein interactions, which are important for correct hormone signal transduction, cell division and immune responses in plants (Turnbull and Hemsley, 2017). For example, the cytokinin biosynthesis enzyme IPT3 is farnesylated. The farnesylation directed the location of IPT3 in the cytoplasm and nuclei, whereas the non-farnesylated form was located in plastids (Galichet et al., 2008). Interestingly, the different subcellular localization of the farnesylated and nonfarnesylated protein was associated with either iP- or Z-type cytokinin biosynthesis (Galichet et al., 2008). The plant protein Rho-related GTPase ROP6 is prenylated, which determine its membrane localization (Sorek et al., 2007).

Prenylation is a weak membrane anchor that usually serves as a primary signal that targets prenylated protein to the membrane, where a second signal, such as S-acylation, is added to the protein for a stable membrane attachment (Hemsley, 2015). S-acylation is another lipid modification, which involves the addition of saturated fatty acids to Cys residues of proteins through thioester bonds (Li and Qi, 2017). In the case of ROP6, the protein is not only

prenylated, which provide a signal for membrane anchoring, but also S-acylated, which is required for active ROP function (Sorek et al., 2007). Similar double-lipid modification responsible for a stable attachment to the plasma membrane has been recently reported for the NbHIPP26 protein (Cowan et al. 2018).

Protein prenylation has also been found to be important for mediating protein-protein interactions. This is more evidenced in yeast and mammals. For instance, deletion of the CaaX motif or substitution of the Cys residue within the CaaX motif to Ser of a prenyled protein RPGR in mammalian cells completely abolished the interaction with its partner protein (Lee and Seo, 2015). In plants, RhoGDI proteins are reported to bind the prenyl group of inactive ROPs to shuttle the ROP proteins between membrane and cytosolic compartment (Bischoff et al., 2000).

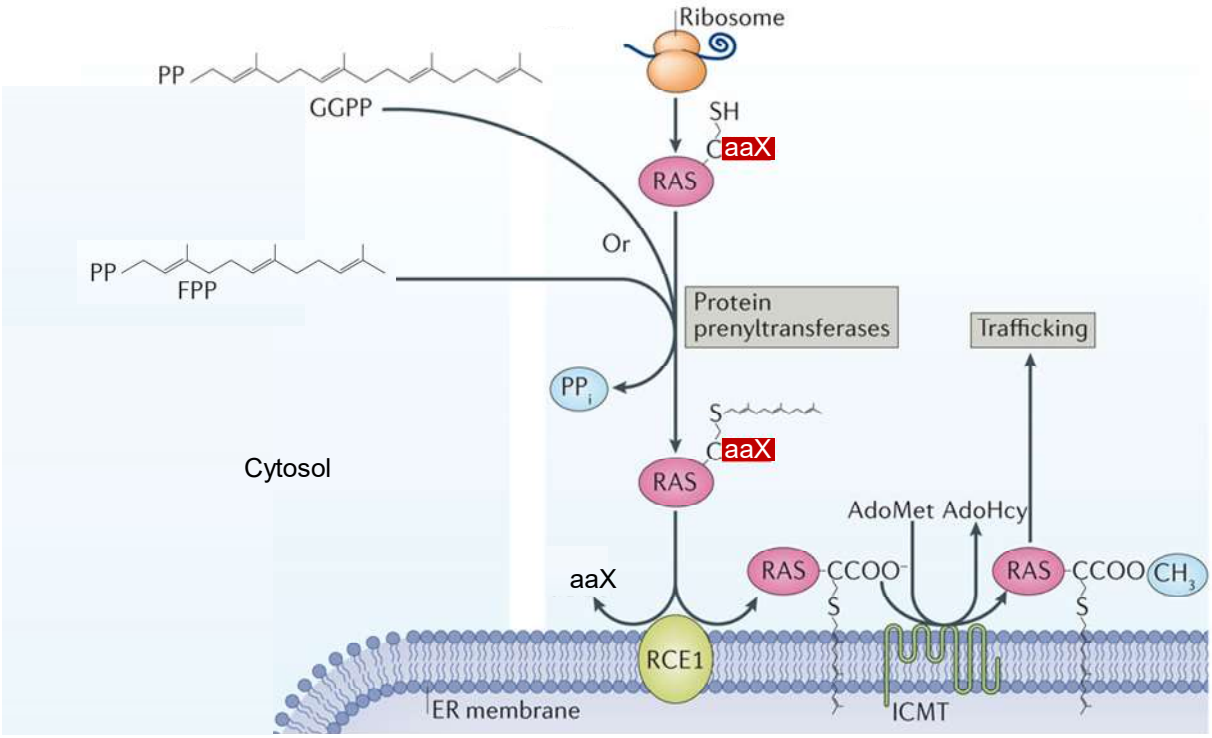

Figure 7. Overview of the protein prenylation pathway.
Proteins that contain a carboxy-terminal CaaX motif are initially modified by the cytosolic protein prenyltransferases farnesyltransferase (PFT) or geranylgeranyltransferase I (PGGT I), which add a 15-carbon farnesyl or a 20-carbon geranylgeranyl, respectively, to the Cys residue of the CaaX motif of the substrate proteins such as RAS. Following prenylation, the CaaX protein travels to the cytosolic surface of the ER, where the three C-terminal amino acids (aaX) are proteolytically cleaved by Ras-converting CaaX endopeptidase (RCE1) resulting in the prenylcysteine is exposed at the C terminus. The newly exposed Cys residue is then carboxyl methylated by isoprenylcysteine methyltransferase (ICMT), which is also an intrinsic ER membrane protein. The fully processed prenylated proteins are directed to their final destinations, which are often the endomembrane system. AdoHcy, S-adenosyl-L-homocysteine; AdoMet, S-adenosyl methionine; FPP, farnesyl diphosphate; GGPP, geranylgeranyl diphosphate. The figure has been adapted from Wang and Casey (2016).

1.3.3 Biological function of HIPP proteins

HIPP proteins have been previously mainly discussed as functioning in heavy metal homeostasis and detoxification, because of the capability of the HMA domain to bind and distribute metal ions (Dykema et al., 1999; Suzuki et al., 2002; Gao et al., 2009; Tehseen et al., 2010). For instance, Arabidopsis plants overexpressing *CdI19*/*HIPP6* gene has been shown more tolerant to Cd stress than WT plants (Suzuki et al., 2002). Similarly, overexpression of the *HIPP26* gene from cluster IV confers Cd tolerance in transgenic Arabidopsis plants, whereas mutation of the three genes (*HIPP20*, *HIPP21* and *HIPP22*) from the same cluster increases the plants sensitive to Cd, suggesting the role of HIPPs in Cd detoxification (Gao et al., 2009; Tehseen et al., 2010). Recently, several studies have shown that HIPP proteins are involved in plant adaptation to biotic and abiotic stresses (Barth et al., 2009; de Abreu-Neto et al., 2013; Zhang et al., 2015; Imran et al., 2016; Cowan et al., 2018; Radakovic et al., 2018). For example, the expression of a wheat *HIPP* gene (*TaHIPP1*) is shown to be induced by exogenous ABA application and wounding (Zhang et al., 2015). Similarly, overexpression of one clade-I *HIPP* gene (*HIPP3*) affected expression of genes involved in pathogen responses, and in abiotic stress responses (Zschiesche et al., 2015). Moreover, the expression of *AtHMAD1* (*HIPP40*) is significantly increased when exposed to nitrosative-mediated stress conditions, and the *athmad1* knock-out is more resistant to virulent *Pseudomonas syringae* (DC3000) (Imran et al. 2016). Although all these studies indicate a role of HIPP proteins in plant responses to biotic and abiotic stresses, the mechanisms underlying their functioning in these biological processes, are unknown.

1.4 Research objectives and work flow

The aim of the present work was to elucidate the biological function of the CKX-interacting HIPP proteins. Recent studies have shown that most of the CKX proteins in Arabidopsis are secretory proteins, and the steady-state levels of these proteins are controlled by the ER protein quality control system, which significantly impacts on the cytokinin responses in Arabidopsis. However, the molecular mechanisms underlying the regulation of CKX proteins are largely unknown. Yeast two-hybrid (Y2H) screen with CKX1 proteins as bait, which has previously been performed in the Dr. Werner's group, identified several CKX-interacting candidate proteins which could be a key component involved in the regulation of CKX proteins. The proteins analyzed in this work belong to a largely uncharacterized family of plant-specific heavy metal-associated isoprenylated plant proteins (HIPPs). Selected group of HIPP proteins belonging to a phylogenetic cluster I were specifically addressed.

In order to study the feature of the CKX-HIPP interaction and to understand the mechanism behind it, the full-length cDNA encoding several HIPP and CKX proteins were cloned, respectively, and the interactions between CKX and HIPP proteins were tested in independent interaction assays. HIPP protein variants with mutations in distinct functional motifs were also tested for their requirement for the protein-protein interactions. Previous studies have demonstrated that most of the Arabidopsis CKX proteins are localized to various compartments of the secretory pathway, including the ER. To gain insight into cellular mechanism underlying the CKX-HIPP interaction, the subcellular localizations of individual HIPP proteins and CKX-HIPP interacting complexes were investigated. In addition, the potential protein-protein interactions among the isolated HIPP proteins were tested.

The second part of this work aimed to explore the physiological function of the isolated HIPP proteins. Therefore, the phenotypes of *HIPP* gain- and loss-of-function plants were isolated and studied in details, with particular emphasis on changes in responses to cytokinin and other phytohormones. To gain further information about the biological function of the individual *HIPP* genes in cluster I, their expression patterns were studied.

Last but not least, several HIPP proteins have been shown to be involved in plant adaptation to biotic and abiotic stresses. Therefore, it was addressed whether the analyzed cluster I-HIPP proteins play a role in stress responses. For that, the endogenous levels of the classic stress hormones ABA and SA were determined and the behaviors of the isolated *HIPP* gain- and loss-of-function plants were investigated under drought stress.

2 Materials and Methods

2.1 Chemicals and consumables

Standard chemicals and consumables were purchased from AppliChem (Darmstadt, DE), Bioline (London, UK), Bio-Rad (Munich, DE), ChromoTek (Planegg-Martinsried, DE), Clontech (California, US), Fluka (Buchs, CH), Invitrogen/Thermo Fisher Scientific (Waltham, US), Macherey-Nagel (Düren, DE), Merck (Darmstadt, DE), OlchemIm (Olomouc, CZ), Qiagen (Hilden, DE), Roche (Mannheim, DE), Roth (Karlsruhe, DE), Sarstedt (Nümbrecht-Rommelsdorf, DE) and Sigma Aldrich (Steinheim, DE). The chemicals for culture media were from Becton Dickinson (Sparks, US) and Duchefa Biochemie (Haarlem, NL).

2.2 Enzymes, kits, DNA and protein ladders

The enzymes, kits, DNA and protein ladders that were used in this study are listed in Table 1.

Table 1: Enzymes, kits and DNA ladders.

Name	Manufacturer
Restriction enzymes	Thermo Fisher Scientific, Waltham, US
DNase I	Thermo Fisher Scientific, Waltham, US
Immolase DNA Polymerase	Bioline, Luckenwalde, DE
Phusion High-Fidelity DNA Polymerase	Thermo Fisher Scientific, Waltham, US
SuperScript® III Reverse Transcriptase	Invitrogen/Thermo Fisher Scientific, Waltham, US
Taq DNA Polymerase	AG Schuster, FU Berlin, DE
NucleoSpin RNA Plant	Macherey-Nagel, Düren, DE
Gateway® BP Clonase™ enzyme mix	Invitrogen/Thermo Fisher Scientific, Waltham, US
Gateway® LR Clonase™ enzyme mix	Invitrogen/Thermo Fisher Scientific, Waltham, US
Pierce™ BCA Protein Assay Kit	Pierce Biotechnology, Rockford, US
QIAGEN Plasmid Mini Kit	Qiagen, Hilden, DE
Wizard® SV Gel and PCR Clean-Up System	Promega, Mannheim, DE
HyperLadder™ I	Bioline, Luckenwalde, DE
P405	MBBL, Bielefeld, DE
PageRuler™ Prestained Protein Ladder (10-180kDa)	Thermo Fisher Scientific, Waltham, US

2.3 Cloning vectors

The cloning vectors used and generated in this work are listed in Table 2.

Table 2: Plasmids list.

Plasmid names	Selection markers in Bacteria	Selection markers in Plants	References
pCB302	Kan^R	$Basta^R$	Xiang et al., 1999
pCB308	Kan^R	$Basta^R$	Xiang et al., 1999
pDONR221	Kan^R	-	Invitrogen/Thermo Fisher Scientific, Waltham, US
pB2GW7	$Spec^R$	$Basta^R$	Karimi et al., 2002
pK7WGF2	$Spec^R$	Kan^R	Karimi et al., 2002
pB7WGF2	$Spec^R$	$Basta^R$	Karimi et al., 2002
pB7WGFUBQ102	$Spec^R$	$Basta^R$	This study
pGWB18	Kan^R, Hyg^R	Kan^R, Hyg^R	Nakagawa et al., 2007
pACT2-GW	Amp^R	-	pACT2 Clonetech®, mofidied by Dortay et al. 2006
pACT2-GW-empty	Amp^R	-	pACT2 Clonetech®, mofidied by Dortay et al. 2006
pBTM116-D9-GW	Amp^R	-	Goehler et al., 2004; Dortay et al., 2006
pBTM116-D9-GW-empty	Amp^R		Goehler et al. 2004, modified by Dortay et al., 2006
pDOE-08	Kan^R	$Basta^R$	Gookin and Assmann, 2014
pDOE-08-CKX1	Kan^R	$Basta^R$	Niemann et al., 2018
pRS300	Amp^R	-	Ossowski et al., 2008
pJet	Amp^R	-	Invitrogen/Thermo Fisher Scientific, Waltham, US

2.4 Yeast and bacteria strains

The yeast and bacteria strains used in this work are listed in Table 3.

Table 3: Yeast and bacteria strains.

Organism	Strain	Genetic marker	Reference
Saccharomyces cerevisiae	L40ccua	*MATa his3Δ200 trp1-901 leu2-3, 112 LYS::(lexAop)4-HIS3 URA3::(lexAop)8-lacZ ADE2::(lexAop)8- URA3 GAL4 gal80 can1 cyh2*	Goehler et al., 2004
Escherichia coli	*DH5α*	F- *endAI hsdRJ7* (rk^-, mk^+) *supE44 thi-J λ⁻ recAI gyrA96 relAI deoRΔ(lacZYA-argF)* U169 *Φ*80d*lacZ*ΔM15	Grant et al., 1990
Escherichia coli	*DH3.1*	F- *gyrA462 endA1 glnV44 Δ(sr1-recA) mcrB mrr hsdS20*(rB -, mB-) *ara14 galK2 lacY1 proA2 rpsL20(Smr) xyl5 Δleu mtl1*	Bernard and Couturier, 1992
Agrobacterium tumefaciens	GV3101:pMP90	Rif^R, $Gent^R$	Koncz and Schell, 1986

2.5 Antibiotics, herbicides and amino acids

The antibiotics, herbicides and amino acids used in this study are listed in Table 4.

Table 4: Antibiotics and herbicides used in this study.

Antibiotic/herbicide	Stock solution	Final concentration in medium
Carbenicillin	50 mg/ml in ddH_2O	50 mg/L
Gentamicin	25 mg/ml in ddH_2O	25 mg/L
Hygromycin B	50 mg/ml in HEPES	50 mg/L
Kanamycin	50 mg/ml in ddH_2O	50 mg/L
Phosphinothricin	10 mg/ml in ddH_2O	10 mg/L
Rifampicin	50 mg/ml in DMSO	50 mg/L
Spectinomycin	50 mg/ml in ddH_2O	50 mg/L
BASTA	-	0.1%
Amino acid	**Stock solution**	**Final concentration in medium**
L-Histidine HCl (His)	2 mg/ml in ddH_2O	20 mg/L
L-Leucine (Leu)	10 mg/ml in ddH_2O	100 mg/L
L-Tryptophane (Trp)	2 mg/ml in ddH_2O	20 mg/L
Uracil (pH 8) (Ura)	2 mg/ml in ddH_2O	20 mg/L

2.6 Plants

In the present study *Nicotiana benthamiana* (*N. benthamiana*) WT plants were used for transient protein expression and if not stated otherwise *Arabidopsis thaliana* ecotype Columbia-0 (Col-0) plants were used as wild type (WT) in all other plant experiments. Table 5 lists all transgenic and mutant Arabidopsis plants used throughout this work.

Table 5: Transgenic and mutant Arabidopsis plants.

Name	References	Source[1)]/Comments
Transgenic Arabidopsis plants		
35S:HIPP6 *35S:HIPP7*	This study	Created by Dr. Henriette Weber, FU Berlin[2)]
UBQ10:HIPP1	This study	--
UBQ10:HIPP7 *UBQ10:HIPP7^{hma}* *UBQ10:HIPP7^{C352G}*	This study	--
pHIPP1S:GUS *pHIPP1L:GUS* *pHIPP5:GUS* *pHIPP6S:GUS* *pHIPP6L:GUS* *pHIPP7:GUS*	This study	--
rock4	Bartrina, 2006; Jensen, 2013	Dr. Isabel Bartrina, FU Berlin
35S:ARR15	Ren et al., 2009	Prof. Dr. Jianru Zuo, Chinese Academy of Sciences (China)

TCSn:GFP	Zürcher et al., 2013	Dr. Bruno Müller, University of Zürich (Switzerland)
ATML1:CKX1-myc	Werner, 2016	Dr. Sören Werner, FU Berlin
pARR5:GUS	D'Agostino et al., 2000	Prof. Dr. Joe Kieber, University of North Carolina (Chapel Hill, USA)
amiRNA-Tri	This study	--
amiRNA-Mul		
Insertion mutant Arabidopsis plants		
hipp1-1, SALK_028133C	This study	N659265
hipp3-1, SALK_021602C		N665488
hipp5-1, SALK_004387		N504387
hipp5-2, SALK_069207		N569207
hipp6-1, SALK_111020C		N656867
hipp7-1, SALK_091924C		N663322
hipp8-1, SM_3_25599	This study	N113215
hipp9-1, SM_3_30660		N117371
hipp3,5	This study	Derived from crosses between *hipp* single mutants
hipp3,6		
hipp3,8		
hipp5,6		
hipp5,7		
hipp6,7		
hipp6,8		
hipp5,6,7	This study	Derived from crosses between *hipp5,6* and *hipp6,7*

1) NASC ID if ordered from The Nottingham Arabidopsis Stock Centre or seeds kindly provided by the indicated researcher.
2) The selection of *35S:HIPP7* homozygous plants were conducted by Dr. Henriette Weber, FU Berlin. The selection of *35S:HIPP6* homozygous plants and the characterization of both *35S:HIPP6* and *35S:HIPP7* transgenic plants were conducted by myself (see also 3.2).

2.7 Growth conditions

If not stated otherwise all described media were autoclaved at 1 bar for 20 min at 120°C. Appropriate antibiotics, amino acids or hormones were added to media after autoclaving, and heat instable components were sterile filtrated before use.

2.7.1 Bacteria and yeast growth conditions

The microbiological cultures were grown under standard conditions as described (Bertani, 1951; Rose et al., 1990; Sambrook and Russell, 2001). *E. coli* and *A. tumefaciens* strains were grown in liquid or on solid Luria Broth (LB) media (10 g/L tryptone, 5 g/L yeast extract, 5 g/L NaCl and 15 g/L agar for solid LB-medium, pH 7.5) (Bertani, 1951) containing the

appropriate antibiotics (Table 4). Liquid YEBS medium (1 g/L yeast extract, 5 g/L beef extract, 5 g/L sucrose, 5 g/L bacto-peptone, 0.5 g/L $MgSO_4$, pH 7.0) was used for the propagation of *A. tumefaciens* cells which were used for plant transformation (Davis et al., 2009). *E. coli* strains were grown overnight at 37°C and *A. tumefaciens* at 28°C for 2-3 days.

S. cerevisiae was grown at 30°C in liquid or on solid YPD medium (10 g/L yeast extract, 20 g/L peptone and 15 g/L agar for solid medium, pH 6.5) with 50 ml/L 40% glucose added after autoclaving or minimal SD medium (6.7 g/L YNB, yeast nitrogen base without amino acids, and 15 g/L agar for solid medium, pH 5.8) with 50 ml/L 40% glucose added after autoclavation (Rose et al., 1990). The appropriate amino acids were added to SD medium for plasmid selection and different concentrations of 3-amino-1,2,4-triazole (3-AT, a competitive inhibitor of the product of the *HIS3* gene) were added to SD medium for autoactivation tests. Liquid cultures were grown while shaking with 200 rpm (*E. coli*), 160 rpm (*A. tumefaciens*) or 150 rpm (*S. cerevisiae*) at the respective temperatures. The selection medium used for *S. cerevisiae* was listed in Table 6.

Table 6: Selection medium used for *S. cerevisiae*.

Plasmid	Selection medium	Amino acid
pACT2-GW	SDI-L	His, Ura, Trp
pBTM116-D9-GW	SDI-T	His, Ura, Leu
pACT2-GW/pBTM116-D9-GW	SDII	His, Ura
	SDIV	--

2.7.2 Plant growth conditions

2.7.2.1 *In vitro* culture

For growth of Arabidopsis seedlings under sterile conditions, seeds were surface-sterilized by soaking and shaking for 5 min in 70% ethanol with the addition of 0.01% (v/v) Triton X-100. Afterwards, seeds were rinsed three times with 70% ethanol under a clean bench and finally transferred by pipetting for drying to a sterile filter paper. The dried seeds were transferred onto solid Murashige and Skoog (MS) medium (4.3 g/L MS basal salt mixture, 0.5 g/L MES, 30 g/L sucrose and 10 g/L agar for solid medium, pH 5.7) (Murashige and Skoog, 1962). After stratification (4°C) for two days, plants were transferred to a climate chamber and cultivated under long day (LD) conditions (light/dark: 16 h/8 h) at 21°C and light intensities of 110-140 µmol m^{-2} s^{-1}.

2.7.2.2 Growth on soil

Arabidopsis seeds were sown on thoroughly watered “sowing soil” (2:2:1, Soil Type P:Soil Type T:Sand). After stratification (4°C) for three days, plants were transferred to a greenhouse or a climate chamber. For the first 2-3 days the plant trays were covered with a clear plastic dome to protect seeds and germinating seedlings from desiccation. Twelve days after germination, plantlets were singled out onto soil containing Perligran G instead of sand. If not otherwise specified, plants were grown under ILD conditions at 20-22°C and light intensities of 130-160 µE m^{-2} s^{-1}.
N. benthamiana was grown at 24°C under 14 h light/10 h dark conditions.

2.8 Genetic crosses

To perform genetic crosses, parental plants were grown until they reached the stage of flowering. Two to three flower buds from one parent were selected in which the tips of the petals were barely visible and before the anthers began to release pollen. Siliques, open flowers as well as flower buds which were not used for crosses were removed. Afterwards, a selected flower bud was opened with a small pair of precision clamping tweezers and emasculated by removing all stamens. Anthers of a newly opened flower from the second parent were used to fertilize the receptive gynoeceum by brushing the anthers over the bare stigma of the female parent. Crosses were successful when siliques started elongating after 2-3 days. Finally, seeds from the developed siliques were harvested and used for propagation. The progeny (F2) of the heterozygous F1 plants were used for genotyping.

2.9 Transformation techniques

2.9.1 Bacteria transformation

For transformation of plasmid DNA to *E. coli* cells, chemical competent cells were used. For heat shock transformation, tube containing 100 µl chemically competent *E. coli* cells was thawed on ice for 5 min and 1 µl plasmid DNA (approximately 50-200 ng) was added and thoroughly mixed. The cell suspension was incubated on ice for 30 min, then incubated at 42°C in a water bath for exactly 45 s and immediately transferred on ice for 2 min. 400 µl of SOC medium (20 g/L tryptone, 5 g/L yeast extract, 500 mg/L NaCl, 2.5 mM KCl, 10 mM $MgSO_4$, 10 mM $MgCl_2$, 20 mM glucose, pH 7.4) were added and incubated for 60 minutes at 37°C on a shaker. Aliquots of the transformation mix were then plated on LB-agar plates supplemented with the appropriate antibiotics (Table 4) and incubated at 37°C over night.

Transformation of *A. tumefaciens* cells was done by electroporation. 1 µl plasmid DNA (approximately 50-150 ng) was added to tubes containing 50 µl thawed electrocompetent *A. tumefaciens* cells and thoroughly mixed. The transformation mixture was transferred into a pre-chilled electroporation cuvette and an electric pulse (200 Ω, 1.8 kV, 2.5 to 5 ms) was applied by using the Genepulser II (Bio-Rad, Munich, DE). Immediately 950 µl of SOC medium was added to the transformation. The mixture was transferred into a 1.5 ml reaction tube, incubated at 28°C on a shaker for 2 h, plated on selection medium and incubated at 28°C for two days.

2.9.2 Yeast transformation

Yeast transformation was performed according to the protocol from Gietz and Woods (2002) with minor modifications: The yeast strain was inoculated in 4 ml YPD medium, incubated overnight at 30°C on a shaker, and the freshly grown 4 ml *S. cerevisiae* culture was used to adjust 50 ml YPD medium to an OD_{600} of 0.3. This starting culture was incubated on a shaker at 30°C until reaching an OD_{600} of 0.6–0.9. Cells were centrifuged at 2.000 rpm for 5 min at room temperature (RT). The pellet was resuspended by pivoting in 10-15 ml freshly made Mix 1 solution (0.1 M LiAc, 1 M sorbitol, 0.5 mM EDTA and 5 mM Tris/HCl pH 7.5) and centrifuged again 5 min with 2.000 rpm at RT. The pellet was resuspended in 1 ml Mix 1 and incubated at RT for 10 min. In a 2 ml reaction tube, 1 µg plasmid-DNA, 15 µl (10 µg/µl) salmon sperm DNA, 700 µl Mix 2 solution (0.1 M LiAc, 40% PEG 3350, 1 mM EDTA and 10 mM Tris/HCl pH 7.5) and 100 µl of the in Mix 1 resuspended cells were mixed by vortexing. The transformations were incubated at 30°C for 30 min. After incubation, 30 µl DMSO were added, mixed by vortexing and heat shock transformation was conducted in a water bath at 42°C for 15-30 min. The transformed cell suspension was centrifuged for 3 min with 4.000 rpm at RT, and resuspended in 200 µl ddH_2O, plated on SD media lacking the appropriate amino acid and incubated for 3 days at 30°C.

2.9.3 Stable transformation of *Arabidopsis thaliana*

Plasmids were transformed into Arabidopsis plants by the floral dip method according to the protocol from Clough and Bent (1998) with minor modifications. A single colony of *A. tumefaciens* bearing the desired binary vector was inoculated into 4 ml of LB medium containing selective antibiotics and grown as starting culture at 28°C for two days. 1 ml of this culture was then added into 250 ml LB selection media and grown for another 24 h at 28°C. Bacteria were centrifuged at 5,500 × g for 20 min at RT and resuspended in 250 ml infiltration medium (50 g/L sucrose, 2.19 g/L MS salts, 50 µl/L Silwet 77). Inflorescences of

four-week-old plants were dipped into the *A. tumefaciens* suspension for 30 seconds, under gentle agitation. Dipped plants were then sealed in a plastic bag for 24 hours to maintain high humidity and then transferred to the greenhouse. Transformants were selected using appropriate antibiotics or herbicides (Table 4).

2.9.4 Transient expression in *N. benthamiana*

Plasmids were transiently expressed in *N. benthamiana* epidermal cells following the method described by Sparkes et al., (2006) using *A. tumefaciens* and 6-weeks-old *N. benthamiana* plants. For co-expression, the *Agrobacterium* cultures harbouring different expression constructs were mixed in infiltration medium to a final OD_{600} of 0.1 for each sample. *35S:p19* (Voinnet et al., 2003) was included in all infiltrations.

2.10 Nucleic acid methods

2.10.1 Nucleic acid extraction methods

2.10.1.1 Extraction of plasmid DNA from bacteria

The plasmid DNA from bacteria was isolated by the QIAGEN Plasmid Mini Kit from Qiagen (Hilden, DE), according to the manufacturer's instructions.

2.10.1.2 Extraction of genomic DNA from Arabidopsis

Genomic DNA was isolated from Arabidopsis by the CTAB method according to the protocol from Weigel and Glazebrook (2002), if DNA was used for PCR amplification and construct cloning.
A "quick prep" method was used, if the genomic DNA was used for genotyping. One or two younger leaves were shredded in 400 µl extraction buffer (250 mM NaCl, 25 mM EDTA, 200 mM Tris/HCl pH 7.5) using a Retsch mill (Retsch, Haan, DE). 20 µl of 5% SDS was added, mixed and plant material centrifuged at 13.000 rpm for 3 min at RT. The supernatant was transferred into a new reaction tube and one volume of isopropyl alcohol was added, thoroughly mixed, incubated at RT for 2 min and centrifuged at 10.000 rpm for 5 min at RT. The pellet was washed with 70% ethanol, air dried and resuspended in 100 µl ddH_2O.

2.10.1.3 Extraction and purification of total RNA from Arabidopsis

Arabidopsis plant material for the extraction of total RNA was shock frozen in liquid nitrogen in 2 ml tubes containing two steel beads and homogenized in pre-cooled (liquid nitrogen) adapters using a Retsch mill (Retsch, Haan, DE). Total RNA was extracted from tissues using the NucleoSpin RNA Plant Kit (Macherey-Nagel, Düren, DE) according to the manufacturer's protocol, including an on-column DNase (Table 1) digestion.
In order to check the quality and quantity of the isolated RNA, the RNA samples were measured photometrically using the NanoDrop ND-1000 spectrophotometer (PeqLab, Erlangen, DE) with the RNA-40 program. The RNA was considered clean if the ratios of 260/280 and 260/230 were both >2.

2.10.2 Polymerase chain reactions (PCR)

2.10.2.1 Standard polymerase chain reaction (PCR)

Standard polymerase chain reaction (PCR) (Mullis and Faloona, 1987) was performed for validation of bacterial or yeast clones and genotyping plants by using the heat resistant *Taq* polymerase and 10x *Taq* PCR buffer (160 mM $(NH4)_2SO_4$, 0.1% (v/v) Tween 20, 20 mM $MgCl_2$, 670 mM Tris/HCl pH 8.8). For the amplification of DNA used for cloning, the Phusion high-fidelity DNA polymerase (Thermo Fisher Scientific, Waltham, US) with proofreading-function (3´→5´ exonuclease) was used according to manufacturer's instructions. The compositions of the PCR reaction mixtures are shown in Table 7.

Table 7: PCR reaction mixtures.

Component	Volume for *Taq* PCR	Volume for Phusion PCR
Buffer	2 µl (10x Taq buffer)	4 µl (5x Phusion HF buffer)
5 mM dNTPs	0.5 µl	0.4 µl
10 µM forward primer	1 µl	0.5 µl
10 µM reverse primer	1 µl	0.5 µl
Polymerase	0.5 µl (1 U/µl)	0.2 µl (2 U/µl)
DNA/cDNA[1)]	x µl	x µl
ddH_2O	ad 20 µl	ad 20 µl

1) For genotyping bacteria or yeast, a single colony was picked with a pipette tip and stirred in the PCR reaction mixture. For genotyping plants or amplification of promoters used for cloning, 1 µl DNA (50–100 ng) was used as template. For amplification of genes used for cloning, 10 µl cDNA (50 ng) was used as template.

Programs used for PCR were dependent on the enzyme and the length of the amplification product and the annealing temperature of primers (Table 8). Primers used for PCRs can be found in the respective chapters.

Table 8: PCR programs.

PCR step	Program for *Taq* PCR	Program for Phusion PCR
Initial denaturation step	95°C, 2 min	98°C, 1 min
Denaturation	95°C, 30 sec	98°C, 10 sec
Primer annealing[1)]	x°C, 30 sec	x°C, 30 sec
Elongation	72°C, 1 kb/min	72°C, 2 kb/min
Final elongation	72°C, twice as long as the amplicon, 16°C hold	72°C, 5-10min, 4°C hold

1) The annealing temperature of primers depended on the melting temperature of the primers and was calculated 5°C lower than the averaged melting temperature of forward and reverse primer when used in *Taq* PCR.

2.10.2.2 Reverse transcriptase (RT)-PCR

For cDNA synthesis 1 µg RNA and SuperScript® III Reverse Transcriptase (see Table 1) were used. First, 1 µg RNA was mixed with 2 µl dNTPs (5 mM), 1 µl oligo(dT) primers (50 µM), 1.8 µl random hexamers (50 µM) and ddH_2O added to 14.5 µl and incubated for 5 min at 65°C. Afterwards, the reaction mixture was placed on ice for at least 2 min and 4 µl 5x first strand buffer,1 µl DTT (0.1 M) and 0.5 µl SuperScript® III (200 U/µl) were added. This reaction mixture was incubated for 5 min at 25°C, 60 min at 50°C, and 15 min at 70°C. After cDNA synthesis the cDNA was diluted 1:10 and stored at -20°C.

2.10.2.3 Semi-quantitative RT-PCR

The semi-quantitative RT-PCR was used to determine whether the isolated T-DNA insertion lines are loss-of-function mutants by analyzing transcripts of the respective genes of interest. For semi-quantitative RT-PCR, 10 µl cDNA (50 ng) was used as template. Control reactions were performed by using *Actin7*-specific primers. The sequences of primers (see in 3.3.2) are shown in Table 9.

Table 9: Primer sequences used for RT-PCR.

Name	Forward sequence (5'-3')	Reverse sequence (5'-3')
hipp3-1, SALK_021602C	AAACGCCTTCCATCACCG	ACAACACAAGCATTCGGATTC
hipp5-2, SALK_069207	ATGGGAGAGGTCCAAGAAG	TTACATAACAGAGCAAC
hipp6-1, SALK_111020C	TTCTCCAAACCAGAC	ATCACGAACTTCCAC
hipp7-1, SALK_091924C	GTTGTCTCAAAGGCTTCG	TTACATTACAGTACATGC
hipp9-1, SM_3_30660	TTAGGGGTCCAAACAACTGTG	GATACCAAACACACGTAC
Actin7, (At5G09810)	TACAACGAGCTTCGTGTTGC	TCCACATCTGTTGGAAGGTG

2.10.2.4 Quantitative real-time PCR (qRT-PCR)

Quantitative real-time PCR (qRT-PCR) reactions were performed in an ABI PRISM 7500 sequence detection system (Applied Biosystems/Thermo Fisher Scientific, Waltham, US), using SYBR Green I (Fluka, Buchs, CH) to monitor dsDNA synthesis and Immolase DNA Polymerase (Bioline, Luckenwalde, DE) as hot start enzyme. The reactions were prepared in 20 µL volume containing 10 ng cDNA as template, 0.01 U/µl Immolase DNA-Polymerase, the corresponding 1x buffer, 2 mM $MgCl_2$, 100 µM each dNTP, 0.1x SYBR Green I, 50 nM ROX as internal reference dye (Sigma, Buchs, CH) and 300 nM each primer. For qRT-PCRs, the "FAST" cycling set up of the Applied Biosystems 7500 Software was used. After heat activation of the DNA polymerase (95°C, 15 min), 40 PCR cycles followed comprised of denaturation (95°C, 5 sec), annealing (55°C, 15 sec), and elongation (72°C, 10 sec). Finally, a dissociation curve was generated to analyze the specificity of amplification. Two housekeeping genes (*PP2AA2* and *UBC10*) were used as a control to normalize the relative transcript abundance of each gene of interest according to Vandesompele et al., (2002). All primers used for qRT-PCR are listed in Table 10.

Table 10: Primer sequences for quantitative real-time PCR.

Gene	AGI number	Forward Primer	Reverse Primer
PP2AA2	AT3G25800	CCATTAGATCTTGTCTCTCTGCT	GACAAAACCCGTACCGAG
UBC10	AT5G53300	CCATGGGCTAAATGGAAA	TTCATTTGGTCCTGTCTTCAG
HIPP1	AT2G28090	AGACTCAGACTGTGGTTGCTGTG	TCTTGATGCAACCATCACAAGAG
HIPP3	AT5G60800	AACCGATTCATCATGGGCGAGAA	GGTGATGGAAGGCGTTTCGTTC
HIPP5	AT2G36950	CGGTGGCGATGGTGAATAAGAT	TGCCAATGCATAGGAGCCGTTG
HIPP6	AT5G03380	GAAGAAACCTACCGATGGTG	GGATCTACGTTTCCGATCAC
HIPP7	AT5G63530	GACGGTGAAAGGAGTTTTTG	TCAGGTGGTGGTGGAG
HIPP8	AT3G02960	ACATGCACTGTGAAGGATGTGTT	TCTGGTTCCACCGATTGAATGCC
HIPP9	AT5G24580	GCCTCCACCCTTCATACTC	ATCACCACTTCTTCCACACC
GA3OX1	AT1G15550	CCCAACATCACCTCAACTACTGC	GGCCCATTCAATGTCTTCTTCGC
GA20OX1	AT4G25420	AGATTACTTCTGCGATGCGTTGG	TCTTGATACACCTTCCCAAATGG
GA2OX1	AT1G78440	AACGTTGGTGACTCTCTCCAGGT	AACCCTATGCCTCACGCTCTTG
GA2OX2	AT1G30040	AGATGGAAGTTGGGTCGCTGTC	CCCGTTAGTCATAACCTGAAGAG
TCSn:GFP		ACAACAACAAACAACAAACAACA	GAATTCGGCCGAGGATAATGA
IPT1	AT1G68460	TCACCAAACGAAGACGAAAA	AAGGGAAACGAGTAGCGAGA
IPT3	AT3G63110	ACCATCTCCTCGGCGTCT	CCATTCCACTCTCCACCATC
IPT5	AT5G19040	ATCATAGCCGGTGGTTCCAA	GCAATCGTTGACCAGAGCCT
ARR5	AT3G48100	CTACTCGCAGCTAAAACGC	GCCGAAAGAATCAGGACA
ARR6	AT5G62920	GAGCTCTCCGATGCAAAT	GAAAAAGGCCATAGGGGT
ARR7	AT1G19050	CTTGGAACCAATCTGCTCTC	ATCATCGACGGCAAGAAC

ARR8	AT2G41310	CATCGCCACAAATTCATCAG	GCCGCTGATTCCTTAACTTTC
ARR9	AT3G57040	TCACCAGGTAGTTGAAGTGAATC	TCTCTGAGGACATGATAACTACT
ARR15	AT1G74890	GAGAGGTGGTGAAGCTGAA	GATGGAGTGTCGTCATCAAG
ARR16	AT2G40670	CCTGTAACGTTATGAAGGTGAGT	GACTCCTTCACTTTCTTGAGTAG
CKX1	AT2G41510	GGATTGACCTCATCCTTACG	GAAGAAGGTAATTCTTTTGGGG
TCP4	AT3G15030	CACGACGGTCTCACTCACAA	AATCTAAGTCAAGCTTCAATGTG
TCP5	AT5G60970	TATTCCCGACATACCCTTCG	CTCCATCGACGACATGATGA
TCP10	AT2G31070	CCACGGAGAAGAAGCTACTCA	TCATCATGAATTTGAACCTCCA
TCP12	AT1G68800	AGAAGTTTCTTGGACTAACCAGT	ATTCCTCGGAGTCACCAAAA
TCP14	AT3G47620	TTCAACAAGCTGAACCATCTGT	AATTCGCCGGGATTGTTC
TCP18	AT3G18550	ATCGCGACAACCCTTTCTC	GAAGATGTGTCCATGGATCCTAA

All primer pairs were designed using the Primer-BLAST (https://www.ncbi.nlm.nih.gov/tools/primer-blast/) under the following conditions: optimum Tm at 60 °C, GC content between 20 % and 80 %, product size 100-200 bp. These primers were used in a final concentration of 300 nM.

* Specific qRT primer pair for *TCSn*-driven *GFP*.

2.10.3 Agarose gel electrophoresis

Agarose gel electrophoresis was performed to check RNA quality (2.10.1.3), to detect PCR amplification products (2.10.2), or to separate DNA fragments by size after restriction digests (2.10.6). Depending on the expected DNA/RNA fragment size, 1% to 3.5% agarose gels in 1x TAE (40 mM Tris, 20 mM acetic acid, 1 mM EDTA (pH 8.0)) were used. The 1x TAE buffer was used as running buffer. DNA/RNA fragments were visualized by staining with ethidium bromide (0.2 µg/mL gel) using an ultraviolet (UV) transilluminator (SynGene Bioimaging system, SynGene, Cambridge, UK). Prior to electrophoresis the samples were mixed with the suitable amount of 10x gel loading buffer (30% glycerol, 0.25% bromophenol blue, 0.25% xylene cyanol). For DNA size determination, the DNA ladder P405 (154-2176 bp, MBBL, Bielefeld, DE) or the HyperLadder™ I (200-10000 bp, Bioline, Luckenwalde, DE) were used.

2.10.4 Purification of PCR products

In order to directly purify PCR products or to isolate DNA fragments after restriction digests from agarose gels, the Wizard® SV Gel and PCR Clean-Up System (Promega, Mannheim, DE) was used according to manufacturer's instruction manual. After that DNA concentration was measured photometrically using the NanoDrop ND-1000 spectrophotometer (PeqLab, Erlangen, DE).

2.10.5 Genotyping of plants

T-DNA insertion lines were genotyped after ordering seeds from NASC or in the F2 and F3 generation following genetic crosses by PCR (2.10.2). Insertional mutants were genotyped via PCR using two primer pairs. One pair comprised of a gene-specific and a T-DNA-specific primer (binding to the left border of the T-DNA) was used to amplify the mutant allele. The second primer pair flanking the insertion was used to amplify the WT allele. All primers used for genotyping are listed in the following Table 11.

Table 11: Primer sequences for genotyping.

Primer	Sequence (5'-3')	Purpose of use
LBb1.3	ATTTTGCCGATTTCGGAAC	T-DNA-specific primer to amplify the mutant allele of SALK lines, e.g. *hipp1-1*
Spm32	TACGAATAAGAGCGTCCATTTTAGAGTGA	T-DNA-specific primer to amplify the mutant allele of SM lines, e.g. *hipp8-1*
HIPP1 RP	AAACGCCTTCCATCACCG	Gene-specific primer to amplify both the WT and mutant alleles of *HIPP1*
HIPP1 LP	TCCTTCAGACTTTACTT	Gene-specific primer to amplify the WT allele of *HIPP1*
HIPP3 RP	ACAACACAAGCATTCGGATTC	Gene-specific primer to amplify both the WT and mutant alleles of *HIPP3*
HIPP3 LP	TTCCACGGAATCTGTAACTGG	Gene-specific primer to amplify the WT allele of *HIPP3*
HIPP5 RP	CATTAGTTGATCGAGAAAATGGC	Gene-specific primer to amplify both the WT and mutant alleles of *HIPP5*
HIPP5 LP	TTGTTTGTTGTTCAGAGCGTG	Gene-specific primer to amplify the WT allele of *HIPP5*
CKXin2_228bp_3	ATCACGAACTTCCAC	Gene-specific primer to amplify the mutant allele of *HIPP6*
proHIPP6_-948_FW	CAGTCTAGAGAAAACCCTAGACGGCTAACC	Gene-specific primer to amplify the WT allele of *HIPP6*
proHIPP6_-25_RV	CAGCCCGGGCGTAGTAGTAGTAGTAGAGAGAATC	Gene-specific primer to amplify the WT allele of *HIPP6*
HIPP7 RP	CCTACCAATACACCCCATGTG	Gene-specific primer to amplify the mutant allele of *HIPP7*
HIPP7_qRT_RV1	ATCGGAGACAGAAGCTGAAC	Gene-specific primer to amplify the WT allele of *HIPP7*
FW-hipp7-exon2	GTTGTCTCAAAGGCTTCG	Gene-specific primer to amplify the WT allele of *HIPP7*
HIPP8 RP	TTGATCGTAAAACCTCTCTGACC	Gene-specific primer to amplify the mutant allele of *HIPP8*
Hipp8_gen_3	TCACATGATTGAACAAG	Gene-specific primer to amplify the WT allele of *HIPP8*
hipp8-exon-B	GGAGAATCAGACAACAAG	Gene-specific primer to amplify the WT allele of *HIPP8*

HIPP9 RP	TTAGGGGTCCAAACAACTGTG	Gene-specific primer to amplify both the WT and mutant alleles of *HIPP9*
HIPP9 LP	ATCCCTTCCAAAACATTCCAC	Gene-specific primer to amplify the WT allele of *HIPP9*

2.10.6 Restriction digestion

Restriction enzymes were purchased from Thermo Fisher Scientific (Waltham, US) and used with supplied buffers. A typical reaction mixture consisted of 50-500 ng DNA, 10 units of the appropriate restriction enzymes, 1x of the recommended reaction buffer and water to a final volume of 20 µl. The reaction mixture was incubated at recommended temperatures for at least 2 hours.

2.10.7 Gateway® recombination

The cloning of constructs in Gateway® compatible vectors was done according to the manufacturer's protocol (Invitrogen/Thermo Fisher Scientific, Waltham, US). The first step of Gateway® cloning was to amplify DNA fragments with gene-specific primers including Gateway attachment attB-sites (Table 12). The Gateway® Entry- and Destination-Vectors which were used in this study are listed in Table 2.

Table 12: Primer sequences for Gateway® cloning.

Amplification of	**Primer sequences (5'-3')[1)]**
HIPP1 (AT2G28090)[2)]	F: ggggacaagtttgtacaaaaaagcaggctTGATGGATCCAGTGAAG
for N-terminal fusion	R: ggggaccactttgtacaagaaagctgggtTCACATAACGCTGC
HIPP5 (AT2G36950)	F: ggggacaagtttgtacaaaaaagcaggctTGATGGGAGAGGTCCAAGAAG
for N-terminal fusion	R: ggggaccactttgtacaagaaagctgggtTTACATAACAGAGCAAC

1) Small letters in the primer sequences indicate the integrated attB1- or attB2-sites for cloning DNA fragments into pDONR 221. Underlined letters are the nucleotides added to keep the sequence in the right frame.
2) The cloning was based on the gene model AT2G28090.2 and the full length cDNA clone AY924752 was used as template (see 3.3.4).

2.10.8 Sequencing of DNA

DNA sequencing was done by the company GATC Biotech (Konstanz, DE).

2.11 DNA cloning

2.11.1 Generation of *HIPP*-overexpressing lines

To generate the binary destination vectors for driving the gene expression by the *UBQ10* promoter, the *UBQ10* promoter was amplified by PCR (2.10.2) creating *Hind*III and *Spe*I restriction sites at the 5'- and 3'-ends, respectively. The fragment was subsequently cloned into the Gateway destination vector pB7WGF2 via *Hin*dIII/*Spe*I sites, replacing the cauliflower mosaic virus (CaMV) 35S promoter (final vector is called pB7WGFUBQ102).
To generate N-terminal fusion constructs overexpressing *HIPP* genes of cluster I, the respective cDNAs were first cloned. It was not possible to amplify the *HIPP1* cDNA corresponding to the annotated *At2g28090.1* gene model. Likewise, none of the publically available EST sequences supports this model. Therefore, a cDNA sequences corresponding to the full-length cDNA clone AY924752 and representing an alternative *HIPP1* gene model, named here *At2g28090.2* (see 3.3.4), was amplified using 500 ng cDNA as template and cloned in this work. *HIPP6* and *HIPP7* genes were amplified using 50 ng cDNA as template. PCR products were cloned into pDONR221 and subsequently subcloned by Gateway LR recombination into the pB7WGFUBQ102 destination vector for an N-terminal GFP-fusion of HIPP1, and into the pK7WGF2 for N-terminal GFP-fusions of HIPP6 and HIPP7.
The $HIPP7^{C352G}$ and $HIPP7^{hma}$ point mutations were introduced by PCR based mutagenesis by Dr. Henriette Weber (FU Berlin). The mutations in the constructs were confirmed by DNA sequencing. The $HIPP7^{C352G}$ and $HIPP7^{hma}$ cDNA sequences were amplified by PCR (2.10.2). PCR products were cloned into pDONR221 and transferred subsequently into the pB7WGFUBQ102 destination vector for N-terminal GFP-fusions.

2.11.2 Generation of amiRNA lines

Because the homologous genes from the same family usually share a large degree of functional redundancy, the technique of artificial microRNA (amiRNA) was used (Schwab et al., 2006b) to target several genes at once. Two amiRNAs with multiple potential targets from clade I of the *HIPP* gene family were designed (see 3.3.1). The amiRNA sequence targeting *HIPP5*, *HIPP6* and *HIPP7* was 5'-TTTCACAGTGCATGCGAACTT-3'. The amiRNA sequence targeting *HIPP3*, *HIPP5*, *HIPP6*, *HIPP7* and *HIPP8* was 5'-TTTCACAGTGCATGTCAACCT-3'. Sequences were selected and expression constructs were made using the Web MicroRNA Designer (WMD3) and the protocol available under http://wmd3.weigelworld.org. The amiRNA precursor was cloned into pDONR221 (Invitrogen/Thermo Fisher Scientific, Waltham, US)

and subsequently into pB2GW7 (Karimi et al., 2002) harbouring the cauliflower mosaic virus (CaMV) 35S promoter to yield 35S:amiRNA-Tri and 35S:amiRNA-Mul, respectively.

2.11.3 Generation of *pHIPP:GUS* lines

In order to analyze the expression patterns of individual *HIPP* genes of cluster I, promoter regions upstream of the translational start ATG of four individual *HIPP* genes, i.e. the 795 bp region of *HIPP1* (upstream of the ATG of the *At2g28090.1*), the 2056 bp region of *HIPP5*, the 949 bp region of *HIPP6*, and the 1580 bp region of *HIPP7*, were amplified by PCR introducing specific restriction sites at the 5'- and 3'-ends.The promoter fragments were subsequently cloned into pCB308 destination vector harboring the *GUS* reporter gene. Additionally, because of the alternative *HIPP1* gene annotation model (3.3.4), the 1491 bp region, which is upstream of the alternative translational start ATG of *At2g28090.2*, was amplified by PCR and fused to the *GUS* gene. Moreover, promoter-proximal introns can have a large influence on the level and pattern of gene expression (Wang et al., 2002; Jeong et al., 2007; Rose et al., 2008). In order to determine whether the promoter-proximal introns have effects on the expression of the *HIPP6* gene, a second *HIPP6* reporter gene construct was cloned. This 1364 bp-long construct includes the same ATG-upstream region (see above) as well as parts of the coding region and the first two introns (see 3.3.2).
Primers used for generation of transgenic lines are listed in Table 13.

Table 13: Primer sequences for generation of transgenic lines.

Amplification of	Primer sequences (5'-3')
Promoter of *HIPP1* (At2g28090.1)	F: CAGTCTAGAGGGTCTTGAAAGATTTTAGTGAC
	R: CAGCCCGGGTTTCGTCTCTAACTTCTTCTGC
Promoter of *HIPP1* (At2g28090.2; *pHIPP1L*)	F: CAGTCTAGAGGGTCTTGAAAGATTTTAGTGAC
	R: CCCGGGGATAAACCCAATCAGAGTCAGC
Promoter of *HIPP5* (At2g36950)	F: GCGCGGATCCATGTGTTGAAATCGTATTTAG
	R: GCGCGGATCCTTCTTGGTTGAAGATAAGG
Promoter of *HIPP6* (At5g03380; *pHIPP6S*)	F: CAGTCTAGAGAAAACCCTAGACGGCTAACC
	R: CAGCCCGGGCGTAGTAGTAGTAGTAGAGAGAATC
Promoter of *HIPP6* (At5g03380; *pHIPP6L*)[1)]	F: CAGTCTAGAGAAAACCCTAGACGGCTAACC
	R: CAGCCCGGGTTGTCGGCCACTTTATCACG
Promoter of *HIPP7* (At5g63530)	F: GCGCTCTAGACGATTATTGCTTGAAGATG
	R: GCGCGGATCCATTTATTTTTTTTGGTTTGAAG
Promoter of *UBQ10* (AT4G05320)	F: CAGAAGCTTCGACGAGTCAGTAATAAAC
	R: CAGACTAGTCTCGAGTGTTAATCAGAAAAACTC

1) Construct includes the same ATG-upstream region of *HIPP6* (*pHIPP6S*) as well as some parts of the coding region and the first two introns (see 3.4).

2.11.4 Cloning of gene constructs in Y2H, Co-IP and BiFC assays

For yeast two-hybrid (Y2H) studies, *HIPP* and *CKX* gene constructs were generated by cloning the corresponding cDNAs into destination vectors pACT2 (prey) and pBTM116 -D9 (bait). Most of the constructs were generated by Dr. Henriette Weber (FU Berlin) as described previously (Weber et al., 2005). The *HIPP1* and *HIPP5* cDNAs were cloned into destination vectors pACT2 (prey) and pBTM116-D9 (bait) by me according to the Gateway® recombination protocol as described (2.10.7). Primers used for generation of the constructs are listed in Table 12. CKX1 to CKX5 were cloned without N-terminal signal peptide/signal anchor sequences (Niemann et al., 2018) (http://www.cbs.dtu.dk/services/SignalP) to avoid targeting to the secretory pathway.

Following gene constructs were used for Co-Immunoprecipitation (Co-IP) experiments: *35S:GFP-HIPP6* (see 2.11.1), *35S:GFP-HIPP7* (see 2.11.1), *35S:GFP-CKX1* (Niemann et al., 2018) and *35S:myc-CKX1* (Niemann et al., 2015). For the myc-fusion proteins, *HIPP6* and *HIPP7* genes in pDONR221 (see 2.11.1) were subcloned by Gateway LR recombination into the pGWB18 destination vector for N-terminal myc-fusions of HIPP6 and HIPP7.

For protein-protein interaction by the bimolecular fluorescence complementation (BiFC) assay, the *HIPP1* and *HIPP7* cDNAs were amplified using primer pairs listed in Table 14. For *HIPP7*^{hma}, the cDNA sequence of *HIPP7*^{hma} (see 2.11.1) was used as template, and all the resulting fragments were cloned into pJet vector. For CKX-HIPP BiFC, *HIPP1* and *HIPP7* cDNAs were subcloned into the *Kfl*I site of MCS3 in pDOE-08-CKX1 (Niemann et al., 2018), resulting in pDOE-08-CKX1-HIPP constructs, expressing CKX1 N-terminally tagged with the N-terminal fragment of monomeric Venus split at residue 210 (NVen-CKX1) and HIPP N-terminally tagged with the C-terminal Venus fragment (CVen-HIPP). For the HIPP7 homodimeration test, *HIPP7* cDNAs was subcloned into *Bam*HI site of the MCS1 in pDOE-08 (Gookin and Assmann, 2014), resulting in pDOE-08-HIPP7 parent vector expressing NVen-HIPP7 and unfused CVen. In the next step, the second *HIPP7* cDNA fragment was subcloned into the *Kfl*I site within MCS3 of the pDOE-08-HIPP7 parent vector, resulting in the vector expressing NVen-HIPP7/CVen-HIPP7.

Table 14: Primer sequences for BiFC system.

Amplification of	Primer sequences (5'-3')
HIPP1 (At2g28090.2)	F: AGGGGTCCCCGATGGATCCAGTGAAGATTGC
for *MCS3*	R: AGGGGACCCTCACATAACGCTGCAATAG
HIPP7 (At5g63530)	F: AGGGATCCGGAGAGGAAGAGAAG
for *MCS1*	R: AGACTAGTTTACATTACAGTACATGC
HIPP7 (At5g63530)	F: AGGGGTCCCCGGGAGAGGAAGAGAAG
for *MCS3*	R: AGGGGACCCTTACATTACAGTACATGC

HIPP7^{C352G} (At5g63530) for *MCS3*	F: AGGGGTCCCCGGGAGAGGAAGAGAAG R: AGGGGACCCTTACATTACAGTACCTGC

2.12 Histochemical analysis of GUS expression

Histochemical analysis of GUS expression was performed as described by Jefferson et al. (1987) with some modifications. Sample tissues were incubated for 1 h in 90% acetone at -20°C and washed twice with 50 mM sodium phosphate buffer (pH 7.0). The enzymatic reaction was conducted with staining solution (0.5 mg/ml X-Gluc (5-bromo-4-chloro-3 -indolyl-β-D-glucuronide), 50 mM sodium phosphate buffer (pH 7.0), 10 mM potassium ferrocyanide, 10 mM potassium ferricyanide, 0.2% Triton X-100) for 4 h to overnight at 37°C in the dark. After staining, plant material was washed with 50 mM sodium phosphate buffer (pH 7.0) and destained with 70% ethanol and cleared with a chloral hydrate: glycerole: water solution (8:1:2, w/v/v) (Berleth and Jurgens, 1993). The GUS staining pattern was visualized and recorded with a light stereomicroscope (SZX12; Olympus, Shinjuku, JP) or a microscope (Axioskop 2 plus; Zeiss, Jena, DE) equipped with an Olympus C-4040ZOOM (Olympus, Shinjuku, JP) photographic device.

2.13 Confocal laser scanning microscopy

To determine the subcellular localization of GFP-HIPP fusion proteins, leaf discs from *N. benthamiana* two day-after-infiltration (DAI) with *A. tumefaciens* (2.9.4) harboring the individual constructs (2.11.1) were used. GFP-fusion proteins and mCherry-marker proteins were analyzed by an inverted fluorescence microscope (Leica DMI 6000 CS), equipped with a Leica TCS SP5 laser scan unit (Leica Microsystems, Wetzlar, DE) and operated with the Leica Application Software. GFP and mCherry were excited at 488 nm and 561 nm and the fluorescence detected at 498-538 nm and 600-630 nm, respectively. Analysis of the subcellular localization of the interaction complexes in the bimolecular fluorescence complementation (BiFC) assay was performed as described by Gookin and Assmann (2014).

2.14 Protein methods

2.14.1 Protein extraction

For the extraction of the total proteins from Arabidopsis and tobacco, the plant material was quickly frozen in liquid nitrogen and homogenized using a Retsch mill in precooled (liquid

nitrogen) adapters using two steel beads. After that, 500 µl of protein extraction buffer was added to approximately 0.5 g homogenized leaf material. The buffer consisted of 150 mM NaCl, 50 mM Tris/HCl pH 7.5, 0.1-0.3% Triton X-100 and prior to use the recommended amount of protease inhibitor cocktail tablets (1 tablet/10 ml, Roche, Cat. No. 11836170001) was added. After the samples have been thoroughly vortexed, they were incubated on ice for 20 min. The samples were centrifuged for 10 min at 6,000 x g at 4°C and the protein concentration of the supernatants were determined prior protein blot analysis.

2.14.2 Determination of protein concentrations

Protein concentrations were determined by the bicinchoninic acid method (Smith et al., 1985). This method is based on the reduction of Cu^{+2} to Cu^{+1} by protein in an alkaline medium, which forms a light blue complex with bicinchoninic acid (BCA). Absorption of the complex at 562 nm is measured photometrically. The measurement was carried out with the aid of the BCA protein assay Kit (Pierce Biotechnology, Rockford, USA). BSA (bovine serum albumin) dilution series (1.0, 0.75, 0.5, 0.25, 0.125 and 0.0 mg/ml) were used to prepare a standard curve. Protein extraction buffer was used as blank. Standards, samples, and blanks were measured in triplicates. 200 µl of detection reagent was added to 10 µl of BSA standard, blank, or sample (see 2.14.1) which was diluted 1:10 or 1:20. The mixture was incubated for 30 min at 37 °C before measuring at 562 nm in microplates using the Synergy 2 Microplate Reader (Biotek, Winooski, USA). In order to calculate the protein concentrations in the samples, linear regression analysis was performed using the values of the BSA standards to obtain the equation for the standard curve.

2.14.3 SDS polyacrylamide gel electrophoresis (SDS-PAGE) and protein blotting

Proteins were separated according to their sizes using denaturing discontinuous SDS-PAGE (Laemmli, 1970). The upper (stacking) and lower (resolving) gel contained 4% and 10% acrylamide, respectively. The composition of gels is shown in Table 15. The electrophoresis buffer used consisted of 192 mM glycine, 25 mM Tris and 0.1% SDS. Protein extracts (see 2.14.1) were mixed with the adequate amount of 4x Laemmli buffer (Laemmli, 1970) and protein extraction buffer. The samples were heat treated for 5 min at 95°C and then a specific volume (corresponding to 30 µg total protein) loaded onto the stacking gel. PageRuler Prestained Protein Ladder (Fermentas/Thermo Scientific, 5 µL) was used as protein molecular weight marker. Gel electrophoresis was performed using 20 mA (constant) per gel until sufficiently separated (visualized by prestained marker) in a Bio-Rad (Hercules, USA) running chamber.

Table 15: Composition of SDS polyacrylamide gels.

Components	Stacking gel	Separating gel
Tris-HCl pH 8	-	375 mM
Tris-HCl pH 6,8	125 mM	-
Acrylamid/Bis-Acrylamid (19:1)	4%	10%
SDS[1)]	0.075%	0.1%
APS[2)]	0.0375%	0.05%
TEMED[3)]	0.06%	0.05%

1) SDS, sodium dodecyl sulfate
2) APS, ammonium persulfate
3) TEMED, *N,N,N′,N′*-tetramethylethane-1,2-diamine

The protein blotting was performed using the Mini Trans-Blot Electrophoretic Transfer Cell System (Bio-Rad). For that gels were rinsed briefly with ddH_2O after the PAGE and then equilibrated for 10 min in the blotting buffer (192 mM glycine, 25 mM Tris). Meanwhile, the PVDF membrane (Immobilon-P Membrane, Cat. No. IPVH00010, pore size 0.45 µm, EMD Millipore) was activated with methanol (20 sec), rinsed with ddH_2O (2 min) and equilibrated in the blotting buffer. Also foam (fiber) pads and Whatman papers (grade 3MM Chr, Cat. No. 3030917) were pre-soaked in the blotting buffer. The blotting sandwich (in the direction of transfer: cathode, foam pad, two Whatman papers, gel, PVDF membrane, one Whatman paper, foam pad, anode) was inserted into the blotting module and blotting was carried out overnight at 4°C with 55 mA (constant). Successful transfer was verified when prestained protein marker was visible on the PVDF membrane.

2.14.4 Immuno-detection

After overnight blotting, the PVDF membrane was rinsed briefly with 1x PBS (137 mM NaCl, 2.7 mM KCl, 10 mM Na_2HPO_4, 1.8 mM KH_2PO_4), and then blocked for 1 h in 5% Skim Milk (Fluka/Sigma-Aldrich) in 1x PBS-T (1x PBS, 0.1% Tween-20) at RT. Afterwards the primary antibody was added to the 5% Skim Milk in PBS-T and incubated at RT for 2 h. Blots were washed for 15 min (3x5 min) in 1x PBS-T and incubated with the secondary antibody in the 5% Skim Milk in PBS-T for 2.5 h at RT. The same washing procedure was carried out after the incubation with the secondary antibody. Chemiluminescence assay using the SuperSignal West Pico Chemiluminescent Substrate Kit (Pierce, Rockford, USA) was performed according to the manufacturer's instructions. After incubation with the ECL substrate a CL-XPosure film (Thermo Fisher Scientific, Waltham, USA) was used to detect the chemiluminescence (exposure time varied, 5 sec to 5 min). The detection of myc epitope was performed with anti-myc antibody (clone 4A6; Millipore, Billerica, USA) (dilution 1:2,500) in combination with the secondary goat anti-mouse antibody IgG-HRP (sc-2005; Santa Cruz, Dallas, USA) (dilution 1:5,000). The detection of GFP was performed with the anti-GFP antibody (JL-8;

Clontech, California, USA) (dilution 1:2,000) in conjunction with the secondary bovine anti-rabbit antibody IgG-HRP (sc-2370; Santa Cruz, Dallas, USA) (dilution 1:3,000).

2.14.5 Coomassie blue staining

To check whether equal amounts of protein were loaded, the Coomassie blue staining method was used as described by Welinder and Ekblad (2011). For this, the membrane was washed twice with 1x PBS-T and then stained with 0.1% Coomassie R-250 (Applichem, Darmstadt, DE) in methanol/water, 1:1, for 1 min. The membrane was destained in acetic acid/ethanol/water, 1:5:4 for 20 min. Finally, the membrane was washed with water and air-dried. Pictures were taken (membranes were put in a transparent plastic bag and scanned) and the protein bands corresponding to the large subunit of ribulose-1,5-bisphosphate carboxylase/oxygenase (RbcL) were used as loading control.

2.15 Yeast two-hybrid and Co-Immunoprecipitation assays

For Y2H studies, yeast transformations were performed (2.9.2) and SDII selection medium was used as transformation control, whereas, SDIV minimal medium was used for interaction tests. Surviving yeast colonies were picked as primary positives and restreaked on SDIV plates. Freshly-grown yeast colonies on SDIV medium were dissolved in liquid SD medium to OD_{600} = 0.1. 2 µL of the resuspended clones were subjected to PCR test. The dissolved clones were then diluted 1:10 in liquid SD medium, and 10 µl of the diluted suspension were dropped on SDIV minimal medium or SDIV supplemented with 5 mM 3-AT for interaction tests. Photographs were taken 5 d after plating.

For CoIP, GFP- and myc-fusion proteins were co-expressed transiently in tobacco leaves. Total protein extracts (50 mM Tris-HCl pH 7.5, 150 mM NaCl, 0.3% Triton X-100, 0.2% Igepal) were incubated with GFP-Trap A beads (ChromoTek, Planegg-Martinsried, DE). Extraction and washing buffers contained at all times 1 mM PMSF (Sigma Aldrich, Steinheim, DE) or complete protease inhibitor cocktail (Roche, Mannheim, DE) and 10 µM MG132 (Sigma Aldrich, Steinheim, DE) to prevent proteolytic and proteasomal activities, respectively. In general, proteins were incubated at least 2 h at 4°C under shaking conditions before being centrifuged. Precipitates were washed five times to remove unspecific bindings, before they were taken up in 1x Laemmli buffer (Laemmli, 1970) and boiled (5 min, 95°C).

2.16 Plant experiments

2.16.1 Hormone and CKX inhibitor experiments

For analyzing the responses of *HIPP*-overexpressing plants to phytohormones, plants were sprayed with cytokinin or CKX inhibitor and GA, respectively. For the plants sprayed with CKX inhibitor, INCYDE (Zatloukal et al., 2008; Niemann et al., 2015) was used to treat the plants in a 3-day interval for four weeks with different concentrations (0, 10 and 50 µM inhibitor; 0.01% Silwet 77) after the first two leaves appeared. The fully expanded leaf 7 was photographed and the leaf area was measured with ImageJ (Abràmoff et al., 2004). For cytokinin treatment, ten plants of each genotype were sprayed in a 3-day interval for three weeks with 50 µM BA (Sigma Aldrich, Steinheim, DE) or with Mock (0.05% DMSO) after the first two leaves appeared. For the GA treatment, ten plants of each genotype were sprayed in a 3-day interval for three weeks with 50 µM GA_3 (OlchemIm, Olomouc, CZ) or with Mock (0.05% DMSO) after the first two leaves appeared.
For cytokinin sensitivity tests on root or shoot growth, Arabidopsis seedlings were grown on half strength MS medium containing different concentrations of iP (5, 10, 25 and 50 nM for root assays; 5, 10 and 25 nM for shoot assays) or 0.002% DMSO as control.

2.16.2 Analysis of growth and developmental parameters

Plants were grown on soil in the greenhouse under the conditions as described (2.7.2.2). During the life cycle of the plants the phenotype was monitored. The rosette diameter was calculated as a mean value of two measurements per rosette at 23 day-after-germination (DAG). Plant shoot height was measured after termination of flowering with a ruler. The final number of siliques on the main stem was determined after termination of flowering.
For flowering time analysis, seeds were stratified for three days at 4°C and then sown on soil and grown in the greenhouse under long day conditions (2.7.2.2) or in a phytochamber under short day (SD) conditions (light/dark: 8 h/16 h) at 22°C and light intensities of 120-170 µmol m^{-2} s^{-1}. Onset of flowering was defined as the point of time where the first flower was visible. Termination of flowering was defined when no more new flowers were formed. The number of rosette leaves was scored at the start of flowering.
For *in vitro* root measurements, plants were grown *in vitro* (2.7.2.1) on vertical plates on half strength MS medium containing 12 g/L agar under standard long day conditions. The elongation of the primary root was determined between three and ten days after germination using the software ImageJ (Abràmoff et al., 2004). The number of emerged lateral roots was determined ten days after germination.

For cell size analysis, leaf tissue was fixed in ethanol/acetic acid (3:1), rehydrated in an ethanol series and cleared with chloral hydrate: glycerole: water solution (8:1:2, w:v:v) (Berleth and Jurgens, 1993) for 2-3 days and analyzed by a stereomicroscope (SZX12; Olympus, Shinjuku, JP) and microscope (Axioskop 2 plus; Zeiss, Jena, DE) equipped with an Olympus C-4040ZOOM (Olympus, Shinjuku, JP) photographic device. The 6th leaf of plants 28 DAG were mounted on microscope slides, and photographed. The average cell size and stomatal index were calculated as described by Holst et al., (2011).

2.16.3 Drought stress experiments

For drought stress experiments, plants were grown on soil under long day conditions. Three-week-old plants were exposed to drought stress by withholding water for 5-6 days. Plants were photographed after the indicated drought stress periods.

2.17 Databases and software

Sequences were obtained from the National Center for Biotechnology Information (NCBI, http://www.ncbi.nlm.nih.gov). Arabidopsis genome sequences and annotated gene model were obtained from the Arabidopsis Information Resource (TAIR, http://www.arabidopsis.org). Statistical analyses were performed by Microsoft Office Excel 2007 (Redmond, Washington, US). The nuclear localization signal (NLS) was predicted by the cNLS Mapper (Kosugi et al., 2009). The analysis of confocal image was performed by using the LAS AF software (Leica Microsystems, Wetzlar, DE). Photographs on the Zeiss Axioskop 2 plus microscope were taken with the software AxioVision Release 4.6 (Zeiss, Jena, DE) and the photographs on the stereomicroscope with the Olympus software DP-Soft 3.2. Corel Photo-Paint 12 (Corel Corporation, Ottawa, Canada) was used to edit image. The elongation of the primary root and the leaf area was measured with the software ImageJ (Abràmoff et al., 2004). The gel images were taken with the software GeneSnap (SynGene, Cambridge, UK).

2.18 Contributions

I worked together with Dr. Michael Niemann and Dr. Henriette Weber on the HIPP project. Dr. Michael Niemann performed most of the analysis of subcellular localization of GFP-HIPP7 fusion proteins in *N. benthamiana* and Arabidopsis (Fig. 12B-G). Dr. Henriette Weber performed the CoIP assays as well as parts of the Y2H assays in the CKX-HIPP interaction section (3.1). Nevertheless, these data have been included here to provide this essential

information in the framework of my thesis. My own contribution to results shown in Figures 8-10 is specified in Table 16.

Table 16: Contributions to the results shown in the CKX-HIPP interaction section (chapter 3.1).

Figures	My part*	Dr. Henriette Weber*
Fig. 8	A and C (*HIPP1* and *HIPP5* cDNAs cloning into destination vectors, yeast transformations)	A-C
Fig. 9	A	B and C
Fig. 10	A and B	C and D

* Capital letters refer to the respective figure panels.

Dr. Michael Niemann performed cell fractionation and membrane association experiments in Arabidopsis. He showed that the membrane association of the HIPP7 protein strongly but not exclusively depended on the protein prenylation. The interaction domain of CKX1 has been mapped by a deletion approach by Dr. Henriette Weber. The experiments showed that the C-terminal part of CKX1 is required for the interaction. These unpublished data are not shown in this work, but are mentioned in the discussion, since these data closely relate to the results of this study.

The hormone measurements were carried out in collaboration with Dr. Ondřej Novák and Dr. Danuše Tarkowská (Laboratory of Growth Regulators, Centre of the Region Haná for Biotechnological and Agricultural Research, Palacký University and Institute of Experimental Botany ASCR, Olomouc, Czech Republic). The plant growth, treatment and sampling as well as data evaluation were conducted by myself (see also 3.2).

Prof. Dr. Jianru Zuo, Prof. Dr. Joe Kieber, Dr. Bruno Müller, Dr. Isabel Bartrina and Dr. Sören Werner kindly provided seeds of mutant and transgenic plants that were used for this study (see Table 5). Prof. Dr. Rongda Qu (Department of Crop Science, North Carolina State University, Raleigh, US) kindly provided the pCAMBIA-mCherry vector. Prof. Dr. Sarah M. Assmann (Department of Biology, The Pennsylvania State University, PA, US) kindly provided the pDOE-08 vector.

3 Results

3.1 CKX proteins interact with distinct members of HIPP protein family

It has been shown that the cellular levels of CKX proteins are regulated by the protein quality control pathway, which significantly impacts on the cytokinin responses in Arabidopsis (Niemann et al., 2015). To explore further molecular mechanisms regulating CKX proteins, and to identify new CKX-interacting proteins, a genome-wide yeast two-hybrid (Y2H) screen with the CKX1 protein as bait has previously been performed in the Dr. Werner's group. Among the positive clones, coding sequences corresponding to six different HIPP proteins were recovered with high frequency (~65% of all isolated interactions). Interestingly, the isolated HIPP proteins fall into two phylogenetically distinct clades of the HIPP protein family: HIPP5, HIPP6 and HIPP7 belong to cluster I, and HIPP32, HIPP33 and HIPP34 form a separate cluster III (Fig. 6) (Tehseen et al., 2010).

3.1.1 Confirmation of the interaction between HIPP and CKX proteins

In order to verify the identified protein-protein interactions, the full-length cDNA encoding HIPP5, HIPP6 and HIPP7 were cloned and the interactions with CKX1 were confirmed in one-on-one Y2H interaction assays. The detected interactions were strong, as only partial growth suppression was observed on media supplemented with 3-amino-1,2,4-triazole (Fig. 8A).

To test that CKX1 interacts with HIPP proteins and forms complexes in planta, GFP-CKX1 was transiently coexpressed with myc-HIPP6 and myc-HIPP7 in *Nicotiana benthamiana* leaves and total protein extracts were used for Co-Immunoprecipitation (Co-IP) assays with anti-GFP antibody. As shown in Fig. 8B, both tested HIPP proteins were clearly detected in the GFP-CKX1 immunocomplex, but they did not coimmunoprecipitate with GFP alone, supporting the notion of a direct CKX1-HIPP interaction. Interestingly, immunoblot analysis suggested that the CKX1-HIPP complexes are rather stable as the monomeric myc-HIPP proteins were not detected upon Co-IP (Fig. 8B).

Result of our Y2H screen also suggested that only a specific subset of HIPP proteins can form complex with CKX1. To test this idea further, additional members of the HIPP family were cloned, and their interactions with CKX1 were tested in Y2H assays. Fig. 8A shows that HIPP1 and HIPP9, additional members of cluster I, interacted with CKX1. Randomly chosen

HIPP proteins outside the cluster I and III, HIPP19 and HIPP35, showed no interaction with CKX1 in yeast (Fig. 8A), confirming selectivity in CKX1-HIPP protein interactions.

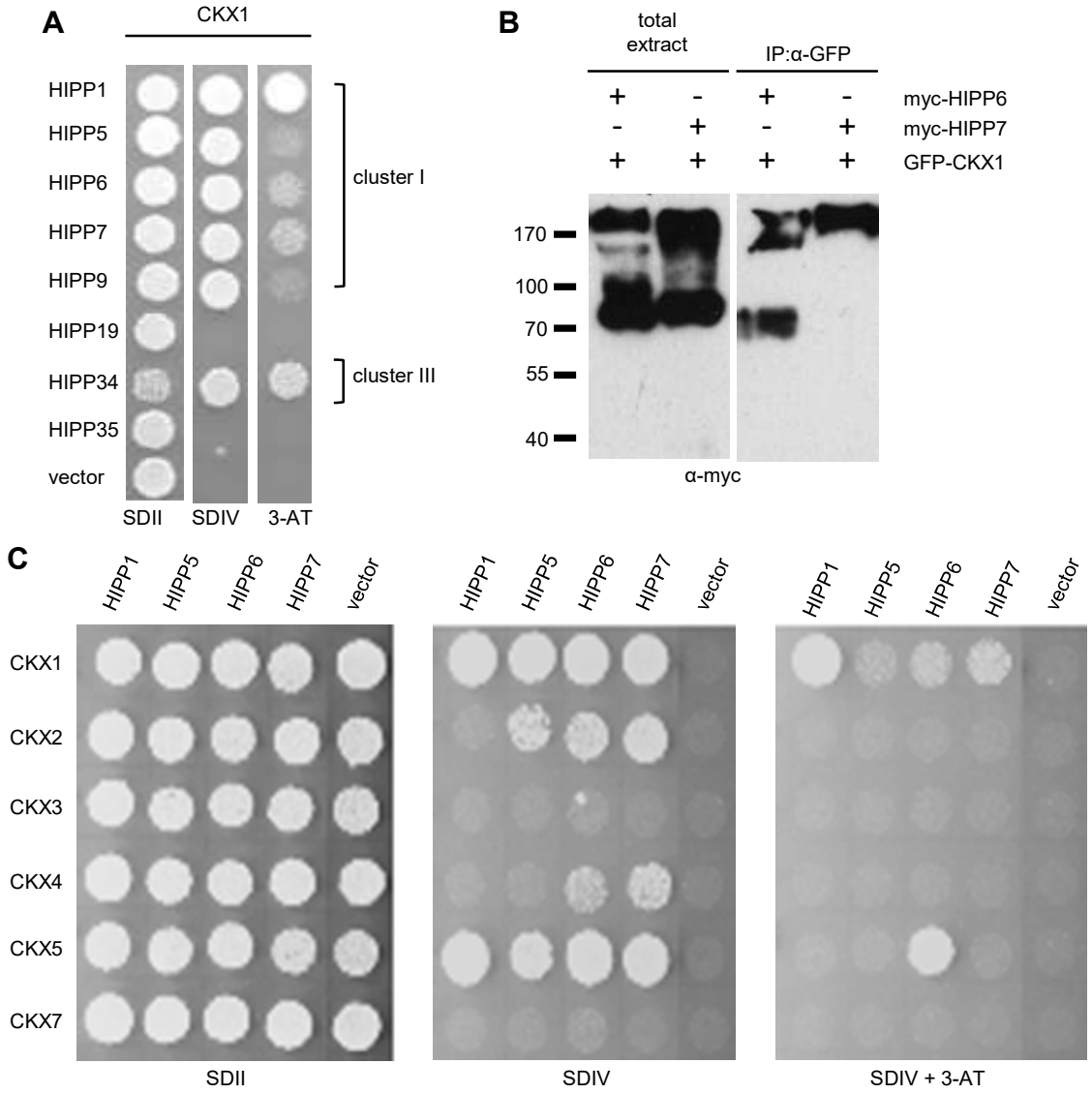

Figure 8. CKX and HIPP proteins interact *in vitro* and *in vivo*.
(A) Interaction between CKX1 and different HIPP proteins detected by yeast two-hybrid (Y2H) assays. Growth of yeast strains harboring CKX1 as bait and the indicated HIPP proteins as prey on control medium (SDII) lacking Leu and Trp, interaction medium also lacking Ura and His (SDIV), and SDIV supplemented with 10 mM 3-amino-1,2,4-triazole (3-AT). Empty vector pACT2-GW was used as negative control.
(B) *In vivo* interaction of CKX1 with HIPP proteins. The GFP-CKX1 protein was transiently coexpressed with myc-HIPP6 or myc-HIPP7 in *N. benthamiana* and the protein extracts were used for immunoprecipitations with anti-GFP antibody followed by SDS-PAGE and immunoblot detection with anti-myc antibody. The left panel shows the input (20 µg of crude extracts used for Co-IP assay); the right panel shows the pellet fractions from the Co-IP assays. Control Co-IP between myc-HIPP7 and free GFP is shown in Fig. 10D. It should be noted that myc-HIPP6 and myc-HIPP7 migrates with apparent molecular sizes higher than predicted for monomeric proteins (50 kDa and 47 kDa, respectively).
(C) Interaction between different CKX and HIPP proteins detected by Y2H assays as described in **(A)**.

To analyze whether CKX proteins other than CKX1 are interacting partners of identified HIPP proteins, five other CKX proteins were tested for the interaction with HIPPs in Y2H. Fig. 8C shows that all four tested HIPP proteins from clade I interacted with CKX5 in yeast; the strongest interaction conferred by HIPP6. In contrast, CKX2 seems to weakly interact with only HIPP5, HIPP6 and HIPP7, and even weaker interaction was detected between CKX4 and HIPP6 and HIPP7. Interestingly, CKX3 and CKX7 showed no interaction with tested HIPP proteins in Y2H assays.

3.1.2 Isoprenylation of HIPP proteins is essential for the interaction with CKX1

To understand the mechanism of CKX-HIPP interaction, HIPP protein domains were mutated to test whether they are required for the interaction, taking the CKX1-HIPP7 complex as a case example (Fig. 9A).

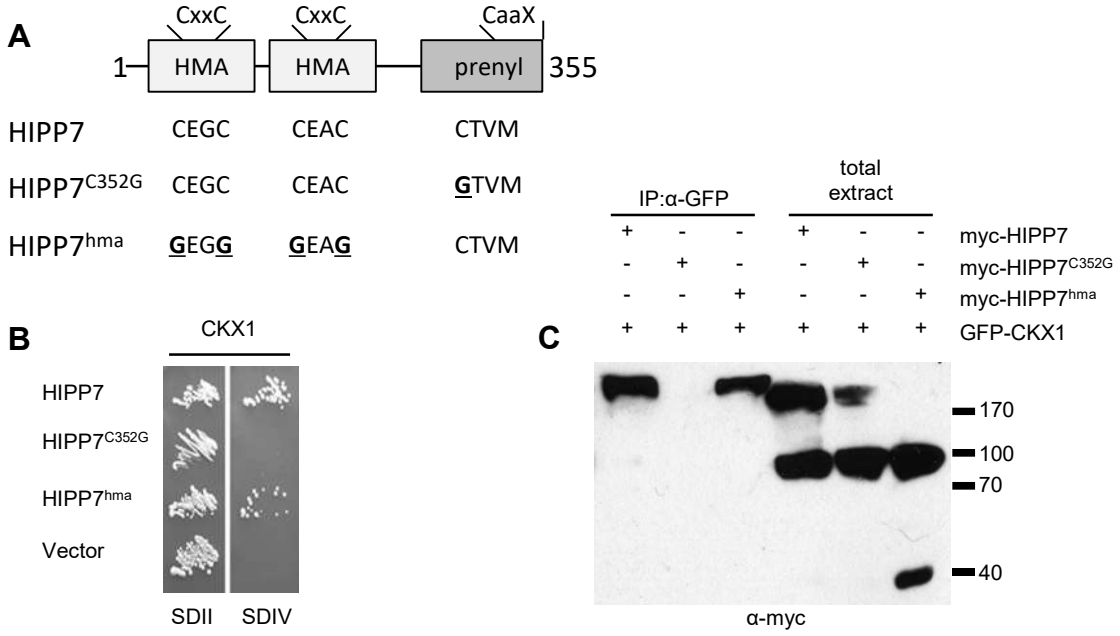

Figure 9. Analysis of interaction motifs in HIPP7 and CKX1.
(A) Scheme of HIPP7 protein structure with conserved motifs. Introduced mutations are indicated in bold/underlined.
(B) Interaction between CKX1 and HIPP7 mutant variants detected by yeast two-hybrid (Y2H) assays. Growth of yeast strains harboring CKX1 as bait and the indicated HIPP7 mutant proteins as prey on control medium (SDII) lacking Leu and Trp, and interaction medium also lacking Ura and His (SDIV). Empty vector pACT2-GW was used as negative control. HIPP7^{C352G}, HIPP7 variant with mutated prenyl-accepting Cys-residue within the isoprenylation motif. HIPP7^{hma}, HIPP7 variant with mutated HMA domains.
(C) Co-IP assays reveal the loss of CKX1-HIPP7 interaction upon mutating isoprenylation site in HIPP7 (HIPP7^{C352G}), whereas mutation of HMA domains (HIPP7^{hma}) does not affect the interaction. The GFP-CKX1 protein was transiently coexpressed with myc-HIPP7, myc-HIPP7^{C352G} or myc- HIPP7^{hma} in *N. benthamiana* and the protein extracts were used for immunoprecipitations with anti-GFP antibody followed by SDS-PAGE and immunoblot detection with anti-myc antibody. The pellet fractions from the Co-IP assays are shown on the left; the input (20 µg of crude extracts used for Co-IP) is on the right.

Protein prenylation can increase protein-membrane association or mediate protein-protein interactions (Sinensky, 2000). To test whether prenylation of HIPP proteins is relevant for

CKX-HIPP complex formation, a mutation of the prenyl-accepting Cys-residue within the isoprenylation motif of HIPP7 was generated (Fig. 9A) and the interaction of this HIPP7^{C352G} mutant with CKX1 was analyzed. As shown in Fig. 9B, the mutation completely abolished the interaction in yeast. Similarly, no interaction was detected using the *in vivo* Co-IP experiments (Fig. 9C), indicating that the prenylation of HIPP7 is required for the interaction with CKX1.
Several HIPP proteins, including HIPP7, were previously shown to bind various heavy metals via their HMA domain (Dykema et al., 1999; Suzuki et al., 2002). Both HMA domains in HIPP7 protein were mutated by exchanging metal-binding Cys residues in each HMA domain to glycine (HIPP7^{hma}; Fig. 9A) and the resulting mutant variant were tested for interaction with CKX1. Y2H and Co-IP assays clearly showed that the interaction was not affected (Fig. 9B and C) suggesting that heavy-metal binding is dispensable for CKX-HIPP interactions.

3.1.3 Homodimerization of HIPP proteins requires prenylation and heavy metal binding

Next, the potential protein-protein interactions among the isolated HIPP proteins were tested. Results showed that HIPP1, HIPP5 and HIPP7 proteins could form homodimers in yeast, but did not interact with other tested HIPP proteins (Fig. 10A-C). Similarly, HIPP7 -homodimerization was also detected in using the *in vivo* Co-IP experiments (Fig. 10D). Interestingly, not like the CKX1-HIPP7 complex, the HIPP7-homodimerization was lost when either the HIPP7^{C352G} or HIPP7^{hma} mutant variants was used, suggesting that both the protein isoprenylation and metal binding are essential for the HIPP7 homocomplex formation.

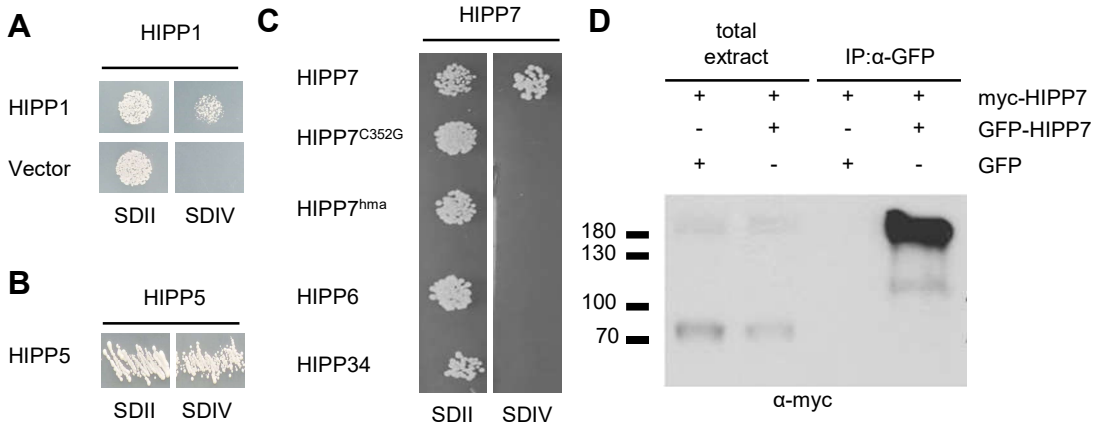

Figure 10. HIPP7 homodimerization requires prenylation and heavy-metal binding.
(A) and **(B)** HIPP1 **(A)** and HIPP5 **(B)** homodimerizes in Y2H assay. Empty vector pACT2-GW was used as negative control.
(C) HIPP7 homodimerizes in Y2H assay but does not form heterodimers with HIPP6 or HIPP34. The homodimerization is abolished when HIPP7^{C352G} and HIPP7^{hma} mutants are used as preys.
(D) Co-IP assays corroborate the *in vivo* homodimerization of HIPP7. myc-HIPP7 was transiently coexpressed with GFP-HIPP7 and free GFP as control in *N. benthamiana*. The protein extracts were used for immunoprecipitations with anti-GFP antibody followed by SDS-PAGE and immunoblot detection with anti-myc antibody. The input (10 µg of crude extracts used for Co-IP) is on the left; the pellet fractions from the Co-IPs are shown on the right.

3.1.4 Subcellular localization of clade-I HIPP proteins

To gain insight into cellular mechanism underlying the activity of HIPP proteins, their subcellular localizations were investigated. HIPP1, HIPP5 and HIPP7 were fused to GFP at their N termini to avoid interference with the potential C-terminal prenalytion, and the fusion proteins were expressed under the control of the 35S promoter, transiently in *N. benthamiana* leaf epidermis and in stably-transformed Arabidopsis.

Confocal laser scanning microscopy revealed that the GFP-HIPP1 fusion protein was localized mainly in the nucleus and in the cytoplasm in *N. benthamiana* leaf cells (Fig. 11A). In the nucleus, the fluorescence labeled nucleoplasm and small bright foci, which were usually localized to nucleolus (Fig. 11B). With lower frequency, GFP-HIPP1 fluorescence was observed in distinct puncta at the cell periphery (Fig. 11A); a pattern characteristic of plasmodesmal localization (Oparka et al., 1997; Crawford and Zambryski, 2001; Yuan et al., 2016). Very similar subcellular localization of GFP-HIPP1 was observed also in the stable transgenic Arabidopsis plants (Fig. 11C-H), however, the frequency and intensity of GFP-HIPP1 signal at the plasmodesmata was significantly stronger than in *N. benthamiana* (Fig. 11G and H).

The GFP-HIPP5 and GFP-HIPP7 were localized mainly in the cytosol of *N. benthamiana* cells, as indicated by a diffuse staining of the cytoplasmic strands and nucleoplasm (Fig. 12A and B). However, in comparison to free mCherry cytoplasmic/nuclear marker, GFP-HIPP7 also accumulated at the nuclear envelope (Fig. 12B, arrowhead) and less frequently associated with plasmodesmata (Fig. 12C). In the cortical region, GFP-HIPP7 showed cytosolic localization adjacent to the ER network labeled with the coexpressed ER marker protein RFP-p24 (Fig. 12D) (Lerich et al., 2011). An apparent colocalization of GFP-HIPP7 with RFP-p24 was observed, but with only very low frequency (Fig. 12E). Similarly, in stably-transformed Arabidospis, GFP-HIPP7 localized to the cytosol, but, in contrast to the *N. benthamiana* system, the protein strongly labeled the plasmodesmata in the analyzed leaf cells (Fig. 12F). Interestingly, the frequency of plasmodesmal localization was lower and the fluorescence signal associated with plasmodesmata was significantly weaker in Arabidopsis plants expressing the GFP-HIPP7^{C352G} mutant form lacking the prenylation site (Fig. 12G). These results show that the prenylation is largely required for the localization of HIPP7 to plasmodesmata, however, the weak plasmodesmal localization of GFP-HIPP7^{C352G} suggests that other targeting determinants might be involved.

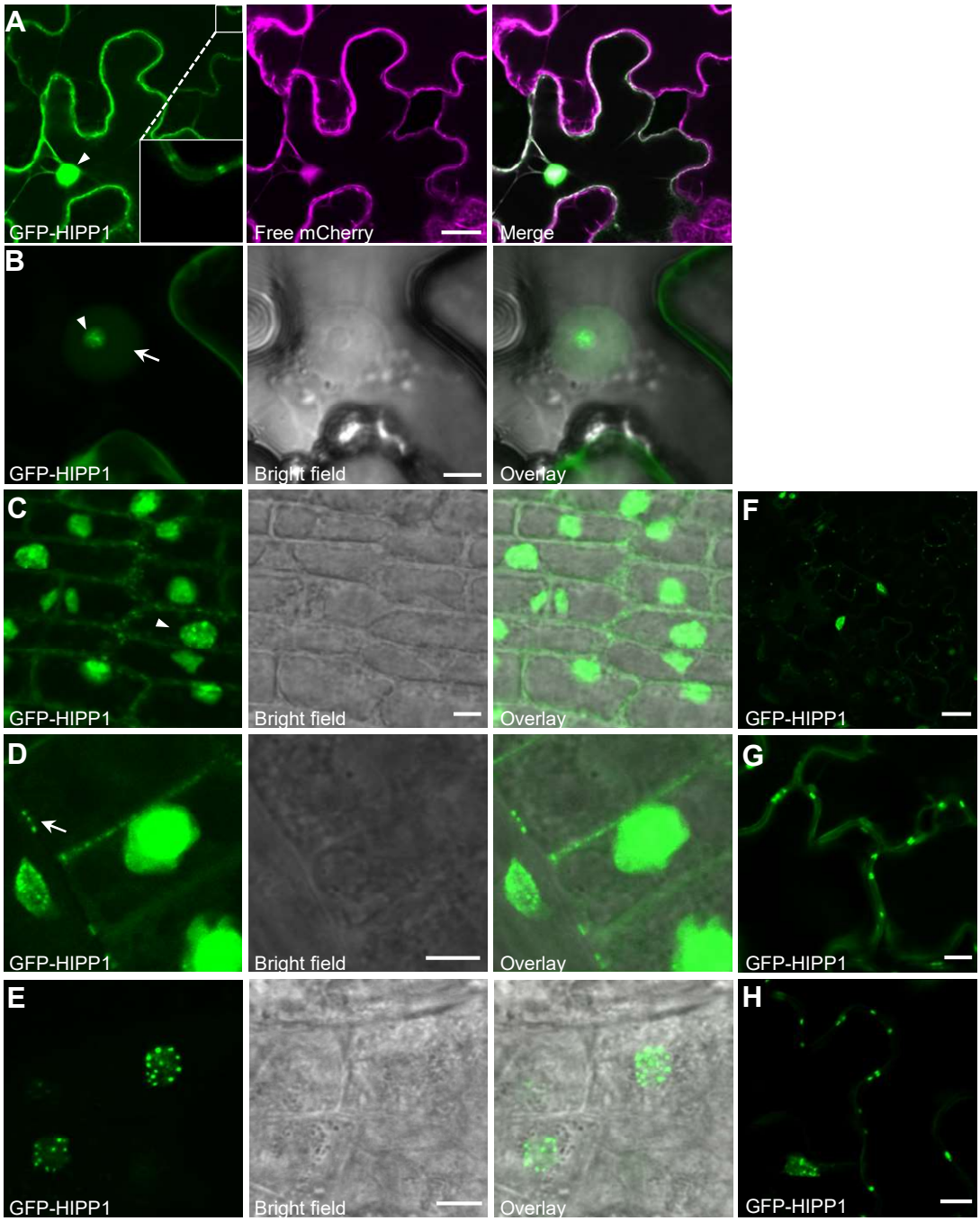

Figure 11. Analysis of subcellular localization of GFP-HIPP1 fusion protein in *N. benthamiana* and Arabidopsis.
(A) and **(B)** Representative confocal microscopy images of *N. benthamiana* leaf epidermal cells coexpressing GFP-HIPP1 with the cytosolic marker pCAMBIA-mCherry (magenta). GFP-HIPP1 localizes strongly in the nucleus (arrowhead) and in the cytoplasm. Occasionally, GFP-HIPP1 fluorescence was associated with plasmodesmata (magnified in the inset) **(A)**. In the nucleus, the GFP-HIPP1 fluorescence labels the nucleoplasm (arrow) and small bright foci within the nucleolus (arrowhead) **(B)**.
(C) to **(E)** Confocal microscopy of Arabidopsis root meristem cells expressing GFP-HIPP1. Similar to the results observed in *N. benthamiana*, the fusion protein localizes in the nucleus (arrowheads), cytosol **(C)** and plasmodesmata (arrow) **(D)**. In nucleus, the GFP-HIPP1 fluorescence is particularly associated with small bright foci **(E)**.
(F) to **(H)** GFP-HIPP1 localizes to the cytosol and strongly to plasmodesmata in Arabidopsis leaf epidermal cells.
The microscopy of *N. benthamiana* was performed 2 DAI. Scale bars = 5 µm (B, C, D,E), 7.5 µm (G and H) and 25 µm (A and F).

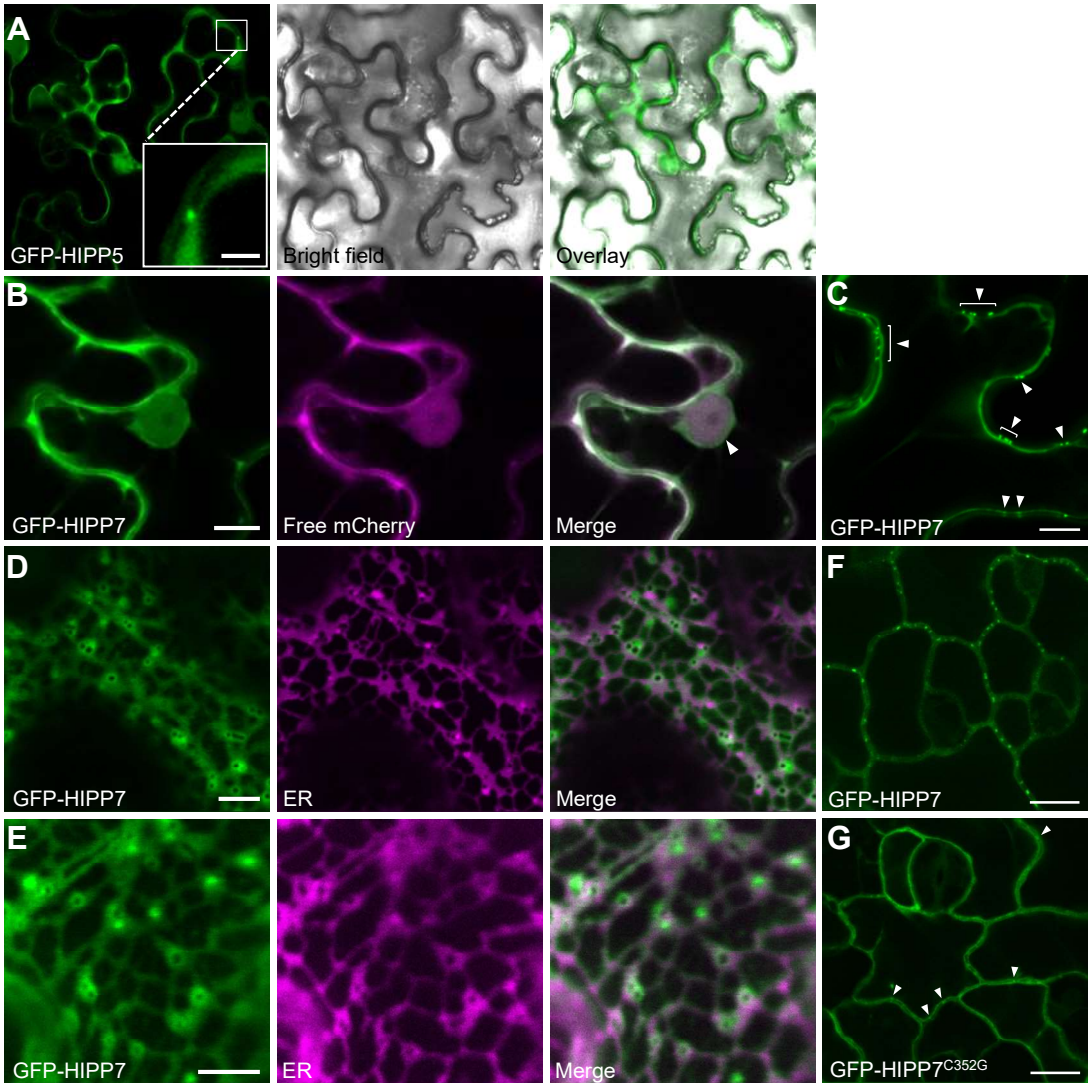

Figure 12. Analysis of subcellular localization of GFP-HIPP5 and GFP-HIPP7 fusion proteins in *N. benthamiana* and Arabidopsis.

(A) Representative confocal microscopy images of *N. benthamiana* leaf epidermal cells expressing GFP-HIPP5. GFP-HIPP5 localizes strongly in the cytosol. Occasionally, GFP-HIPP5 fluorescence was associated with plasmodesmata (magnified in the inset).

(B) to **(E)** Confocal microscopy analysis of *N. benthamiana* leaf epidermal cells transiently expressing GFP-HIPP7. In central plane of the cell, the protein is seen localized in the cytosol, in the nucleoplasm, and at the nuclear membrane (arrowhead) **(B)**. At the cell periphery, it additionally localizes to punctate structures reminiscent of plasmodesmata (arrowheads) **(C)**. In the cell cortex, GFP-HIPP7 localizes mainly adjacent to the ER (RFP-p24, magenta) **(D)**; less frequently, they colocalize **(E)**.

(F) and **(G)** Confocal microscopy of Arabidopsis leaf epidermal cells stably expressing GFP-HIPP7 **(F)** and GFP-HIPP7^{C352G} **(G)**. In addition to the cytosol, GFP-HIPP7 localizes strongly to plasmodesmata. HIPP7^{C352G} is mainly cytosolic with only weak plasmodesmal localization (arrowheads).

3.1.5 HIPP7 interacts with the CKX1 protein apparently relocated from the ER

Previous studies have demonstrated that CKX proteins, identified in this work as interacting with HIPP proteins, are localized to various compartments of the secretory pathway including the ER (Werner et al., 2003; Niemann et al., 2018). In view of the described CKX-HIPP protein interactions, it is therefore intriguing that HIPP1, HIPP5 and HIPP7 proteins are apparently localized outside of the secretory system, raising the question about cellular mechanisms underlying these protein-protein interactions.

To address this question, CKX1-HIPP7 interaction was tested using the optimized bimolecular fluorescence complementation (BiFC) system which utilizes monomeric Venus split at residue 210 (Gookin and Assmann, 2014). For this, CKX1 and HIPP7 were fused at their N termini to the N- and C-proximal halves of the Venus (NVen and CVen, respectively) in the double ORF expression vector pDOE-08. To monitor non-specific assembly of NVen and CVen, the parent vector expressing NVen-CKX1 together with unfused CVen was used as control. We performed transient transformations of *N. benthamiana* leaves and examined the fluorescence by confocal microscopy. The expressing epidermal cells were identified by monitoring the fluorescence of the integrated Golgi-localized mTurquoise2 marker (Golgi-mTq2; Gookin and Assmann, 2014). As illustrated in Fig. 13A, no or very weak BiFC was detected in cells expressing the control vector. In contrast, all cells transformed with the vector expressing NVen-CKX1 and CVen-HIPP7 showed strong Venus fluorescence (Fig. 13B), indicating BiFC between the fusion proteins and suggesting that CKX1 and HIPP7 interact also *in planta*. Most interestingly, in contrast to the GFP-HIPP7 signal predominantly localized to cytosol (Fig. 12), the fluorescence of the NVen-CKX1/CVen-HIPP7 complex clearly localized to the cortical and perinuclear ER and small punctate structures (Fig. 13I and J). This pattern closely resembled the subcellular localization of CKX1-GFP (Niemann et al., 2018). The BiFC experiments thus indicate that, at least in the *N. benthamiana* system, the CKX1-HIPP7 complex formation involves the HIPP7 protein fraction detected at the ER and/or is associated with relocation of HIPP7 to the ER. Moreover, it has been shown that CKX1 exhibits a transmembrane topology with the C-terminus residing in the ER lumen (Niemann et al., 2018) and, therefore, BiFC between CKX1 and HIPP7 implicates that the CKX1 protein in the detected complex represents a form which was relocated to the cytosolic site of the membrane. This is consistent with the recent finding that CKX1 is targeted to the ERAD pathway (Niemann et al., 2015), which requires retrotranslocation of target proteins from the ER prior delivery to the cytosolic/nuclear proteasome (Römisch, 2005). The results therefore suggest that HIPP7 might play a role during retrotranslocation of CKX1 or function in post-retrotranslocation steps.

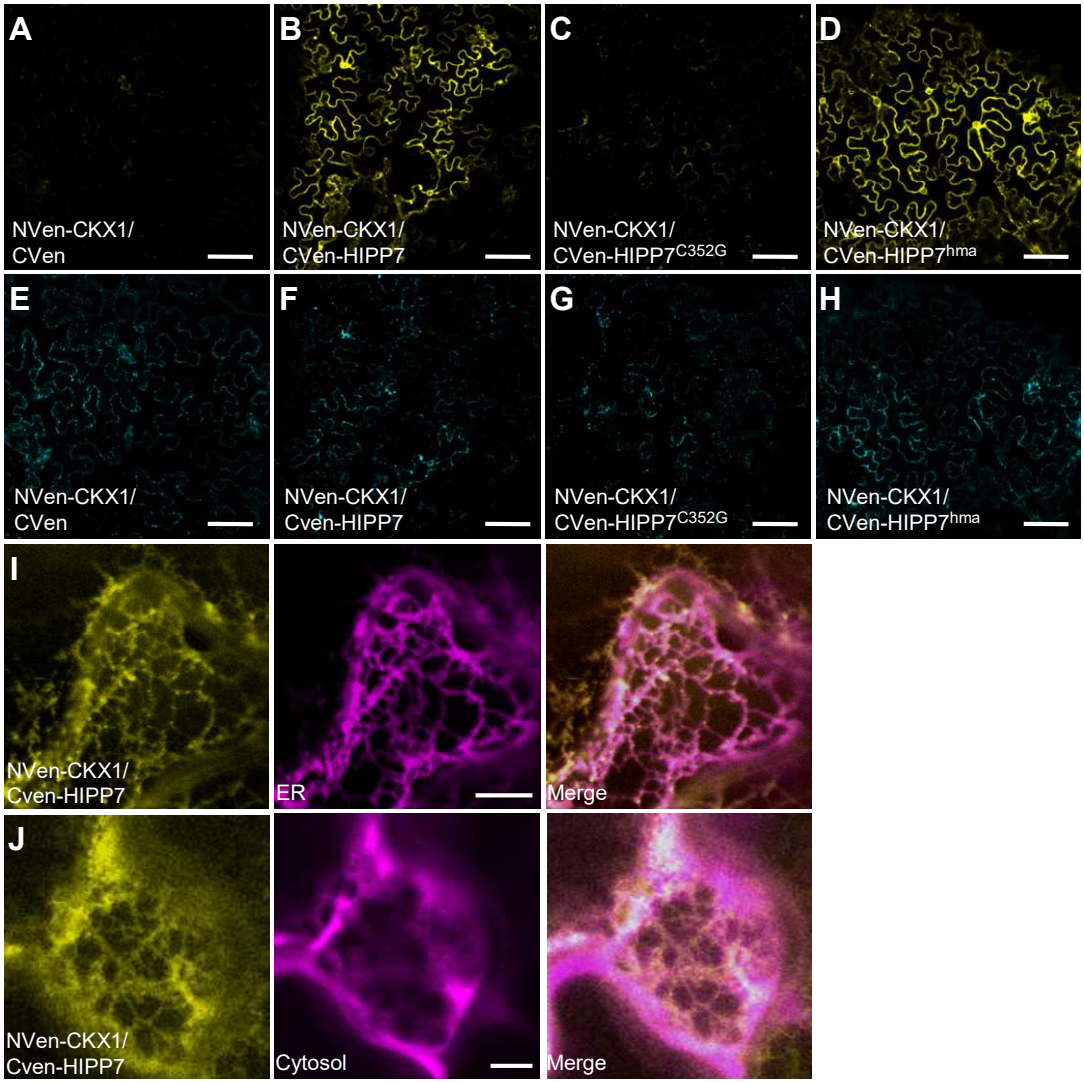

Figure 13. CKX1 interacts with HIPP7 protein *in planta*.
(A) and **(E)** Confocal microscopy analysis of bimolecular fluorescence complementation assay (BiFC) in *N. benthamiana* epidermal leaf cells shows that no background BiFC fluorescence **(A)** is produced when the NVen-CKX1/CVen parent vector is expressed as indicated by the mTq2 fluorescence **(E)**.
(B) and **(F)** The reconstitution of the Venus-derived fluorescence (yellow) demonstrates NVen-CKX1 interaction with CVen-HIPP7 **(B)**. mTq2 control **(F)**.
(C) and **(G)** No or very weak BiFC signal is produced when NVen-CKX1 is co-expressed with CVen-HIPP7^{C352G} **(C)**. mTq2 control **(G)**.
(D) and **(H)** The reconstitution of the Venus-derived fluorescence (yellow) demonstrates NVen-CKX1 interaction with CVen-HIPP7^{hma} **(D)**. mTq2 control **(H)**.
(I) NVen-CKX1/CVen-HIPP7 BiFC fluorescence signal localizes to the cortical ER and small punctate structures. Yellow, Venus BiFC; magenta, RFP-p24.
(J) NVen-CKX1/CVen-HIPP7 BiFC fluorescence (yellow) does not colocalize with the cytosolic marker pCAMBIA-mCherry (magenta). The BiFC fluorescence mainly labels the cortical ER.
The microscopy was performed 2 days after infiltration (DAI).Scale bars = 100 µm (A-H), 10 µm (I) and 5µm (J).

HIPP7 mutant lacking the prenylation site did not or only very weakly interact with CKX1 in the BiFC assay (Fig. 13C), confirming the hypothesis that the posttranslational modification is required for the complex formation. The interaction of CKX1 with HIPP7 was not affected in the BiFC system when both metal-binding cysteine residues in each of the two HMA domains were mutated to glycine, suggesting that heavy metal binding is dispensable for CKX-HIPP interactions. Interestingly, unlike the NVen-CKX1/CVen-HIPP7, the NVen-CKX1/CVen -HIPP7^{hma} complex signal was mainly localized in the cytoplasm (Fig. 13D).

Similar BiFC experiment was designed to test interaction between CKX1 and HIPP1. As shown in Fig. 14A, a clear BiFC signal was detected for the NVen-CKX1/CVen-HIPP1 pair. The fluorescence signal was mainly localized in the nucleus and in the cytoplasm (Fig. 14B), suggesting that the protein complex also involves the cellular fraction of the CKX1 protein presumably retrotranslocated to the cytosol. However, unlike NVen-CKX1/CVen-HIPP7, the NVen-CKX1/CVen-HIPP1 complex was not detected in the ER, suggesting that the CKX1/CVen-HIPP1 complex was extracted from the ER membrane upon CKX1 retrotranslocation. It is worth to note, that the microscopic evaluation of multiple BiFC experiments revealed consistently weaker fluorescence of the CKX1-HIPP1 BiFC complex in comparison to that of CKX1-HIPP7 BiFC pair, which contrast with the strongest protein-protein interaction observed between CKX1 and HIPP1 in yeast.

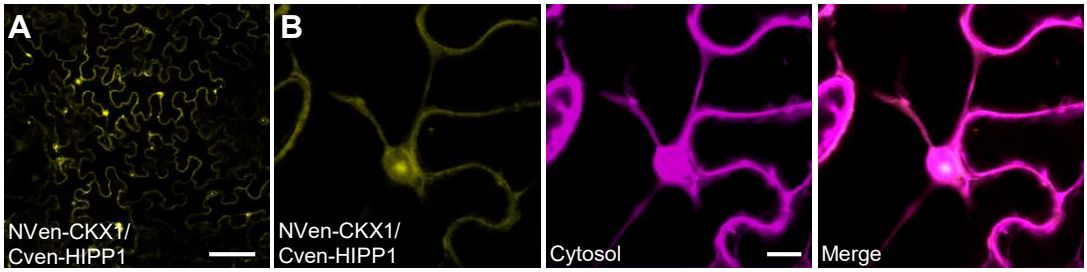

Figure 14. CKX1 interacts with HIPP1 protein *in planta*.
(A) The reconstitution of the Venus-derived fluorescence demonstrates NVen-CKX1 interaction with CVen-HIPP1.
(B) NVen-CKX1/CVen-HIPP1 BiFC (yellow) signal is distributed mainly in the nucleus and weakly in the cytoplasm as indicated by the colocalization with pCAMBIA-mCherry (magenta).
The microscopy was performed 2 days after infiltration (DAI). Scale bars = 100 µm (A) and 10 µm (B).

To verify the HIPP7 homodimerization and to confirm the results revealed by Y2H that both isoprenylation and metal binding are essential for the HIPP7 homocomplex formation, BiFC assays with HIPP7, HIPP7^{C352G}, and HIPP7^{hma} cloned into pDOE-08 vector were performed. The parent vector expressing NVen-HIPP7 together with unfused CVen was used as control. As illustrated in Fig. 15A, no or very weak BiFC was detected in cells expressing the control vector. Similar to the parent vector, the cells expressing the NVen-HIPP7/CVen-HIPP7^{C352G} or NVen-HIPP7/CVen-HIPP7^{hma} constructs showed no or weak fluorescence (Fig. 15C and D), indicating that both motifs contribute essentially to the formation of HIPP homodimers. In

contrast, all cells transformed with the vector expressing NVen-HIPP7 and CVen-HIPP7 showed strong Venus fluorescence (Fig. 15B), indicating the formation of HIPP7 homocomplex *in planta*.

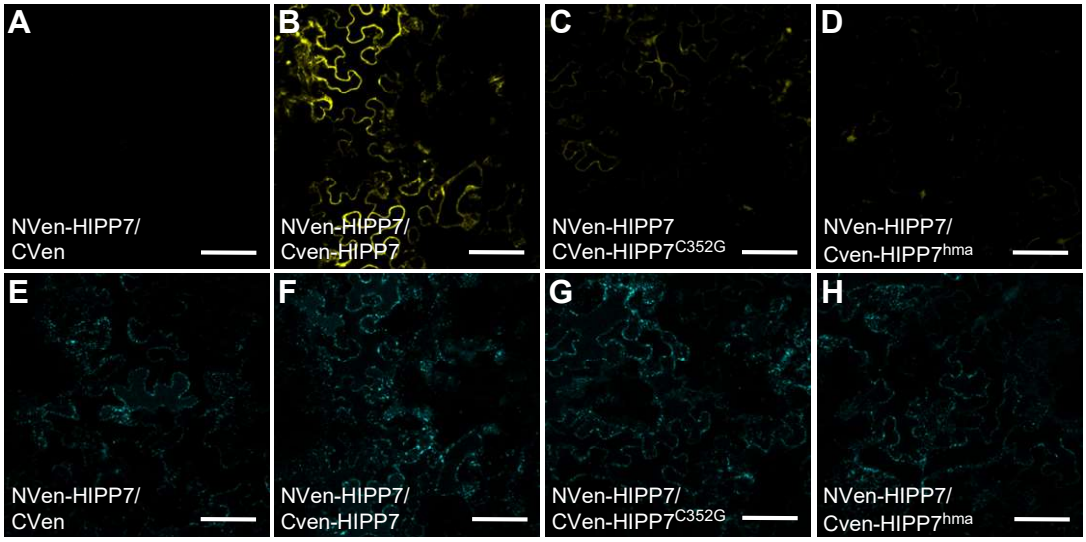

Figure 15. HIPP7 homodimerization in BiFC requires prenylation and heavy-metal binding.
(A) and **(E)** Confocal microscopy analysis of bimolecular fluorescence complementation assay (BiFC) in *N. benthamiana* epidermal leaf cells shows that no background BiFC fluorescence **(A)** is produced when the NVen-HIPP7/CVen parent vector is expressed as indicated by the mTq2 fluorescence **(E)**.
(B) and **(F)** The reconstitution of the Venus-derived fluorescence (yellow) demonstrates NVen-HIPP7 interaction with CVen-HIPP7 **(B)**. mTq2 control **(F)**.
(C) and **(G)** No or very weak BiFC signal is produced when NVen-HIPP7 is co-expressed with CVen-HIPP7^{C352G} **(C)**. mTq2 control **(G)**.
(D) and **(H)** No BiFC signal is produced when NVen-HIPP7 is co-expressed with CVen-HIPP7^{hma} **(D)**. mTq2 control **(H)**.
The microscopy was performed 2 days after infiltration (DAI). Scale bars = 100 µm

3.2 Overexpression of clade-I *HIPP* genes causes pleiotropic phenotypes and alters cytokinin activity

Strategy to explore the physiological function of the isolated HIPP proteins is to enhance or reduce levels of gene activity. To this end, we first performed gain-of-function experiments by expressing HIPP6 and HIPP7 N-terminally fused to GFP tag under the control of the cauliflower mosaic virus 35S promoter in Arabidopsis plants. Independent homozygous lines expressing *35S:GFP-HIPP6* and *35S:GFP-HIPP7* (called *35S:HIPP6* and *35S:HIPP7*, respectively, in the following) were identified. The transcript levels of *HIPP6* or *HIPP7* were enhanced in all of the overexpression lines as compared to WT plants (Fig. 16A and C). In accordance, immunoblot analysis confirmed that high levels of the GFP-HIPP6 and GFP-HIPP7 proteins accumulated in the respective overexpression lines (Fig. 16B and D). Interestingly, immunoblot analysis suggested that an apparently stable HIPP7 complex, which is more abundant than the monomeric GFP-HIPP7 protein.

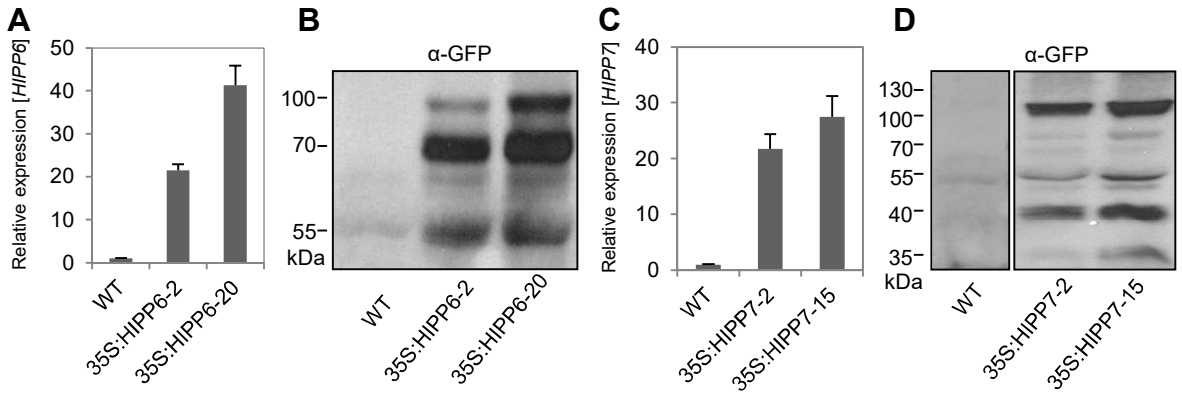

Figure 16. *HIPP* gene expression and protein levels in transgenic Arabidopsis plants.
(A) Relative transcript abundances of the *HIPP6* gene in shoots of the *35S:HIPP6* seedlings grown on soil for 15 days as measured by qRT-PCR. Data are means ± SE (n = 4).
(B) Representative Western blot analysis of the GFP-HIPP6 protein levels in two independent homozygous transgenic lines.
(C) Relative transcript abundances of the *HIPP7* gene in shoots of the *35S:HIPP7* seedlings grown on soil for 15 days as measured by qRT-PCR. Data are means ± SE (n = 4).
(D) Representative Western blot analysis of the GFP-HIPP7 protein levels in two independent homozygous transgenic lines.

During the course of the PhD project, the 35S-driven *HIPP* expression was found to be occasionally silenced. This part of the project was elaborated in more detail in a master thesis, which I co-supervised (Alcaniz Rolli, 2016). In order to avoid gene silencing by using the viral 35S promoter, transgenic lines expressing *GFP-HIPP1* under the control of the *UBQ10* promoter were generated (called *UBQ10:HIPP1* in the following). Independent homozygous

lines were identified and the transcript abundances and protein levels determined (Fig. 17A and B).

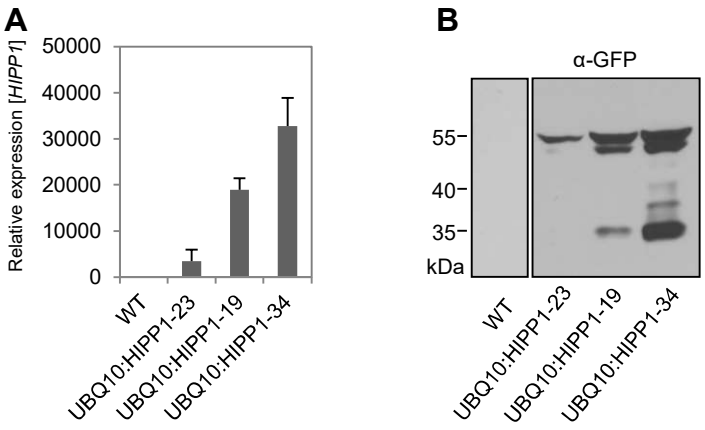

Figure 17. mRNA and protein levels in *HIPP1*-overexpression plants.
(A) Relative transcript abundances of the *HIPP1* gene in shoots of the *UBQ10:HIPP1* seedlings grown on soil for 15 days as measured by qRT-PCR. Data are means ± SE (n = 4). It should be noted that relative transcript abundances of the *HIPP1* gene in the WT was low and 100 ng instead of 10 ng cDNA was used as template.
(B) Representative Western blot analysis of the GFP-HIPP1 protein levels in three independent homozygous transgenic lines.

3.2.1 Phenotypic characterization of *HIPP*-overexpression plants

The *35S:HIPP6* and *35S:HIPP7* overexpression lines developed very similar pleiotropic phenotypes which have not been observed during previous attempts to overexpress *HIPP6*/*Cdl19* (Suzuki et al., 2002). Transgenic lines expressing either construct did not differ from WT in their seedling morphology. However, the *35S:HIPP6* and *35S:HIPP7* plants developed smaller rosettes leaves with strongly altered morphology in their later growth and development (Fig. 18A and B). The rosette diameter was 74 to 75% of the WT diameter for the two *35S:HIPP6* transgenic lines and 65 to 85% of the WT diameter for *35S:HIPP7* individual transgenic lines (Fig. 18C). The leaves of the transgenic plants were characterized by shorter petioles and smaller and crinkly lamina in comparison to WT (Fig. 18D). As leaf size and shape is determined by patterns of cell division and cell expansion, the cell size of epidermal cells in the fully developed rosette leaves of WT and *35S:HIPP7* plants were compared. Microscopic analysis revealed a strongly increased number of the *35S:HIPP7* epidermal cells, which were reduced in size by ~60% in comparison to WT (Fig. 18E).
Moreover, whereas differentiated adaxial epidermal pavement cells of WT plants had characteristic puzzle shape morphology, the *35S:HIPP7* cells developed much less convoluted shape with fewer lobes and indentations (Fig. 18G), suggesting a delayed differentiation. This notion was corroborated by frequent occurrence of apparently recent cell division events in the expanded *35S:HIPP7* leaves (newly formed cell walls with a straight appearance are indicated by arrowheads in Fig. 18G).

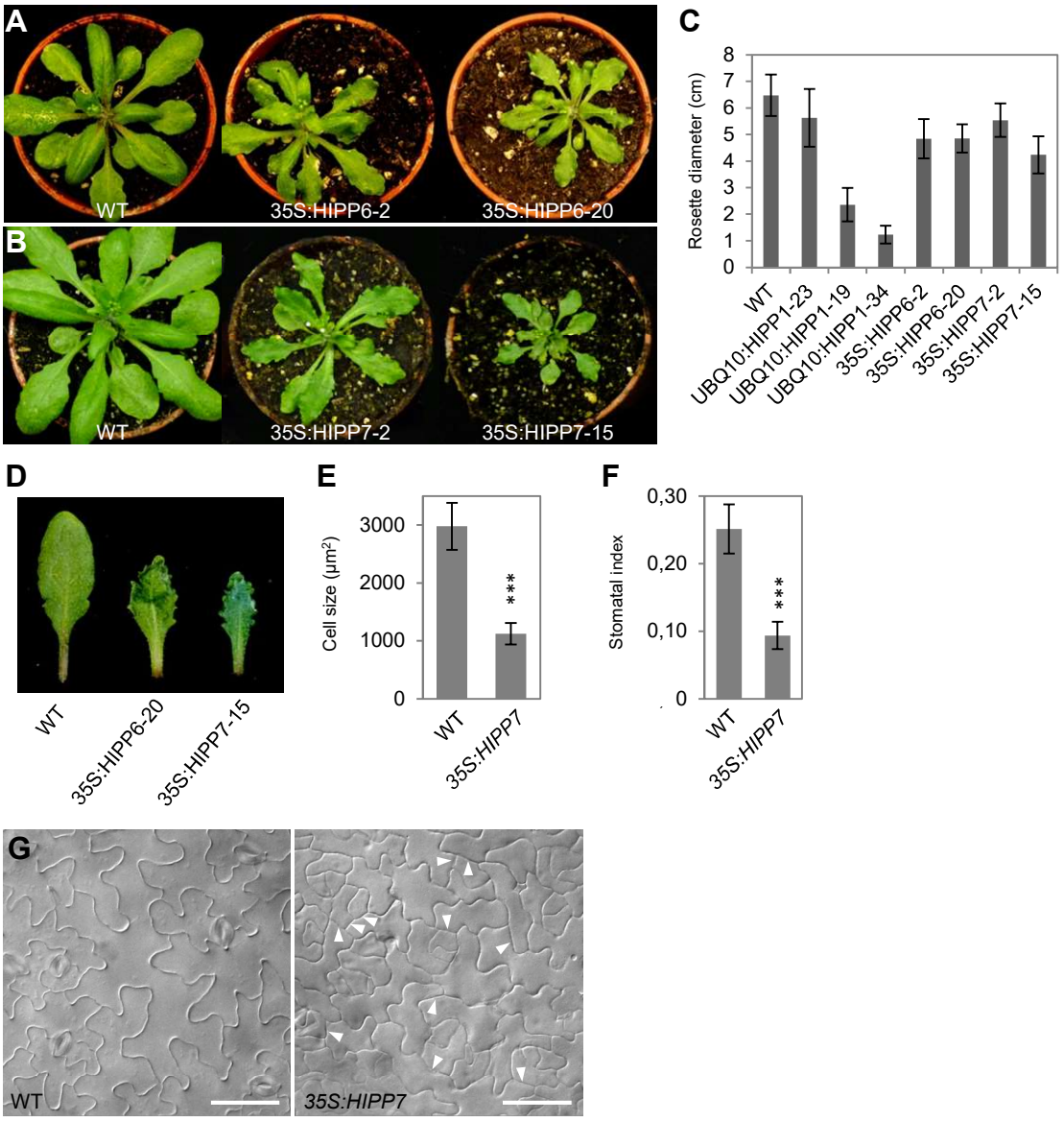

Figure 18. Overexpression of clade-I *HIPP* genes alters the leaf development.
(A) and **(B)** 4-week-old plants overexpressing *35S:HIPP6* **(A)** and *35S:HIPP7* **(B)**. Two independent lines are show for each construct.
(C) Rosette diameter of the wild type (WT) and independent homozygous lines of plants overexpressing *UBQ10:HIPP1, 35S:HIPP6* and *35S:HIPP7*. The rosette diameter was determined 23 DAG. Data are means ± SD (*n* = 25).
(D) Morphology of 6th rosette leaves of the WT and transgenic plants shown in **(A)** and **(B)**.
(E) and **(F)** Average size of abaxial epidermal cells **(E)** and the stomatal index **(F)** of the 5th and 6th rosette leaves of the WT and 35S:HIPP7-15 line 28 DAG. Data are means ± SD (*n* ≥ 15). ***P < 0.005, calculated by Student's *t* test.
(G) Abaxial epidermis of 6th leaf of WT and 35S:HIPP7-15 line 28 DAG. Cells at 25% distance from tip to base are shown. Examples of apparently recent cell walls are indicated by arrowheads. Scale bars = 50 µm.

Next we analyzed the stomatal cells, which originate in the leaf epidermis through a series of cell divisions followed by differentiation of cells of the stomatal lineage (Bergmann and Sack, 2007). The number of stomata per unit area was decreased by 45% in *35S:HIPP7* leaves and the stomatal index, which is the fraction of stomata in the total epidermal cell population, was decreased by >60% in comparison to WT (Fig. 18F). Therefore, consistent with the observed

delay in differentiation of the pavement cells, the data indicate that *HIPP7* expression inhibits also differentiation of other cell types in the leaf.

In addition to the leaf phenotype, the reproductive development of *35S:HIPP6* and *35S:HIPP7* transgenic lines was also delayed as the transgenic plants flowered significantly later than the WT. The WT plants flowered at 22 days after germination (DAG) under LD conditions. In contrast, the *35S:HIPP6* and *35S:HIPP7* flowered at 34 and 28 DAG under LD conditions, respectively (Fig. 19A). These results indicate that *HIPP*-overexpression delays the onset of flowering.

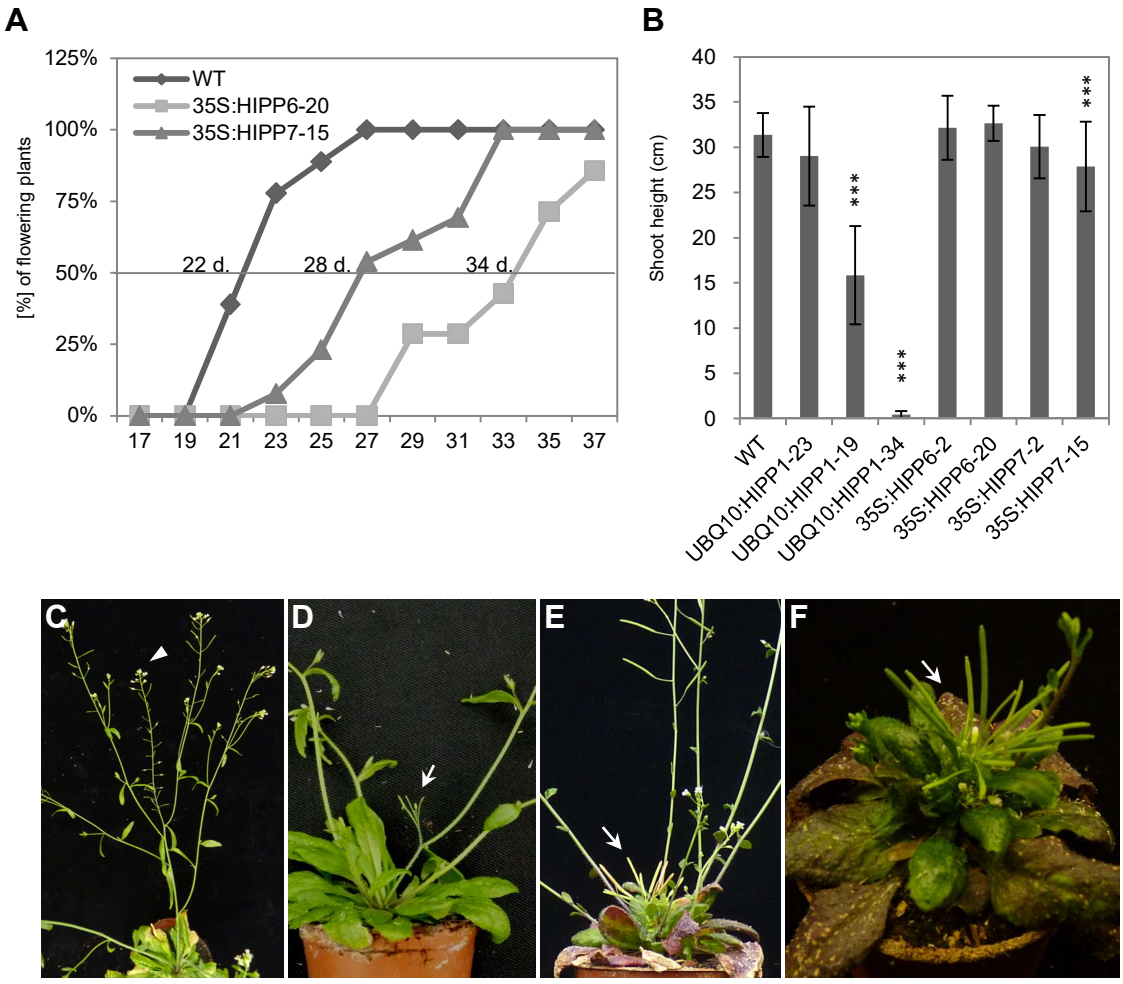

Figure 19. *HIPP* overexpression delays flowering and inhibits inflorescence shoot growth.
(A) Flowering time under long-day conditions of WT, *35S:HIPP6* and *35S:HIPP7* ($n > 20$).
(B) Shoot height of fully grown plants of the wild type (WT) and independent homozygous lines of plants overexpressing *UBQ10:HIPP1, 35S:HIPP6* and *35S:HIPP7*. Data are means ± SD ($n = 25$). ***$P < 0.005$, calculated by Student's *t* test.
(C) to **(F)** Reduced apical dominance of the primary inflorescence stem (arrowhead) and reduced or arrested inflorescence meristems (arrows) in *UBQ10:HIPP1* **(C)**, *35S:HIPP6* **(D)**, and *UBQ10:HIPP7* **(E)** and **(F)** plants.

The selected *UBQ10:HIPP1* transgenic lines displayed overall similar, in part more severe, phenotypic changes as the *35S*-driven *HIPP6* and *HIPP7* (Fig. 21). The rosette diameter was 18 to 86% of the WT diameter for the three analyzed *UBQ10:HIPP1* transgenic lines (Fig.

18C), and the phenotypic severity correlated with the transgene transcript and protein levels (Fig. 17A and B).

Moreover, the transgenic plants overexpressing clade-I *HIPP* genes had a significantly retarded shoot height in comparison to WT plants, which was most evident in the *UBQ10:HIPP1* transgenic plants (Fig. 19B). Furthermore, several *HIPP*-overexpressing plants displayed with incomplete penetrance a loss of primary inflorescence shoot dominance and a reduced inflorescence meristem activity (Fig. 19C-E). Interestingly, some transgenic lines, in particular the *UBQ10*-driven *HIPP7* transgenic plants (3.2.2.1), exhibited more severe defects in shoot apical with completely arrested and differentiated inflorescence meristems (Fig. 19F).

Together, the results described above show that the enhanced expression of different clade-I *HIPP* genes causes similar phenotypic changes. Many of those changes, including the leaf margin serration, the promotion of division and inhibition of differentiation of the epidermal cells strongly resemble those in plants with increased cytokinin content or activity (Rupp et al., 1999; Steiner et al., 2012; Efroni et al., 2013; Li et al., 2013a).

3.2.2 Cytokinin status in shoot

3.2.2.1 Clade-I HIPPs enhance leaf responses to cytokinin in a prenylation-dependent manner

To find out whether the phenotypic changes in the *HIPP*-overexpressing plants are related to altered cytokinin responses and to know how HIPP proteins influence the cytokinin activity, we increased the endogenous cytokinin content in the analyzed plants by treatment with INCYDE, an effective inhibitor of CKX proteins (Zatloukal et al., 2008; Niemann et al., 2015), and analyzed the leaf growth responses. Fig. 20A and B show that WT responded to the low INCYDE concentration by increasing the leaf surface area, which is typical for plants treated with low cytokinin concentrations (Efroni et al., 2013) or for plants displaying enhanced cytokinin activity (Bartrina et al., 2017). In contrast, the leaf areas of *35S:HIPP6* and *35S:HIPP7* plants were reduced in response to already low INCYDE concentration and the reduction was significantly stronger after treatment with higher concentrations of the inhibitor in comparison to WT. Moreover, the crinkly leaf phenotype was strongly enhanced after the inhibitor treatment (Fig. 20A). Together, these results suggest that the *35S:HIPP6* and *35S:HIPP7* plants are hypersensitive to cytokinin.

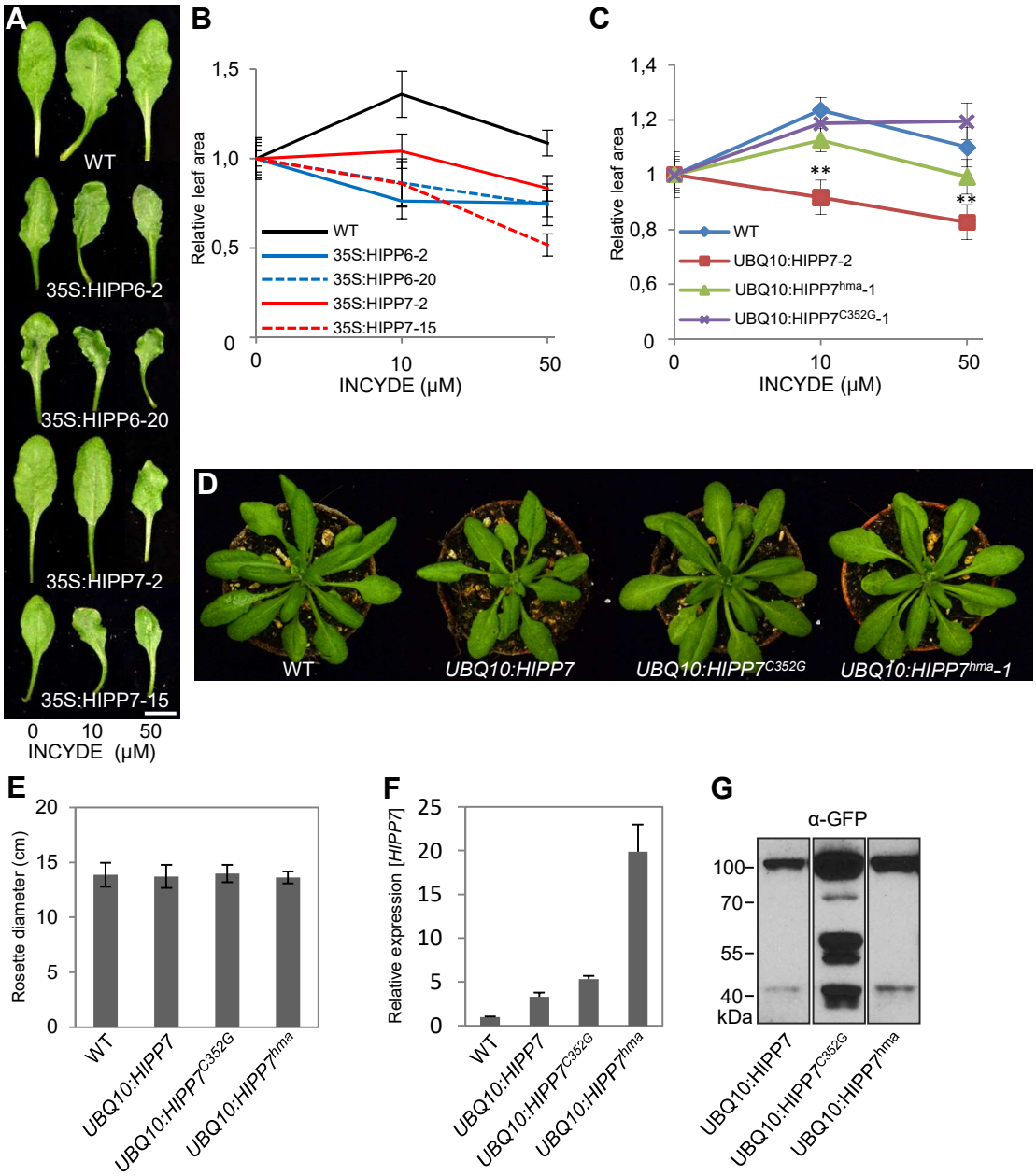

Figure 20. Clade-I HIPPs enhance leaf responses to cytokinin in a prenylation-dependent manner.

(A) Leaf 7 from wild type (WT) and two independent homozygous lines expressing *35S:HIPP6* and *35S:HIPP7* treated repeatedly with INCYDE (10 and 50 µM) for 4 weeks. Bar = 1 cm.

(B) Relative growth of rosette leaf 7 of WT and plants expressing *35S:HIPP6* and *35S:HIPP7* after 4 weeks of repeated INCYDE application. Data are means ± SE (n = 8-9). All mutant lines differed significantly from the WT for both INCYDE treatments (Student's t test, $P < 0.05$).

(C) Relative growth of rosette leaf 7 of WT and plants expressing *UBQ10:HIPP7*, *UBQ10:HIPP7*^{C352G} and *UBQ10:HIPP7*^{hma} after 4 weeks of repeated INCYDE application. Data are means ± SE (n = 8). $^{**}P < 0.01$, calculated by Student's t test.

(D) Four-week-old plants expressing *UBQ10;HIPP7*, *UBQ10:HIPP7*^{C352G} and *UBQ10:HIPP7*^{hma} under the control of the *UBQ10* promoter.

(E) Rosette diameter of the wild type (WT) and independent homozygous lines of plants overexpressing *UBQ10;HIPP7*, *UBQ10:HIPP7*^{C352G} and *UBQ10:HIPP7*^{hma}. The rosette diameter was determined 23 DAG. Data are means ± SD (n = 25).

(F) Relative transcript abundances of the *HIPP7* transgenes in shoots of the *UBQ10;HIPP7*, *UBQ10:HIPP7*^{C352G} and *UBQ10:HIPP7*^{hma} seedlings grown on soil for 15 days as measured by qRT-PCR. Data are means ± SE (n = 4).

(G) Representative Western blot analysis of the GFP-HIPP7, GFP-HIPP7^{C352G} and GFP-HIPP7^{hma} protein levels in selected homozygous transgenic lines.

To test the effect of *HIPP* expression on cytokinin sensitivity in more detail and to avoid the strong leaf morphological changes associated with the *35S:HIPP* expression, transgenic lines expressing *GFP-HIPP7* under the control of the *UBQ10* promoter (called *UBQ10:HIPP7* in the following) were generated. Selected *UBQ10:HIPP7* lines displayed no detectable changes in leaf morphology under the control conditions (Fig. 20D and E). Nevertheless, the *UBQ10:HIPP7* leaves responded more sensitive towards the INCYDE treatment than WT (Fig. 20C), corroborating the notion of the increased cytokinin sensitivity through *HIPP* expression. Most importantly, the hypersensitive responses were completely abolished in plants expressing the HIPP7 mutant form lacking the prenyl-accepting site (*UBQ10:HIPP7*^{C352G}; Figure 20C), although the mutant protein was expressed higher than the respective HIPP7 WT protein form in *UBQ10:HIPP7* plants (Fig. 20F and G). Plants expressing the HIPP7 mutant with mutated HMA domains (*UBQ10:HIPP7*^{hma}) displayed a reproducible, but statistically not significant, increase in cytokinin sensitivity (Fig. 20C). These data suggest that the CKX-HIPP complex formation triggered by the *HIPP7*-expression is causal for the enhanced cytokinin sensitivity.

Similarly to *HIPP6* and *HIPP7*, an increased sensitivity towards cytokinin was observed also in the generated independent *UBQ10:HIPP1* lines. As shown in Fig. 21, compared to WT plants, the *UBQ10:HIPP1* lines produced smaller yellow leaves with excessive serrations when repeatedly sprayed with exogenous cytokinin. Together, these results suggest that overexpressing of HIPP proteins elevated plants responses to cytokinin.

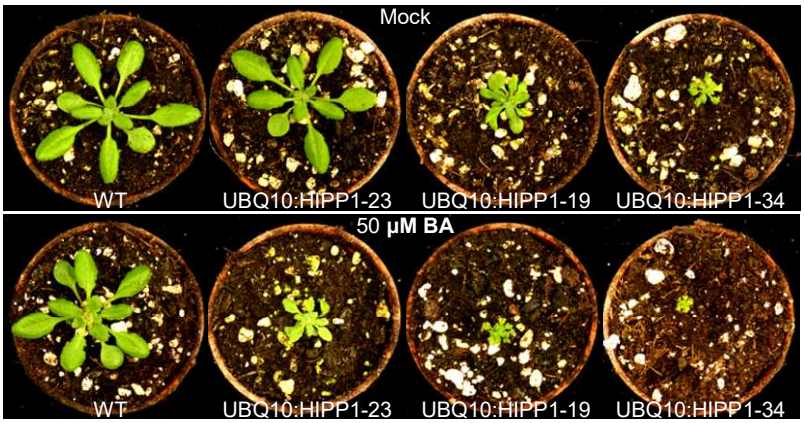

Figure 21. HIPP1 enhances cytokinin sensitivity in leaves.
Effects on the growth of shoots of independent *UBQ10:HIPP1* transgenic lines after 3 weeks of repeated 50 µM benzyladenine (BA) application.

3.2.2.2 *IPT3* gain-of-function mutation enhances the *HIPP*-overexpression phenotypes

To further explore the influence of altered cytokinin activity on the development of *HIPP*-overexpressing plants, *35S:HIPP7* plants were crossed with *repressor of cytokinin*

deficiency4 (*rock4*), which is a dominant gain-of-function mutation of cytokinin biosynthesis *IPT3* gene with increased endogenous cytokinin content (Jensen, 2013). This mutant was isolated based on its ability to suppress the cytokinin-deficient phenotypes (Niemann et al., 2015). Fig. 22 illustrates that the elevated cytokinin biosynthesis in the hybrid plants severely enhanced the *35S:HIPP7* leaf developmental defects corroborating the enhanced cytokinin sensitivity of the transgenic line.

Figure 22. A gain-of-function mutation in *IPT3* enhances the *35S:HIPP7* leaf phenotypic changes.
A dominant gain-of-function mutation of cytokinin biosynthesis *IPT3* gene (*rock4*; *repressor of cytokinin deficiency4*) enhances the *35S:HIPP7* leaf developmental defects. Please note the reduced leaf size and extensive serration in the hybrid plants. F1 hybrid plants 28 DAG are shown.

3.2.2.3 Impact of *HIPP* overexpression on endogenous cytokinin concentration

As next we analyzed whether the observed phenotypic changes in *HIPP*-overexpressing plants were reflected by the content of the endogenous cytokinins. The analysis of 2-week-old *35:HIPP6* and *35S:HIPP7* shoots revealed that the content of most cytokinin metabolites was relatively weakly changed (Table 17).

Table 17: Cytokinin content of *35S:HIPP6* and *35S:HIPP7* Arabidopsis plants.

Genotype	iP	iPR	iPRMP	iP9G	tZ	tZR	tZRMP	tZ9G
WT	0.46 ± 0.09	8.28 ± 1.85	17.62 ± 4.35	0.83 ± 0.03	1.93 ± 0.19	13.09 ± 0.73	33.73 ± 5.94	18.86 ± 0.68
35S:HIPP6-2	0.55 ± 0.09	6.78 ± 1.44	11.22 ± 2.23	0.84 ± 0.07	1.74 ± 0.31	12.90 ± 2.53	26.14 ± 5.29	18.20 ± 1.92
35S:HIPP6-21	0.36 ± 0.09	7.64 ± 1.29	8.91 ± 0.87	0.64 ± 0.04	1.29 ± 0.27	12.45 ± 1.74	19.75 ± 4.92	15.65 ± 0.86
35S:HIPP7-2	0.48 ± 0.09	8.14 ± 0.64	13.84 ± 1.81	0.96 ± 0.12	1.86 ± 0.22	16.07 ± 2.24	29.90 ± 6.02	21.81 ± 2.63
35S:HIPP7-15	0.48 ± 0.11	6.48 ± 0.90	11.38 ± 2.17	0.97 ± 0.10	1.66 ± 0.18	11.58 ± 2.19	24.36 ± 3.90	20.90 ± 0.62

Genotype	tZOG	tZROG	cZ	cZR	cZRMP	cZOG	cZROG
WT	5.27 ± 0.87	1.12 ± 0.16	0.05 ± 0.01	0.58 ± 0.14	3.21 ± 0.59	0.27 ± 0.04	0.26 ± 0.01
35S:HIPP6-2	6.14 ± 0.70	1.00 ± 0.03	0.13 ± 0.03	1.67 ± 0.42	6.22 ± 0.37	0.43 ± 0.10	0.40 ± 0.10
35S:HIPP6-21	7.48 ± 0.52	1.06 ± 0.09	0.14 ± 0.03	3.13 ± 0.91	7.07 ± 0.78	0.60 ± 0.08	0.66 ± 0.14
35S:HIPP7-2	6.09 ± 0.13	1.04 ± 0.09	0.10 ± 0.01	1.36 ± 0.25	4.66 ± 0.18	0.38 ± 0.03	0.24 ± 0.04
35S:HIPP7-15	6.02 ± 0.35	0.95 ± 0.13	0.09 ± 0.02	1.81 ± 0.52	5.25 ± 0.47	0.43 ± 0.06	0.26 ± 0.02

Whole rosettes (15 DAG) were analyzed. iP, N^6-(Δ^2-isopentenyl)adenine; iPR, N^6-(Δ^2-isopentenyl)adenosine; iPRMP, N^6-(Δ^2-isopentenyl)adenosine 5'-monophospate; iP9G, N^6-(Δ^2-isopentenyl)adenine 9-glucoside; tZ, *trans*-zeatin; *t*ZR, *trans*-zeatin riboside; *t*ZRMP, *trans*-zeatin riboside 5'-monophosphate; *t*Z9G, *trans*-zeatin 9-glucoside; *t*ZOG, *trans*-zeatin *O*-glucoside; *t*ZROG, *trans*-zeatin riboside *O*-glucoside; *c*Z, *cis*-zeatin; *c*ZR,

cis-zeatin riboside; *c*ZRMP, *cis*-zeatin riboside 5'-monophosphate; cZOG, *cis*-zeatin *O*-glucoside; *c*ZROG, *cis*-zeatin riboside *O*-glucoside. Data shown are pmol/g fresh weight ± SD; *n* = 3.

The strongest changes were detected for isopentenyladenine (iP) and *trans*-zeatin (tZ) nucleotides, which were reduced to 50% of the WT levels, whereas the concentrations of cytokinin *O*-glucosides were significantly increased (Table 17). Interestingly, in contrast to iP- and tZ-type cytokinins, all *cis*-zeatin (cZ) metabolites, including the free cZ base, were strongly increased in all transgenic lines in comparison to WT (Table 17).
Similar changes were detected at the later developmental stages (Table 18). Together, the complex changes of the cytokinin profiles indicate that a number of homeostatic reactions were activated in response to the expression of different *HIPP* genes.

Table 18: Cytokinin content of *HIPP*-overexpressing Arabidopsis plants.

genotype	iP	iPR	iPRMP	iP9G	tZ	tZR	tZRMP	tZ9G
WT	0.97 ± 0.22	1.43 ± 0.21	38.25 ± 6.13	1.28 ± 0.15	1.78 ± 0.35	4.55 ± 1.13	50.89 ± 8.94	30.95 ± 4.09
UBQ10:HIPP1-23	0.42 ± 0.06	0.89 ± 0.26	15.74 ± 1.80	1.01 ± 0.19	1.44 ± 0.24	2.09 ± 0.53	29.02 ± 4.21	22.70 ± 2.87
UBQ10:HIPP1-19	1.22 ± 0.35	1.98 ± 0.44	11.85 ± 1.31	0.66 ± 0.06	0.88 ± 0.13	1.74 ± 0.41	13.50 ± 2.96	15.04 ± 0.89
UBQ10:HIPP1-34	0.85 ± 0.02	1.46 ± 0.11	9.67 ± 0.40	0.77 ± 0.02	0.74 ± 0.07	1.41 ± 0.05	9.59 ± 0.92	11.29 ± 0.61
35S:HIPP6-2	0.55 ± 0.06	1.05 ± 0.26	23.43 ± 1.38	0.81 ± 0.06	1.24 ± 0.10	3.76 ± 0.64	36.83 ± 3.06	21.24 ± 0.45
35S:HIPP6-21	0.51 ± 0.15	0.96 ± 0.16	22.65 ± 1.78	0.96 ± 0.08	1.39 ± 0.15	3.72 ± 1.02	36.49 ± 4.87	22.66 ± 1.02
35S:HIPP7-2	0.62 ± 0.08	1.48 ± 0.34	22.86 ± 3.26	1.20 ± 0.15	1.54 ± 0.12	4.98 ± 0.87	42.45 ± 3.26	25.95 ± 2.28
35S:HIPP7-15	0.54 ± 0.15	1.73 ± 0.24	18.74 ± 2.35	0.83 ± 0.08	1.28 ± 0.16	4.29 ± 0.59	25.72 ± 3.34	19.09 ± 1.43

genotype	tZOG	tZROG	cZ	cZR	cZRMP	cZOG	cZROG
WT	8.04 ± 1.49	1.28 ± 0.30	0.05 ± 0.01	0.36 ± 0.08	4.98 ± 0.81	0.89 ± 0.18	1.06 ± 0.10
UBQ10:HIPP1-23	7.69 ± 0.77	1.32 ± 0.18	0.05 ± 0.01	0.41 ± 0.08	4.95 ± 0.44	0.79 ± 0.16	1.25 ± 0.22
UBQ10:HIPP1-19	11.31 ± 0.94	1.85 ± 0.11	0.30 ± 0.08	1.33 ± 0.20	10.39 ± 1.32	4.23 ± 0.47	8.93 ± 1.03
UBQ10:HIPP1-34	14.04 ± 1.17	2.40 ± 0.44	0.33 ± 0.04	1.58 ± 0.16	12.00 ± 0.69	7.10 ± 0.55	21.42 ± 2.57
35S:HIPP6-2	9.25 ± 1.07	1.01 ± 0.18	0.06 ± 0.01	0.42 ± 0.09	6.49 ± 1.07	1.28 ± 0.11	1.81 ± 0.11
35S:HIPP6-21	9.66 ± 1.28	1.10 ± 0.21	0.06 ± 0.01	0.46 ± 0.04	6.66 ± 0.58	1.32 ± 0.10	1.93 ± 0.17
35S:HIPP7-2	8.43 ± 0.84	1.12 ± 0.17	0.04 ± 0.00	0.46 ± 0.06	5.56 ± 0.59	0.97 ± 0.12	1.08 ± 0.11
35S:HIPP7-15	9.52 ± 0.87	1.03 ± 0.19	0.10 ± 0.02	0.78 ± 0.13	6.94 ± 0.53	1.25 ± 0.17	1.78 ± 0.32

The 6th and 7th rosette leaves (23 DAG) were analyzed. iP, N^6-(Δ^2-isopentenyl)adenine; iPR, N^6-(Δ^2-isopentenyl)adenosine; iPRMP, N^6-(Δ^2-isopentenyl)adenosine 5'-monophospate; iP9G, N^6-(Δ^2-isopentenyl)adenine 9-glucoside; tZ, *trans*-zeatin; *t*ZR, *trans*-zeatin riboside; *t*ZRMP, *trans*-zeatin riboside 5'-monophosphate; *t*Z9G, *trans*-zeatin 9-glucoside; *t*ZOG, *trans*-zeatin *O*-glucoside; *t*ZROG, *trans*-zeatin riboside *O*-glucoside; *c*Z, *cis*-zeatin; *c*ZR, *cis*-zeatin riboside; *c*ZRMP, *cis*-zeatin riboside 5'-monophosphate; cZOG, *cis*-zeatin *O*-glucoside; *c*ZROG, *cis*-zeatin riboside *O*-glucoside. Data shown are pmol/g fresh weight ± SD; *n* = 3.

3.2.2.4 *HIPP* overexpression enhances cytokinin activity in shoot

To analyze directly the cytokinin status of the *HIPP*-overexpressing plants, we introgressed the cytokinin output sensor *TCSn:GFP* (Zürcher et al., 2013) in *HIPP1 and*

HIPP7-overexpressing lines. Because the *TCSn:GFP* reporter displays relatively low fluorescence signal in rosette leaves, which was not possible to analyze by microscopy, we analyzed the *TCSn:GFP* expression levels by qRT-PCR. Fig. 23 shows that the *TCSn:GFP* expression levels were significantly increased in the transgenic lines compared to WT. These results correlate with the increased sensitivity of leaves towards the cytokinin and suggest that clade-I HIPP proteins increase cytokinin activities in shoot.

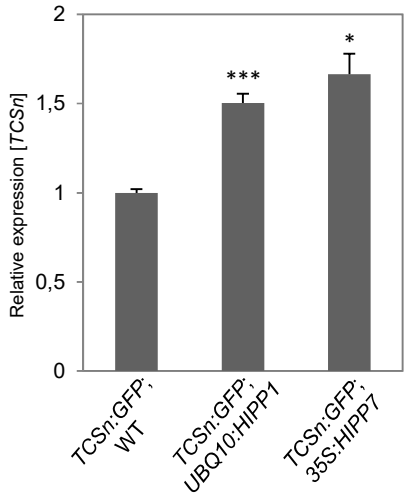

Figure 23. *HIPP*-overexpression enhances cytokinin activity in shoot.
Quantitative RT-PCR (qRT-PCR) analysis of *GFP* transcript levels in rosettes of 15 DAG F1 plants from the crosses of *TCSn:GFP* with the wild-type (WT), UBQ10:HIPP1-19 and 35S:HIPP7-15 plants. Data are means ± SE (n = 3). *P < 0.05, ***P < 0.005, calculated by Student's t test.

3.2.2.5 Differential regulation of type-A *ARR* genes in response to *HIPP*-expression

To further corroborate the results that *HIPP*-expression increased the sensitivity of leaves towards the cytokinin and elevated the expression of cytokinin output sensor *TCSn:GFP*, we analyzed expression of type-A *ARR* genes encoding downstream component of the cytokinin signaling pathway (To et al., 2004). The qRT-PCR analysis revealed a strong upregulation of *ARR5* and *ARR7* in *HIPP*-overexpressing plants (Fig. 24A). Interestingly, the steady-state transcript levels of most analyzed *ARR* genes were unaltered or decreased in comparison to WT (Fig. 24A), suggesting differential regulation of type-A *ARR* genes in response to *HIPP*-expression. Among the strongly downregulated type-A *ARR*s were genes which have previously been shown to be specifically expressed in the expanding leaves and to inhibit cytokinin response, which promotes cell differentiation during the leaf development (Efroni et al., 2013). For example, the *ARR16* transcript levels were severely reduced in *HIPP*-overexpressing leaves in comparison to WT. Moreover, the reduction was progressively stronger during the later stages of leaf maturation (Fig. 24B), which correlates with the

appearance of the severe leaf developmental defects in the transgenic plants. Therefore, in agreement with the inhibitory function of the type-A *ARR* genes on cytokinin response, their diminished expression in *HIPP*-overexpressing plants correlates with the higher steady-state cytokinin signaling detected by *TCSn:GFP*, and with the enhanced cytokinin responsiveness.

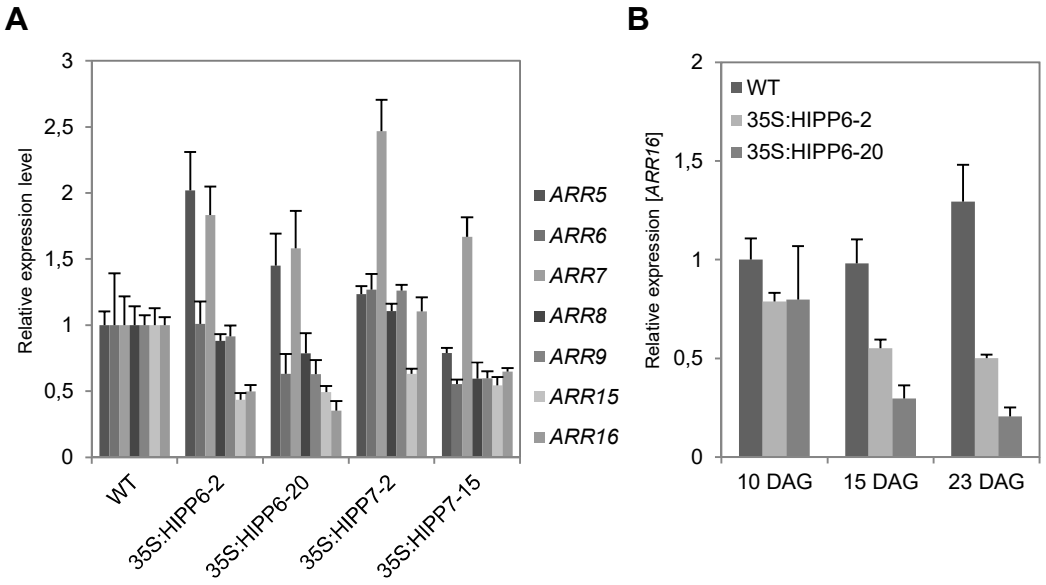

Figure 24. Differential regulation of type-A *ARR* genes in *HIPP*-overexpressing transgenic Arabidopsis plants.
(A) qRT-PCR analysis of type-A *ARRs* steady-state transcript levels in rosettes of WT, *35S:HIPP6*, and *35S:HIPP7* plants 15 DAG. Data are means ± SE (*n* = 4).
(B) qRT-PCR analysis of *ARR16* transcript levels in rosettes of WT and *35S:HIPP6* lines of at indicated developmental time points. Data are means ± SE (*n* = 4).

3.2.2.6 *IPT* gene expression is reduced in shoot of *HIPP*-overexpression lines

On one hand, the elevated *TCSn:GFP* expression levels indicated increased cytokinin activities in shoots of *HIPP*-overexpression lines. On the other hand, the content of some cytokinin metabolites such as iP and tZ nucleotides were reduced. To understand the apparent discrepancy between higher cytokinin activity and reduced cytokinin levels, the expression of several genes for ATP/ADP isopentenyltransferases (IPT) were analyzed. IPTs catalyze the first step of cytokinin biosynthesis in Arabidopsis and are downregulated by cytokinin through a negative feedback loop (Miyawaki et al., 2004). The qRT-PCR analysis revealed a strong downregulation of three analyzed *IPT* genes in *35S:HIPP6* and *35S:HIPP7* overexpressing plants (Fig. 25A). Similarly to *HIPP6* and *HIPP7*, all three *IPT* genes were downregulated in the independent *UBQ10:HIPP1* lines (Fig. 25B). These results thus indicate that cytokinin biosynthesis was partially reduced in response to a higher steady-state cytokinin signaling in the *HIPP*-overexpressing plants.

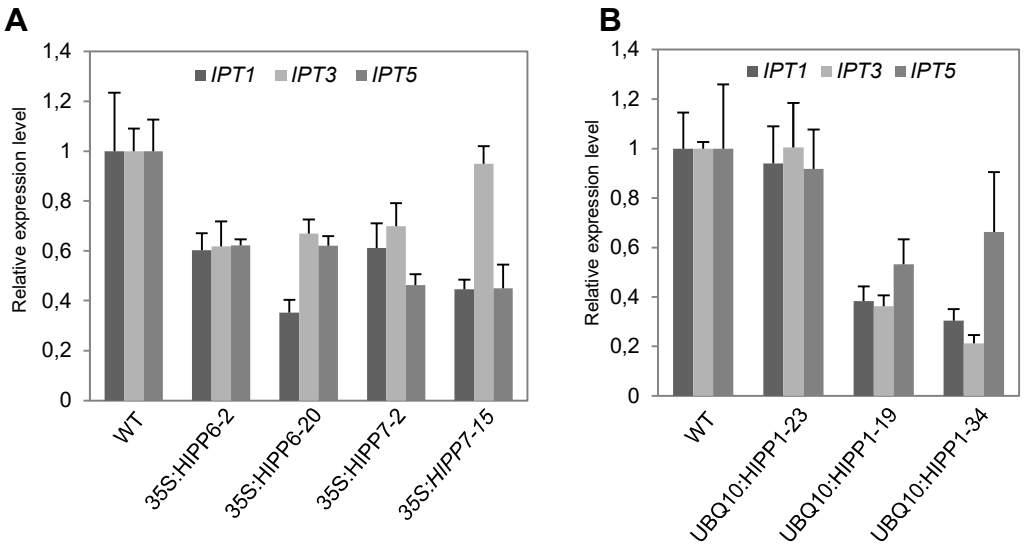

Figure 25. Expression of *IPTs* in the *HIPP*-overexpressing plants.
(A) Quantitative RT-PCR (qRT-PCR) analysis of *IPTs* steady-state transcript levels in rosettes of WT, *35S:HIPP6*, and *35S:HIPP7* plants 15 DAG. Data are means ± SE (*n* = 4).
(B) qRT-PCR analysis of *IPTs* steady-state transcript levels in rosettes of the *UBQ10:HIPP1* plants 15 DAG. Data are means ± SE (*n* = 4).

3.2.2.7 *35S:ARR15* suppresses the *HIPP*-overexpression phenotypes

To test whether the enhanced cytokinin activity is causally involved in the establishment of the *HIPP*-overexpression leaf phenotype, we performed a genetic cross between a *35S:HIPP6* transgenic line, which has a pronounced crinkly leaf phenotype, and a *ARR15* overexpression line, which has a reduced cytokinin sensitivity, but does not display any leaf phenotypic changes compared with WT (Ren et al., 2009). The resulting hybrid phenotypes were analyzed in the F1 generation. Fig. 26A-C show that the leaf phenotype of *35S:HIPP6* plants was strongly suppressed by the introgression of *ARR15*. The rosette diameter and fresh weight of the *35S:HIPP6; 35S:ARR15* double transgenic line was 121% and 138% compared to the *35S:HIPP6;* WT control F1 hybrid. The transcript levels of the *HIPP6* transgene were comparable to control cross (Fig. 26D and E). Together, this genetic analysis suggested that the altered leaf development in *HIPP*-overexpressing plants is largely caused by enhanced cytokinin activity.

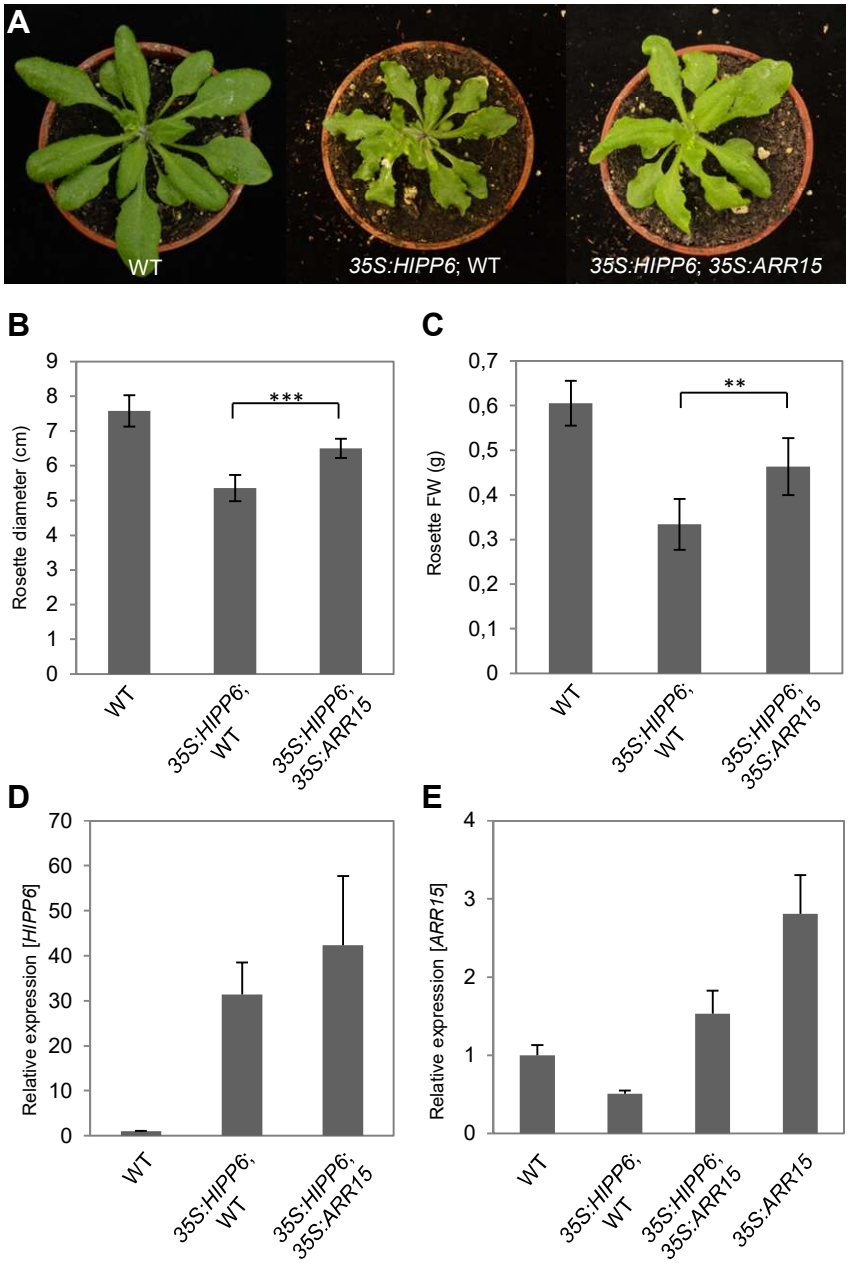

Figure 26. *35S:HIPP6* shoot phenotype is suppressed by the expression of *35S:ARR15*.
(A) Suppression of the altered leaf morphology of *35S:HIPP6* plants by the expression of *35S:ARR15*. F1 hybrid plants 23 DAG are shown.
(B) Rosette diameter of the wild type (WT) and F1 hybrid plants from the cross of *35S:HIPP6* with WT or *35S:ARR15* shown in **(A)**. Data are means ± SD (n = 5). ***P < 0.005, calculated by Student's t test.
(C) Rosette fresh weight (FW) of plants shown in **(A)**. Data are means ± SD (n = 4). **P < 0.01, calculated by Student's t test.
(D) qRT-PCR analysis of *HIPP6* transcript levels in rosettes of plants shown in **(A)**. Data are means ± SE (n = 4).
(E) qRT-PCR analysis of *ARR15* transcript levels in rosettes of the WT, F1 hybrid plants shown in **(A)** and *35S:ARR15* homozygous plants. Data are means ± SE (n = 4).

3.2.3 Cytokinin responses in root

3.2.3.1 Overexpression of clade-I *HIPP* genes inhibits root growth and development

To understand whether the ectopic *HIPP* expression influences the root development, we tested the primary root elongation and lateral root development in various *HIPP* overexpressing lines.

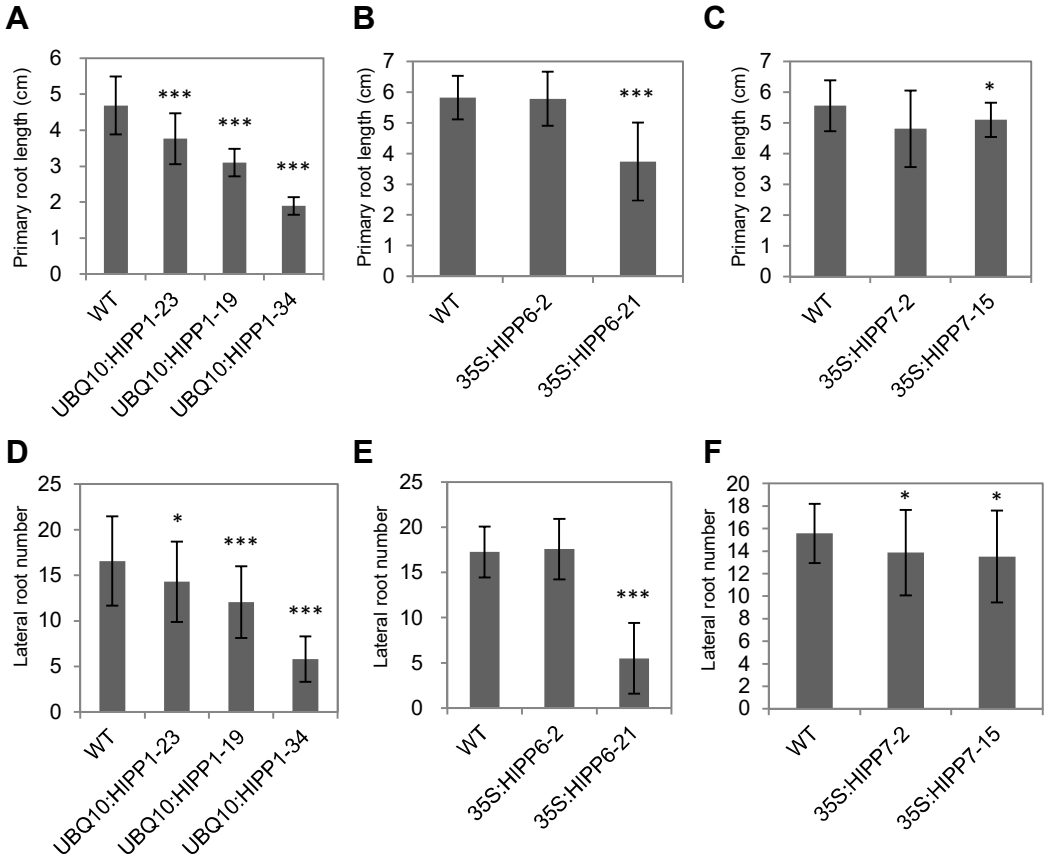

Figure 27. Arabidopsis plants overexpressing *HIPPs* exhibit altered root growth and development.
(A) to **(C)** Primary root length of the wild type (WT) and independent homozygous lines of plants overexpressing *UBQ10:HIPP1* **(A)**, *35S:HIPP6* **(B)** and *35S:HIPP7* **(C)**. Elongation of primary roots between day 3 and 10 after germination were measured. Data are means ± SD (n = 15). *P < 0.05, **P < 0.01 and ***P < 0.005, calculated by Student's t test.
(D) to **(F)** Number of emerged lateral roots in plants shown in **(A)** to **(C)** 10 DAG. Data are means ± SD (n = 15).

It was observed that the *UBQ10:HIPP1* lines, which displayed the most severe changes in shoot morphology, developed also strongly retarded root system. As presented in Fig. 27A, the primary root elongation was reduced to about 40% of the WT in several independent lines. The reduction correlated with the degree of the transgene expression (Fig. 27A, Fig. 17A and B). Moreover, the formation of lateral roots was also severely affected. The *HIPP1*-overexpressing plants showed a strong decrease of lateral root numbers (65%) compared with the WT seedlings (Fig. 27D). Similarly to *HIPP1*, *35S:HIPP6* and *35S:HIPP7*

overexpressing plants displayed a retarded primary root growth and a decreased lateral root number (Fig. 27).

3.2.3.2 The retarded root development of *HIPP*-overexpressing plants is associated with enhanced cytokinin activity

Provided the altered cytokinin sensitivity in the shoot, it was important to analyze whether the observed changes in root development might be a result of altered cytokinin activity in this organ as well. As cytokinin has been shown to regulate the size of the root apical meristem (Werner et al., 2003; Dello Ioio et al., 2007), the root meristem size was compared in different *UBQ10:HIPP1* lines and WT by scoring the number of the cortex cells between the quiescent center and transition zone. The cortex cell number was strongly reduced in *UBQ10:HIPP1* root meristems (Fig. 28A-D), indicating a premature cell differentiation and suggesting that the altered root meristem activity was due to enhanced cytokinin response.

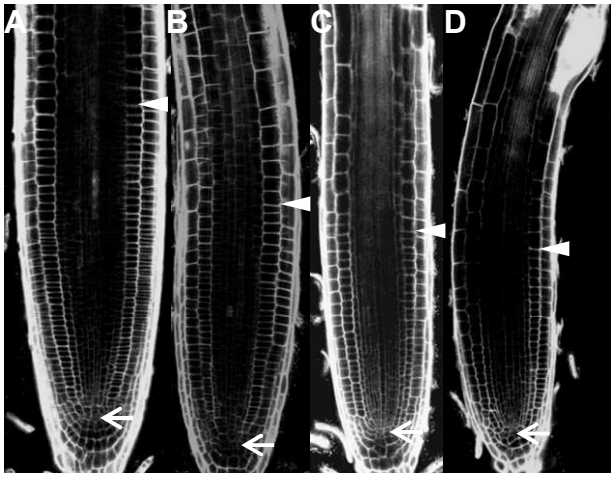

Figure 28. *HIPP1*-overexpression plants display a reduced root-meristem cell number.
(A) to **(D)** Root meristems of WT **(A)**, UBQ10:HIPP1-23 **(B)**, UBQ10:HIPP1-19 **(C)**, and UBQ10:HIPP1-34 **(D)** plants 7 DAG. Arrows indicate the quiescent center and arrowheads indicate the first elongating cortex cell at the transition zone.

To address this experimentally, the *TCSn*:GFP activity in the root meristems was visualized by the confocal microscopy. The analysis revealed that in comparison to control roots (Fig. 29), the GFP signal was stronger in the procambial cells and it further expanded upward into the root vasculature in *UBQ10:HIPP1* roots (Fig. 29B). Correlating with the increased cytokinin activities in the shoot, these results confirm that the *HIPP* overexpression enhances cytokinin activities also in the root.

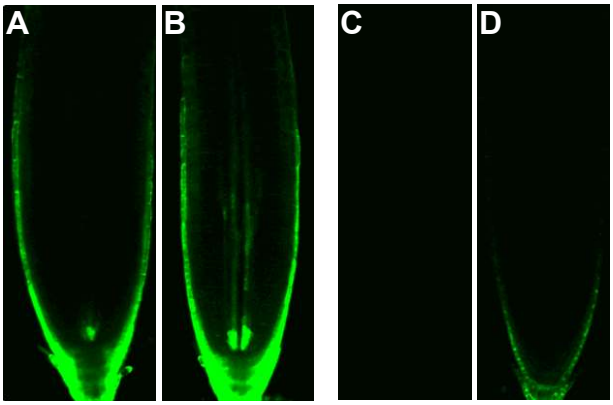

Figure 29. Increased cytokinin signaling activity in Arabidopsis plants overexpressing *HIPP1*.
(A) to **(D)** Confocal microscopy analysis of root meristems of F1 plants with *TCSn:GFP* crossed into WT **(A)** and UBQ10:HIPP1-19 **(B)**. Images in **(A)** and **(B)** were captured using identical confocal settings. **(C)** and **(D)** The background GFP fluorescence corresponding to the GFP-HIPP1 protein expressed in the UBQ10:HIPP1-19 line was very low **(D)** and thus not interfering with the analysis of the fluorescence signal resulting from *TCSn:GFP* activity shown in **(A)** and **(B)**. WT is shown in **(C)**. Images were captured using identical confocal settings as in the analysis shown in **(A)** and **(B)**.

3.2.3.3 Clade-I HIPPs suppress root development in a prenylation dependent manner

Since it was shown that prenylation of HIPP7 was necessary for the establishment of the overexpression phenotypes in leaves, it was further tested whether this posttranslational protein modification is also important for the HIPP activity in roots. Fig. 30A and B, shows that transgenic line expressing *UBQ10:HIPP7* displayed significantly reduced (~10%) elongation of the primary root and the formation of the lateral roots (~20%). Importantly, the expression of the prenylation-deficient HIPP7 protein (*UBQ10:HIPP7*^{C352G}) did not produce a significant change in root development in comparison to WT, suggesting that the changes of cytokinin activity in roots were dependent on the HIPP7 prenylation. Plants expressing the HIPP7 mutant with mutated HMA domains (*UBQ10:HIPP7*^{hma}) displayed a slightly, but statistically not significant, reduced elongation of the primary root and the formation of the lateral roots (Fig. 30).

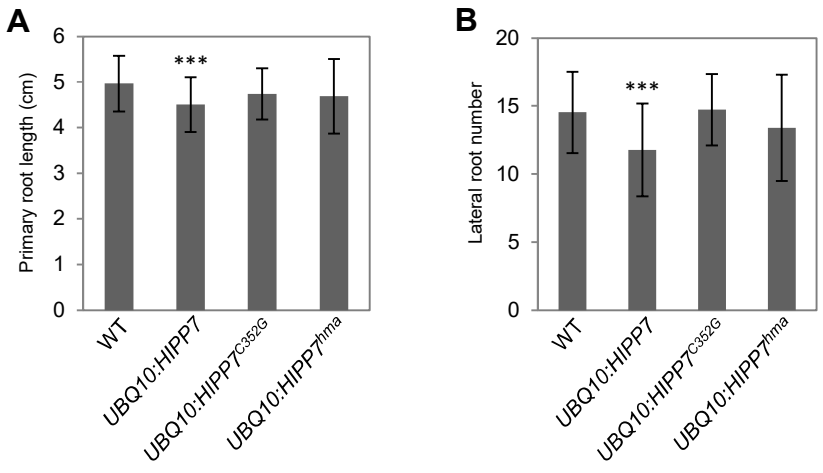

Figure 30. Clade-I HIPPs perturb root development in a prenylation dependent manner.
(A) Length of the primary root of the WT and plants expressing *UBQ10:GFP-HIPP7*, *UBQ10:GFP-HIPP7*^{C352G} and *UBQ10:GFP-HIPP7*^{hma}. Elongation of primary roots between day 3 and 10 after germination were measured. Data are means ± SD (*n* = 30). ***P < 0.005, calculated by Student's *t* test.
(B) Number of emerged lateral roots in plants shown in **(A)** 10 DAG. Data are means ± SD (*n* = 30). ***P < 0.005, calculated by Student's *t* test.

3.2.4 Clade-I HIPPs regulate CKX1 protein abundance in Arabidopsis plants

The phenotypic and molecular analysis of *HIPP*-overexpressing plants provided several indications that their cytokinin activity is increased. This suggests that the cytokinin metabolic homeostasis or cytokinin responses are altered. Having shown that the HIPP proteins interact with CKX *in vitro* and *in vivo*, it was aimed to study how HIPP expression influences the CKX protein levels. To approach this question experimentally, we crossed the lines expressing *UBQ10:HIPP1*, *35S:HIPP6* and *35S:HIPP7* respectively, with a transgenic line expressing the CKX1-myc fusion protein under the control of the *Arabidopsis thaliana MERISTEM LAYER 1* (*ATML1*) promoter (*AtML1:CKX1-myc*) (Werner, 2016). Analysis of the *AtML1:CKX1-myc*, *UBQ10:HIPP1*, F1 progenies revealed that the levels of the CKX1-myc were strongly reduced in comparison to the control cross (Fig. 31A and C), suggesting that the CKX1/HIPP1 complex formation is associated with the enhanced degradation of CKX1. This results correlates with the enhanced cytokinin activity in the *HIPP1*-overexpressing plants.
In contrast to this, CKX1-myc protein levels were significantly increased upon the expression of *35S:HIPP6* and *35S:HIPP7* (Fig. 31B and D), suggesting that the CKX-myc protein was more stable in the complex with the respective HIPP proteins. Since the BiFC experiments indicated that CKX1/HIPP7 complex is localized at the cytosolic site of the ER membrane, the increased CKX1-myc levels suggest that the protein was stabilized in a cytosolic complex. Nonetheless, the increased cytokinin activity in *HIPP6* and *HIPP7* overexpressing plants

implicate that CKX1 protein was withdrawn from the ER and less CKX degradation occurs in this compartment.

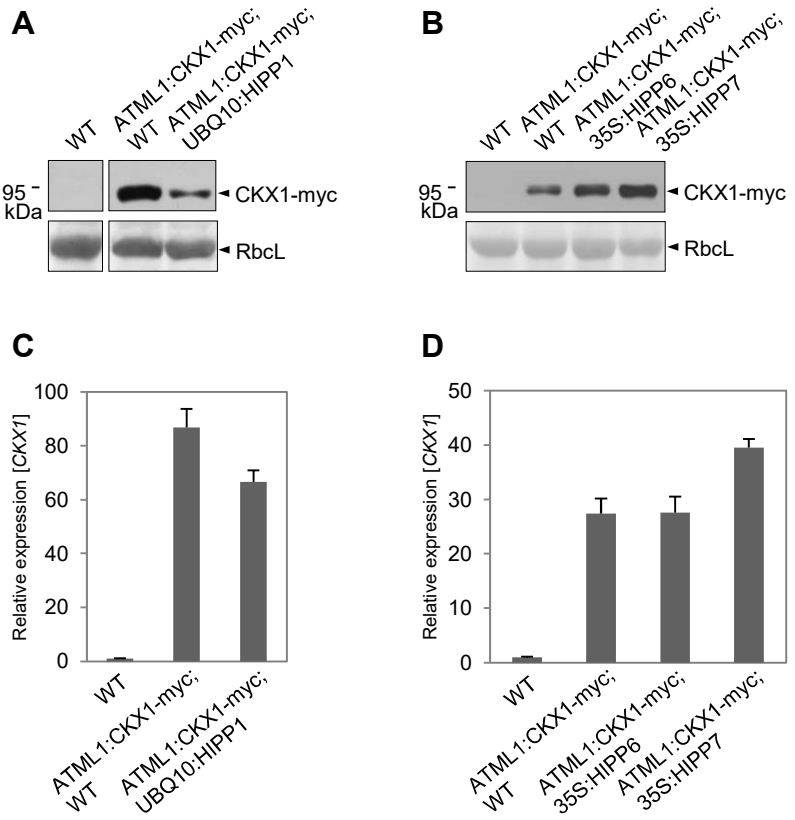

Figure 31. Overexpression of *HIPP* genes alters the CKX1 protein levels.
(A) and **(B)** Comparison of the *CKX1-myc* protein abundances in the F1 plants resulting from the crosses between the *ATML1:CKX1-myc* Arabidopsis line and plants expressing *UBQ10:HIPP1* **(A)**, *35S:HIPP6* and *35S:HIPP7* **(B)**. Hemizygous F1 plants from the cross between *ATML1:CKX1-myc* and wild type (WT) were used as a control. 30 µg of the crude protein extracts from shoots 20 DAG were resolved by SDS-PAGE and submitted to immunoblot analysis with anti-myc antibody. Coomassie blue staining of Rubisco large subunit (RbcL) was used as loading control.
(C) and **(D)** Comparable expression of the *CKX1-myc* transgene in the F1 plants resulting from the crosses between the *ATML1:CKX1-myc* Arabidopsis line with plants expressing *UBQ10:HIPP1* **(C)**, *35S:HIPP6* and *35S:HIPP7* **(D)** and the F1 plants from the cross with wild type (WT). qRT-PCR analysis of transcript levels in shoots 15 DAG. Expression in WT was set to 1. Data are means ± SE (*n* = 4).

3.2.5 Changes in the expression of genes encoding TCP transcription factors

The dynamic progress of leaf growth and development is modulated by multiple regulatory cues, including several transcription factors and phytohormones. It has been reported that the TEOSINTE BRANCHED1/CYCLOIDEA/PROLIFERATING CELL FACTOR1 (TCP) transcription factors regulate leaf morphogenesis via mediating cytokinin signaling. For example, overexpression of *TCP14*, encoding class I TCP, leads to plants hypersensitive to cytokinin (Steiner et al., 2012). In contrast, the reduction in expression of class II *TCP* increased plants sensitivity to cytokinin and produced crinkly leaves (Efroni et al., 2013). To

test whether the changes in leaf development in *HIPP*-overexpressing plants are linked to altered expression of *TCPs*, the mRNA levels of several *TCP* were analyzed by qRT-PCR. As shown in Figure 32A, the expression level of the *TCP14* was not increased in *35S:HIPP6* plants. In contrary, a slight, but not significant, reduction of *TCP14* expression was detected, suggesting that the *35S:HIPP6* leaf phenotype was not due to the alteration of the expression of *TCP14*. Interestingly, the transcript levels of several class II *TCP* genes were reduced in *HIPP6*-overexpressing plants. Especially, there was a significant reduction for *TCP10* and *TCP18* (Fig. 32A). The expression of class II *TCP* was further tested in *35S:HIPP7* plants. Intriguingly, a similar reduction in *TCP4* and *TCP18* transcript levels was detected in these transgenic plants (Fig. 32B). These results together suggest that *HIPP* overexpression could affect the leaf development, at least in part, via regulating the expression of class II type *TCP*s.

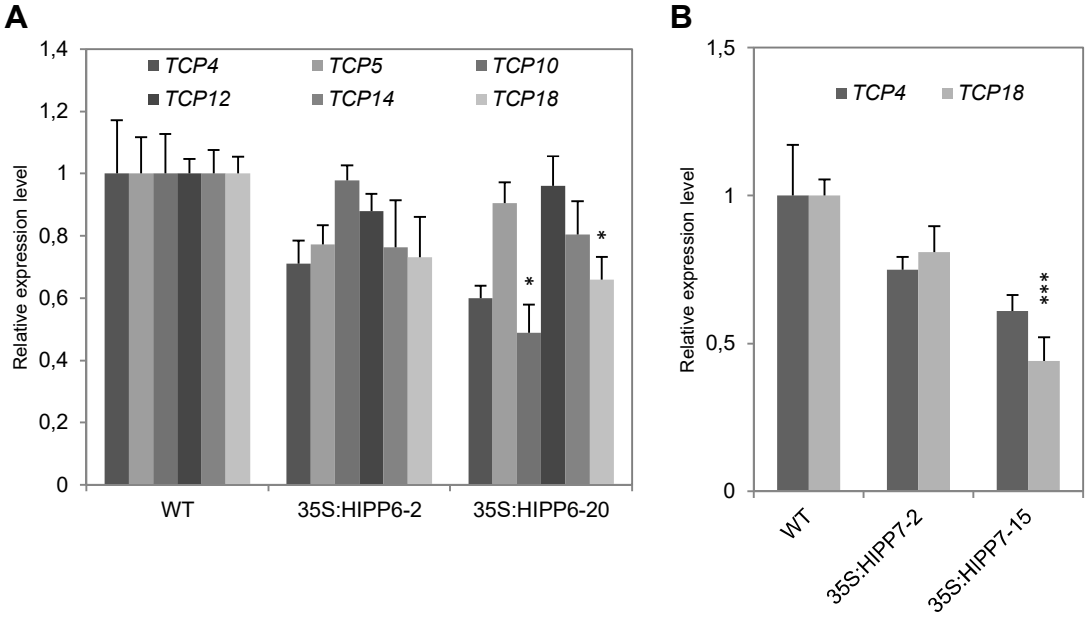

Figure 32. Expression of *TCP* genes in *HIPP*-overexpressing Arabidopsis plants.
(A) qRT-PCR analysis of *TCP* genes steady-state transcript levels in rosettes of wild type (WT) and two independent homozygous lines expressing *35S:HIPP6* at 15 DAG. Data are means ± SE (n = 4). *P < 0.05, calculated by Student's t test.
(B) qRT-PCR analysis of *TCP* genes transcript levels in rosettes of WT and *35S:HIPP7* plants 15 DAG. Data are means ± SE (n = 4). ***P < 0.005, calculated by Student's t test.

3.2.6 Overexpression of clade-I *HIPPs* affects the expression of gibberellin metabolism genes and gibberellin homeostasis

Leaf shape is determined by a highly flexible process that modulates the balance between leaf cell proliferation and differentiation (Bar and Ori, 2014). This flexibility is regulated by several phytohormones, one of which is cytokinin as discussed above. Another important

plant hormone is gibberellin (GA) which promotes cell differentiation and leaf maturation (Achard et al., 2009). To test whether GA is affected in *HIPP*-overexpressing plants, the expression levels of several GA biosynthesis and deactivation genes were analyzed by qRT-PCR. Fig. 33A shows that the transcript levels of *GA3OX1*, which encodes the crucial enzyme catalyzing the last step of the biosynthesis of active GA form in Arabidopsis (Sun, 2008; Yamaguchi, 2008), were reduced to less than 20% in two independent *35S:HIPP6* lines in comparison to the WT control. Similarly, the transcript levels of *GA20OX1*, which also modulate active GA content in the late stages (Sun, 2008; Yamaguchi, 2008), were reduced in the *35S:HIPP6* lines (Fig. 33A), suggesting a lower GA content in the transgenic plants. Moreover, similar to the expression of *ARR16* in the *35S:HIPP6* transgenic plants, the reduction in the *GA3OX1* transcripts was progressively stronger during the later stages of leaf maturation (Fig. 33B). Interestingly, the expression level of *GA2OX1*, which catalyzes the deactivation reaction of GA, was also downregulated in the analyzed *35S:HIPP6* lines, but another GA 2-oxidase, the *GA2OX2* was upregulated (Fig. 33A), suggesting a differential regulation of GA deactivation genes in response to *HIPP*-overexpression.

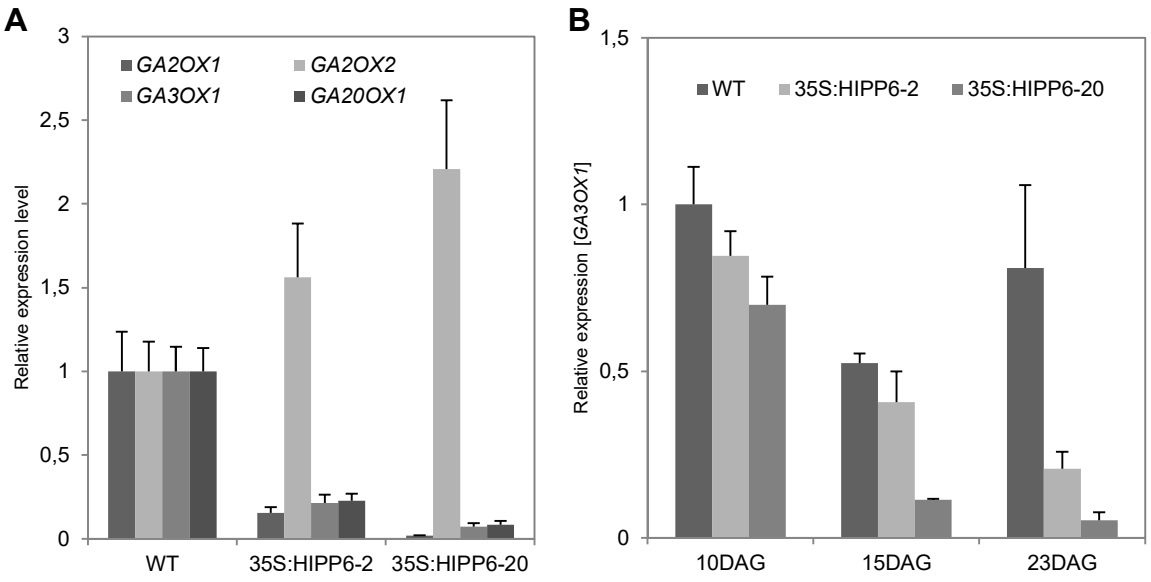

Figure 33. Differential regulation of GA metabolism genes in *HIPP*-overexpressing Arabidopsis plants.
(A) qRT-PCR analysis of the steady-state transcript levels of GA metabolism genes in rosettes of WT and *35S:HIPP6* plants 15 DAG. Data are means ± SE (*n* = 4).
(B) qRT-PCR analysis of *GA3OX1* transcript levels in rosettes of WT and *35S:HIPP6* lines at indicated developmental time points. Data are means ± SE (*n* = 4).

Next, we examined whether the deregulated expression of GA metabolism genes resulted in changes of the endogenous GA content. The analysis of 2-week-old *35:HIPP6* and *35S:HIPP7* shoots revealed that the content of most GA metabolites was relatively weakly changed (Appendix Fig. A.1). Interestingly, the GA_4, which is thought to be the major bioactive

GA in Arabidopsis (Yamaguchi, 2008), was strongly reduced to less than 50% of the WT levels in the two *35:HIPP6* lines (Fig. 34A). A slight but not significant reduction of GA_4 was also detected in the analyzed *35:HIPP7* lines (Fig. 34A). Both the WT and *HIPP* overexpression lines had very low or undetected amount of GA_1, GA_3 and GA_7, which are also the bioactive GA forms (Appendix Fig. A.1). In contrast to the reduced GA_4 levels, the concentrations of GA_{15}, one of the precursors of GA_4, were significantly accumulated in all transgenic lines (Fig. 34B). Together, the complex changes of the GA profiles could due to the different regulation of the GA metabolism genes responding to the overexpression of *HIPP* genes.

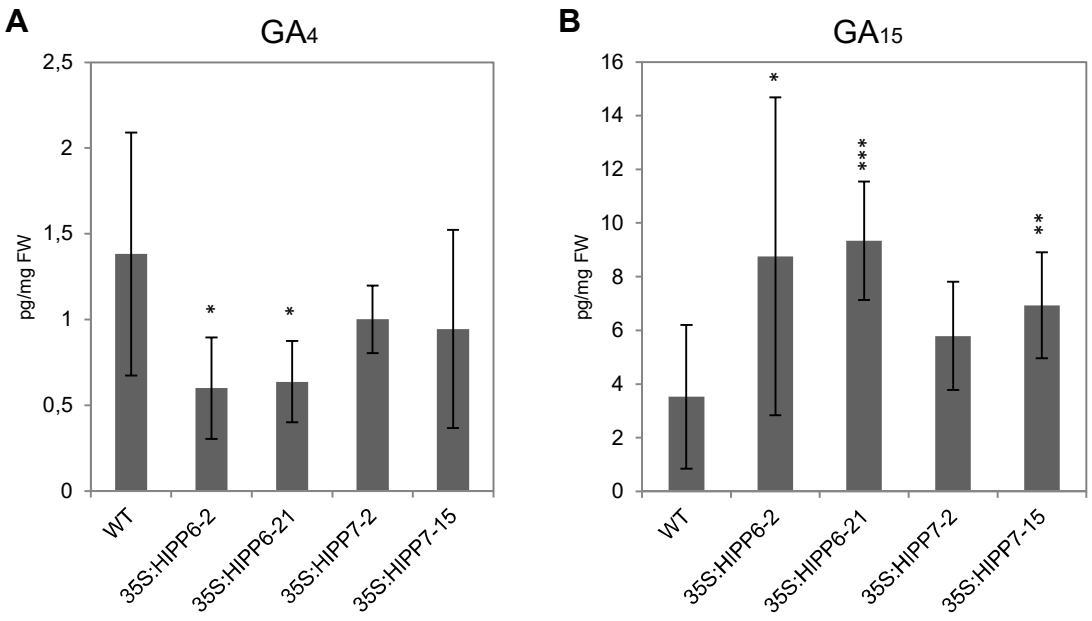

Figure 34. GA content in *HIPP*-overexpressing transgenic Arabidopsis plants.
(A) and **(B)** GA_4 **(A)** and GA_{15} **(B)** contents in wild type (WT) and two independent homozygous lines expressing *35S:HIPP6* and *35S:HIPP7.* Rosettes (15 DAG) were analyzed. Data shown are means ± SD; $n = 3$. *$P < 0.05$, **$P < 0.01$, ***$P < 0.005$, calculated by Student's *t* test.

To find out whether the reduced GA levels are causal for the altered leaf development in the *HIPP*-overexpressing plants, exogenous GA_3 was applied to *35S:HIPP6* plants and the phenotypic changes scored. As shown in Fig. 35A and B, the application of GA promoted WT leaf growth and resulted in an enlarged rosette compared with the mock control. GA application had a similar effect on promoting the leaf growth of the *35:HIPP6* plants. However, neither the smaller rosette diameter nor the crinkly leaf phenotype of the *35S:HIPP6* plants was rescued by the GA application. Even after 3 weeks of GA application, the *35S:HIPP6* plants displayed obvious overexpression leaf morphology (Fig. 35C), suggesting that the leaf phenotypes of the *HIPP*-overexpression plants was not caused by reduced GA content.

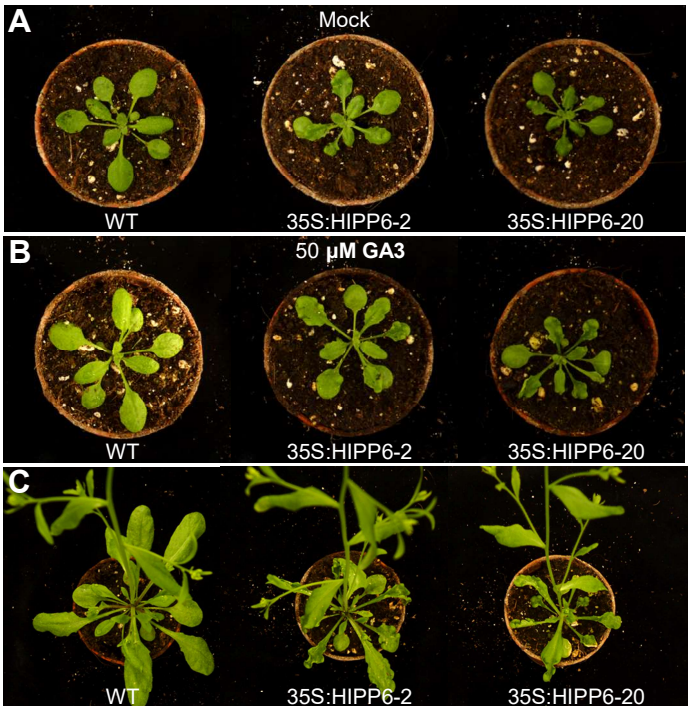

Figure 35. GA application does not rescue the leaf phenotypes of the *35:HIPP6* plants.
(A) and **(B)** Wild type (WT) and two independent homozygous lines expressing *35S:HIPP6* treated repeatedly with 0 µM (DMSO) **(A)** and 50 µM GA_3 **(B)** for 2 weeks.
(C) WT and two independent homozygous lines expressing *35S:HIPP6* treated repeatedly with 50 µM GA_3 for 3 weeks.

3.2.7 Overexpression of clade-I *HIPPs* elevates the concentrations of ABA and SA

As only little is known about biological processes controlled by HIPP proteins, the function of clade-I HIPP proteins in controlling other plant hormones was further investigated by measuring the contents of abscisic acid (ABA) and salicylic acid (SA) in *HIPP*-overexpression plants. The analysis of 2-week-old *35:HIPP6* and *35S:HIPP7* shoots revealed that the concentration of ABA is elevated in one *35S:HIPP6* overexpression line and in both *35S:HIPP7* overexpression lines (Fig. 36A). Especially in the 35S:HIPP7-15 line, the concentration of ABA was increased by 86% in comparison to the WT control (Fig. 36A). Strong changes in the concentrations of SA were detected in the *HIPP*-overexpression plants. As shown in Fig. 36B, there was a 3 and 4-fold increase of SA content in the 35S:HIPP6 line 2 and line 20, respectively. Elevated concentrations of SA were also detected in the stronger *35S:HIPP7* overexpression line. Together, these results suggest that the overexpression of clade-I *HIPPs* affected the expression of genes associated with ABA and SA metabolism or altered the distribution of these hormones in the plant.

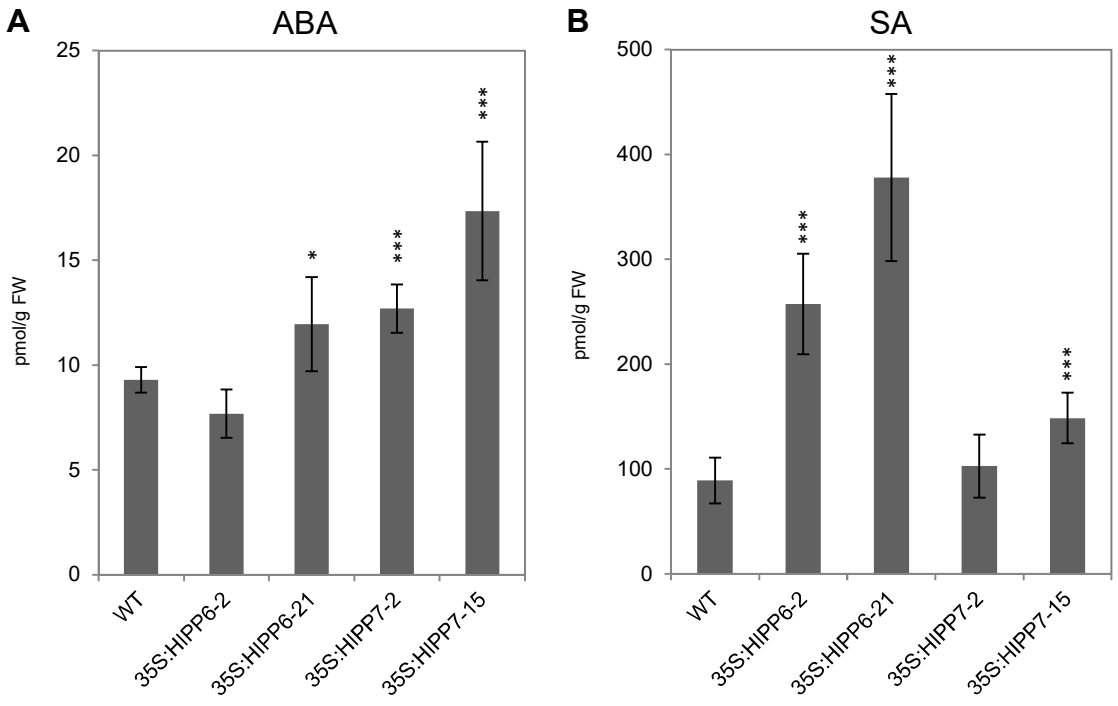

Figure 36. ABA and SA contents in *HIPP*-overexpressing Arabidopsis plants.
(A) ABA content in wild type (WT) and two independent homozygous lines expressing *35S:HIPP6* and *35S:HIPP7.* Rosettes (15 DAG) were analyzed. Data shown are means ± SD; $n = 3$. *$P < 0.05$, ***$P < 0.001$, calculated by ANOVA.
(B) SA content in plants shown in **(A)**. Data shown are means ± SD; $n = 3$. ***$P < 0.001$, calculated by ANOVA.

3.2.8 Overexpression of clade-I *HIPPs* increases drought tolerance in Arabidopsis

To examine whether the changes in the level of endogenous HIPP proteins can affect plant tolerance to abiotic stress, drought experiments were performed. Arabidopsis WT and various *HIPP*-overexpression lines were cultivated on soil for 3 weeks under LD conditions with regular irrigation. Subsequently, plants were kept under the same conditions except that water was completely withdrawn. As early as 6 day after withdrawing water, most of the WT plants showed severe damage due to the drought stress, whereas a significantly higher number of *HIPP*-overexpression plants maintained turgor and stayed green (Fig. 37). Importantly, it was observed that the drought resistance phenotypes of the *HIPP*-overexpression plants correlated with the transgene expression levels (Fig. 16 and 17), suggesting that the HIPP proteins might play a positive role in mediating responses to drought stress.

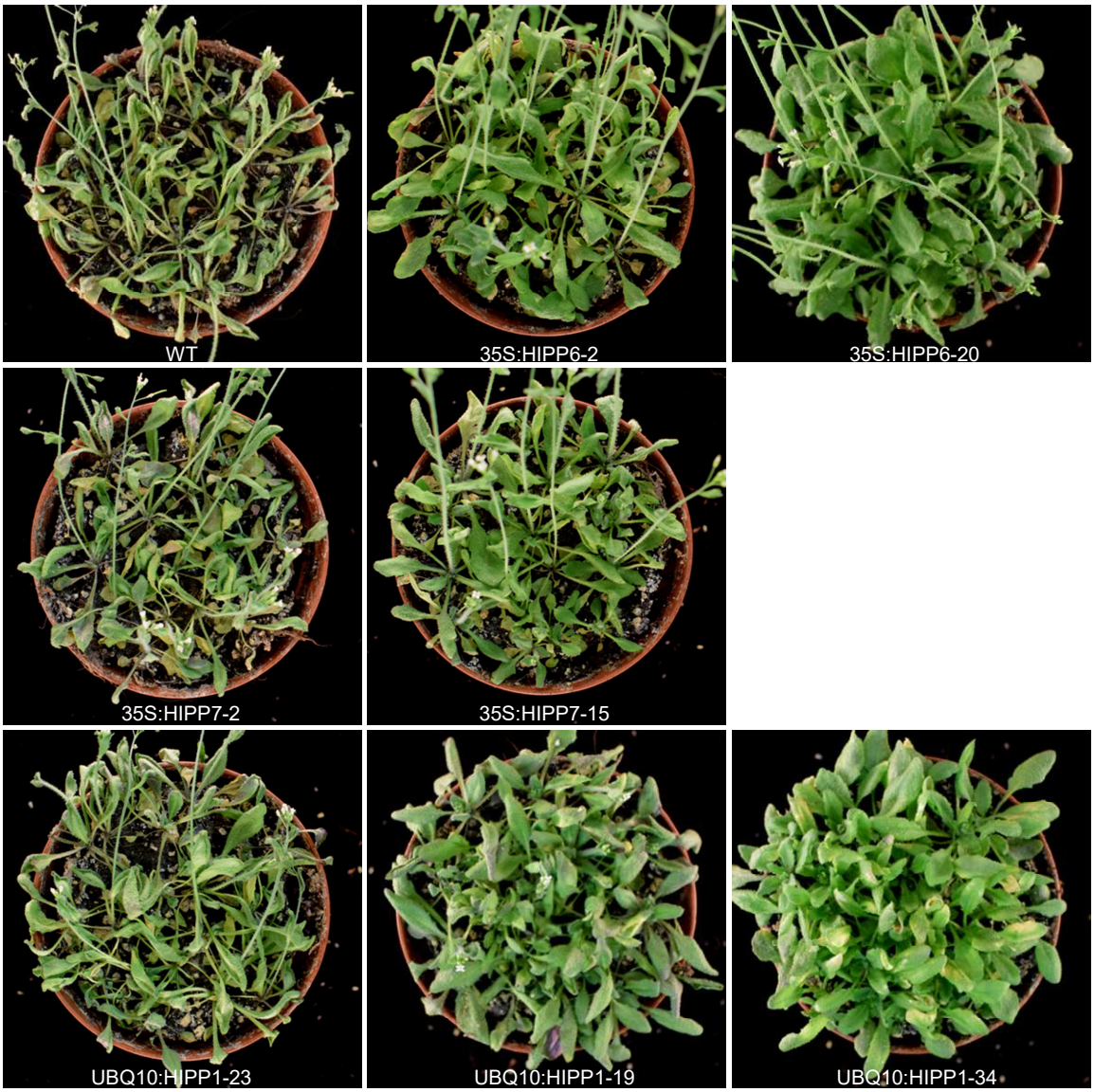

Figure 37. Increased drought tolerance of the *HIPP*-overexpression plants.
Three-week-old wild type (WT) and *HIPP*-overexpression plants were exposed to drought for 6 days and photographed.

3.3 Characterization of *hipp* loss-of-function mutants in Arabidopsis

An important strategy to explore the physiological function of the isolated HIPP proteins is to reduce levels of their respective gene activities by employing reverse genetic methods. However, the homologous genes from the same family may share a large degree of functional redundancy, which may impede the genetic analysis. Furthermore, the generation of multigene knockouts for closely linked genes, especially those present as tandem duplications, has imposed further challenges and constraints. In order to circumvent these problems and to generate higher-order *hipp* mutants, an approach employing the expression of artificial microRNA targeting multiple *HIPP* genes was pursued. In an alternative approach, T-DNA insertional mutants of individual *HIPP* genes were isolated and higher-order mutants created by genetic crosses.

3.3.1 Generation and characterization of Arabidopsis plants expressing single amiRNA constructs for multiple *HIPP* gene silencing

Artificial microRNA (amiRNA) technology exploits the biogenesis and silencing machineries for endogenous miRNA precursors to generate sRNAs that direct gene silencing in either plants or animals (Ossowski et al., 2008; Sablok et al., 2011). An amiRNA is designed from a native endogenous miRNA precursor, in which the miRNA-miRNA* duplex is replaced with a customized sequence. The high-level accumulation of an amiRNA of desired sequence redirects the miRNA-induced silencing complex to silence the mRNA target of interest (Zeng et al., 2002; Parizotto et al., 2004; Alvarez et al., 2006; Schwab et al., 2006; Ossowski et al., 2008). Plant amiRNA has significant advantages due to its small size, which make it possible to generate constructs expressing multiple and unrelated amiRNAs (Alvarez et al., 2006; Niu et al., 2006; Schwab et al., 2006; Ossowski et al., 2008; Li et al., 2013b). Because the homologous genes from the same family usually share a large degree of functional redundancy, two amiRNAs with multiple potential targets from clade I of the *HIPP* gene family were designed. The amiRNA construct amiRNA-Tri targets three *HIPP* genes, *HIPP5*, *HIPP6* and *HIPP7*. The second amiRNA construct, amiRNA-Mul, was designed to target five *HIPP* genes (*HIPP3*, *HIPP5*, *HIPP6*, *HIPP7* and *HIPP8*), which represent a theoretical maximal number of cluster I *HIPP* genes to be targeted by a single amiRNA according to the bioinformatic prediction (Fig. 38A). The amiRNA constructs were placed under the control of the 35S promoter and transformed into Arabidopsis. T3 transgenic lines were analyzed by means of qRT-PCR. The results revealed that, among four selected homozygous lines expressing amiRNA-Tri, the transcript levels of *HIPP7* were reduced to around 40 to 70% in comparison with that of the WT, while lower transcript levels of *HIPP6* were detected only in

one transgenic line. None of the selected lines showed reduced *HIPP5* mRNA levels (Fig. 38B). Similarly, none of the analyzed T3 transgenic lines expressing amiRNA-Mul was effective in silencing all five potential *HIPP* target genes. In fact, only the transcript levels of *HIPP7* were effectively reduced (to around 20% of the WT levels) in the selected homozygous lines. There was about 30% decrease in the *HIPP3* mRNA levels, while the expression of *HIPP5* and *HIPP6* was not altered in the selected transgenic lines (Fig. 38C). These results suggested an intrinsic difficulty in silencing multiple *HIPP* genes using a single amiRNA. Although it can not be excluded that the expressed amiRNA caused translational repression of the target HIPPs (Li et al., 2013b), the lack of any obvious morphological changes of the selected plants suggested that the approach was ineffective and it was abandoned.

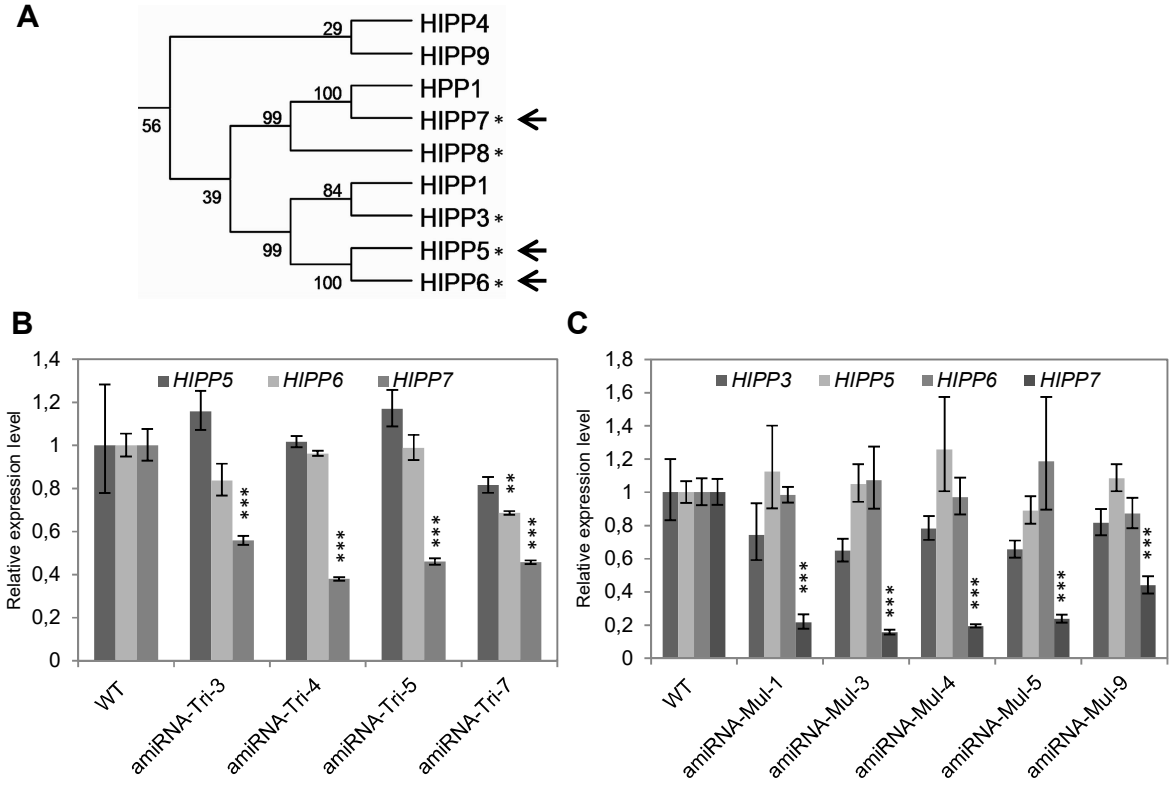

Figure 38. Genetic approach to target multiple clade-I *HIPP* genes by a single amiRNA.
(A) Predicted *HIPP* targets for two designed amiRNA. Arrows and stars indicate genes targeted by amiRNA-Tri and amiRNA-Mul, respectively.
(B) Relative transcript abundances of the *HIPP5*, *HIPP6* and *HIPP7* genes in independent T3 lines expressing the amiRNA-Tri construct. Seedlings 10 DAG were measured by qRT-PCR. Data are means ± SE (n = 3). $^{**}P < 0.01$, $^{***}P < 0.005$, calculated by Student's t test.
(C) Relative transcript abundances of the *HIPP3*, *HIPP5*, *HIPP6* and *HIPP7* genes in independent T3 lines expressing the amiRNA-Mul construct. Seedlings 10 DAG were measured by qRT-PCR. Data are means ± SE (n = 3). $^{***}P < 0.005$, calculated by Student's t test.

3.3.2 Isolation and molecular characterization of *hipp* T-DNA insertion mutants

Even though the amiRNA can be designed to target any gene of interest, there are still some disadvantages such as off-target effects and the low efficacies to silence gene of interest as described above. Traditional genetic crossing is an alternative approach to produce multiple gene knockouts and study their respective functions. In an attempt to gain more information on the functions of individual *HIPP* genes in Arabidopsis, a reverse genetic approach was followed. Eight T-DNA insertion alleles were obtained from screening different insertional populations (Fig. 39).

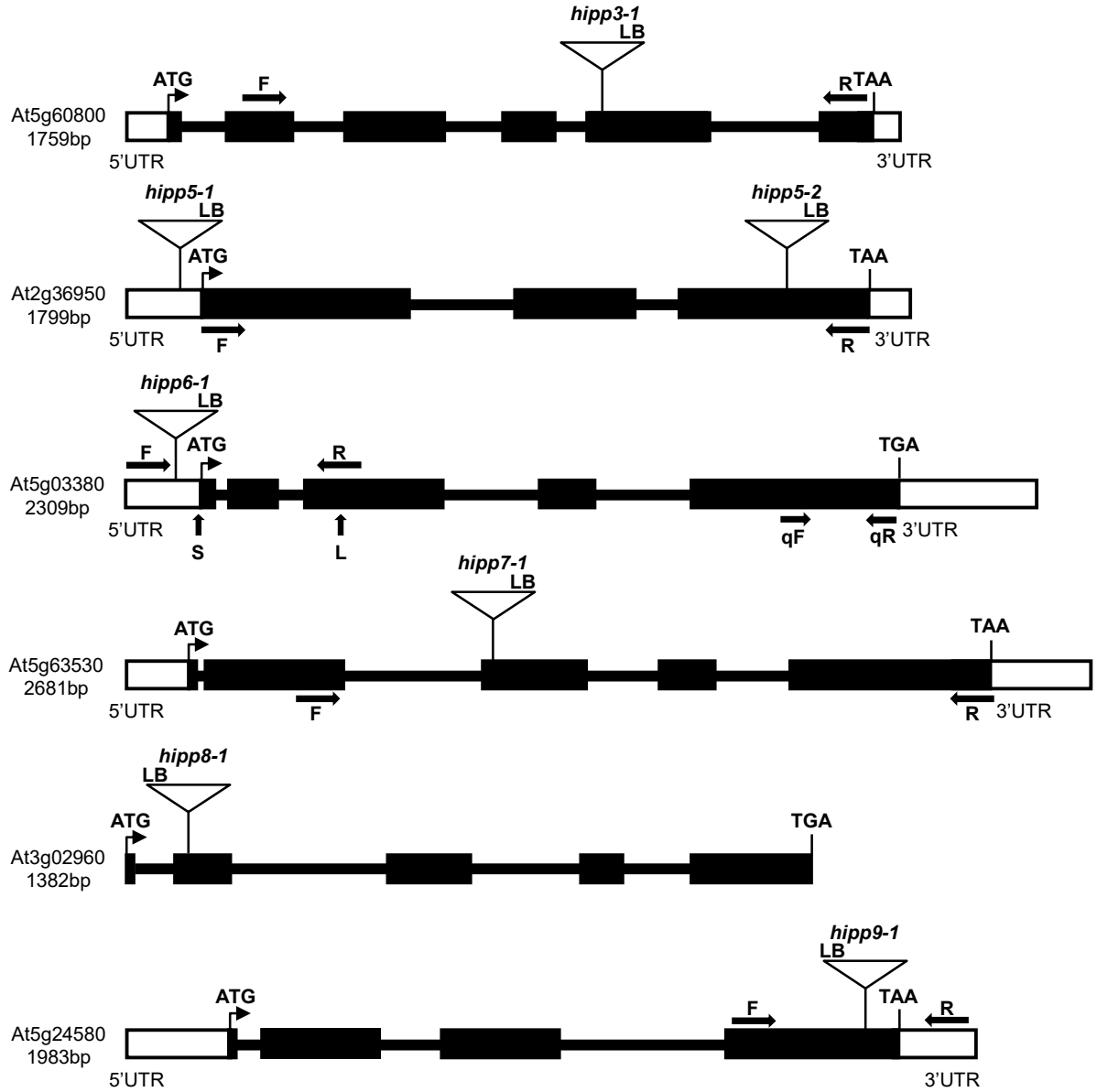

Figure 39. Positions of T-DNA insertions in the analyzed *HIPP* genes.
The length of the genomic *HIPP* gene sequences are given in base pairs. LB, Left border. Triangles indicate the T-DNA insertion sites. White and black boxes indicate untranslated regions (UTRs) and exons, respectively. F and R indicate positions of PCR primers used for RT-PCR analysis in Fig. 40B. qF and qR indicate positions of *HIPP6*-specific qRT-PCR primers used in Fig. 40C. S (short) and L (long) indicate the 3' termini of the two *HIPP6* promoters (3.4).

Homozygous mutant lines were isolated by PCR using genomic DNA as template (Fig. 40A). In order to determine the exact position of the insertion, the junctions between the left border of the inserted T-DNA and adjacent genomic regions were sequenced. In the *hipp3-1* allele (SALK_021602C), the T-DNA is inserted 1010 bp downstream of the predicted ATG start codon. For *HIPP5*, two T-DNA insertions were found in the SALK collection (Alonso et al., 2003), *hipp5-1* (SALK_004387) located in the 5'-UTR, and *hipp5-2* (SALK_069207) was localized in the third exon 1459 bp downstream of the presumed ATG start codon. The *hipp5-2* allele was used for all experiments. In the *hipp6-1* mutant allele (SALK_111020C), the T-DNA is inserted in the 5' UTR, 68 bp upstream of the presumed ATG. For the *HIPP7* gene, the *hipp7-1* allele (SALK_091924C) with a T-DNA insertion 907 bp downstream of the ATG was identified. In the JIC-SM collection (Tissier et al., 1999) T-DNA insertions SM_3_25599 and SM_3_30660 were found for *HIPP8* and *HIPP9*, respectively. In the *hipp8-1* allele (SM_3_25599), the T-DNA is located 221 bp downstream of the predicted start codon. The T-DNA insertion site in *hipp9-1* (SM_3_30660) is 1664 bp downstream of the ATG.

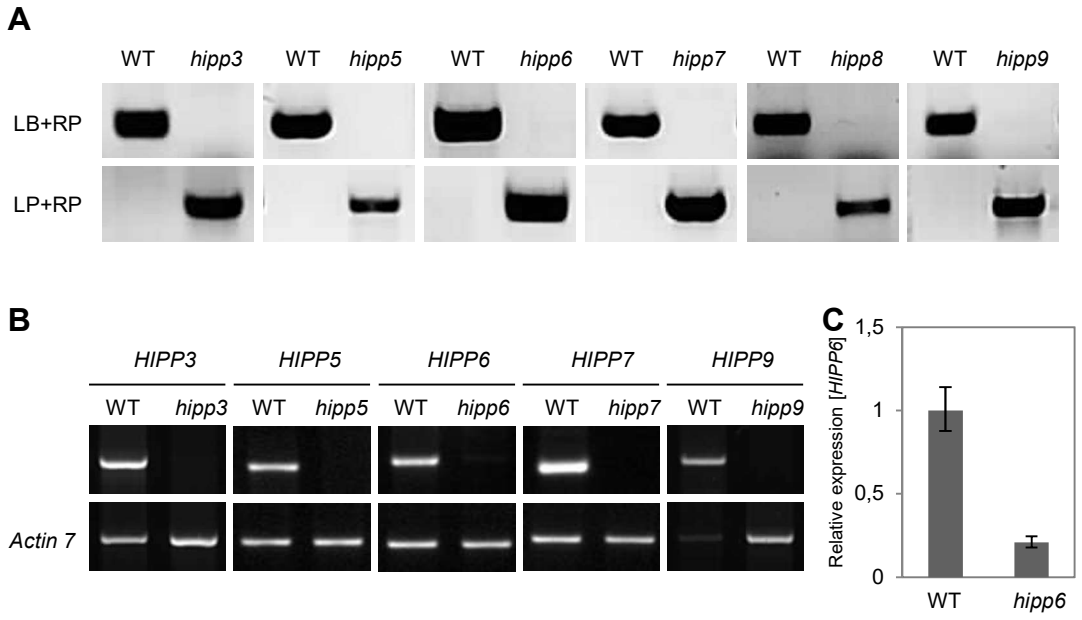

Figure 40. Molecular characterization of *hipp* T-DNA insertion alleles.
(A) Genotyping PCR. DNA from the wild-type (WT) and insertional mutant seedlings 10 DAG was used as template for the PCR. LB, left border T-DNA primer; RP, right genomic primer; LP left genomic primer, according to the SALK primer design tool. Primers used are further detailed in the Table 11.
(B) *HIPP* transcript levels in WT and individual insertional mutants. RNA from seedlings 10 DAG was used as template for the RT-PCR. Primers used for the analysis are depicted in Fig. 39. *Actin7* was included as a control.
(C) Relative *HIPP6* transcript abundances in the WT and *hipp6* mutant seedlings grown on soil for 10 days as measured by qRT-PCR. Data are means ± SE (*n* = 3).

Individual *hipp* homozygous mutants were isolated by PCR-based genotyping (Fig. 40A). Semi-quantitative RT-PCR analyses showed an absence of the respective WT transcripts in

the homozygous mutants of *hipp3*, *hipp5*, *hipp7* and *hipp9* (Fig. 40B), indicating complete knockouts of the corresponding genes. The *hipp6-1* has an insertion in the 5' UTR of the gene, and RT-PCR did not detect any *HIPP6* transcripts using primers flanking the T-DNA insertion sequence (Fig. 40B). However, a reduced *HIPP6* expression to about 20% of the WT level could be detected in the homozygous plants by qRT-PCR using primers downstream of the insertion (Fig. 40C), suggesting that the *hipp6-1* represents a hypomorphic allele.

3.3.3 *hipp* single mutant plants display distinct phenotypic changes during shoot development

Compared to the WT plants, no visible effects on vegetative growth were observed in the analyzed *hipp* single knockout and knockdown mutants grown under LD conditions (Fig. 41).

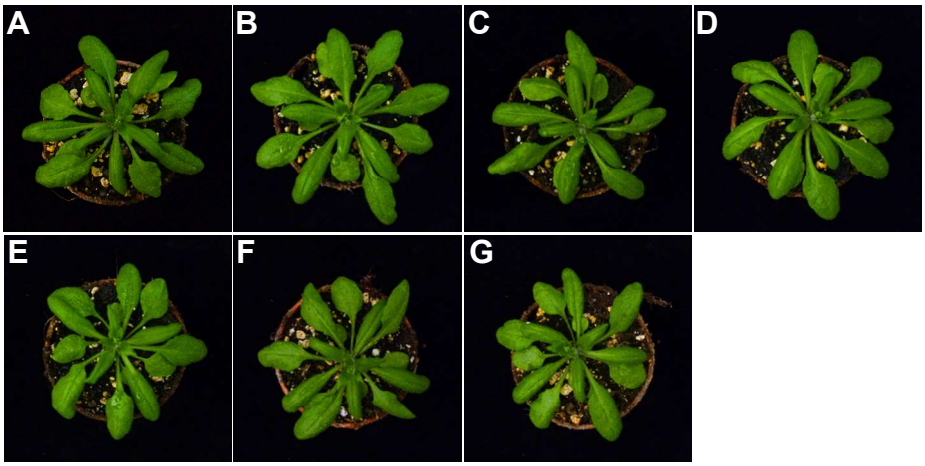

Figure 41. *hipp* single mutants do not exhibit phenotypic changes during vegetative growth.
(A-G) In comparison to WT **(A)**, no visible differences were observed in single knockout or knockdown mutants of *hipp3* **(B)**, *hipp5* **(C)**, *hipp6* **(D)**, *hipp7* **(E)**, *hipp8* **(F)** and *hipp9* **(G)** at 20 DAG.

Interestingly, phenotypic analysis revealed that the *hipp5*, *hipp6* and *hipp7* single mutants exhibited an earlier flowering phenotype under SD conditions (Fig. 42A). The strongest effect was observed for *hipp7*, which flowered about 10 days earlier than WT (Fig. 42A). The early flowering correlated with a reduced number of rosette leaves being formed at the bolting time (Fig. 42B). These results indicated a role of *HIPP* genes in regulation of timing of transition from vegetative to reproductive phase.
Moreover, the *hipp7* mutant exhibited an about 13% reduction of shoot height as well as 10% less siliques on the main stem compared to the WT under LD conditions (Fig. 42C and D). The *hipp5* mutant plants also formed 7% less siliques on the main stem compared to the WT (Fig. 42D). The data suggest that the activity of the shoot apical meristem was reduced and that the *HIPP* genes may play a role in controlling this process.

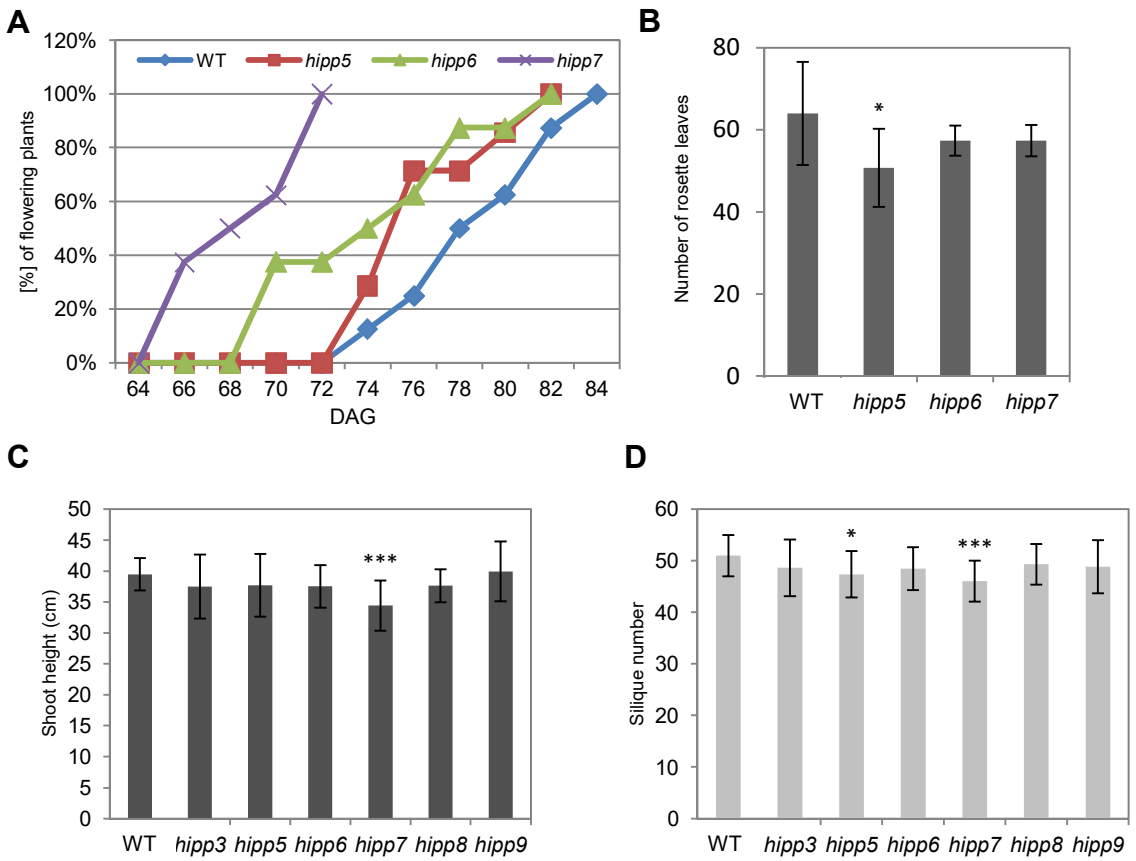

Figure 42. Phenotypic changes of *hipp* mutants during reproductive development.
(A) Flowering time under SD conditions of WT, *hipp5*, *hipp6* and *hipp7* mutants. ($n > 20$).
(B) Number of rosette leaves as counted at the flowering time point under SD conditions. Data are means ± SD ($n > 20$). *$P < 0.05$, calculated by Student's *t* test.
(C) Shoot height of fully mature plants under LD conditions. Data are means ± SD ($n > 20$). ***$P < 0.005$, calculated by Student's *t* test.
(D) Number of siliques on the main stem determined at full maturity. Data are means ± SD ($n > 20$). *$P < 0.05$, ***$P < 0.005$, calculated by Student's *t* test.

Overexpression of clade-I *HIPP* genes caused pleiotropic phenotypes and altered cytokinin activity as described above (3.2). To investigate whether cytokinin activity was affected in *hipp* mutants, responses of selected *hipp* mutants to various concentrations of exogenous cytokinin were assessed. Fig. 43 shows that the primary root growth as well as lateral root development were not altered compared to WT upon cytokinin or mock treatment, suggesting eventually a higher degree of functional redundancy among the clade-I *HIPP* genes in controlling cytokinin responses.

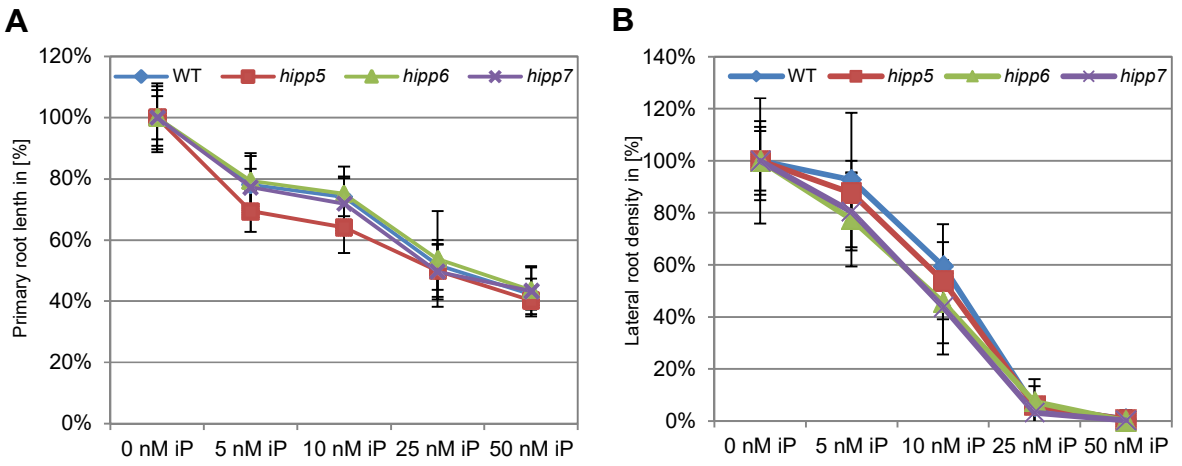

Figure 43. Effects of exogenous cytokinin on root development in *hipp* single mutants.
(A) and **(B)** The inhibitory effect of cytokinin on primary root growth **(A)** and lateral root density **(B)** are showed. WT, *hipp5*, *hipp6* and *hipp7* mutants were grown on vertical agar plates supplemented with 0, 5, 10, 25 and 50 nM iP. Primary root length and lateral root density were evaluated 10 DAG, and the results expressed relative to the mock (0 nM iP) treatment. Data are means ± SE (*n* = 20).

To investigate the impact of exogenous cytokinin on shoot development, the shoot fresh weight of plants grown in the presence of various concentrations of cytokinin was measured. As shown in Fig. 44, cytokinin significantly reduced the WT shoot growth in a concentration -dependent manner. Whereas *hipp6* and *hipp7* showed similar responses, the *hipp5* mutant was significantly less sensitive to cytokinin treatment than the WT control (Fig. 44).

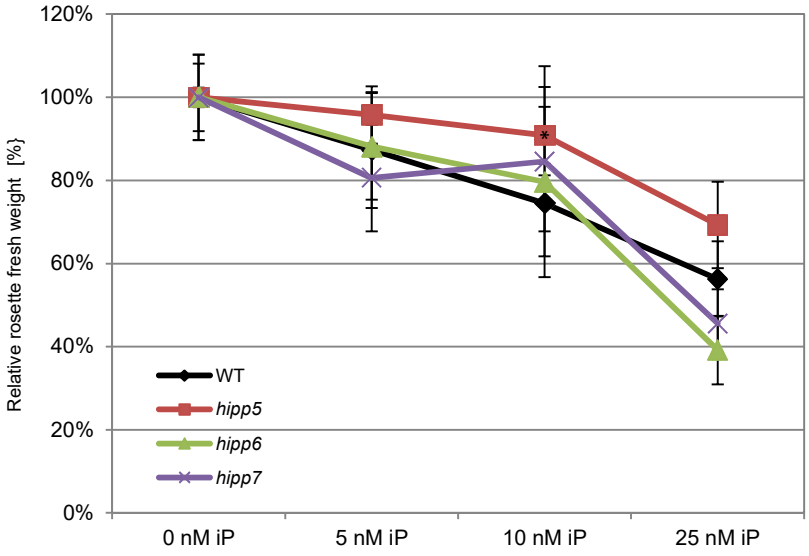

Figure 44. Shoot growth of the *hipp5* mutant is less sensitive to exogenous cytokinin.
Effects of exogenous cytokinin on shoot growth of WT and *hipp* mutant plants. Seedlings were grown on agar plates supplemented with 0, 5, 10 and 25 nM iP. Fresh weight of 10 rosettes 10 DAG was measured per one sample and the results expressed relative to the mock (0 nM iP) treatment. Data are means ± SE (*n* = 3). **P* < 0.05, calculated by Student's *t* test.

Although *hipp6* and *hipp7* mutant plants showed similar morphological responses to WT, it might be that the mutant plants differed from WT at the molecular level. Indeed, a reduced expression of type-A *ARR* genes *ARR5* and *ARR7* was detected in *hipp5*, *hipp6*, *hipp7* mutant plants. However, the reduced expression of the type-A *ARR* genes could not be confirmed in all independent biologic experiments and the data are not shown.

3.3.4 *hipp1* is a gain-of-function mutant and displays retarded root growth

For the *HIPP1* gene, a homozygous T-DNA insertion line *hipp1-1* (SALK_028133C) was isolated and characterized. The T-DNA insertion site has been annotated in the middle of the last exon (Fig. 45A). However, sequencing of the junction between the left border of the T-DNA and the genomic region revealed that the insertion was located exactly in the stop codon of the gene (Fig. 45A). The insertion changed the original TGA stop codon into the TAA stop codon (Fig. 45A), but apparently did not affect the protein coding capacity of the locus. However, the influence of the altered sequence of the 3'UTR on the expression of the *HIPP1* gene is unclear. Semi-quantitative RT-PCR was used to analyze this question. However, no transcripts of the *HIPP1* gene was detected in both WT and *hipp1* mutant plants when using primers located directly at the beginning and end of the *HIPP1* coding sequence *At2g28090.1* according to the TAIR10 genome annotation. Similarly, qRT-PCR did not detect any *HIPP1* transcripts when using PCR primers located in the first annotated exon.

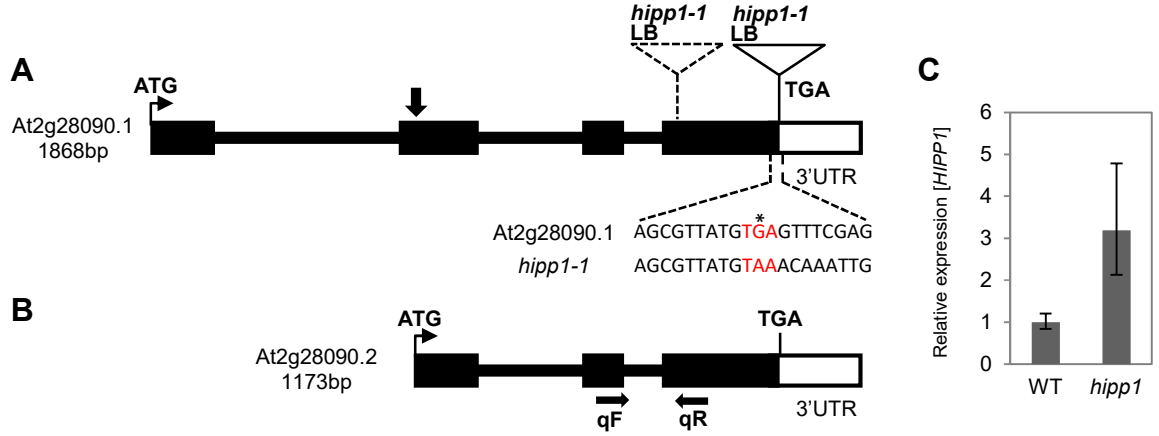

Figure 45. Identification and characterization of the T-DNA insertion mutant of *HIPP1*.
(A) *At2g28090.1* is the annotated protein-coding gene model for *HIPP1*. The length of the genomic *HIPP1* gene sequences is given in base pairs. LB, Left border. Arrow indicates the position of the alternative start codon in **(B)**. Dashed-lined and full-lined triangle indicates the annotated and the experimentally determined T-DNA insertion sites, respectively. White box indicates the 3' untranslated regions (UTR), and black boxes indicated exons. No 5' UTR is annotated. The *hipp1* T-DNA insertion is located in the stop codon of the *HIPP1* gene. The original and newly formed stop codon are indicated in red. * indicated the T-DNA insertion site.
(B) *At2g28090.2* gene annotation model. The length of the genomic *HIPP1* gene sequences is given in base pairs. White box indicates the 3' untranslated regions (UTR), and black boxes indicated exons. No 5' UTR is annotated. qF and qR indicate positions of *HIPP1*-specific qRT-PCR primers used in **(C)**.
(C) Relative *HIPP1* transcript abundances in the WT and *hipp1* mutant seedlings grown on soil for 10 days as measured by qRT-PCR. Data are means ± SE (*n* = 3).

Interestingly, there is apparently another, as yet unannotated, open reading frame with an alternative start codon located in the second exon of *At2g28090.1* (Fig. 45B). This alternative gene model, named here *At2g28090.2* (Fig. 45B) is supported, for example, by the full length cDNA clone AY924752 available through the ABRC stock centre. This clone was also used for other experimental works in this thesis (3.1 and 3.2). According to the new gene model, new primers were designed (Fig. 45B) to analyze the *HIPP1* transcript abundances in the *hipp1* mutant and WT plants. The analysis showed that *HIPP1* transcript levels were increased by 3-fold in *hipp1-1* in comparison to WT (Fig. 45C), suggesting that *hipp1-1* might be a gain-of-function mutant allele.

Phenotypic analysis revealed that the *hipp1-1* mutant displayed a strongly retarded root growth phenotype (Fig. 46A). As presented in Fig. 46B, the primary root elongation of the *hipp1* mutant line was reduced to about 65% of the WT. The root meristem size was compared by scoring the number of the cortex cells between the quiescent center and transition zone. The cortex cell number was strongly reduced in the *hipp1* root meristems in comparison to WT (Fig. 46C-E). Interestingly, these phenotypic changes of *hipp1* are very similar to those observed in the *HIPP1*-overexpressing plants (see 3.2.3), supporting the idea that *hipp1-1* is a gain-of-function allele. Interestingly, as shown in Fig. 45C, the increase of the *HIPP1* transcript levels in the *hipp1-1* mutant were not dramatic compared to WT, but the *hipp1* mutant plants revealed a stronger short root phenotype (35% reduction in primary root elongation) compared to the *UBQ10:HIPP1* overexpression line 23 (20% reduction in primary root elongation), in which the expression of *HIPP1* was increased 3000 times (Fig. 17). This raised the question whether the short root phenotype of *hipp1-1* might have been duo to another insertion in the genome. To test this, the *hipp1-1* was backcrossed to WT, and the F3 homozygous *hipp1-1* plants were reanalyzed. Fig. 46F shows that the backcrossed *hipp1* homozygous plants still had a retarded root growth in comparison to the WT control. Intriguingly, the root phenotype was weaker in comparison to the original *hipp1-1* mutant, indicating some factor enhancing the *hipp1-1* effect in the original genetic background.

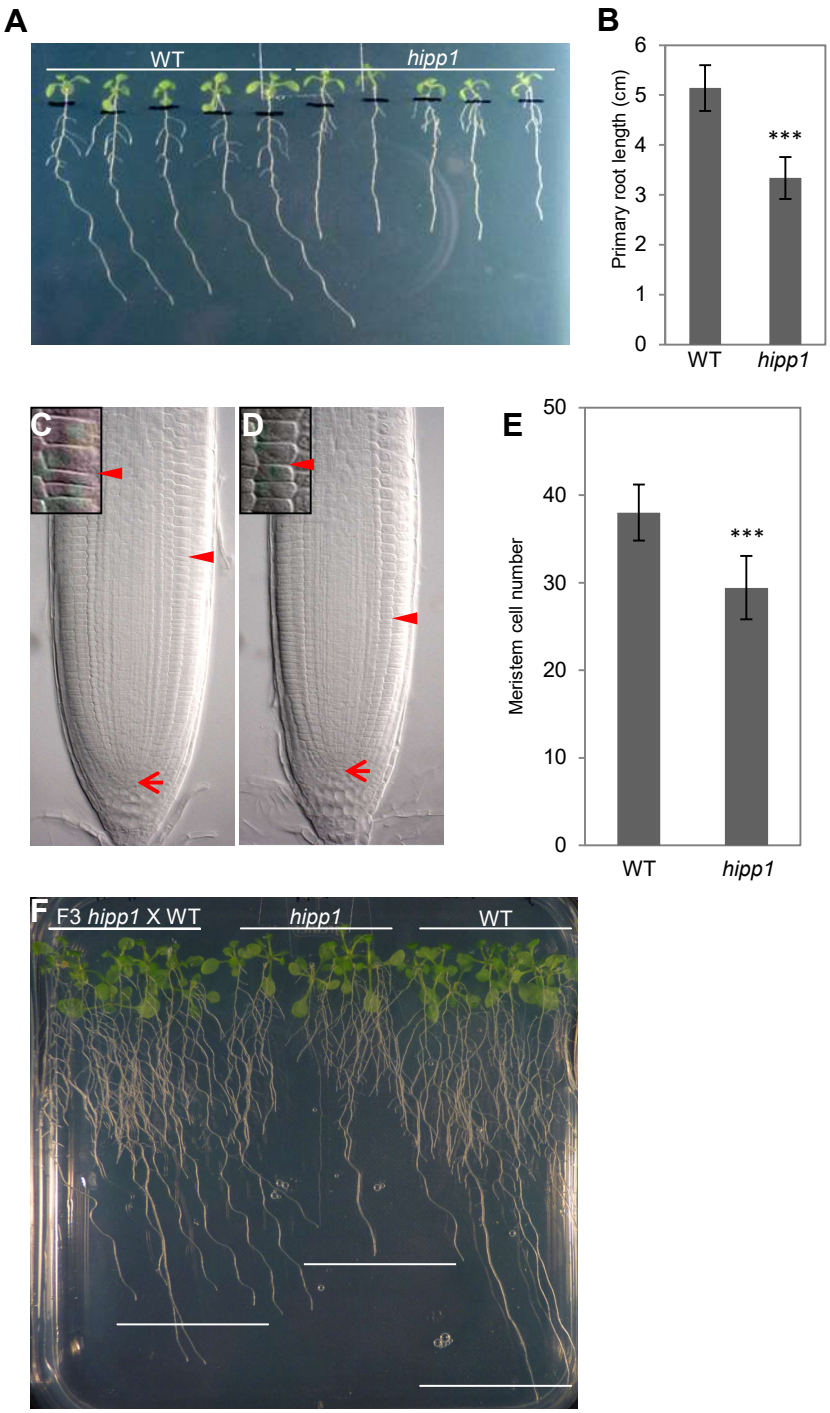

Figure 46. *hipp1* displays retarded root growth.
(A) Primary root of the wild type (WT) and *hipp1-1* plants 10 DAG.
(B) Primary root length of the WT and *hipp1-1* plants. Primary root length was evaluated 10 DAG. Data are means ± SD ($n > 20$). ***$P < 0.005$, calculated by Student's *t* test.
(C) and **(D)** Root meristems of WT **(C)** and *hipp1-1* **(D)** 7 DAG. Arrows indicate the QC and arrowheads indicate the cortex cells at the transition zone. The insert shows a blow-up of elongating cells exiting from the meristem at the transition zone.
(E) Root-meristem cell number of the WT and *hipp1-1* mutants depicted in **(C)** and **(D)**. Data are means ± SD ($n = 20$). ***$P < 0.005$, calculated by Student's *t* test.
(F) Primary root growth of the homozygous *hipp1-1* backcrossed to WT (F3 *hipp1* x WT) compared to the *hipp1-1* mutant line and WT plants at 10 DAG.

3.3.5 Phenotypic analyses of *hipp* higher-order Arabidopsis mutants

The isolated *hipp* single knockout and knockdown mutants displayed no obvious differences during vegetative growth under normal growing conditions. However, homologous genes from the same family may share a large degree of functional redundancy. Therefore, *hipp* double or triple mutants were generated and phenotypically assessed. However, under normal conditions *hipp* double mutants also did not show any visible morphologic changes during vegetative growth (Fig. 47).

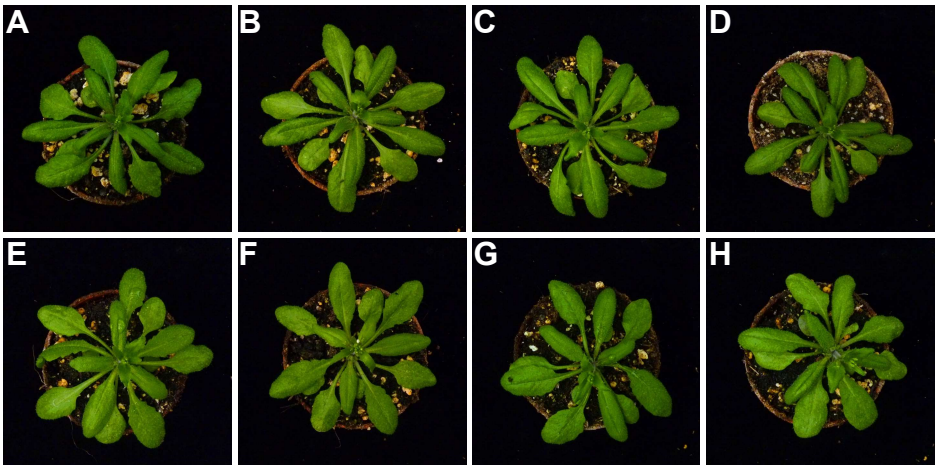

Figure 47. *hipp* double mutants have no visible phenotypic changes during vegetative growth.
(A-H) In comparison to WT, no visible differences were observed in *hipp* double mutants. Rosettes of WT **(A)**, *hipp3,5* **(B)**, *hipp3,6* **(C)**, *hipp3,8* **(D)**, *hipp5,6* **(E)**, *hipp5,7* **(F)**, *hipp6,7* **(G)** and *hipp6,8* **(H)** plants 20 DAG.

Whereas, the *hipp6,7* mutant displayed an early flowering phenotype, the flowering time of *hipp5,7* and *hipp5,6* was not changed compared with WT control (Fig. 48A).
During reproductive development, *hipp5,6*, *hipp5,7* and *hipp6,7* exhibited a reduced shoot height compared to WT under LD conditions (Fig. 48B). Moreover, the *hipp5,6* mutant plants produced significantly less siliques on the main stem than WT (Fig. 48C). Surprisingly, the changes were not stronger than those detected in the single mutants (Fig. 42).
Since the *hipp5* shoots showed a slightly insensitive reaction to cytokinin, the growth responses to various cytokinin concentrations were studied in the *hipp5,6* and *hipp5,7* double mutants. The analysis revealed that the response of *hipp5,7* to 10 nM cytokinin was further compromised in comparison to either of the *hipp5* or *hipp7* single mutants (Fig. 48D), suggesting that these two *HIPP* genes have partially overlapping functions in regulating responses to cytokinin. Intriguingly, *hipp5,6* double mutant, did not show any difference comparing with WT under these conditions, although the *hipp5* single mutant was less sensitive to cytokinin (Fig. 44).

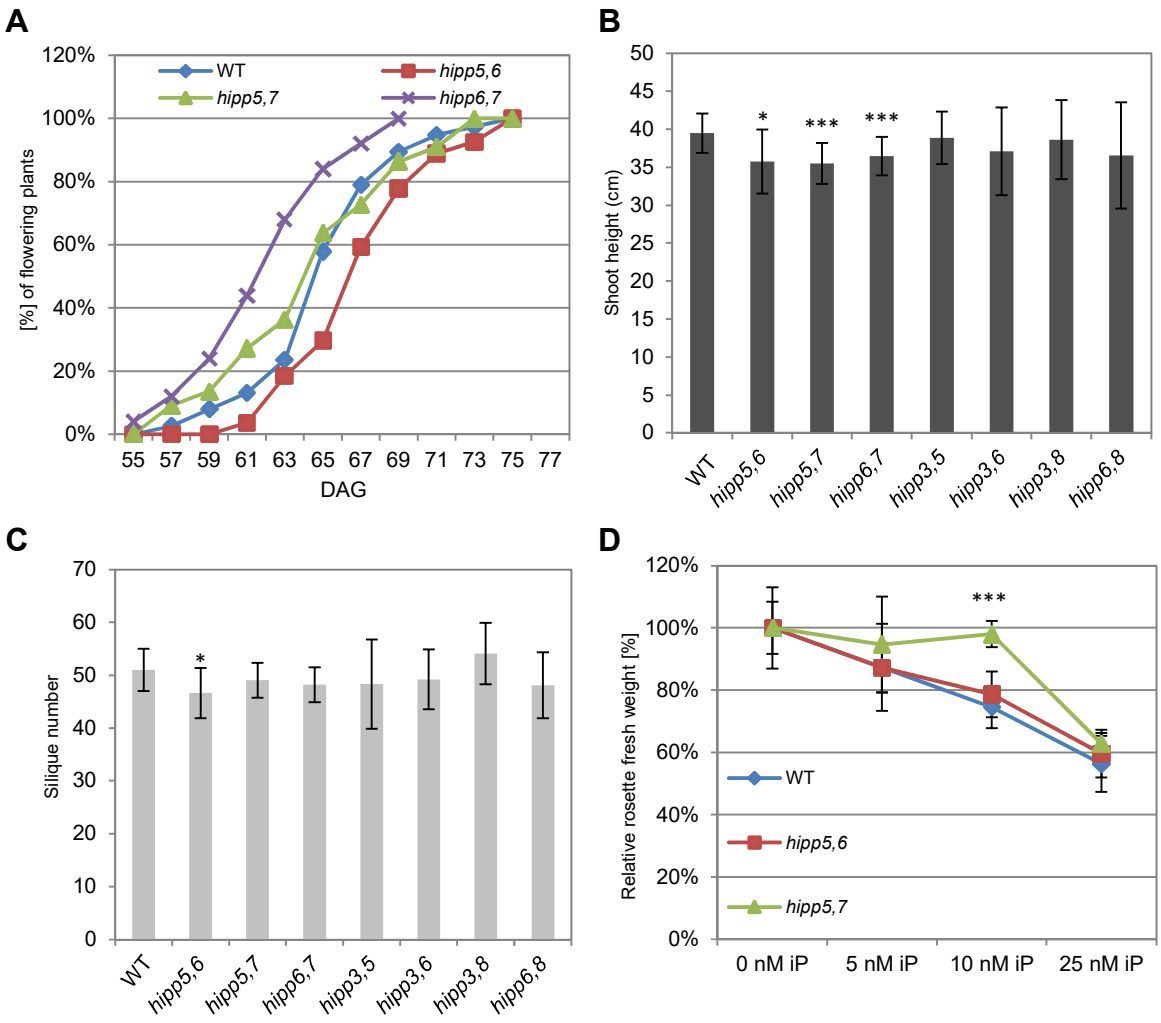

Figure 48. *hipp* double mutants exhibited phenotypic changes during reproductive development and altered sensitivity to exogenous cytokinin.
(A) Flowering time under SD conditions of WT, *hipp5,6*, *hipp5,7* and *hipp6,7* double mutants. ($n > 20$).
(B) Shoot height of fully grown plants under long-day conditions. ($n > 20$). $^{*}P < 0.05$, $^{***}P < 0.005$, calculated by Student's *t* test.
(C) Number of siliques on main stem per plant. ($n > 20$). $^{*}P < 0.05$, calculated by Student's *t* test. It should be noted that the results shown in **(B)** and **(C)** originate from the same biological experiments as shown in Fig. 42C and D.
(D) Exogenous cytokinin inhibits *hipp* double mutants shoot growth. Seedlings were grown on agar plates supplemented with 0, 5, 10 and 25 nM iP. Fresh weight of 10 rosettes 10 DAG was measured per one sample and the results expressed relative to the mock (0 nM iP) treatment. Data are means ± SE ($n = 3$). $^{***}P < 0.005$, calculated by Student's *t* test. The presented results originate from the same biological experiments as shown in Fig. 44.

Next, the triple mutant was generated by crossing the double mutants *hipp5,6* and *hipp6,7*. Preliminary results showed that the *hipp5,6,7* triple mutant developed leaves, which were pale green in comparison to WT and which were rounded leaf margin compared to the WT (Figure 49A-D), suggesting a lower chlorophyll content in this mutant. In addition, the mutants leaves were slightly smaller and developed less pronounce serration and crinkly leaf margins as compared to WT (Fig. 49). Together, these results may indicate a role of the respective *HIPP* genes during the process of the acquisition of leaf shape and size.

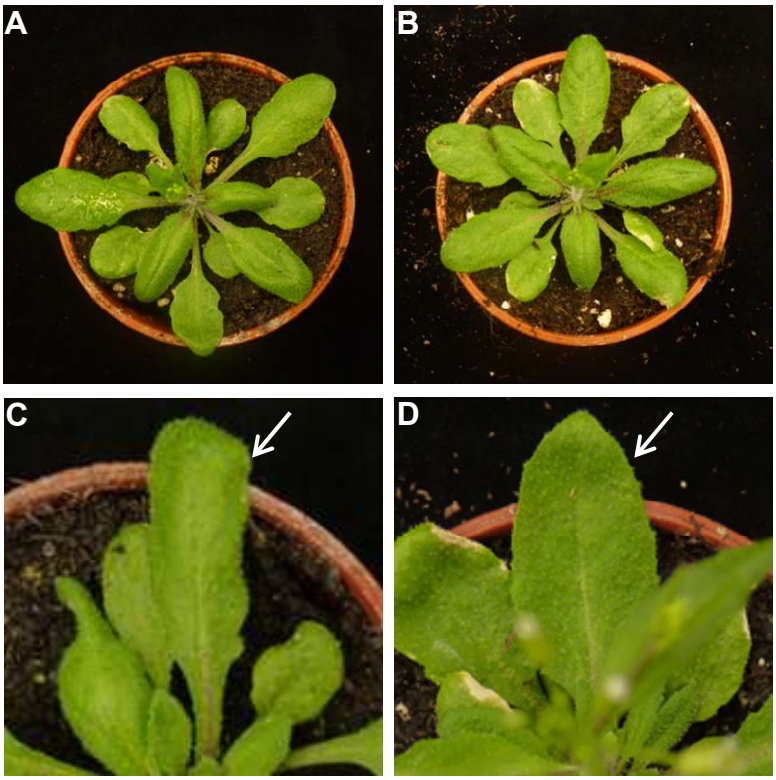

Figure 49. The leaf development in the *hipp5,6,7* triple mutants.
(A) to **(D)** In comparison to WT **(A)**, the *hipp5,6,7* triple mutant plants showed paled and smooth leaf margins **(B)** at 20 DAG. Arrows indicate leaf 7 from the WT **(C)** and *hipp5,6,7* triple mutant **(D)** after bolting at 23 DAG.

Interestingly, phenotypic analyses revealed that the *hipp5,6,7* triple mutant formed significantly less rosette leaves at the bolting time compared to WT under LD conditions (Fig. 50), suggesting that the flowering of *hipp5,6,7* was also slightly accelerate under LD conditions. However, this needs to be further analyzed.

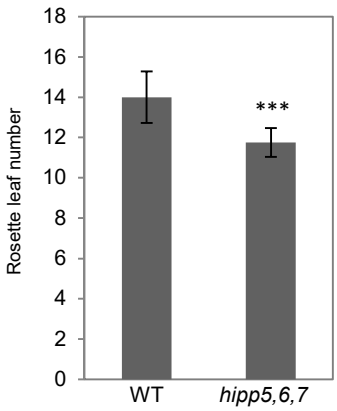

Figure 50. *hipp5,6,7* display a reduced number of rosette leaves being formed at bolting time.
Number of rosette leaves as counted at the bolting time point under LD conditions. Data are means ± SD ($n > 7$). ***$P < 0.005$, calculated by Student's *t* test.

3.3.6 The *hipp5,6,7* triple mutants display enhanced drought sensitivity

To examine whether the reduced expression of *HIPPs* alters plant's responses to drought, the *hipp5,6,7* triple mutant was analyzed under the same drought stress treatment as described in chapter **3.2.8**. *hipp5,6,7* triple mutant seedlings revealed severe significant wilting and damage already 5 days after completely withdrawing water, whereas a significantly high number of WT plants maintained turgor (Fig. 51). In agreement with the results that the *HIPP*-overexpression plants displayed increased drought tolerance, these results together indicate that the HIPP proteins play a positive role in regulating responses to drought stress.

Figure 51. Drought-sensitive phenotype of the *hipp5,6,7* triple mutant.
Three-week-old wild type (WT) and *hipp5,6,7* triple mutant plants were exposed to drought for 5 day and photographed. Note that the results shown in this figure originate from the identical biological experiments as shown in Fig. 37.

3.4 Tissue specific expression of individual *HIPP* gene family members

In order to analyze expression patterns of individual *HIPP* genes of cluster I, promoter regions upstream of the translational start ATG of four individual *HIPP* genes, i.e. the 795 bp region of *HIPP1*, the 2056 bp region of *HIPP5*, the 949 bp region of *HIPP6*, and the 1580 bp region of *HIPP7*, were fused to the *GUS* gene. The resulting reporter gene constructs are called *pHIPP1S:GUS*, *pHIPP5:GUS*, *pHIPP6S:GUS* and *pHIPP7:GUS*, respectively, in the following. Additionally, because of the alternative gene annotation model (3.3.4) of *HIPP1*, the 1491 bp region, which is upstream of the alternative translational start ATG of *At2g28090.2*, was fused to the *GUS* gene and is called *pHIPP1L:GUS* in the following. Moreover, promoter-proximal introns can have a large influence on the level and pattern of gene expression (Wang et al., 2002; Jeong et al., 2007; Rose et al., 2008). In order to determine whether the promoter-proximal introns have effects on the expression of the *HIPP6* gene, a second *HIPP6* reporter gene construct was cloned. This 1364 bp-long construct includes the same ATG-upstream region (see above) as well as some parts of the coding region and the first two introns as indicated in Fig. 39. The reporter is called *pHIPP6L:GUS* in the following. Arabidopsis plants were stably transformed with these constructs and at least three independent lines for each *pHIPP:GUS* construct were analyzed by scoring the GUS activity at different developmental stages.

3.4.1 Individual members of the *HIPP* gene in clade-I are expressed differentially

No GUS signal was detected in plants expressing neither the *pHIPP1S:GUS* nor *pHIPP1L:GUS* construct (data not shown), which correlates to the low expression of the *HIPP1* gene as described above (see 3.2).

The *pHIPP5:GUS* reporter was expressed highly and predominantly in the root meristem. It was first detectable in the tip of the radicle after its emergence (Fig. 52A). At 2 DAG, the activity was detected specifically in the center of the primary root apical meristem (RAM), including the stem cell niche and partially the cells of the lateral root cap (Fig. 52B). The GUS activity was detected also in the vascular cylinder (Fig. 52C). No *pHIPP5:GUS* signal was detected in the early or late stages of lateral root primordia (LRP) development (Fig. 52D and E), in the emerged lateral roots (Fig. 52F), or at the beginning of the fast lateral root elongation (Fig. 52G). Interestingly, staining signal appeared later in the lateral root meristem, and became progressively stronger with the maturation of the lateral root (Fig. 52H and I). In shoot, the *pHIPP5:GUS* activity was detected in the shoot apex and in the vasculature of cotyledons and true leaves (Fig. 52J and K). A strong *pHIPP5:GUS* expression was also

detected at the root-hypocotyl junction (Fig. 52L). During flower development, *pHIPP5:GUS* activity was observed in young developing stamen primordia (Fig. 52M) and was later restricted to the central part of filament (Fig. 52N). Overall, the *pHIPP5:GUS* showed the strongest activity among the analyzed *HIPP:GUS* reporter constructs, potentially indicating a higher *HIPP5* expression levels at least at the analyzed developmental time points.

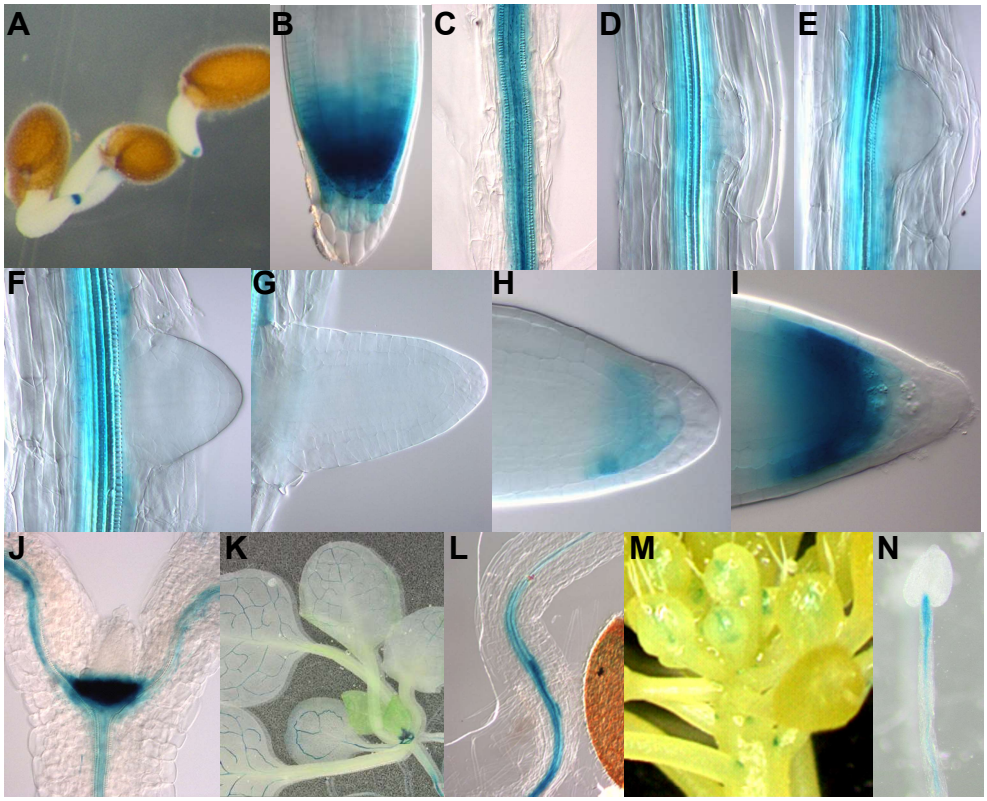

Figure 52. Expression analysis of the *HIPP5* gene promoter.
(A) to **(N)** The earliest activity of *pHIPP5:GUS* is detected in the root tip of germinating seedlings **(A)**, in apical meristem **(B)**, and in the vasculature **(C)** of the primary root. *pHIPP5:GUS* activity is not detected during early **(D)** or late **(E)** stage of lateral root primordia formation, in the emerged **(F)** and early elongating **(G)** lateral roots. The staining appeared in the lateral root apical meristem at later stages **(H)** and became stronger with the maturation of lateral root **(I)**. Expression in the shoot is confined mainly to the shoot apex **(J)**, the vascular system of young tissues (e.g., cotyledons **[J]** and young true leaves **[K]**). The *pHIPP5:GUS* expression at the root-hypocotyl junction **(L)**. In flowers, expression is detected in developing stamen **(M)** and in the filament **(N)**.

For *pHIPP6S:GUS*, the expression was first detectable also in the tip of the radicle after its emergence (Fig. 53A). In contrast to the specific meristem expression of *HIPP5*, the maximum expression of *HIPP6* was restricted to the lateral root cap of the primary root (Fig. 53B) and no GUS expression was detected in the LRPs or in the apical meristems of mature lateral roots (data not shown). Similar to *pHIPP5:GUS*, the signal could be also detected in the root vasculature (Fig. 53C) and at the root-hypocotyl junction (Fig. 53D). Weak *pHIPP6S:GUS* activity was detected in the vasculature of cotyledons (not shown) and occasionally at the hypocotyl-cotyledon vascular junction (Fig. 53E). Interestingly, GUS activity disappeared in the emerging radicle when promoter-proximal introns were included in

the *pHIPP6L:GUS* construct (Fig. 53F). Moreover, in comparison to the strong expression of *pHIPP6S:GUS* in the lateral root cap, only faint staining was detected in this tissue in plants expressing *pHIPP6L:GUS* (Fig. 53G). Furthermore, the GUS signal was mostly detected in the central cylinder of the primary root (Fig. 53G). In contrast to *pHIPP6S:GUS*, weak or no signal was detected in the root vasculature, root-hypocotyl junction and hypocotyl-cotyledon vascular junction of the *pHIPP6L:GUS* plants (Fig. 53H-J). These results indicate presence of negative *cis* regulatory elements in the exon/intron region included in the *pHIPP6L:GUS* reporter.

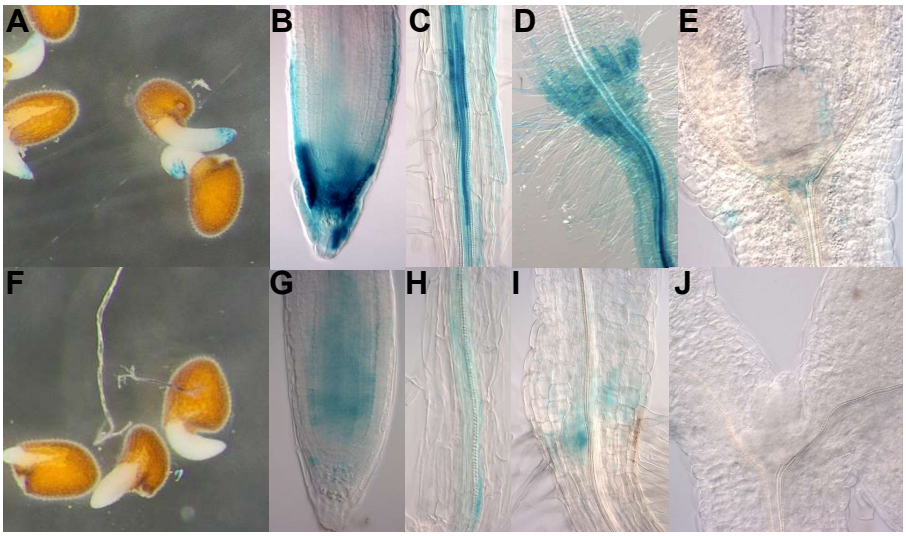

Figure 53. Expression pattern of two different *HIPP6* gene promoter constructs.
(A) to **(E)** Localization of *pHIPP6S:GUS* activity. The earliest expression of *pHIPP6S:GUS* is detected in the root tip of germinating seedlings **(A)**, in the lateral root cap **(B)**, root vasculature **(C)** and at the root-hypocotyl junction **(D)**. Weak *pHIPP6S:GUS* expression at the hypocotyl-cotyledon vascular junction **(E)**.
(F) to **(J)** Localization of *pHIPP6L:GUS* activity. The activity is weaker or undetectable in the same tissues as shown in **(A)** to **(E)**.

For *pHIPP7:GUS*, no GUS activity was detected in the tip of the radicle after its emergence (Fig. 54A). At 2 DAG, weak expression was detected in the columella and lateral root cap (Fig. 54B). GUS signal was also associated with the vasculature and apical meristem of lateral roots (Fig. 54C-G). The expression of *pHIPP7:GUS* was observed in the inner cell layers of early stage lateral root primodia (Fig. 54C), and the GUS signal expanded to all cells of the LRPs at later stage (Fig. 54D). Strong staining signal was detected in the basal part of lateral roots and weakly in the forming vascular cylinder (Fig. 54E). Interestingly, the *pHIPP7:GUS* signal became weaker with the progression of lateral root development (Fig. 54F), and was later restricted to the QC and the stem cell niche (Fig. 54G). Only faint GUS signal was detected at the root-hypocotyl junction (Fig. 54H). In the shoot, the greatest *pHIPP7:GUS* activity was present in the stomatal guard cells of cotyledons (Fig. 54I). During reproductive development, the expression of *pHIPP7:GUS* was found in anthers (Fig. 54J).

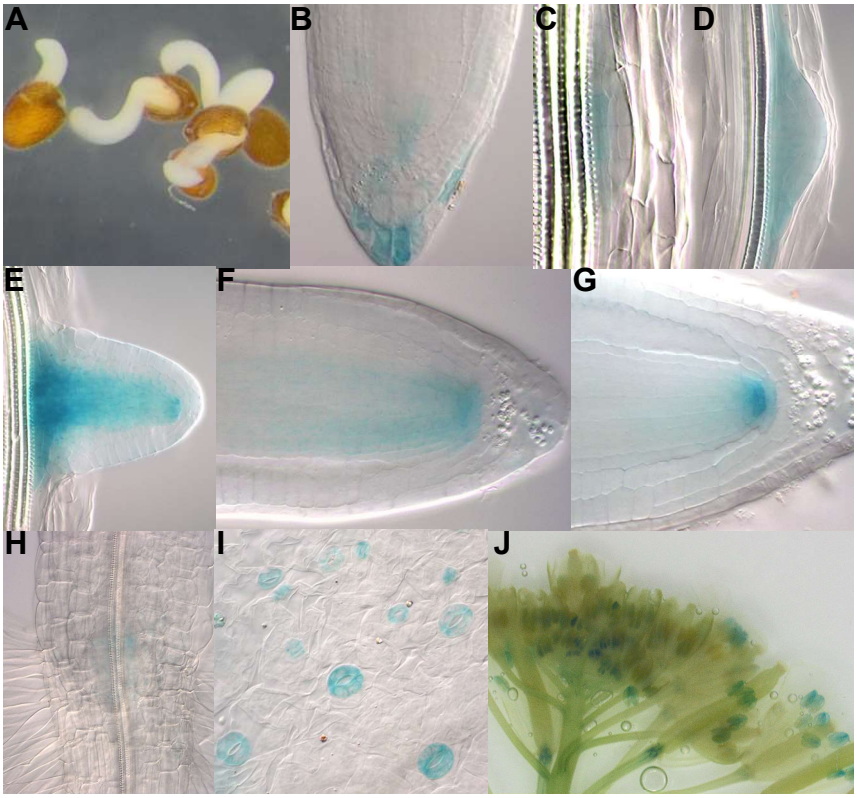

Figure 54. Expression analysis of *HIPP7* gene promoter.
(A) to **(J)** No *pHIPP7:GUS* expression is detected in the root tip of germinating seedlings **(A)**. Weak expression in the columella and lateral root cap of the primary root **(B)**. GUS signal is detectable during early **(C)** and late **(D)** stages of lateral root primordia development. Signal in the emerging lateral root **(E)** becomes weaker **(F)** and restricted to the stem cell niche **(G)**. Root-hypocotyl junction **(H)**. *pHIPP7:GUS* activity in the stomatal guard cells of cotyledons **(I)** and in anthers **(J)**.

Because the two different *HIPP1* reporter gene constructs did not show activity, the *HIPP1* expression in different tissues was analyzed by qRT-PCR. The analysis confirmed that the *HIPP1* expression is overall very low (Fig. 55A). The highest transcript levels were detected specifically in the inflorescence (Fig. 55A), suggesting its potential function in this restricted tissue. The *HIPP6* transcripts were most abundant in the root (Fig. 55B), which correlated with the histochemical reporter gene analysis. The qRT-PCR analysis revealed that, in contrast to *HIPP1* and *HIPP6*, the *HIPP7* exhibits a relatively broad expression, with the exception of roots (Fig. 55C).

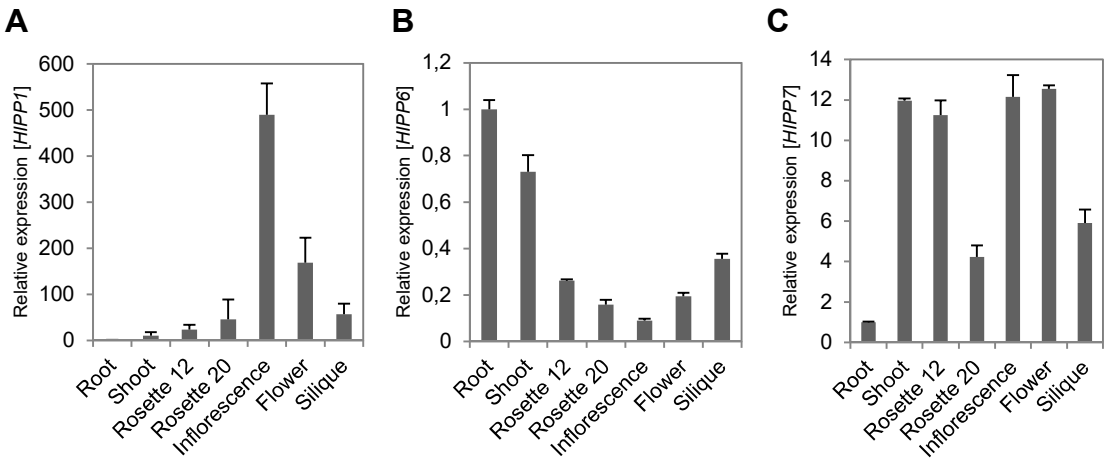

Figure 55. Tissue-specific expression of *HIPP1*, *HIPP6* and *HIPP7*.
(A) to **(C)** Relative transcript abundances of the *HIPP1* **(A)**, *HIPP6* **(B)**, and *HIPP7* **(C)** genes as measured by qRT-PCR. Tissues analyzed were root and shoot from seedlings 10 DAG grown on agar plates, 12 and 20 DAG soil-grown rosettes, inflorescences, flower buds and flowers, and young siliques. The expression in root was set to 1 and the other samples were expressed relative to it. Data are means ± SE (*n* = 3).

3.4.2 Cytokinin regulates *HIPP* gene expression in Arabidopsis

Analysis of microarray data from Arabidopsis exposed to cytokinin has shown that most *HIPP* transcript levels did not change under these conditions. However, the expression levels of *HIPP5* and *HIPP6* were down-regulated in response to cytokinin (Bhargava et al., 2013). To examine this in more detail, qRT-PCR analysis of the clade-I *HIPP* genes in Arabidopsis seedlings exposed to cytokinin was performed. As shown in Fig. 56A, the *ARR5* transcript levels were elevated by 17-fold after 30 min of cytokinin application and then the expression declined to 6 fold after 120 min. This was consistent with the previous results (Brandstatter and Kieber, 1998; D'Agostino et al., 2000) and confirmed that the cytokinin induction was sufficient. After 30 min cytokinin treatment, the *HIPP5* and *HIPP6* transcript levels were downregulated to about 40% relative to the control plants, and then the expression restored to normal levels after 2 hour-treatment (Figure 56B). Very similar reaction was detected also for *HIPP7*. Little or no reduction was detected for *HIPP3* transcript levels following the cytokinin treatment. By contrast, *HIPP9* was slightly, but not significantly, downregulated after 30-min treatment, but the expression increased 3-fold after 2 hours of cytokinin application (Figure 56B).

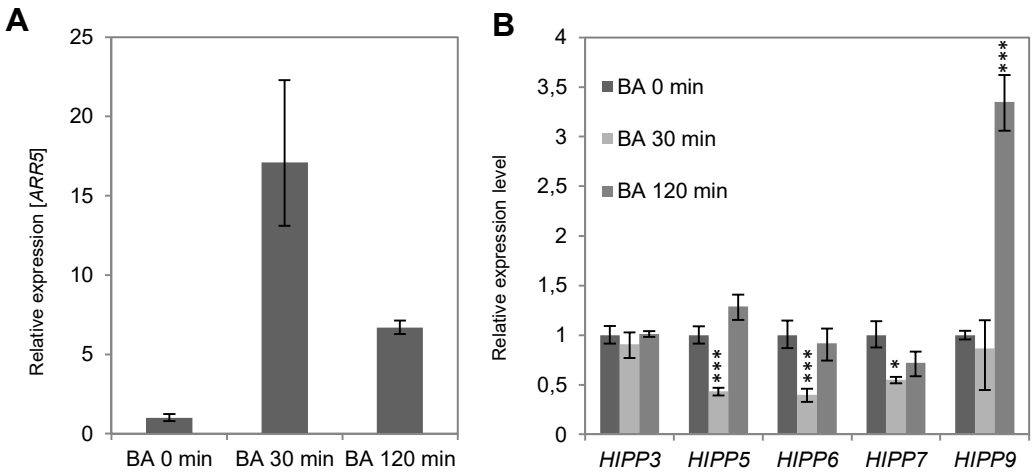

Figure 56. Regulation of the *HIPP* gene expression by cytokinin.
(A) and **(B)** Relative transcript abundances of the *ARR5* **(A)** and clade-I *HIPP* **(B)** genes as measured by qRT-PCR. Total RNA extracted from 10 day-after-germination (DAG) seedlings grown on agar plates treated with 5 μM BA for 0, 30 or 120 min. The expression level at 0 min was put to 1, and other values were expressed relative to it. Control seedlings treated with DMSO for 30 and 120 min displayed no significant changes in the steady-state levels of *ARR5* or *HIPP* transcripts. Data are means ± SE (n = 3). *P < 0.05, ***P < 0.005, calculated by Student's t test.

To further confirm the down-regulation of *HIPP* genes by cytokinin, the expression of the *pHIPP:GUS* constructs in the presence of 10 nM BA was examined. Figure 57 shows that control plants harboring the *pARR5*:*GUS* fusion displayed higher GUS activity in response to cytokinin. In contrast, significantly weaker GUS activity was observed in the *pHIPP5:GUS* and *pHIPP6S:GUS* reporter lines grown on media with 10 nM BA, indicating that the downregulation of these *HIPP* genes by cytokinin was due to transcriptional repression.

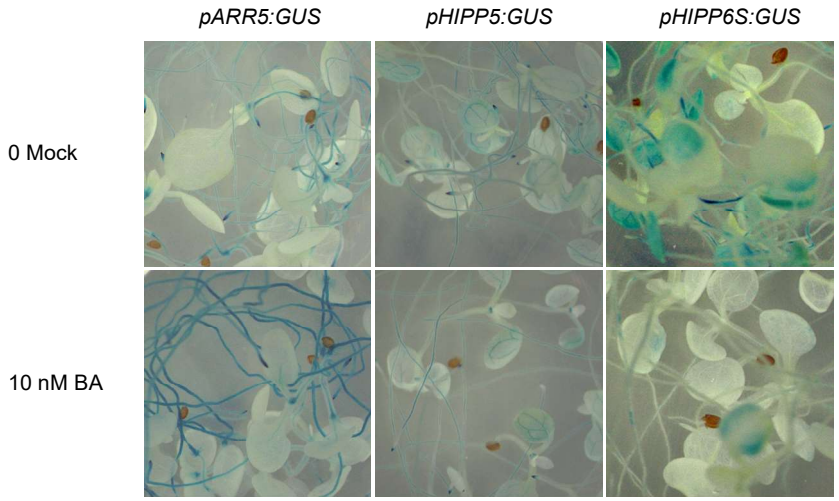

Figure 57. Reduced *pHIPP5:GUS* and *pHIPP6S:GUS* expression in response to exogenous cytokinin.
Weaker GUS staining signals were observed in lines harboring the *pHIPP5:GUS* and *pHIPP6S:GUS* constructs when grown on media supplemented with 10 nM BA for 7 days. Three independent lines for each construct were examined with similar results and one representative line is shown.

4 Discussion

4.1 The interaction between CKXs and HIPPs

The main aim of this work was to identify proteins which could physically interact with CKX proteins and sequentially influence cytokinin homeostasis. For that, a genome-wide yeast two-hybrid (Y2H) screen with the CKX1 protein as bait has previously been performed in the Dr. Werner's group, and a group of positive CKX-interacting proteins have been characterized molecularly and genetically in this work. Intriguingly, six of the candidates are from the plant-specific HIPP protein family, which is characterized by the presence of one or two HMA domains and an isoprenylation motif at the protein C terminus. The results demonstrated that CKX1-HIPP7 interactions were completely abolished when the Cys-residue within the isoprenylation motif was mutated (Fig. 9). Furthermore, the yeast results revealed that the conserved HMA domains was dispensable for the CKX1-HIPP7 interaction, but was required for the formation of HIPP7 homodimer (Fig. 9 and 10). Additional HIPP members from outside cluster I and III did not interact with CKX1. Most, but not all CKXs interacted with four tested HIPP proteins (Fig. 8C). These findings indicate the selectivity in CKX-HIPP protein interactions requiring a specific protein-interacting interface provided apparently by both the posttranslational modification of HIPPs and by conserved protein-protein binding motifs in HIPP and CKX proteins. BiFC assays revealed that in contrast to the GFP-HIPP7, which predominantly localized to cytosol (Fig. 12), the CKX1-HIPP7 complex clearly localized to the cortical and perinuclear ER (Fig. 13). These results indicate that the CKX1-HIPP7 complex formation involves the relocation of CKX1 to the cytosolic site of the membrane and the relocation of HIPP7 to the ER. The major results and conclusions regarding the molecular aspects of CKX1-HIPP7 interaction are summarized and will be discussed in details below.

4.1.1 Isoprenylation is required but not sufficient for CKX-HIPP protein interaction

The specific interactions between CKX1 with several HIPP proteins were detected with high frequency in the Y2H screen (~65% of all isolated interactions), indicating occurrence of some particular domains in HIPP proteins, which are specifically required for the interaction. Mutation of the Cys-residue within the isoprenylation motif of HIPP7 completely abolished the CKX1-HIPP7 interactions (Fig. 9), indicating that the HIPP7 prenylation is indispensable for the interaction. However, the fact that other HIPP proteins outside the clade I and III did not interact with CKX1 suggests that HIPP protein prenylation itself is not sufficient for the

interaction and further suggest that the interaction is mediated either indirectly or not exclusively by the prenyl moiety. One possibility is that the isoprenylation mediates the subcellular localization of HIPP protein which directly provides an interface for the interaction. It has been reported that CKX1 is an integral single-pass membrane protein that localizes predominantly to the ER in Arabidopsis to directly regulate the cytokinin signaling output in this compartment (Niemann et al., 2018). This indicates that the interaction of CKX1 with HIPP proteins may require that the HIPP proteins associate with the ER. It is plausible that the ER association is modulated by HIPP prenylation. Although the function of protein prenylation is not precisely understood, current evidence suggests that the lipid modification serving as a membrane anchor regulates the subcellular location of the protein (Hemsley, 2015). The covalent attachment of the isoprenoid intermediates farnesyl diphosphate (FPP) or geranylgeranyl diphosphate (GGPP) to cysteines in conserved carboxy-terminal sequence motifs enhanced the hydrophobicity of the prenylated proteins and, at least partially, result in their association with endomembrane system in the cell, which is essential for their biological activity (Galichet and Gruissem, 2003). For example, current study with *N. benthamiana* NbHIPP26 protein has demonstrated that the protein localized in the plasma membrane, small motile vesicles, the plasmodesmata, the nucleoplasm and the nucleoli. Mutation of the prenylated cysteine residue largely reduced the association of NbHIPP26 with plasma membrane and increased the protein accumulation in the cytosol and nucleus (Cowan et al., 2018). Although the prenylation may promote the protein affinity for the membranes, HIPP proteins studied in this work were found to localize in various compartments outside of the endomembrane system. For example, HIPP1 protein has a predicted nuclear localization signal (NLS; amino acids 100-122 based on gene model of At2G28090.2; cNLS Mapper; Kosugi et al., 2009) and was visible mainly in the nucleus and cytoplasm (Fig. 11). Similarly, HIPP5 and HIPP7 were localized predominantly in the cytosol of *N. benthamiana* epidermal cells and in the nucleoplasm (Fig. 12). Even though GFP-HIPP7 showed apparent colocalization with ER marker of RFP-p24 in the cortical cell region, this colocalization was visible with only low frequency (Fig. 12). A similar nuclear and cytoplasm localization of HIPP3, which also belongs to cluster I of the HIPP protein family, has been observed previously (Zschiesche et al., 2015). Additional, expression of RFP-tagged fusion proteins in protoplasts showed that rice OsHIPP21 and OsHIPP41 localize in the cytosol and in the cell nucleus (de Abreu-Neto et al., 2013). These results together indicate that many HIPP proteins, including those studied in this work, are soluble proteins and are not bound to membranes by the hydrophobic anchor provided by the prenylation, at least when expressed in *N. benthamiana* or protoplasts.

This lack of strong membranes association might be duo to other motifs existing in the HIPP proteins that mediate targeting into other subcellular compartments. For example, transient

expression of GFP-fused rice calmodulin protein, GFP-CaM61, which has a C-terminal CaaX motif, showed that the GFP fluorescence was associated with the cytoplasm, cell periphery, ER and the nucleus (Gerber et al., 2009). By contrast, when expressing a truncated version of the CaM61, that contains only the C-terminal domain with a series of basic amino acid residues followed by the CaaX isoprenylation motif, a clear plasma membrane localization was observed (Gerber et al., 2009).

The association of GFP-HIPP7 with membranes was tested more rigorously by the membrane fractionation and protein gel blot experiments using stable Arabidopsis lines generated in this work. This analysis did not fit the timeframe of this work and was performed by the colleagues in Dr. Werner's group. Interestingly, this analysis revealed that GFP-HIPP7 was predominantly associated with microsomal membranes and almost absent in the supernatant fraction of soluble proteins, whereas the membrane association of HIPP7^{C352G} mutant lacking the prenylation site was strongly reduced (Dr. Werner's group; unpublished data). This indicates that the HIPP7 protein is attached to endomembrane system in the cell and prenylation is important for the membrane association. These results are in discrepancy with the microscopic observations of the cytosol and nuclear localization of GFP-HIPP7 protein in *N. benthamina* cells. One explanation could be that in the subcellular localization studies, the 35S promoter was used for ectopic expression of GFP-HIPP7. By contrast, a weaker promoter, the UBQ10, was used in the protein fractionation studies in Arabidopsis. Thus, in the subcellular localization studies, the overexpressed protein might not be prenylated sufficiently in the *N. benthamiana* epidermal cells, which could partially account for the cytosolic localization of GFP-HIPP7. This could be either because the capacity of the prenylation machinery in *N. benthamiana* cells was exceeded or the *N. benthamiana* enzymes involved in the prenylation do not efficiently recognize the Arabidopsis HIPP7 protein as a substrate. However, in contrast to this idea stands the strong interaction between CKX1 and HIPP proteins expressed in *N. benthamina*; which was dependent on the functionl CaaX motif.

After prenylation, the three C-terminal residues (i.e., the -aaX) are proteolytically clipped off and, in turn, the exposed carboxyl group of the prenylated cysteine is methylated. The proteolysis and carboxyl-methylation are often referred to as CaaX processing (Bracha-Drori et al., 2008). Although prenylation is important for the correct subcellular localization of CaaX proteins, often promoting protein peripheral association to plasma or endomembranes, the membrane localization of prenylated proteins has been shown to also strongly depend on CaaX processing (Hancock et al., 1991). This is more pronounced in the farnesylated (C15) proteins than in the more hydrophobic geranylgeranylated (C20) protein (Michaelson et al., 2005). Interestingly, the two endoproteases STE24 and RCE1, which catalyze the prenyl-dependent endoproteolysis, and the two isoprenyl carboxy methyltransferases (ICMTs)

are all localized in the ER membrane, indicating that prenylated proteins have to reach the ER membrane to undergo the CaaX processing. This implies that, although the final subcellular localization of prenylated proteins can be very different, they have to reach the ER during their biogenesis. Hence, the ER membrane is the compartment where HIPP proteins may encounter CKX1 for interaction.

In general, prenylation is a weak membrane anchor, and usually requires a second signal to enable stable membrane attachment. These signals include S-acylation, a poly basic stretch of amino acids for further interacting with phospholipid head groups, or certain number of hydrophobic residues to penetrate deeper into the membrane core (Hemsley, 2015). The membrane fractionation experiment in Arabidopsis showed that the membrane association of the HIPP7^{C352G} mutant protein was strongly reduced but not totally abolished by the lack of the prenylation site (Dr. Werner's group; unpublished data), indicating that a second signal is existing in HIPP7 for membrane targeting. Interestingly, most of HIPP proteins contain several Cys residues which can be potentially S-acylated (Hemsley et al., 2013). S-acylation is a reversible lipid modification involving the addition of acyl lipids to cysteine residues of proteins through thioester bonds (Li and Qi, 2017). S-acylation has no defined consensus sequence for modification, but usually requires prior modification by N-myristoylation or prenylation (Hemsley, 2015). For example, besides prenylation, the NbHIPP26 has been shown to be lipid modified by S-acylation through a Cys residue at the N terminus. The S-acylation is important for the localization of NbHIPP26 at plasma membrane and PD as the mutation of the Cys residue caused the accumulation of the protein in the nucleus and cytosol (Cowan et al., 2018). HIPP7 contains seven Cys residues: four in the two HMA domains, one as the prenylation site, and two of unknown function (amino acids 93 and 107). The Cys^{93} residue is strongly predicted as a S-acylation site (Ren et al., 2008). S-acylation usually requires a prior protein prenylation (Hemsley, 2015). If the membrane association of HIPP7 is required for the interaction with CKX1, the lack of prenylation in the HIPP7^{C352G} mutant could prevent its S-acylation and reduce thus the ability of the protein to interact. Moreover, an insufficient S-acylation of GFP-HIPP7 expressed in *N. benthamiana* could also partially account for the apparent cytosolic localization. However, further experiments are required to clarify whether S-acylation exists in HIPP7 and acts as a membrane association anchor.

The second hypothesis how the prenylation might determine the CKX-HIPP interaction is that the prenyl moiety directly mediates the interaction. Indeed, in the case of the interaction studies performed in the yeast two hybrid system, CKX1 and HIPP7 proteins were targeted to the nucleus by the NLS encoded by the prey and bait vectors. One can thus assume that both proteins were in soluble form and not membrane associated when expressed in yeast. However, the interaction with CKX1 was strictly dependent on the prenylation, because the prenylation mutant HIPP7^{C352G} lost the ability to interact with CKX1 (Fig. 9). This suggests that

the prenylation of HIPP7 is not only required for the membrane association (as shown in Arabidopsis) but also for the direct protein-protein interaction. However as mentioned above, not all tested HIPP proteins interacted with CKX1 suggesting that some amino acid residues within the HIPP protein, together with the prenyl moiety, may be required to form the protein interaction interface. Indeed, it has been shown that protein residues in close proximity to the prenylation site are relevant for mediating the interaction, as for example in the case of RPGR-PDE6D interaction (Lee and Seo, 2015). RPGR is an isoprenylation protein with a C-terminal CaaX box motif. Deletion of the CaaX motif or substitution of the Cys residue within the CaaX motif to Ser completely abolished the RPGR-PDE6D interaction. Interestingly, substitution of a Ser residue at the -3 position from the CaaX motif to Ala did not impair the RPGR prenylation but largely reduced the ability of RPGR to bind PDE6D, indicating that the prenylation and also the amino acid residues near the prenylation site might directly form an interaction motif (Lee and Seo, 2015). It is therefore plausible that certain amino acid residues, or motifs, which occur only in specific HIPP proteins, are necessary to facilitate the interaction with CKX.

Interestingly, the prenylation appears to be also involved in HIPP7 homodimerization as indicated by the complete loss of homodimerization in HIPP7^{C352G} mutant. The hypothesis that HIPP-amino acid residues are also relevant for the protein-protein interaction is supported by the fact that HIPP7 homodimerization was abolished by the mutation of two Cys residues within the HMA domain. HMA domains are found in bacteria, yeast, animal and plants, and are characterized by the conserved M/LXCXXC heavy metal binding sequence which usually forms a ferredoxin-like structural fold. Several HMA containing proteins displayed a function in transporting metallic ions to specific cellular sites or in heavy metal homeostasis (Dykema et al., 1999; Chu et al., 2005). Nevertheless, there are also reports showing that the HMA domain is essential for protein-protein interaction. For example, the NaKR1 (HPP2) is reported to interact with FLOWERING LOCUT T (FT) *in vitro* and *in vivo*. Interestingly, a truncated protein containing only the HMA domain of NaKR1 has been shown to be sufficient for interacting with FT, indicating that the interaction between NaKR1 and FT might be related to HMA function in metal binding (Zhu et al., 2016). Similarly, substitution of the two central Cys residues of the M/LXCXXC core sequence in HIPP26 completely abolished the interaction between HIPP26 and ATHB29 (Barth et al., 2009). However, although the HMA is relevant for HIPP7 homodimerization, mutation of the Cys residues in HMA domains of HIPP7 did not interrupt the CKX1-HIPP7 interaction (Fig. 9). Similarly, the mutation of the HMA domain of NbHIPP26 retained the TBG1-NbHIPP26 interaction (Cowan et al., 2018). These results suggest that the mechanisms of the HIPP7 homodimerization and CKX-HIPP heterocomplex formation are apparently different.

In addition to the cytosol and nuclear localization that were seen in the analyzed leaf cells, the GFP fused HIPP1, HIPP5 and HIPP7 proteins were also visible in the plasmodesmata (PD) (Fig. 11 and 12). Interestingly, in comparison to GFP-HIPP7, the frequency of PD localization was lower and the fluorescence signal associated with PD was significantly weaker in Arabidopsis plants expressing the GFP-HIPP7^{C352G} mutant form (Fig. 12), indicating that the prenylation of HIPP7 is important for the association with the PD. Interestingly, Cowan et al., (2018) recently reported that NbHIPP26 was associated with a population of PD in *N. benthamiana* epidermal cells and the PD-localization was weaker in the prenylation-lacking mutant protein. Cowan et al., (2018) have proposed that prenylation is not only relevant for HIPP protein localization to the PD, but also for the long-distance movement of HIPP proteins or for the PD-meditated intracellular signaling. What is the mechanism of targeting HIPP proteins to PD and how the prenylation is precisely involved in this process is currently unclear. However, interestingly, a proteomics approach has revealed that more HIPP proteins might be associated with PD (Fernandez-Calvino et al., 2011).

4.1.2 What are the additional CKX-HIPP interaction determinants in HIPP proteins?

As discussed above, HIPP protein prenylation itself is indispensable but not sufficient for the CKX-HIPP interaction. Some specific amino acid residues or motifs within the HIPP protein may be required to form the protein interaction interface. Interestingly, in addition to the characterized HMA domain and isoprenylation motif, most of HIPP proteins have a number of glycine-rich and proline-rich regions localized between these elements (de Abreu-Neto et al., 2013). In plants, glycine- and proline-rich proteins have been reported to be involved in cellular stress responses and signaling (Bai et al., 2009; Czolpinska and Rurek, 2018). In general, these regions are discussed to be important for structural protein conformation, subcellular localization and protein-protein interaction. With respect to the latter, it has been proposed that these proteins may act as assembly pieces of multicomponent complexes and that the glycine- and proline-rich domains are functioning as structural features that define their position and function in such large complexes (Mangeon et al., 2010). For instance, the glycine-rich domains can assume a secondary structure as β-pleated sheets composed of a varying number of antiparallel strands that generate a large surface with strongly hydrophobic regions to interact with other hydrophobic partners (Sachetto-Martins et al., 2000). The recognition of proline-rich sequences by intracellular protein domains is essential for coordinated assembly of multiprotein complexes during the process of signaling transduction (Kay et al., 2000; Gu et al., 2005). The sequence PxxPxxP (x can be any residue) represents a majority of proline-rich target sequences, which forms a unique recognition motif for

protein-binding (Ball et al., 2005). Interestingly, two such putative core sequences (PIPPPPP and PPPPPPP) are present in the proline-rich region (amino acids 141-PIPPPPPPP-149) of HIPP7, suggesting that this domain might be involved in the interactions of HIPP7 with other proteins. However, further studies are required to clarify whether the proline- and glycine-rich regions found in different HIPP proteins are functionally relevant for protein-protein interactions.

4.1.3 Are HIPP proteins involved in the ER-associated degradation of CKX proteins?

The interaction domain of the CKX1 has been mapped by a deletion approach in Dr. Werner's group (unpublished data). The experiments showed that the C-terminal part of CKX1 is required for the interaction and amino acid residues at position 409 to 430 are crucial for the interaction in particular. Furthermore, an Asn-Ile-Leu-Thr (NILT) sequence motif within this region was identified to be conserved among all CKX proteins interacting with HIPP, but not in CKX7. Mutation of this motif abolished the CKX1-HIPP7 protein interaction, which supports the idea that the interaction depends on the CKX protein sequence itself and that the C terminus of CKX is mediating it.

CKX1 has been shown to be a type II membrane protein with a short cytosolic N terminus and a C-terminal catalytic domain oriented to the ER lumen (Niemann et al., 2018). Interestingly, the fluorescence of the NVen-CKX1/CVen-HIPP7 BiFC complex clearly localized to the cortical and perinuclear ER and small punctate structures (Fig. 13I and J), indicating that either the HIPP7 protein had to enter the ER lumen to encounter the C terminus of CKX1 or the CKX1 protein was transported to the cytosol and interacted with HIPP7 at the cytosolic side of the ER membrane. The first hypothesis appears very unlikely in the light of the current understanding of protein prenylation. Although the prenylated proteins have to reach the ER to undergo the CaaX processing, because the corresponding endoproteases (Rce1 and Ste24) and ICMTs are localized in the ER membrane (Bracha-Drori et al., 2008), many studies have shown that the respective catalytic reactions take place at the cytosolic side of the ER membrane (Choy et al., 1999; Apolloni et al., 2000; Romano and Michaelis, 2001; Wright and Philips, 2006; Wright et al., 2009; Pryor et al., 2013). For example, studies of the crystal structure of an Rce1 homolog from the archaea *Methanococcus maripaludis* have revealed that the core catalytic cavity, which contains the conserved catalytic glutamate and histidine residues, opens to the cytosol (Manolaridis et al., 2013; Hampton et al., 2018). Similarly, the crystal structure analysis has revealed that the *Methanosarcina acetivorans* ICMT is an integral membrane protein containing several transmembrane helices and a highly conserved C-terminal cytosolic loop serving as a catalytic domain (Yang et al., 2011). It is,

therefore, reasonable to assume that, similar to other prenylated proteins, HIPP proteins do not enter the ER lumen but undergo the CaaX processing at the cytosolic side of the ER. This could also partially account for the occasionally observed ER localization of GFP-HIPP7 in the *N. benthamiana* epidermal cells.

Hence, the second, more plausible, hypothesis how the HIPP7 protein could encounter an access to the C-terminal domain of CKX1 protein is that CKX1 is retrotranslocated to the cytosol. This hypothesis is strongly supported by the work of Niemann et al., (2015) who have demonstrated that CKX1, as well as other CKX proteins targeted to secretory pathway, are ERAD substrates and their protein abundances are reduced by the loss of ROCK1, which functions as an important part of the ERQC system. ERAD is a conserved, multistep degradation process that involves protein retrotranslocation across the ER membrane, ubiquitination, and cytosolic/nuclear 26S proteasome (Smith et al., 2011). Misfolded proteins must ultimately arrive at the membrane-anchored ERAD complexes for ubiquitination and, because the catalytic domain of the core component of the ERAD complexes are on the cytosolic surface of the ER membrane, there is a requirement for the retrotranslocation of the ERAD substrates into the cytosol to undergo ubiquitination and to access the cytosolic proteasome system for their degradation (Deshaies and Joazeiro, 2009). This indicates that the CKX1-HIPP interaction may take place during the retrotranslocation of CKX1 to the cytosolic side of the ER and the interaction might influence the efficiency of the process and thereby the degradation rate of the CKX1 protein. Similar scenario is also conceivable for other CKX isoforms capable to interact with the characterized HIPP proteins. It is interesting to note that CKX7, which is the single cytosolic CKX isoform apparently not controlled by ROCK1-mediated ERQC, did not interact with any of the tested HIPP proteins (Fig. 8). The mechanism of how the HIPP proteins connect to ERAD of secretory CKX proteins is currently unclear. The fact that all transgenic Arabidopsis lines overexpressing different HIPP proteins showed increased cytokinin responses may suggest that HIPP proteins promote protein retrotranslocation, which results in reduced CKX protein levels in the ER and upregulated cytokinin concentrations in the compartment lumen. This hypothesis is supported by the result that the levels of the CKX1-myc were strongly reduced in the *AtML1:CKX1-myc*, *UBQ10:HIPP1* double transgenics (Fig. 31A and C), which suggests that the degradation of CKX1 by 26S proteasome was increased. Interestingly, in contrast to HIPP1, CKX1-myc protein levels were significantly increased upon the expression of *35S:HIPP6* and *35S:HIPP7* (Fig. 31B and D). This discrepancy could be explained by the different subcellular localization of CKX1-HIPP1 and CKX1-HIPP7 complexes in the cell as revealed by the BiFC assays. The fluorescence of the NVen-CKX1/CVen-HIPP7 complex clearly localized to the cortical and perinuclear ER and small punctate structures (Fig. 13I and J), whereas the fluorescence signal of the NVen-CKX1/CVen-HIPP1 complex was mainly localized in the nucleus and

cytoplasm (Fig. 14). These results together indicate that, although the interaction between CKX1 and different HIPP proteins apparently facilitates the retrotranslocation, the CKX1-HIPP7 complex is retained and eventually accumulates at the cytosolic side of the ER membrane without being further processed by the ERAD machinery. In contrast, the cytosolic/nuclear localization of the CKX1-HIPP1 BiFC complex together with the lowered CKX1-myc levels in *UBQ10:HIPP1* plants suggest that the interaction with HIPP1 enhances the proteasomal degradation of CKX1. More experimental data will be needed to explain this discrepancy. One possibility is that different HIPP proteins regulate different steps of the ERAD pathway. Whereas HIPP7 might, for example, control more upstream processes such as the retrotranclocation at the membrane, HIPP1 may promote more downstream steps of ERAD such as to escort the substrate proteins to the proteasome. The observed accumulation of CKX1-myc in *35S:HIPP6*- and *35S:HIPP7*-expressing plants might imply that some intrinsic factors are rate-limiting for the protein degradation in the experimental system used. However, it should be noted that the knowledge about the plant ERAD processes is rather limited, especially for the later stages of the ERAD pathway, such as how the misfolded proteins undergo retrotranslocation and sequentially the delivery of the ERAD substrates to the 26S proteasome (Liu and Li, 2014). More experiments are required to understand the molecular function of the HIPP proteins during the ERAD of the CKX. It will be also interesting to explore whether other ERAD substrate proteins are regulated by HIPPs.

4.2 A role of clade-I *HIPP* genes in regulating plant growth and development

4.2.1 Overexpression of *HIPP* genes increases cytokinin signaling output

The cytokinin signal is perceived by three AHK cytokinin receptor proteins, which have been reported to localize to plasma membrane and to a larger extend to the ER (Fig. 58) (Caesar et al., 2011; Wulfetange et al., 2011). The ligand binding domain of the latter receptors is oriented into the lumen of the ER, whereas the C-terminal kinase domain and receiver domain are exposed to the cytoplasm. The current model predicts that the bulk of cytokinin signaling is initiated from the ER and the cellular response to this hormone is determined by the steady-state concentration in the ER lumen (Fig. 58) (Romanov et al., 2018). The hypothesis proposed in this work that the interaction between CKX and HIPP proteins facilitates the retrotranslocation of CKX from the ER provides a model for how the overexpression of HIPP proteins influence the subcellular levels and degradation of secretory CKX proteins and thereby modulate cytokinin homeostasis and cytokinin responses in the cell (Fig. 58). The enhanced retrotranslocation of the CKX proteins into the cytosol could reduce the abundance

of the active CKX proteins in the ER lumen resulting in less cytokinin degradation in the ER (Fig. 58). Increased cytokinin levels in the ER lumen would consequently enhance cytokinin signaling through the ER-localized AHK receptors (Fig. 58). Such an elevated signaling will trigger cytokinin-related transcriptional programs and corresponding developmental changes.

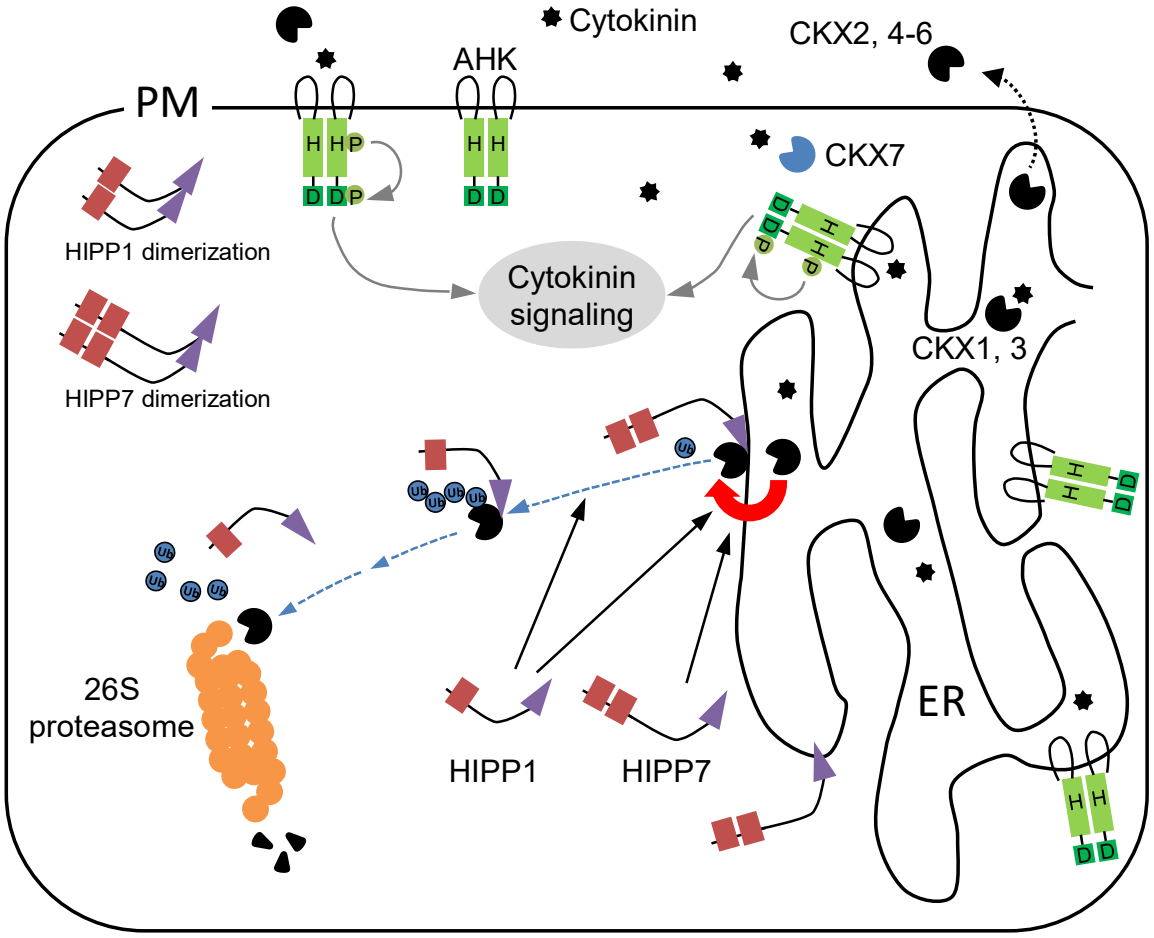

Figure 58. Model of CKX-HIPP interaction and its effect on cytokinin homeostasis.
Cytokinin is perceived by AHK receptors localized to the plasma membrane and, to a larger extend, to the ER. The steady-state concentrations of cytokinin in the ER are regulated by CKX1, which is an ER-localized membrane protein, and presumably CKX3. CKX2, 4-6 are most likely secreted to the apoplast. The ER-resident as well as apoplastic CKXs are monitored by ERQC to attain their native conformations. The misfolded proteins are degraded by the ERAD pathway, including retrotranslocation (red arrow) from the ER to cytosol, polyubiquitination, and degradation by the ubiquitin-proteasome system. The interaction with HIPPs facilitates the retrotranlocation of CKXs from the ER to cytosol, resulting in less cytokinin degradation in the ER, which triggers cytokinin-related transcriptional programs and corresponding developmental changes. Whereas the CKX-HIPP7 complex is retained at the cytosolic side of the ER membrane, the interaction with HIPP1 promotes CKX protein degradation. Gray arrows denote cytokinin signaling pathway; red arrow indicates protein retrotranslocation from the ER to cytosol; blue dashed arrows indicate ERAD processes; black arrows indicate a positive effect on the particular process; black dashed arrow indicates protein secretion; red rectangles and purple arrowhead indicate the HMA domains and prenyl residue in HIPP proteins, respectively.

Several results from this work support this hypothesis. For instance, the expression levels of the cytokinin output sensor *TCSn:GFP* were significantly increased in the shoots of *HIPP1 and HIPP7*-overexpressing lines compared to WT (Fig. 23). Similarly, the GFP signal of the

TCSn:GFP reporter was stronger in the root procambial cells and the reporter activity expanded upwards into the root vasculature in *UBQ10:HIPP1* roots (Fig. 29). The synthetic *TCSn* promoter harbors 24 DNA consensus sequence, as recognized by the type-B ARRs, in optimized number and spacing, and demonstrates higher sensitivity in response to cytokinin signaling in comparing with *TCS* (Sakai et al., 2000; Hosoda et al., 2002; Imamura et al., 2003; Zürcher et al., 2013). *TCS* or the improved *TCSn* reporter have been widely used in monitoring the cytokinin signaling output in cells, leading to refined existing models of cytokinin functions in numerous contexts (Gordon et al., 2009; Bielach et al., 2012; Chickarmane et al., 2012) and directing the discovery of previously unknown cytokinin activities in different tissues (Müller and Sheen, 2008; Bencivenga et al., 2012; Marsch‐Martínez et al., 2012; Reid et al., 2017). The higher activities of this reporter detected in the different *HIPP*-overexpressing plants showed that the *HIPP* overexpression enhances cytokinin signaling output in the plant. The elevated cytokinin signaling output is further supported by the increased expression levels of two type-A *ARRs*, *ARR5* and *ARR7*, in the *HIPP*-overexpression lines (Fig. 24). The type-A *ARRs* genes represent the cytokinin primary-response genes, and their expression has been used to monitor transcriptional activity in response to cytokinin signal (D'Agostino et al., 2000; Hwang and Sheen, 2001; Zubo et al., 2017). However, not all tested type-A *ARR* genes showed increased transcription levels in the *HIPP*-overexpression lines. Indeed, the expression levels of several type-A *ARR* genes were reduced, such as *ARR15* and *ARR16*. This could be due to the fact that their transcription might not be exclusively controlled by cytokinin but also by additional inputs and transcription factors, which are eventually expressed in a tissue-specific fashion. Such examples have been reported previously. For example, *ARR6* and *ARR16* are direct target genes transcriptionally activated by the TCP transcription factor, such as TCP4, and changes in the TCP4 levels have pronounced effects on the expression of these *ARR* genes and thus influence the overall leaf growth (Efroni et al., 2013). Similarly, the transcription factor WUS, for example, controls shoot meristem size by directly repressing the transcription of several type-A *ARR* genes (Leibfried et al., 2005). Interestingly, reduced transcript levels of several class II *TCP* genes were detected in *HIPP*-overexpressing plants, suggesting that the reduced expression of several type-A *ARR* genes in *HIPP*-overexpression plants could be duo to the regulation of class II type *TCP*s. Importantly, as the type-A ARR proteins generally function as inhibitors of cytokinin responses (Hwang and Sheen, 2001; To et al., 2004; To et al., 2007), reduction of their expression in *HIPP*-overexpressing plants could contribute to the enhanced cytokinin responses.

Interestingly, the contents of most cytokinin metabolites were relatively weakly changed. The strongest changes were detected for iP- and tZ-nucleotides, which were reduced to 50% of the WT levels (Table 17 and 18). Whereas the free cytokinin bases are the major active

cytokinin forms in Arabidopsis (Lomin et al., 2015), Cytokinin nucleotides and nucleosides are the precursors of the active bases, and the metabolic interchanges between these forms determine cytokinin homeostasis *in planta* (Kieber and Schaller, 2018). The first and rate-limiting step in cytokinin biosynthesis, leading to cytokinin nucleotides, is catalyzed by IPT proteins. It has been shown that *IPT1* and its homologs *IPT3*, *IPT5* and *IPT7* were downregulated by a cytokinin feedback regulation loop (Miyawaki et al., 2004). Similarly, to maintain the balance of cell division and differentiation during root development, cytokinin feeds back to negatively regulate *IPT7* via repressing the expression of a HD-ZIPIII transcription factor *PHABULOSA*, which directly activates *IPT7* (Dello Ioio et al., 2012). Therefore, the reduced levels of cytokinin nucleotides in *HIPP*-overexpressing plants indicated that the cytokinin biosynthesis was suppressed as a result of increased cytokinin signaling in these plants. Indeed, the strong downregulation of three analyzed *IPT* genes in *HIPP*-overexpressing plants (Fig. 25) supported this idea and further strengthens the hypothesis that the stronger retrotranslocation of CKX proteins from the ER by *HIPP*-overexpression enhanced the ER cytokinin concentrations and cytokinin signaling output. It is interesting to note that, in contrast to the enhanced cytokinin signaling, the overall concentrations of main active cytokinins were not dramatically increased in HIPP overexpressers. This eventually implicates that the cytokinin pool in the ER is small relative to the whole cell cytokinin content. Comparably mild changes of overall cytokinin concentrations were detected in *rock1* plants displaying enhanced ERAD of CKX proteins (Niemann et al. 2015).

Interestingly, in contrast to iP- and tZ-type cytokinins, all cZ metabolites, including the free cZ bases, were strongly increased in all *HIPP*-transgenic lines (Table 17 and 18). In Arabidopsis, the synthesis of the cZ-type cytokinins is catalyzed by two tRNA-IPTs (IPT2 and IPT9). In contrast to the key function of adenylate-IPTs in iP- and tZ-type cytokinins biosynthesis, the isopentenylation by tRNA-IPTs is not the rate-limiting step of cZ biosynthesis, and the expression of these *tRNA-IPT* genes is not regulated by cytokinin or other phytohormones (Miyawaki et al., 2004; Miyawaki et al., 2006). This suggests that the biosynthesis of the cZ-type cytokinins was probably not repressed by the enhanced cytokinin signaling in *HIPP*-overexpressing plants. Moreover, it has been shown that individual CKX isoforms possess different capacity to degrade cZ-, tZ-, and iP-type cytokinins (Gajdošová et al., 2011). It is conceivable that individual CKX isoforms were differentially affected by *HIPP* overexpression depending, for example, on the relative protein-protein interaction affinities. In this respect, it is particularly interesting that CKX3, which showed almost no degradation of cZ (Gajdošová et al., 2011) did not interact with the characterized HIPP proteins in Y2H tests. Although cZ exhibits generally lower biological activities than tZ and iP in Arabidopsis

(Gajdošová et al. 2011), it is possible that the increased cZ concentrations contributed to the enhanced cytokinin responses in *HIPP*-overexpressing plants.

Another interesting discovery is that, in contrast to the reduced iP- and tZ-nucleotides, the concentrations of cytokinin *O*-glucosides were significantly increased in *HIPP*-overexpressing plants (Table 17 and 18). Cytokinin conjugation involves *N*- and *O*-glycosylation (Hou et al., 2004). In contrast to the *N*-glycosylation, which is usually irreversible conjugation, the *O*-glucosylated forms of cytokinin can be easily converted into active cytokinin and seem to serve as storage, transport and deactivated forms because of their resistance to CKX (Auer, 2002). The conjugation process is precisely regulated to maintain the steady state concentration of cytokinin appropriately in a respective tissue (Bajguz and Piotrowska, 2009). The enhanced *O*-glycosylation in *HIPP*-overexpressing plants may be a compensation of the impaired cytokinin degradation in the ER to maintain the steady-state cytokinin concentration.

4.2.2 Ectopic overexpression of *HIPP* genes and regulation of leaf morphology

Cytokinin has been reported to play an important role in determining the final size and shape of leaves (Riefler et al., 2006; Shani et al., 2010; Bartrina et al., 2017). For instance, cytokinins induce the expression of *CYCD3* genes, which accelerates the progression through the G1-to-S phase, promoting cell division (Riou-Khamlichi et al., 1999). Li et al., (2013a) reported that cytokinins control the local expansion of pavement cells through a subset of *ARR* genes. However, it is not well understood how the cytokinin metabolism is coordinated during the leaf development. For example, it is unclear how and which CKX proteins are involved in the regulation of cytokinin concentration during leaf development. The most obvious phenotypic changes displayed by the *HIPP*-overexpressing plants are their smaller rosettes leaves with shorter petioles and crinkly lamina (Fig. 18). Interestingly, very similar changes in leaf development have been previously reported for plants overexpressing *IPT* genes (Rupp et al., 1999; Efroni et al., 2013), reinforcing the hypothesis that the leaf phenotype of the *HIPP*-overexpressing plants was directly linked to the increased cytokinin activity in these plants. In line with this, microscopic analysis revealed that the number of epidermal cells was strongly increased in *35S:HIPP7* plants, whereas the cell size was dramatically reduced in comparison to WT (Fig. 18). Moreover, the *35S:HIPP7* pavement cells developed much less convoluted shape with fewer lobes and indentations (Fig. 18). These cell phenotypes are in accord with the current model of cytokinin activity in leaves, in which the hormone controls the duration of the proliferation phase by delaying the onset of cell differentiation (Holst et al., 2011; Efroni et al., 2013).

As discussed above, the CKX-HIPP protein-protein interactions are proposed to cause reduced levels of CKX proteins in the ER and thereby stronger cytokinin signaling (see 4.1.3).

The phenotypic changes of *HIPP*-overexpressing leaves suggest that the HIPP-interacting CKX proteins are involved in the regulation of leaf growth and that changes in their levels altered cytokinin signaling and caused the leaf phenotypic changes in the *HIPP*-overexpressing plants. It has been reported that most of the *CKX* genes encoding respective CKX isoforms, which interacted with HIPPs, are expressed in the shoot (Werner et al., 2003). For instance, the *CKX1* gene is expressed in the shoot apex and lateral shoot meristems. The expression of *CKX4* has been detected in epidermal pavement cells and stomatal meristemoids within the basal, mitotically active, part of young leaves. The CKX5, which displayed strong interaction with most tested HIPP proteins in the Y2H assays, is expressed to the edges at the most basal part of the young leaves, specifically the elongating leaf petioles (Werner et al., 2003). These leaf-expressed CKX isoforms apparently control the cytokinin levels during leaf growth processes and can be hypothesized to be causally involved in the *HIPP*-overexpressing leaf phenotypes. To clarify this, it will be important to analyze leaf development in various higher-order *ckx* mutant combinations.

Another interesting phenotypic change displayed by the *HIPP*-overexpressing plants is that the number of stomata per unit area and the stomatal index (SI), which is the fraction of stomata in the total epidermal cell population, was dramatically decreased in comparison to WT (Fig. 18). Recently, Vatén et al., (2018) reported that cytokinin mediates stomatal lineage asymmetric division diversity through interaction with SPEECHLESS regulator. Exogenous cytokinin application or higher cytokinin signaling input sensed by the stomatal lineage ground cell (SLGC) leads to SLGCs undergoing additional asymmetric division (called spacing division), resulting in the increased cell number and SI, whereas overexpression of the *CKX3* or *ARR16* genes prevent the SLGC division (Vatén et al., 2018). The apparent discrepancy between the model of the regulation of stomatal division by cytokinin proposed by Vatén et al., (2018) and reduced SI in *HIPP*-overexpressing plants is currently difficult to explain. *CKX4* has been reported to be expressed in the developing stomata of young growing leaves, specifically in stomatal meristemoids (Werner et al., 2003; Pillitteri et al., 2011), it is plausible that CKX4 is involved in the cytokinin mediated stomata development. It is therefore interesting that SI was unexpectedly not increased in higher-order *ckx* mutants lacking stomatal lineage abundant CKXs (Vatén et al., 2018), suggesting that cytokinin controlled by CKX in leaves may regulate other cell division types, including the amplifying cell division leading to more pavement cells and lower SI. It should be noted that the *ckx4-1* allele employed by Vatén et al., (2018) is most probably not a null allele (Bartrina et al., 2011). Moreover, the experimental model used in the work by Vatén et al., (2018) has been cotyledons whereas true leaves were analyzed in this work. It is probable that true leaves will display a more complex pattern of cell divisions during the leaf maturation. In this respect, it is interesting to note that mitotic activity was observed in *HIPP7*-overexpressing epidermal

pavement cells very late during the leaf ontogenesis (Fig. 18), which could account for the increased number of pavement cells and the reduced relative proportion of stomata in the total epidermal cell population. However, more experiments are required to clarify the function of CKXs in regulating stomata development.

Leaf growth is dependent on leaf cell proliferation and cell expansion (Czesnick and Lenhard, 2015). Cytokinin has been reported to modulate both of these two processes during leaf development (Holst et al., 2011; Li et al., 2013a). Interestingly, cytokinin has been shown to regulate leaf growth in a dose-dependent manner, in which low cytokinin concentrations promote the leaf growth and increase the blade surface area and higher cytokinin concentrations inhibit the leaf expansion (Efroni et al., 2013). However, in this work, exogenous application of low concentrations of BA or CKX inhibitor (INCYDE) to the *HIPP*-overexpressing plants dramatically repressed the leaf expansion and resulted in the reduction of the final leaf area (Fig. 20 and 21). These results indicate that the steady-state levels of cytokinin signaling in the *HIPP*-overexpressing plants were higher than the physiological optimum required for leaf growth. This also hints that CKX proteins might play an important role in restricting cytokinin to optimal concentrations, which coordinate the processes of cell division and cell expansion during different stages of leaf development.

4.2.3 Effect of *HIPP* overexpression on root development

The most severe changes in root morphology were displayed by the *UBQ10:HIPP1* lines. The primary root elongation as well as the formation of lateral roots was severely affected in independent *UBQ10:HIPP1* lines (Fig. 27). Cytokinin control the cells division and cell elongation by dampening auxin output and redistribution to promote cell differentiation in the transition zone (TZ), resulting in the inhibition of the root growth (Dello Ioio et al., 2007; Dello Ioio et al., 2012). Exogenous application of cytokinin or enhancing cytokinin signaling output repress primary root elongation, whereas the overexpression of *CKXs* or dampening cytokinin signaling enhance primary root growth (Werner et al., 2003; Dello Ioio et al., 2007; Kurepa et al., 2014). Cytokinin also acts as a positional cue to regulate lateral root spacing by inhibiting lateral root initiation in Arabidopsis (Laplaze et al., 2007; Chang et al., 2013, 2015). It was shown that HIPP1 could only interact with CKX1 and CKX5 in the Y2H assays (Fig. 8). *CKX1* was reported to specifically express in close to the vascular cylinder at the side of growing lateral roots (Werner et al., 2003), indicating that *CKX1* is plausible involved in the regulation of lateral root development. Interestingly, the *CKX5* has been shown to be gradually expressed from the center of the meristem to the elongation zone; especially strongly expressed in the initial cells proximal to the quiescent center, indicating that CKX5 might play a crucial role in preventing cytokinin accumulation in the root apical meristem (RAM) to control

the sustainable system of cell division and differentiation. Could *HIPP1* overexpression affect the root development through the suppression of CKX1 and CKX5 activity? The enhanced activity of *TCSn:GFP* in *UBQ10:HIPP1* root meristems is in agreement with this idea. However, single *ckx1* and *ckx5* mutants show no obvious changes in root development (Bartrina, 2006; Dr. Werner's group unpublished results), and the respective double mutant needs to be analyzed. It is also plausible that not all interactions between HIPP proteins and different CKX proteins were reliably captured by Y2H tests and, therefore, the phenotypic changes in *UBQ10:HIPP1* roots can be results of suppression of additional CKX isoforms as well. In line with this, the higher-order *ckx* mutants has been shown to develop shorter roots initiating less lateral branches (Bartrina, 2006). However, as already discussed above, caution should be taken when interpreting the *HIPP*-overexpression phenotypes as these eventually may not be fully related to altered cytokinin activity.

4.2.4 HIPPs regulate shoot elongation and flowering time independently of cytokinin

In addition to the leaf phenotype, the transgenic plants overexpressing clade-I *HIPP* genes had a significantly retarded shoot height in comparison to WT plants (Fig. 19). The reproductive development of *HIPP*-transgenic lines was also delayed as the transgenic plants flowered significantly later than the WT (Fig. 19), whereas the *hipp* single mutants exhibited an early-flowering phenotype under SD conditions (Fig. 42A). It is well established that cytokinin plays generally a positive role in regulating shoot development (Zürcher and Müller, 2016; Kieber and Schaller, 2018). For instance, cytokinin regulates the size of shoot apical meristems and the initiation of axillary meristem by inducing the expression of *WUS* (Bartrina et al., 2011; Wang et al., 2017). Similarly, cytokinin-deficient transgenic plants show retarded shoot growth, which is attributable mainly to the reduced meristematic cell number, meristem size and organogenic activity (Werner et al., 2003). Considering the enhanced cytokinin signaling detected in the shoots of *HIPP*-overexpressing plants, the reduced height of the inflorescence stems is plausible caused by other factors than cytokinin that are affected by the *HIPP* overexpression. Similarly, cytokinin acts as a positive regulator in promoting flowering (Galvão and Schmid, 2014). For example, the exogenous application of cytokinin promotes flowering of plants by inducing the expression of *TWIN SISTER OF FT* (*TSF*), as well as *FD*, which encodes a partner protein of TSF, and the downstream gene *SUPPERSSOR OF OVEREXPRESSION OF CONSTANS1* (*SOC1*) (D'Aloia et al., 2011). The *repressor of cytokinin deficiency2* (*rock2*), which encodes a constitutively active gain-of-function variant of the AHK2 cytokinin receptor, flowered significantly earlier than the WT (Bartrina et al., 2017). In contrast, the *HIPP*-overexpressing transgenic plants flowered

significantly later than the WT, indicating that the altered flowering phenotype was independent of cytokinin. Consistent with the delayed flowering in *HIPP* overexpressers, the single *hipp* loss-of-function mutants flower significantly earlier than WT, underpinning the biological function of *HIPP* genes in regulating flowering time. Curiously, the early flowering phenotype was enhanced in respective higher-order *hipp* mutants, suggesting a complex genetic interaction. The molecular basis of *HIPP*-mediated control of flowering needs remains to be clarified.

However, this work provides some evidence that the activity of other hormones such as, for example, GA might have been perturbed by *HIPP* overexpression. GA has been reported to play an important role in regulating plant flowering (Conti, 2017). GA signaling, as one of four quantitative floral pathways initially identified in Arabidopsis, promotes flowering through the transcriptional activation of *FT* by triggering the degradation of DELLA proteins (Mutasa-Göttgens and Hedden, 2009). For instance, under LD conditions, plants with exogenous application of GA or *DELLA* loss-of-function mutants flower early in comparison to the WT, whereas GA-insensitive *sly1-10* mutant, which accumulates DELLA proteins, delayed flowering (Galvão et al., 2012). In this work, the GA_4, which is thought to be the major bioactive GA in Arabidopsis (Yamaguchi, 2008), was strongly reduced in the two *35:HIPP6* lines (Fig. 34), indicating that the reduced GA might account for the delayed flowering displayed by the *HIPP*-overexpressing plants. Moreover, the transcript levels of *GA3OX1* and *GA20OX1*, which catalyze the final steps of the active GA biosynthesis in Arabidopsis (Sun, 2008; Yamaguchi, 2008), were dramatically reduced in *35S:HIPP6* lines (Fig. 33), whereas one of the GA 2-oxidase genes (*GA2OX2*), which contributes to the inactivation and turnover of GA, was increased in the transgenic lines, suggesting that the overexpression of *HIPP* genes changes GA concentration via differential regulation of GA metabolism genes. The expression of GA metabolism genes is controlled by numerous factors (Frigerio et al., 2006; Sun, 2008). Interestingly, the reduction in the *GA3OX1* transcripts was progressively stronger during the later stages of leaf maturation in the *35S:HIPP6* transgenic plants, which was similar to the expression of *ARR16* (Fig. 24). This suggests that the expression of these genes might be under the control of the same factor, which might have been altered by the *HIPP* overexpression. Intriguingly, it has been shown that the expression of *GA3OX1* and *ARR16* genes are similarly regulated by *TCP* genes. TCPs promote the expression of *GA3OX1* and *ARR16* genes, whereas the overexpression of the *miRNA319b*, which targets several *TCP* genes, represses the expression of *GA3OX1* and *ARR16* (Efroni et al., 2013), indicating that the reduced expression of GA metabolism genes might also be a result of the decreased expression of *TCP* genes detected in this work.

4.2.5 Stress-related HIPP protein functions

Cytokinin metabolism and signaling pathways have been recognized to play an important role in plant adaptation to biotic and abiotic stresses because of their intensive crosstalk with other phytohormones, such as ABA and SA (Ha et al., 2012; O'Brien and Benková, 2013). For instance, the activity of ABI5, a positive regulator of ABA signaling, is attenuated by the interaction with type-A ARRs (Wang et al., 2011). Similarly, a type-B ARR (ARR2) interacts directly with the SA transcription factor TGACG sequence-specific (TGA) 3, which promotes the expression of two pathogen resistance genes (*PR-1* and *PR-2*) by binding to their promoter regions (Choi et al., 2010). Interestingly, the results showed that the concentration of ABA was significantly elevated in *HIPP*-overexpression lines (Fig. 36). Moreover, a 3 to 4-fold increase of SA content were detected in the *35S:HIPP6* lines. These results indicate that the enhanced cytokinin signaling output caused by the overexpression of *HIPPs* might account for the increased ABA and SA by the hormonal crosstalk. The drought experiments revealed that *HIPP*-overexpression plants displayed significant drought tolerance in comparison to WT plants (Fig. 37), suggesting that the elevated ABA concentration promoted their resistance to drought stress. Intriguingly, cytokinin is usually reported to act as antagonists to ABA in responses to environmental stresses (Werner et al., 2010; Nishiyama et al., 2011; Nishiyama et al., 2013; Nguyen et al., 2016). Cytokinin signaling deficiency leads to the hypersensitivity to ABA and upregulation of ABA-responsive genes under drought stress (Werner et al., 2010a; Nishiyama et al., 2011; Nishiyama et al., 2013; Nguyen et al., 2016), whereas an increase in cytokinin content results in the repression of stress- and ABA-responsive genes (Wang et al., 2011; Guan et al., 2014). However, in contrasting to this, the ABA contents have been reported to be reduced in cytokinin-deficient plants (Nishiyama et al., 2011). Taken together, it is currently difficult to draw conclusions about causal relation between cytokinin, ABA and SA and it also cannot be excluded that that the elevated ABA and SA contents in *HIPP*-overexpression plants are independent of cytokinin.

Several HIPP proteins have been reported to be involved in plant adaptation to biotic and abiotic stresses (Suzuki et al., 2002; Barth et al., 2009; Gao et al., 2009; de Abreu-Neto et al., 2013; Imran et al., 2016; Cowan et al., 2018; Radakovic et al., 2018). For example, overexpression of one clade-I *HIPP* gene (*HIPP3*) affected expression of ca. 400 genes and almost half of the most strongly affected genes are involved in pathogen responses, and a smaller number in abiotic stress responses (Zschiesche et al., 2015). HIPP26 has been shown to interact with the drought stress-related zinc finger transcription factor 29 (ATHB29) and the potato mop-top virus (PMTV) movement protein, TGB1 (Barth et al., 2009; Cowan et al., 2018). Plants infected with PMTV are shown to be drought tolerant, indicating that HIPP26 might be involved in the upregulation of dehydration-responsive genes leading to the

establishment of a drought-tolerant state in the plant (Cowan et al., 2018). Moreover, the rice *OsHIPP41* gene, which possesses 61.6% coding sequence identity with the Arabidopsis *AtHIPP26*, is shown to be highly induced in response to cold and drought stresses (de Abreu-Neto et al., 2013). All these data suggest that HIPPs play an important role in plant responses to biotic and abiotic stresses and these stress responses might be, at least in part, independent from their influence on cytokinin activity.

4.2.6 Future perspectives

In the present work, several clade-I HIPP proteins have been shown to interact with CKXs in a prenylation dependent manner. Protein prenylation is a post-translational lipid modification, which is important for protein-membrane targeting and protein-protein interaction (Crowell and Huizinga, 2009). In this work, the relevance of prenylation for the function of HIPP proteins was addressed. It was shown that this modification is essential for mediating CKX-HIPP interaction, however, the exact mechanism was not fully resolved. It could serve as a membrane targeting signal, which enables HIPP proteins to encounter CKXs at the cytosolic surface of the ER, because the attachment of the lipid increases the hydrophobicity of the protein per se, and also because the prenylated proteins undergo CaaX processing by enzymes located to the ER membrane. Additionally, protein prenylation could function as a prime determinant, which targets protein to the membrane system to undergo further modification, which is required to confer tight membrane association, such as S-acylation. It is also possible that the prenylation motif directly act as the interaction domain, which forms the correct conformation for the interaction via the lipid modification. In this context, further experiments, such as acyl-RAC assay and mutations of the amino acid residues near the prenylation motif, are required to test whether the studied HIPP proteins are S-acylated and whether the prenylation region could directly form the interaction interface, respectively.

The ERQC system is a highly stringent and efficient protein quality control mechanism that allows only correctly assembled proteins to be exported to their final destinations but retains incompletely folded proteins for additional rounds of chaperone-assisted folding and degrades terminally misfolded proteins via ERAD (Liu and Li, 2014). CKX1, as well as other CKX proteins, which have been shown to be targeted to secretory pathway, are apparently ERAD substrates and their protein abundances are reduced by the loss of ROCK1, which functions as an important part of the ERQC system (Niemann et al., 2015). In this work, several results indicate that the CKX-interacting HIPP proteins are involved in the ERAD of CKXs. However, because the current knowledge of the plant ERAD processes is rather limited, especially about the retrotranslocation and the delivery of the ERAD substrates to the proteasome, it is a big challenge to conclude in which step(s) in ERAD of CKX the identified HIPP proteins are

involved. Similarly, it will be important to examine whether other ERAD clients are regulated by the HIPP identified in this work. To answer these questions, it will be important to identify other proteins interacting with HIPPs, for example, in a new Y2H assays using HIPP as bait. CKXs, which carry out the irreversible degradation of cytokinin, play an important role in maintaining the hormone at the proper physiological levels in certain tissues (Armstrong, 1994; Carabelli et al., 2007; Bartrina et al., 2011; Li et al., 2013c). Overexpressing HIPP proteins in Arabidopsis caused plant growth changes and triggered higher cytokinin response in individual tissues, which might be mediated by controlling the CKX protein levels. However, because of the ectopic expression of these *HIPP* genes, the phenotypic changes may not fully reflect their true spatial and temporal biological functions. Reverse genetic approaches using multiple T-DNA insertional mutants together with CRISPR/Cas9-mediated mutagenesis of candidate *HIPP* genes will certainly promote our understanding of the molecular functions of the HIPP proteins in the plant ERAD system as well as their role in regulating developmental and physiological processes. Unfortunately, the studied *HIPP* genes belong to a large gene family and to a phylogenetic cluster containing nine genes. Given that the homologous genes from the same family may share a large degree of functional redundancy, the genetic analysis of the identified *HIPP* genes may prove to be difficult.

HIPP5 and *HIPP6* genes have been identified as cytokinin downregulated genes by microarray-meta analysis (Bhargava et al., 2013). In this work, qRT-PCR analysis of Arabidopsis seedlings exposed to cytokinin showed that the *HIPP5*, *HIPP6* and *HIPP7* transcript levels were downregulated after 30 min of cytokinin treatment. Moreover, the activity of the *pHIPP:GUS* constructs was reduced in the presence of cytokinin. These results indicate that cytokinin represses the transcription of these *HIPP* genes and the rapid repression suggests that these *HIPP* genes are eventually cytokinin primary response genes. Considering that HIPP proteins enhance cytokinin signaling by controlling CKX protein levels in cells, the repressed transcription of specific *HIPP* genes by cytokinin might represent a cytokinin feedback regulation loop. However, more experiments, such as chromatin immunoprecipitation (ChIP), are required to determine whether the transcription of these *HIPP* genes is directly controlled by cytokinin signaling.

One of the biggest challenges for the plant biologists today is to improve plant performances under numerous environment stresses and pathogen threats. HIPP proteins have been reported to be involved in plant responses to biotic and abiotic stresses (Suzuki et al., 2002; Barth et al., 2009; de Abreu-Neto et al., 2013; Zschiesche et al., 2015; Cowan et al., 2018; Radakovic et al., 2018). In the present work, the *HIPP*-overexpressing plants have been shown to have higher tolerance to drought stress, whereas *hipp* triple mutant plants are more vulnerable to drought stress. Moreover, the concentrations of several stress-related hormones, such as ABA and SA, are elevated in the *HIPP*-overexpressing plants, indicating

that HIPP proteins play a positive role in plant responses to biotic and abiotic stresses. However, whether the stress-tolerant phenotype of the *HIPP*-overexpressing plants is a result of the crosstalk between cytokinin and stress-related hormones or is a cytokinin-independent effect is still not clear. To uncover this, it is necessary to experimentally manipulate the cytokinin activity in the *HIPP*-overexpressing plants and to analyze levels of these stress-related hormones as well as the plant responses to stress stimuli. For instance, approaches such as introducing loss- and gain-of-function mutant variants of AHK receptors into the *HIPP*-overexpressing plants could certainly provide additional knowledge about the mechanism underlying the increased resistance of the *HIPP*-overexpressing plants against the drought stress. It will be also interesting to study whether other abiotic and biotic stresses are controlled by the identified *HIPP* genes.

5 Summary

The plant hormone cytokinin controls various processes in plant development and responses to environmental stresses. Cytokinin degradation is catalyzed by a group of CKX enzymes. Cellular levels of these proteins significantly impact the cytokinin homeostasis in plants and it is, therefore, important to understand the mechanisms regulating their activities. In this study, several CKX-interacting proteins, belonging to a plant-unique protein family (HIPP), were molecularly characterized and their biological function elucidated, particularly in respect to the regulation of cytokinin homeostasis.

In the first part of this work, the molecular basis of the CKX-HIPP interaction, such as the essential interaction motifs, interaction specificity, and the subcellular compartmentation of the CKX-HIPP complex, were investigated. Interaction assays performed in yeast and in planta revealed protein-protein interactions between specific members of the CKX and HIPP protein families. CKX1 interacted with HIPP proteins from the phylogenetic cluster I and III, but not other members of the family. The analyzed cluster I-HIPP proteins interacted additionally with most CKX proteins targeted to the secretory system but did not interact with the cytosolic CKX7 isoform. The CKX1-HIPP7 interaction required the prenylation motif at the C-terminus of HIPP7, implying that the lipid modification mediates the CKX-HIPP interaction. In addition, the tested HIPP proteins were found to form homodimers, which required both the functional prenylation and HMA domains, suggesting that metal binding could mediate the HIPP homodimerization.

The Arabidopsis CKX1 protein, a case example in this study, has been shown to be a type II membrane protein that localizes predominantly to the ER. However, the subcellular localization studies in this work revealed that HIPP1, HIPP5 and HIPP7 are localized apparently outside of the secretory system, predominantly in the cytosol and nucleus. To address this discrepancy, bimolecular fluorescence complementation (BiFC) assays were performed. The fluorescence of the BiFC CKX1/HIPP7 complex clearly showed that the interaction occur at the cortical and perinuclear ER. Moreover, a strong BiFC signal mainly localized in the nucleus and cytosol was detected for the CKX1/HIPP1 pair. These results suggest that CKX1 in the detected complexes represents a protein form that was relocated to the cytosolic site of the ER membrane.

The second part of this work aimed to uncover the biological function of the identified HIPP proteins, especially in respect to their potential role in regulating CKX protein levels and cytokinin responses in Arabidopsis. The *HIPP*-overexpressing plants displayed cytokinin-related phenotypic changes and were hypersensitive to cytokinin. This was correlated with an increased cytokinin activity in these plants. It could be further shown that

HIPP proteins differentially affected the abundance of the CKX1 protein. Given that CKX1 has been previously shown to be an ERAD substrate protein, it is proposed that the analyzed HIPP proteins might play a role during the retrotranslocation of CKX proteins from ER into the cytosol or during their cytosolic proteasomal degradation. It is hypothesized that the increased cytokinin activity displayed by *HIPP*-overexpressing plants is due to reduced levels of CKX proteins in the ER, which results in more cytokinin being sensed by the AHK cytokinin receptors localized in this compartment.

Analysis of the concentration of other phytohormones or key genes determining their biosynthesis revealed that *HIPP*-overexpression resulted in the accumulation of stress-related hormones, i.e. ABA and SA, and downregulation of genes related to GA biosynthesis. These changes probably accounted for the enhanced drought tolerance and delayed onset of flowering of the *HIPP*-overexpressing plants. These data suggest that HIPPs may have broader biological activity beyond the regulation of CKX.

Additionally, the effects of *hipp* loss-of-function mutations and the expression patterns of the analyzed *HIPP* genes were investigated in this work. In comparison to the phenotypic changes of the *HIPP*-overexpressing plants, *hipp* single and double mutants did not display obvious phenotypic changes, suggesting a higher degree of functional redundancy among the cluster I *HIPP* genes in controlling cytokinin responses and plant development. The *HIPP* genes were found to be expressed in distinct tissues, including mainly root and shoot apical meristems, and vascular tissues. Interestingly, *HIPP* transcript levels were repressed by exogenous cytokinin applications, suggesting a regulatory feedback loop between cytokinin and analyzed *HIPP* genes.

6 Zusammenfassung

Das Pflanzenhormon Cytokinin steuert verschiedene Prozesse in der Pflanzenentwicklung und die Reaktion der Pflanzen auf Umweltstress. Der Cytokininabbau wird durch CKX Enzyme katalysiert. Die zelluläre Konzentration dieser Proteine hat einen signifikanten Einfluss auf die Cytokinin-Homöostase der Pflanzen. Daher ist es wichtig die Mechanismen zu verstehen, welche ihre Aktivität regulieren. In dieser Studie wurden mehrere CKX-interagierende Proteine, die zu einer neuen pflanzen-spezifische Proteinfamilie (HIPP) gehören, molekular charakterisiert und ihre biologische Funktion untersucht, insbesondere in Bezug auf die Regulation der Cytokinin-Homöostase.

Im ersten Teil dieser Arbeit wurden die molekularen Grundlagen der CKX-HIPP-Interaktion analysiert, wie z. B. die wesentlichen Proteininteraktionsmotive, die Interaktionsspezifität und die subzelluläre Lokalisation des CKX-HIPP-Komplexes. Durchgeführte Interaktionsassays in Hefe und in Pflanzen demonstrierten Protein-Protein-Wechselwirkungen zwischen spezifischen Mitgliedern der CKX- und der HIPP-Proteinfamilien. CKX1 interagierte mit HIPP-Proteinen aus den phylogenetischen Clustern I und III, jedoch nicht mit Mitgliedern aus anderen Clustern. Die analysierten Cluster-I-HIPP-Proteine interagierten zudem nur mit den sekretorischen CKX-Proteinen jedoch nicht mit der cytosolischen CKX7-Isoform. Die CKX1-HIPP7-Wechselwirkung erforderte das Prenylierungsmotiv am C-Terminus von HIPP7, was impliziert, dass diese Lipidmodifikation die CKX-HIPP-Wechselwirkung vermittelt. Außerdem wurde festgestellt, dass die getesteten HIPP-Proteine Homodimere bilden, was sowohl die funktionelle Prenylierungs- als auch die HMA-Domäne erforderte, was darauf hindeutet, dass Metallbindung die HIPP-Homodimerisierung vermitteln könnte.

Das Arabidopsis CKX1-Protein (ein Fallbeispiel in dieser Studie) ist ein Typ-II-Membranprotein, das vorwiegend im ER lokalisiert ist. Die subzellulären Lokalisationsstudien in dieser Arbeit zeigten jedoch, dass HIPP1, HIPP5 und HIPP7 scheinbar außerhalb des sekretorischen Wegs lokalisiert sind, hauptsächlich im Cytosol und im Zellkern. Um diese Diskrepanz näher zu untersuchen, wurden Bimolekulare Fluoreszenzkomplementation (BiFC) Tests durchgeführt. Die Fluoreszenz des BiFC CKX1/ HIPP7-Komplexes zeigte deutlich, dass die Wechselwirkung am kortikalen und perinukleären ER auftritt. Darüber hinaus wurde für das CKX1/HIPP1-Paar ein starkes, hauptsächlich im Kern und im Cytosol lokalisiertes BiFC-Signal nachgewiesen. Diese Ergebnisse legen nahe, dass CKX1 in den nachgewiesenen Komplexen eine Proteinform darstellt, die an die cytosolische Seite der ER-Membran verlagert wurde.

Der zweite Teil dieser Arbeit zielte darauf ab, die biologische Funktion der identifizierten HIPP-Proteine aufzudecken, insbesondere hinsichtlich ihrer potenziellen Rolle bei der

Regulation des CKX-Proteinspiegels und der Reaktion auf Cytokinin in Arabidopsis. Die HIPP-überexprimierenden Pflanzen wiesen Cytokinin assoziierte phänotypische Veränderungen auf und waren hypersensitiv gegen Cytokinin. Dies korrelierte mit einer erhöhten Cytokininaktivität in diesen Pflanzen. Es konnte weiter gezeigt werden, dass HIPP-Proteine die Menge des CKX1-Proteins unterschiedlich beeinflussten. In Anbetracht dessen, dass CKX1 zuvor als ein ERAD-Substratprotein identifiziert wurde, wurde postuliert, dass die analysierten HIPP-Proteine eine Rolle bei der Retrotranslokation von CKX-Proteinen aus dem ER in das Cytosol oder während ihres cytosolischen proteasomalen Abbaus spielen könnten. Es wird vermutet, dass die erhöhte Cytokininaktivität der HIPP-überexprimierenden Pflanzen auf reduzierte CKX-Proteine im ER zurückzuführen ist, was dazu führt, dass mehr Cytokinin von den in diesem Kompartiment lokalisierten AHK-Cytokininrezeptoren wahrgenommen wird.

Die Analyse der Konzentration anderer Phytohormone oder Schlüsselgene, die deren Biosynthese bestimmen, ergab, dass die HIPP-Überexpression zur Anhäufung von stressbedingten Hormonen, wie ABA und SA, und zur Herunterregulierung von Genen führte, die mit der GA-Biosynthese in Verbindung stehen. Diese Veränderungen waren wahrscheinlich für die erhöhte Toleranz gegenüber Trockenheit und den verzögerten Beginn der Blüte der HIPP-überexprimierenden Pflanzen verantwortlich. Diese Daten deuten darauf hin, dass HIPPs eine breitere biologische Aktivität aufweisen, die über die CKX-Regulierung hinausgeht.

Zusätzlich wurden *hipp*-knockout-Mutanten und die Expressionsmuster der analysierten *HIPP*-Gene in dieser Arbeit untersucht. Im Vergleich zu den phänotypischen Veränderungen der *HIPP*-überexprimierenden Pflanzen wiesen *hipp*-Einzel- und Doppelmutanten keine offensichtlichen phänotypischen Änderungen auf, was auf einen hohen Grad an funktioneller Redundanz zwischen den Cluster I-*HIPP*-Genen bei der Kontrolle von Cytokinin-Antworten und der Pflanzenentwicklung schließen lässt. Es wurde festgestellt, dass die *HIPP*-Gene in verschiedenen Geweben exprimiert werden, hauptsächlich in den apikalen Meristemen der Wurzel und des Sprosses sowie im Vaskulargewebe. Interessanterweise wurden die Expression *HIPP*-Transkripte durch exogene Cytokinin Zugabe unterdrückt, was auf eine regulatorische Rückkopplungsschleife zwischen Cytokinin und den analysierten *HIPP*-Genen schließen lässt.

7 References

A Seif El-Yazal, S., A Seif El-Yazal, M., F Dwidar, E., and M Rady, M. (2015). Phytohormone crosstalk research: cytokinin and its crosstalk with other phytohormones. Current Protein and Peptide Science **16,** 395-405.

Abràmoff, M.D., Magalhães, P.J., and Ram, S.J. (2004). Image processing with ImageJ. Biophotonics international **11,** 36-42.

Achard, P., Gusti, A., Cheminant, S., Alioua, M., Dhondt, S., Coppens, F., Beemster, G.T.S., and Genschik, P. (2009). Gibberellin signaling controls cell proliferation rate in Arabidopsis. Current Biology **19,** 1188-1193.

Aebi, M. (2013). N-linked protein glycosylation in the ER. Biochimica et Biophysica Acta (BBA)-Molecular Cell Research **1833,** 2430-2437.

Albrecht, T., and Argueso, C.T. (2017). Should I fight or should I grow now? The role of cytokinins in plant growth and immunity and in the growth–defence trade-off. Annals of Botany **119,** 725-735.

Alcaniz Rolli, J. (2016). Analyse der Cytokininantwort in HIPP *loss*- und *gain of- function Arabidopsis*-Mutanten. Master Thesis. Institute of Biology/Applied Genetics Berlin, Freie Universität Berlin.

Alonso, J.M., Stepanova, A.N., Leisse, T.J., Kim, C.J., Chen, H., Shinn, P., Stevenson, D.K., Zimmerman, J., Barajas, P., Cheuk, R., Gadrinab, C., Heller, C., Jeske, A., Koesema, E., Meyers, C.C., Parker, H., Prednis, L., Ansari, Y., Choy, N., Deen, H., Geralt, M., Hazari, N., Hom, E., Karnes, M., Mulholland, C., Ndubaku, R., Schmidt, I., Guzman, P., Aguilar-Henonin, L., Schmid, M., Weigel, D., Carter, D.E., Marchand, T., Risseeuw, E., Brogden, D., Zeko, A., Crosby, W.L., Berry, C.C., and Ecker, J.R. (2003). Genome-wide insertional mutagenesis of *Arabidopsis thaliana*. Science **301,** 653-657.

Alvarez, J.P., Pekker, I., Goldshmidt, A., Blum, E., Amsellem, Z., and Eshed, Y. (2006). Endogenous and synthetic microRNAs stimulate simultaneous, efficient, and localized regulation of multiple targets in diverse species. Plant Cell **18,** 1134-1151.

Apolloni, A., Prior, I.A., Lindsay, M., Parton, R.G., and Hancock, J.F. (2000). H-ras but not K-ras traffics to the plasma membrane through the exocytic pathway. Molecular and cellular biology **20,** 2475-2487.

Argueso, C.T., Ferreira, F.J., and Kieber, J.J. (2009). Environmental perception avenues: the interaction of cytokinin and environmental response pathways. Plant, Cell & Environment **32,** 1147-1160.

Argueso, C.T., Raines, T., and Kieber, J.J. (2010). Cytokinin signaling and transcriptional networks. Current Opinion in Plant Biology **13,** 533-539.

Argueso, C.T., Ferreira, F.J., Epple, P., To, J.P., Hutchison, C.E., Schaller, G.E., Dangl, J.L., and Kieber, J.J. (2012). Two-component elements mediate interactions between cytokinin and salicylic acid in plant immunity. PLoS Genetics **8,** e1002448.

Argyros, R.D., Mathews, D.E., Chiang, Y.-H., Palmer, C.M., Thibault, D.M., Etheridge, N., Argyros, D.A., Mason, M.G., Kieber, J.J., and Schaller, G.E. (2008). Type B response regulators of Arabidopsis play key roles in cytokinin signaling and plant development. Plant Cell **20,** 2102-2116.

Armstrong, D.J. (1994). Cytokinin oxidase and the regulation of cytokinin degradation. In Cytokinins: Chemistry, activity, and function (Mok, D. W. S. and Mok, M. C., eds) Boca Raton: CRC, pp. 139-154.

Arnesano, F., Banci, L., Bertini, I., Cantini, F., Ciofi-Baffoni, S., Huffman, D.L., and O'Halloran, T.V. (2001). Characterization of the binding interface between the

copper chaperone Atx1 and the first cytosolic domain of Ccc2 ATPase. Journal of Biological Chemistry **276,** 41365-41376.

Atanasova, L., Pissarska, M., Popov, G., and Georgiev, G. (2004). Growth and endogenous cytokinins of juniper shoots as affected by high metal concentrations. Biologia Plantarum **48,** 157-159.

Auer, C.A. (2002). Discoveries and dilemmas concerning cytokinin metabolism. Journal of Plant Growth Regulation **21,** 24-31.

Bai, L., Zhang, G., Zhou, Y., Zhang, Z., Wang, W., Du, Y., Wu, Z., and Song, C.P. (2009). Plasma membrane-associated proline-rich extensin-like receptor kinase 4, a novel regulator of Ca^{2+} signalling, is required for abscisic acid responses in *Arabidopsis thaliana*. Plant Journal **60,** 314-327.

Bajguz, A., and Piotrowska, A. (2009). Conjugates of auxin and cytokinin. Phytochemistry **70,** 957-969.

Baldridge, R.D., and Rapoport, T.A. (2016). Autoubiquitination of the Hrd1 ligase triggers protein retrotranslocation in ERAD. Cell **166,** 394-407.

Ball, L.J., Kühne, R., Schneider-Mergener, J., and Oschkinat, H. (2005). Recognition of proline-rich motifs by protein-protein-interaction domains. Angewandte Chemie International Edition **44,** 2852-2869.

Banci, L., Bertini, I., Cantini, F., Felli, I.C., Gonnelli, L., Hadjiliadis, N., Pierattelli, R., Rosato, A., and Voulgaris, P. (2006). The Atx1-Ccc2 complex is a metal-mediated protein-protein interaction. Nature Chemical Biology **2,** 367.

Bar, M., and Ori, N. (2014). Leaf development and morphogenesis. Development **141,** 4219-4230.

Bar, M., Israeli, A., Levy, M., Ben Gera, H., Jimenez-Gomez, J.M., Kouril, S., Tarkowski, P., and Ori, N. (2016). CLAUSA is a MYB transcription factor that promotes leaf differentiation by attenuating cytokinin signaling. Plant Cell **28,** 1602-1615.

Barth, O., Vogt, S., Uhlemann, R., Zschiesche, W., and Humbeck, K. (2009). Stress induced and nuclear localized HIPP26 from *Arabidopsis thaliana* interacts via its heavy metal associated domain with the drought stress related zinc finger transcription factor ATHB29. Plant Molecular Biology **69,** 213-226.

Barton, M.K. (2010). Twenty years on: The inner workings of the shoot apical meristem, a developmental dynamo. Developmental Biology **341,** 95-113.

Bartrina, I. (2006). Function of the cytokinin oxidases/dehydrogenases in Arabidopsis. Dissertation. Institute of Biology/Applied Genetics Berlin, Freie Universität Berlin.

Bartrina, I., Otto, E., Strnad, M., Werner, T., and Schmülling, T. (2011). Cytokinin regulates the activity of reproductive meristems, flower organ size, ovule formation, and thus seed yield in *Arabidopsis thaliana*. Plant Cell **23,** 69-80.

Bartrina, I., Jensen, H., Novák, O., Strnad, M., Werner, T., and Schmülling, T. (2017). Gain-of-function mutants of the cytokinin receptors AHK2 and AHK3 regulate plant organ size, flowering time and plant longevity. Plant Physiology **173,** 1783-1797.

Beck, E., and Wagner, B.M. (1994). Quantification of the daily cytokinin transport from the root to the shoot of *Urtica dioica* L. Botanica Acta **107,** 342-348.

Bencivenga, S., Simonini, S., Benková, E., and Colombo, L. (2012). The transcription factors BEL1 and SPL are required for cytokinin and auxin signaling during ovule development in Arabidopsis. Plant Cell **24,** 2886-2897.

Bergmann, D.C., and Sack, F.D. (2007). Stomatal development. Annual Review of Plant Biology **58,** 163-181.

Berleth, T., and Jurgens, G. (1993). The role of the monopteros gene in organising the basal body region of the Arabidopsis embryo. Development **118,** 575-587.

Bernard, P., and Couturier, M. (1992). Cell killing by the F plasmid CcdB protein involves poisoning of DNA-topoisomerase II complexes. Journal of Molecular Biology **226,** 735-745.

Berner, N., Reutter, K.-R., and Wolf, D.H. (2018). Protein quality control of the endoplasmic reticulum and ubiquitin-proteasome-triggered degradation of aberrant proteins: yeast pioneers the path. Annual Review of Biochemistry **87,** 751-782.

Bertani, G. (1951). Studies on lysogenesis i.: The mode of phage liberation by lysogenic escherichia coli1. Journal of Bacteriology **62,** 293.

Besnard, F., Refahi, Y., Morin, V., Marteaux, B., Brunoud, G., Chambrier, P., Rozier, F., Mirabet, V., Legrand, J., and Lainé, S. (2014). Cytokinin signalling inhibitory fields provide robustness to phyllotaxis. Nature **505,** 417.

Beveridge, C.A., Murfet, I.C., Kerhoas, L., Sotta, B., Miginiac, E., and Rameau, C. (1997). The shoot controls zeatin riboside export from pea roots. Evidence from the branching mutant rms4. Plant Journal **11,** 339-345.

Bhargava, A., Clabaugh, I., To, J.P., Maxwell, B.B., Chiang, Y.-H., Schaller, G.E., Loraine, A., and Kieber, J.J. (2013). Identification of cytokinin-responsive genes using microarray meta-analysis and RNA-seq in Arabidopsis. Plant Physiology **162,** 272-294.

Bielach, A., Hrtyan, M., and Tognetti, V. (2017). Plants under stress: Involvement of auxin and cytokinin. International Journal of Molecular Sciences **18,** 1427.

Bielach, A., Podlešáková, K., Marhavý, P., Duclercq, J., Cuesta, C., Müller, B., Grunewald, W., Tarkowski, P., and Benková, E. (2012). Spatiotemporal regulation of lateral root organogenesis in Arabidopsis by cytokinin. Plant Cell **24,** 3967-3981.

Bilsborough, G.D., Runions, A., Barkoulas, M., Jenkins, H.W., Hasson, A., Galinha, C., Laufs, P., Hay, A., Prusinkiewicz, P., and Tsiantis, M. (2011). Model for the regulation of *Arabidopsis thaliana* leaf margin development. Proceedings of the National Academy of Sciences of the United States of America **108,** 3424-3429.

Bilyeu, K.D., Cole, J.L., Laskey, J.G., Riekhof, W.R., Esparza, T.J., Kramer, M.D., and Morris, R.O. (2001). Molecular and biochemical characterization of a cytokinin oxidase from maize. Plant Physiology **125,** 378-386.

Bischoff, F., Vahlkamp, L., Molendijk, A., and Palme, K. (2000). Localization of AtROP4 and AtROP6 and interaction with the guanine nucleotide dissociation inhibitor AtRhoGDI1 from Arabidopsis. Plant Molecular Biology **42,** 515-530.

Bodnar, N.O., and Rapoport, T.A. (2017). Molecular mechanism of substrate processing by the Cdc48 ATPase complex. Cell **169,** 722-735.

Boyartchuk, V.L., Ashby, M.N., and Rine, J. (1997). Modulation of Ras and a-factor function by carboxyl-terminal proteolysis. Science **275,** 1796-1800.

Bracha-Drori, K., Shichrur, K., Lubetzky, T.C., and Yalovsky, S. (2008). Functional analysis of Arabidopsis postprenylation CaaX processing enzymes and their function in subcellular protein targeting. Plant Physiology **148,** 119-131.

Brandstatter, I., and Kieber, J.J. (1998). Two genes with similarity to bacterial response regulators are rapidly and specifically induced by cytokinin in Arabidopsis. Plant Cell **10,** 1009-1019.

Bray, E.A. (1997). Plant responses to water deficit. Trends in Plant Science **2,** 48-54.

Brugière, N., Jiao, S., Hantke, S., Zinselmeier, C., Roessler, J.A., Niu, X., Jones, R.J., and Habben, J.E. (2003). Cytokinin oxidase gene expression in maize is localized to the vasculature, and is induced by cytokinins, abscisic acid, and abiotic stress. Plant Physiology **132,** 1228-1240.

Bürkle, L., Cedzich, A., Döpke, C., Stransky, H., Okumoto, S., Gillissen, B., Kühn, C., and Frommer, W.B. (2003). Transport of cytokinins mediated by purine transporters

of the PUP family expressed in phloem, hydathodes, and pollen of Arabidopsis. Plant Journal **34,** 13-26.

Caesar, K., Thamm, A.M.K., Witthöft, J., Elgass, K., Huppenberger, P., Grefen, C., Horak, J., and Harter, K. (2011). Evidence for the localization of the Arabidopsis cytokinin receptors AHK3 and AHK4 in the endoplasmic reticulum. Journal of Experimental Botany **62,** 5571-5580.

Carabelli, M., Possenti, M., Sessa, G., Ciolfi, A., Sassi, M., Morelli, G., and Ruberti, I. (2007). Canopy shade causes a rapid and transient arrest in leaf development through auxin-induced cytokinin oxidase activity. Genes and Development **21,** 1863-1868.

Caramelo, J.J., and Parodi, A.J. (2008). Getting in and out from calnexin/calreticulin cycles. Journal of Biological Chemistry **283,** 10221-10225.

Carr, J.P., Lewsey, M.G., and Palukaitis, P. (2010). Chapter 3 - Signaling in Induced Resistance. In Advances in Virus Research (Carr, John P. and Loebenstein, Gad., eds.) Academic Press, pp. 57-121.

Casey, P.J., and Seabra, M.C. (1996). Protein prenyltransferases. Journal of Biological Chemistry **271,** 5289-5292.

Chandran, D., Sharopova, N., Ivashuta, S., Gantt, J.S., VandenBosch, K.A., and Samac, D.A. (2008). Transcriptome profiling identified novel genes associated with aluminum toxicity, resistance and tolerance in *Medicago truncatula*. Planta **228,** 151-166.

Chang, L., Ramireddy, E., and Schmülling, T. (2013). Lateral root formation and growth of Arabidopsis is redundantly regulated by cytokinin metabolism and signalling genes. Journal of Experimental Botany **64,** 5021-5032.

Chang, L., Ramireddy, E., and Schmülling, T. (2015). Cytokinin as a positional cue regulating lateral root spacing in Arabidopsis. Journal of Experimental Botany **66,** 4759-4768.

Cheng, C.-Y., Mathews, D., Eric Schaller, G., and Kieber, J.J. (2013). Cytokinin-dependent specification of the functional megaspore in the Arabidopsis female gametophyte. Plant Journal **73,** 929-940.

Chickarmane, V.S., Gordon, S.P., Tarr, P.T., Heisler, M.G., and Meyerowitz, E.M. (2012). Cytokinin signaling as a positional cue for patterning the apical-basal axis of the growing Arabidopsis shoot meristem. Proceedings of the National Academy of Sciences of the United States of America **109,** 4002-4007.

Choi, J., Huh, S.U., Kojima, M., Sakakibara, H., Paek, K.-H., and Hwang, I. (2010). The cytokinin-activated transcription factor ARR2 promotes plant immunity via TGA3/NPR1-dependent salicylic acid signaling in Arabidopsis. Developmental Cell **19,** 284-295.

Choy, E., Chiu, V.K., Silletti, J., Feoktistov, M., Morimoto, T., Michaelson, D., Ivanov, I.E., and Philips, M.R. (1999). Endomembrane trafficking of ras: the CAAX motif targets proteins to the ER and Golgi. Cell **98,** 69-80.

Chu, C.-C., Lee, W.-C., Guo, W.-Y., Pan, S.-M., Chen, L.-J., Li, H.-m., and Jinn, T.-L. (2005). A copper chaperone for superoxide dismutase that confers three types of copper/zinc superoxide dismutase activity in Arabidopsis. Plant Physiology **139,** 425-436.

Clerc, S., Hirsch, C., Oggier, D.M., Deprez, P., Jakob, C., Sommer, T., and Aebi, M. (2009). Htm1 protein generates the N-glycan signal for glycoprotein degradation in the endoplasmic reticulum. The Journal of Cell Biology **184,** 159-172.

Clough, S.J., and Bent, A.F. (1998). Floral dip: a simplified method for *Agrobacterium*-mediated transformation of *Arabidopsis thaliana*. Plant Journal **16,** 735-743.

Conti, L. (2017). Hormonal control of the floral transition: can one catch them all? Developmental Biology **430,** 288-301.

Cowan, G.H., Roberts, A.G., Jones, S., Kumar, P., Kalyandurg, P.B., Gil, J.F., Savenkov, E., Hemsley, P.A., and Torrance, L. (2018). Potato mop-top virus co-opts the stress sensor HIPP26 for long-distance movement. Plant Physiology **176,** 2052-2070.

Crawford, K.M., and Zambryski, P.C. (2001). Non-targeted and targeted protein movement through plasmodesmata in leaves in different developmental and physiological states. Plant Physiology **125,** 1802-1812.

Crowell, D.N., and Huizinga, D.H. (2009). Protein isoprenylation: the fat of the matter. Trends in Plant Science **14,** 163-170.

Czesnick, H., and Lenhard, M. (2015). Size control in plants—lessons from leaves and flowers. Cold Spring Harbor perspectives in biology **7,** a019190.

Czolpinska, M., and Rurek, M. (2018). Plant glycine-rich proteins in stress response: An emerging, still prospective story. Frontiers in Plant Science **9,** 302.

D'Agostino, I.B., Deruere, J., and Kieber, J.J. (2000). Characterization of the response of the Arabidopsis response regulator gene family to cytokinin. Plant Physiology **124,** 1706-1717.

D'Aloia, M., Bonhomme, D., Bouche, F., Tamseddak, K., Ormenese, S., Torti, S., Coupland, G., and Perilleux, C. (2011). Cytokinin promotes flowering of Arabidopsis via transcriptional activation of the FT paralogue TSF. Plant Journal **65,** 972-979.

D'Alessio, C., Caramelo, J.J., and Parodi, A.J. (2010). UDP-GlC: glycoprotein glucosyltransferase-glucosidase II, the ying-yang of the ER quality control. In Seminars in cell & developmental biology. Elsevier, pp. 491-499.

Davis, A.M., Hall, A., Millar, A.J., Darrah, C., and Davis, S.J. (2009). Protocol: Streamlined sub-protocols for floral-dip transformation and selection of transformants in *Arabidopsis thaliana*. Plant Methods **5,** 3.

de Abreu-Neto, J.B., Turchetto-Zolet, A.C., de Oliveira, L.F.V., Bodanese Zanettini, M.H., and Margis-Pinheiro, M. (2013). Heavy metal-associated isoprenylated plant protein (HIPP): characterization of a family of proteins exclusive to plants. FEBS (Federation of European Biochemical Societies) Journal **280,** 1604-1616.

Dello Ioio, R., Linhares, F.S., Scacchi, E., Casamitjana-Martinez, E., Heidstra, R., Costantino, P., and Sabatini, S. (2007). Cytokinins determine Arabidopsis root-meristem size by controlling cell differentiation. Current Biology **17,** 678-682.

Dello Ioio, R., Galinha, C., Fletcher, Alexander G., Grigg, Stephen P., Molnar, A., Willemsen, V., Scheres, B., Sabatini, S., Baulcombe, D., Maini, Philip K., and Tsiantis, M. (2012). A PHABULOSA/cytokinin feedback loop controls root growth in Arabidopsis. Current Biology **22,** 1699-1704.

Deng, Y., Dong, H., Mu, J., Ren, B., Zheng, B., Ji, Z., Yang, W.-C., Liang, Y., and Zuo, J. (2010). Arabidopsis histidine kinase CKI1 acts upstream of HISTIDINE PHOSPHOTRANSFER PROTEINS to regulate female gametophyte development and vegetative growth. Plant Cell **22,** 1232-1248.

Deshaies, R.J., and Joazeiro, C.A. (2009). RING domain E3 ubiquitin ligases. Annual Review of Biochemistry **78,** 399-434.

Dewitte, W., Riou-Khamlichi, C., Scofield, S., Healy, J.M.S., Jacqmard, A., Kilby, N.J., and Murray, J.A.H. (2003). Altered cell cycle distribution, hyperplasia, and inhibited differentiation in Arabidopsis caused by the D-Type cyclin CYCD3. Plant Cell **15,** 79-92.

Dewitte, W., Scofield, S., Alcasabas, A.A., Maughan, S.C., Menges, M., Braun, N., Collins, C., Nieuwland, J., Prinsen, E., Sundaresan, V., and Murray, J.A.H. (2007). Arabidopsis CYCD3 D-type cyclins link cell proliferation and endocycles and are rate-limiting for cytokinin responses. Proceedings of the National Academy of Sciences of the United States of America **104,** 14537-14542.

Dortay, H., Mehnert, N., Burkle, L., Schmulling, T., and Heyl, A. (2006). Analysis of protein interactions within the cytokinin-signaling pathway of *Arabidopsis thaliana*. FEBS (Federation of European Biochemical Societies) Journal **273,** 4631-4644.

Dortay, H., Gruhn, N., Pfeifer, A., Schwerdtner, M., Schmülling, T., and Heyl, A. (2008). Toward an interaction map of the two-component signaling pathway of *Arabidopsis thaliana*. Journal of Proteome Research **7,** 3649-3660.

Durán-Medina, Y., Díaz-Ramírez, D., and Marsch-Martínez, N. (2017). Cytokinins on the Move. Frontiers in Plant Science **8,** 146.

Durner, J., Shah, J., and Klessig, D.F. (1997). Salicylic acid and disease resistance in plants. Trends in Plant Science **2,** 266-274.

Dykema, P., Sipes, P., Marie, A., Biermann, B., Crowell, D., and Randall, S. (1999). A new class of proteins capable of binding transition metals. Plant Molecular Biology **41,** 139-150.

Efroni, I., Han, S.-K., Kim, Hye J., Wu, M.-F., Steiner, E., Birnbaum, Kenneth D., Hong, Jong C., Eshed, Y., and Wagner, D. (2013). Regulation of leaf maturation by chromatin-mediated modulation of cytokinin responses. Developmental Cell **24,** 438-445.

El-Showk, S., Ruonala, R., and Helariutta, Y. (2013). Crossing paths: cytokinin signalling and crosstalk. Development **140,** 1373-1383.

Faiss, M., Zalubìlová, J., Strnad, M., and Schmülling, T. (1997). Conditional transgenic expression of the ipt gene indicates a function for cytokinins in paracrine signaling in whole tobacco plants. Plant Journal **12,** 401-415.

Feng, J., Wang, C., Chen, Q., Chen, H., Ren, B., Li, X., and Zuo, J. (2013). S-nitrosylation of phosphotransfer proteins represses cytokinin signaling. Nature Communications **4,** 1529.

Fernandez-Calvino, L., Faulkner, C., Walshaw, J., Saalbach, G., Bayer, E., Benitez-Alfonso, Y., and Maule, A. (2011). Arabidopsis plasmodesmal proteome. PLoS ONE **6,** e18880.

Ferris, S.P., Kodali, V.K., and Kaufman, R.J. (2014). Glycoprotein folding and quality-control mechanisms in protein-folding diseases. Disease models & mechanisms **7,** 331-341.

Fleishon, S., Shani, E., Ori, N., and Weiss, D. (2011). Negative reciprocal interactions between gibberellin and cytokinin in tomato. New Phytologist **190,** 609-617.

Fonouni-Farde, C., McAdam, E., Nichols, D., Diet, A., Foo, E., and Frugier, F. (2018). Cytokinins and the CRE1 receptor influence endogenous gibberellin levels in *Medicago truncatula*. Plant Signaling & Behavior **13,** e1428513.

Franc, V., Šebela, M., Řehulka, P., Končitíková, R., Lenobel, R., Madzak, C., and Kopečný, D. (2012). Analysis of *N*-glycosylation in maize cytokinin oxidase/dehydrogenase 1 using a manual microgradient chromatographic separation coupled offline to MALDI-TOF/TOF mass spectrometry. Journal of Proteomics **75,** 4027-4037.

Frébort, I., Šebela, M., Galuszka, P., Werner, T., Schmülling, T., and Peč, P. (2002). Cytokinin oxidase/cytokinin dehydrogenase assay: Optimized procedures and applications. Analytical Biochemistry **306,** 1-7.

Frébortová, J., Novák, O., Frébort, I., and Jorda, R. (2010). Degradation of cytokinins by maize cytokinin dehydrogenase is mediated by free radicals generated by enzymatic oxidation of natural benzoxazinones. Plant Journal **61,** 467-481.

Frébortová, J., Fraaije, M.W., Galuszka, P., Šebela, M., Pec, P., Hrbác, J., Novák, O., Bilyeu, K.D., English, J.T., and Frébort, I. (2004). Catalytic reaction of cytokinin dehydrogenase: Preference for quinones as electron acceptors. Biochemical Journal **380,** 121-130.

Frigerio, M., Alabadí, D., Pérez-Gómez, J., García-Cárcel, L., Phillips, A.L., Hedden, P., and Blázquez, M.A. (2006). Transcriptional regulation of gibberellin metabolism genes by auxin signaling in Arabidopsis. Plant Physiology **142,** 553-563.

Frugier, F., Kosuta, S., Murray, J.D., Crespi, M., and Szczyglowski, K. (2008). Cytokinin: secret agent of symbiosis. Trends in Plant Science **13,** 115-120.

Gajdošová, S., Spíchal, L., Kamínek, M., Hoyerová, K., Novák, O., Dobrev, P.I., Galuszka, P., Klíma, P., Gaudinová, A., Žižková, E., Hanuš, J., Dančák, M., Trávníček, B., Pešek, B., Krupička, M., Vaňková, R., Strnad, M., and Motyka, V. (2011). Distribution, biological activities, metabolism, and the conceivable function of *cis*-zeatin-type cytokinins in plants. Journal of Experimental Botany **62,** 2827-2840.

Galichet, A., and Gruissem, W. (2003). Protein farnesylation in plants – conserved mechanisms but different targets. Current Opinion in Plant Biology **6,** 530-535.

Galichet, A., Hoyerová, K., Kamínek, M., and Gruissem, W. (2008). Farnesylation directs AtIPT3 subcellular localization and modulates cytokinin biosynthesis in Arabidopsis. Plant Physiology **146,** 1155-1164.

Galuszka, P., Frébort, I., Šebela, M., Sauer, P., Jacobsen, S., and Pec, P. (2001). Cytokinin oxidase or dehydrogenase? Mechanism of cytokinin degradation in cereals. European Journal of Biochemistry **268,** 450-461.

Galuszka, P., Frébortová, J., Werner, T., Yamada, M., Strnad, M., Schmülling, T., and Frébort, I. (2004). *Cytokinin oxidase/dehydrogenase* genes in barley and wheat: cloning and heterologous expression. European Journal of Biochemistry **271,** 3990-4002.

Galuszka, P., Popelková, H., Werner, T., Frébortová, J., Pospísilová, H., Mik, V., Köllmer, I., Schmülling, T., and Frébort, I. (2007). Biochemical characterization of cytokinin oxidases/dehydrogenases from *Arabidopsis thaliana* expressed in *Nicotiana tabacum* L. Journal of Plant Growth Regulation **26,** 255-267.

Galvão, V.C., and Schmid, M. (2014). Chapter Three - Regulation of flowering by endogenous signals. In Advances in Botanical Research (Fornara. F., eds) Academic Press, pp. 63-102.

Galvão, V.C., Horrer, D., Küttner, F., and Schmid, M. (2012). Spatial control of flowering by DELLA proteins in *Arabidopsis thaliana*. Development **139,** 4072-4082.

Gan, S., and Amasino, R.M. (1995). Inhibition of leaf senescence by autoregulated production of cytokinin. Science **270,** 1986-1988.

Gao, W., Xiao, S., Li, H.-Y., Tsao, S.-W., and Chye, M.-L. (2009). *Arabidopsis thaliana* acyl-CoA-binding protein ACBP2 interacts with heavy-metal-binding farnesylated protein AtFP6. New Phytologist **181,** 89-102.

Gaudin, V., Lunness, P.A., Fobert, P.R., Towers, M., Riou-Khamlichi, C., Murray, J.A., Coen, E., and Doonan, J.H. (2000). The expression of D-cyclin genes defines distinct developmental zones in snapdragon apical meristems and is locally regulated by the Cycloidea gene. Plant Physiology **122,** 1137-1148.

Gemrotová, M., Kulkarni, M.G., Stirk, W.A., Strnad, M., Van Staden, J., and Spíchal, L. (2013). Seedlings of medicinal plants treated with either a cytokinin antagonist (PI-55) or an inhibitor of cytokinin degradation (INCYDE) are protected against the negative effects of cadmium. Plant Growth Regulation **71,** 137-145.

Gerber, E., Hemmerlin, A., Hartmann, M., Heintz, D., Hartmann, M.A., Mutterer, J., Rodríguez-Concepción, M., Boronat, A., Van Dorsselaer, A., Rohmer, M., Crowell, D.N., and Bach, T.J. (2009). The plastidial 2-C-methyl-D-erythritol 4-phosphate pathway provides the isoprenyl moiety for protein geranylgeranylation in tobacco BY-2 cells. Plant Cell **21,** 285-300.

Gietz, R.D., and Woods, R.A. (2002). Transformation of yeast by lithium acetate/single-stranded carrier DNA/polyethylene glycol method. In Methods in Enzymology (Elsevier), pp. 87-96.

Gillissen, B., Bürkle, L., André, B., Kühn, C., Rentsch, D., Brandl, B., and Frommer, W.B. (2000). A new family of high-affinity transporters for adenine, cytosine, and purine derivatives in Arabidopsis. Plant Cell **12,** 291-300.

Goda, H., Sawa, S., Asami, T., Fujioka, S., Shimada, Y., and Yoshida, S. (2004). Comprehensive comparison of auxin-regulated and brassinosteroid-regulated genes in Arabidopsis. Plant Physiology **134,** 1555-1573.

Goehler, H., Lalowski, M., Stelzl, U., Waelter, S., Stroedicke, M., Worm, U., Droege, A., Lindenberg, K.S., Knoblich, M., and Haenig, C. (2004). A protein interaction network links GIT1, an enhancer of huntingtin aggregation, to Huntington's disease. Molecular Cell **15,** 853-865.

Golan, Y., Shirron, N., Avni, A., Shmoish, M., and Gepstein, S. (2016). Cytokinins induce transcriptional reprograming and improve Arabidopsis plant performance under drought and salt stress conditions. Frontiers in Environmental Science **4,** 63.

Gonzalez, N., Vanhaeren, H., and Inzé, D. (2012). Leaf size control: Complex coordination of cell division and expansion. Trends in Plant Science **17,** 332-340.

Gookin, T.E., and Assmann, S.M. (2014). Significant reduction of BiFC non-specific assembly facilitates *in planta* assessment of heterotrimeric G-protein interactors. Plant Journal **80,** 553-567.

Gordon, S.P., Chickarmane, V.S., Ohno, C., and Meyerowitz, E.M. (2009). Multiple feedback loops through cytokinin signaling control stem cell number within the Arabidopsis shoot meristem. Proceedings of the National Academy of Sciences of the United States of America **106,** 16529-16534.

Grant, S.G., Jessee, J., Bloom, F.R., and Hanahan, D. (1990). Differential plasmid rescue from transgenic mouse DNAs into *Escherichia coli* methylation-restriction mutants. Proceedings of the National Academy of Sciences of the United States of America **87,** 4645-4649.

Greenboim-Wainberg, Y., Maymon, I., Borochov, R., Alvarez, J., Olszewski, N., Ori, N., Eshed, Y., and Weiss, D. (2005). Cross talk between gibberellin and cytokinin: The Arabidopsis GA response inhibitor SPINDLY plays a positive role in cytokinin signaling. Plant Cell **17,** 92-102.

Gu, R., Fu, J., Guo, S., Duan, F., Wang, Z., Mi, G., and Yuan, L. (2010). Comparative expression and phylogenetic analysis of maize cytokinin dehydrogenase/oxidase (CKX) gene family. Journal of Plant Growth Regulation **29,** 428-440.

Gu, W., Kofler, M., Antes, I., Freund, C., and Helms, V. (2005). Alternative binding modes of proline-rich peptides binding to the GYF domain. Biochemistry **44,** 6404-6415.

Guan, C., Wang, X., Feng, J., Hong, S., Liang, Y., Ren, B., and Zuo, J. (2014). Cytokinin antagonizes abscisic acid-mediated inhibition of cotyledon greening by promoting the degradation of ABSCISIC ACID INSENSITIVE5 protein in Arabidopsis. Plant Physiology **164,** 1515-1526.

Ha, S., Vankova, R., Yamaguchi-Shinozaki, K., Shinozaki, K., and Tran, L.-S.P. (2012). Cytokinins: metabolism and function in plant adaptation to environmental stresses. Trends in Plant Science **17,** 172-179.

Hampton, R.Y., and Sommer, T. (2012). Finding the will and the way of ERAD substrate retrotranslocation. Current Opinion in Cell Biology **24,** 460-466.

Hampton, S.E., Dore, T.M., and Schmidt, W.K. (2018). Rce1: Mechanism and inhibition. Critical Reviews in Biochemistry and Molecular Biology **53,** 157-174.

Hancock, J.F., Cadwallader, K., and Marshall, C.J. (1991). Methylation and proteolysis are essential for efficient membrane binding of prenylated p21K ‐ ras (B). The EMBO (European Molecular Biology Organization) Journal **10,** 641-646.

Hasson, A., Plessis, A., Blein, T., Adroher, B., Grigg, S., Tsiantis, M., Boudaoud, A., Damerval, C., and Laufs, P. (2011). Evolution and diverse roles of the CUP-SHAPED COTYLEDON genes in Arabidopsis leaf development. Plant Cell **23,** 54-68.

Hejátko, J., Pernisová, M., Eneva, T., Palme, K., and Brzobohatý, B. (2003). The putative sensor histidine kinase CKI1 is involved in female gametophyte development in Arabidopsis. Molecular Genetics and Genomics **269,** 443-453.

Hejátko, J., Ryu, H., Kim, G.-T., Dobešová, R., Choi, S., Choi, S.M., Souček, P., Horák, J., Pekárová, B., Palme, K., Brzobohatý, B., and Hwang, I. (2009). The histidine kinases CYTOKININ-INDEPENDENT1 and ARABIDOPSIS HISTIDINE KINASE2 and 3 regulate vascular tissue development in Arabidopsis shoots. Plant Cell **21,** 2008-2021.

Hemsley, P.A. (2015). The importance of lipid modified proteins in plants. New Phytologist **205,** 476-489.

Hemsley, P.A., Weimar, T., Lilley, K.S., Dupree, P., and Grierson, C.S. (2013). A proteomic approach identifies many novel palmitoylated proteins in Arabidopsis. New Phytologist **197,** 805-814.

Heyl, A., and Schmülling, T. (2003). Cytokinin signal perception and transduction. Current Opinion in Plant Biology **6,** 480-488.

Heyl, A., Wulfetange, K., Pils, B., Nielsen, N., Romanov, G.A., and Schmülling, T. (2007). Evolutionary proteomics identifies amino acids essential for ligand-binding of the cytokinin receptor CHASE domain. BMC Evolutionary Biology **7,** 62.

Hirose, N., Takei, K., Kuroha, T., Kamada-Nobusada, T., Hayashi, H., and Sakakibara, H. (2008). Regulation of cytokinin biosynthesis, compartmentalization and translocation. Journal of Experimental Botany **59,** 75-83.

Hirsch, C., Gauss, R., Horn, S.C., Neuber, O., and Sommer, T. (2009). The ubiquitylation machinery of the endoplasmic reticulum. Nature **458,** 453.

Holst, K., Schmülling, T., and Werner, T. (2011). Enhanced cytokinin degradation in leaf primordia of transgenic Arabidopsis plants reduces leaf size and shoot organ primordia formation. Journal of Plant Physiology **168,** 1328-1334.

Hong, Z., Jin, H., Fitchette, A.-C., Xia, Y., Monk, A.M., Faye, L., and Li, J. (2009). Mutations of an α1,6 mannosyltransferase inhibit endoplasmic reticulum–associated degradation of defective brassinosteroid receptors in Arabidopsis. Plant Cell **21,** 3792-3802.

Hosoda, K., Imamura, A., Katoh, E., Hatta, T., Tachiki, M., Yamada, H., Mizuno, T., and Yamazaki, T. (2002). Molecular structure of the GARP family of plant Myb-related DNA binding motifs of the Arabidopsis response regulators. Plant Cell **14,** 2015-2029.

Hou, B., Lim, E.K., Higgins, G.S., and Bowles, D.J. (2004). N-glucosylation of cytokinins by glycosyltransferases of *Arabidopsis thaliana*. Journal of Biological Chemistry **279,** 47822-47832.

Huang, X., Zhang, X., Gong, Z., Yang, S., and Shi, Y. (2017). ABI4 represses the expression of type-A *ARRs* to inhibit seed germination in Arabidopsis. Plant Journal **89,** 354-365.

Huang, X., Hou, L., Meng, J., You, H., Li, Z., Gong, Z., Yang, S., and Shi, Y. (2018). The antagonistic action of abscisic acid and cytokinin signaling mediates drought stress response in Arabidopsis. Molecular Plant **11,** 970-982.

Hubbard, S.C., and Robbins, P.W. (1979). Synthesis and processing of protein-linked oligosaccharides *in vivo*. The Journal of Biological Chemistry **254,** 4568-4576.

Huffman, D.L., and O'Halloran, T.V. (2001). Function, structure, and mechanism of intracellular copper trafficking proteins. Annual Review of Biochemistry **70,** 677-701.

Hutchison, C.E., Li, J., Argueso, C., Gonzalez, M., Lee, E., Lewis, M.W., Maxwell, B.B., Perdue, T.D., Schaller, G.E., and Alonso, J.M. (2006). The Arabidopsis histidine phosphotransfer proteins are redundant positive regulators of cytokinin signaling. Plant Cell **18,** 3073-3087.

Hüttner, S., Veit, C., Vavra, U., Schoberer, J., Liebminger, E., Maresch, D., Grass, J., Altmann, F., Mach, L., and Strasser, R. (2014). Arabidopsis class I α-mannosidases MNS4 and MNS5 are involved in endoplasmic reticulum–associated degradation of misfolded glycoproteins. Plant Cell **26,** 1712-1728.

Hwang, I., and Sheen, J. (2001). Two-component circuitry in Arabidopsis cytokinin signal transduction. Nature **413,** 383-389.

Hwang, I., Chen, H.-C., and Sheen, J. (2002). Two-component signal transduction pathways in Arabidopsis. Plant Physiology **129,** 500-515.

Igari, K., Endo, S., Hibara, K., Aida, M., Sakakibara, H., Kawasaki, T., and Tasaka, M. (2008). Constitutive activation of a CC-NB-LRR protein alters morphogenesis through the cytokinin pathway in Arabidopsis. Plant Journal **55,** 14-27.

Imamura, A., Kiba, T., Tajima, Y., Yamashino, T., and Mizuno, T. (2003). *In vivo* and *in vitro* characterization of the ARR11 response regulator implicated in the His-to-Asp phosphorelay signal transduction in *Arabidopsis thaliana*. Plant Cell Physiol **44,** 122-131.

Imamura, A., Hanaki, N., Umeda, H., Nakamura, A., Suzuki, T., Ueguchi, C., and Mizuno, T. (1998). Response regulators implicated in His-to-Asp phosphotransfer signaling in Arabidopsis. Proceedings of the National Academy of Sciences of the United States of America **95,** 2691-2696.

Imamura, A., Hanaki, N., Nakamura, A., Suzuki, T., Taniguchi, M., Kiba, T., Ueguchi, C., Sugiyama, T., and Mizuno, T. (1999). Compilation and characterization of *Arabiopsis thaliana* response regulators implicated in His-Asp phosphorelay signal transduction. Plant and Cell Physiology **40,** 733-742.

Imran, Q.M., Falak, N., Hussain, A., Mun, B.-G., Sharma, A., Lee, S.-U., Kim, K.-M., and Yun, B.-W. (2016). Nitric oxide responsive heavy metal-associated gene *AtHMAD1* contributes to development and disease resistance in *Arabidopsis thaliana*. Frontiers in Plant Science **7,** 1712.

Inoue, T., Higuchi, M., Hashimoto, Y., Seki, M., Kobayashi, M., Kato, T., Tabata, S., Shinozaki, K., and Kakimoto, T. (2001). Identification of CRE1 as a cytokinin receptor from Arabidopsis. Nature **409,** 1060-1063.

Ishida, K., Yamashino, T., Yokoyama, A., and Mizuno, T. (2008). Three type-B response regulators, ARR1, ARR10 and ARR12, play essential but redundant roles in cytokinin signal transduction throughout the life cycle of *Arabidopsis thaliana*. Plant and Cell Physiology **49,** 47-57.

Jefferson, R.A., Kavanagh, T.A., and Bevan, M.W. (1987). GUS fusions: Beta-glucuronidase as a sensitive and versatile gene fusion marker in higher plants. EMBO (European Molecular Biology Organization) Journal **6,** 3901–3907.

Jensen, H. (2013). Molecular characterisation of dominant repressors of the cytokinin deficiency syndrome. Dissertation. Institute of Biology/Applied Genetics Berlin, Freie Universität Berlin.

Jeong, Y.M., Mun, J.H., Kim, H., Lee, S.Y., and Kim, S.G. (2007). An upstream region in the first intron of petunia actin-depolymerizing factor 1 affects tissue-specific

expression in transgenic Arabidopsis (*Arabidopsis thaliana*). Plant Journal **50,** 230-239.

Jiang, C.-J., Shimono, M., Sugano, S., Kojima, M., Liu, X., Inoue, H., Sakakibara, H., and Takatsuji, H. (2013). Cytokinins act synergistically with salicylic acid to activate defense gene expression in rice. Molecular Plant-Microbe Interactions **26,** 287-296.

Joshi, M.V., and Loria, R. (2007). *Streptomyces turgidiscabies* possesses a functional cytokinin biosynthetic pathway and produces leafy galls. Molecular Plant-Microbe Interactions **20,** 751-758.

Kamada-Nobusada, T., and Sakakibara, H. (2009). Molecular basis for cytokinin biosynthesis. Phytochemistry **70,** 444-449.

Kang, J., Lee, Y., Sakakibara, H., and Martinoia, E. (2017). Cytokinin transporters: GO and STOP in signaling. Trends in Plant Science **22,** 455-461.

Karimi, M., Inzé, D., and Depicker, A. (2002). GATEWAY vectors for *Agrobacterium*-mediated plant transformation. Trends in Plant Science **7,** 193-195.

Kay, B.K., Williamson, M.P., and Sudol, M. (2000). The importance of being proline: the interaction of proline-rich motifs in signaling proteins with their cognate domains. The FASEB (Federation of American Societies for Experimental Biology) journal **14,** 231-241.

Khan, A.A. (1971). Cytokinins: permissive role in seed germination. Science **171,** 853-859.

Kieber, J.J., and Schaller, G.E. (2014). Cytokinins. The Arabidopsis Book**,** e0168.

Kieber, J.J., and Schaller, G.E. (2018). Cytokinin signaling in plant development. Development **145,** dev 149344.

Kim, H.J., Chiang, Y.-H., Kieber, J.J., and Schaller, G.E. (2013). SCF^{KMD} controls cytokinin signaling by regulating the degradation of type-B response regulators. Proceedings of the National Academy of Sciences of the United States of America **110,** 10028-10033.

Kinoshita-Tsujimura, K., and Kakimoto, T. (2011). Cytokinin receptors in sporophytes are essential for male and female functions in *Arabidopsis thaliana*. Plant Signaling and Behavior **6,** 66-71.

Ko, D., Kang, J., Kiba, T., Park, J., Kojima, M., Do, J., Kim, K.Y., Kwon, M., Endler, A., Song, W.-Y., Martinoia, E., Sakakibara, H., and Lee, Y. (2014). Arabidopsis ABCG14 is essential for the root-to-shoot translocation of cytokinin. Proceedings of the National Academy of Sciences of the United States of America **111,** 7150-7155.

Köllmer, I., Novák, O., Strnad, M., Schmülling, T., and Werner, T. (2014). Overexpression of the cytosolic cytokinin oxidase/dehydrogenase (CKX7) from Arabidopsis causes specific changes in root growth and xylem differentiation. Plant Journal **78,** 359-371.

Koncz, C., and Schell, J. (1986). The promoter of T L-DNA gene *5* controls the tissue-specific expression of chimaeric genes carried by a novel type of *Agrobacterium* binary vector. Molecular and General Genetics MGG **204,** 383-396.

Kong, X., Liu, G., Liu, J., and Ding, Z. (2018). The root transition zone: A hot spot for signal crosstalk. Trends in Plant Science **23,** 403-409.

Kopečný, D., Pethe, C., Šebela, M., Houba-Herin, N., Madzak, C., Majira, A., and Laloue, M. (2005). High-level expression and characterization of *Zea mays* cytokinin oxidase/dehydrogenase in *Yarrowia lipolytica*. Biochimie **87,** 1011-1022.

Kopečný, D., Končitíková, R., Popelka, H., Briozzo, P., Vigouroux, A., Kopečná, M., Zalabák, D., Šebela, M., Skopalová, J., Frébort, I., and Moréra, S. (2016). Kinetic and structural investigation of the cytokinin oxidase/dehydrogenase active site. FEBS (Federation of European Biochemical Societies) Journal **283,** 361-377.

Kosugi, S., Hasebe, M., Tomita, M., and Yanagawa, H. (2009). Systematic identification of cell cycle-dependent yeast nucleocytoplasmic shuttling proteins by prediction of

composite motifs. Proceedings of the National Academy of Sciences of the United States of America **106,** 10171-10176.

Kurakawa, T., Ueda, N., Maekawa, M., Kobayashi, K., Kojima, M., Nagato, Y., Sakakibara, H., and Kyozuka, J. (2007). Direct control of shoot meristem activity by a cytokinin-activating enzyme. Nature **445,** 652-655.

Kurepa, J., Li, Y., Perry, S.E., and Smalle, J.A. (2014). Ectopic expression of the phosphomimic mutant version of Arabidopsis response regulator 1 promotes a constitutive cytokinin response phenotype. BMC Plant Biology **14,** 28.

Kuroha, T., Tokunaga, H., Kojima, M., Ueda, N., Ishida, T., Nagawa, S., Fukuda, H., Sugimoto, K., and Sakakibara, H. (2009). Functional analyses of *LONELY GUY* cytokinin-activating enzymes reveal the importance of the direct activation pathway in Arabidopsis. Plant Cell **21,** 3152-3169.

Laemmli, U.K. (1970). Cleavage of structural proteins during the assembly of the head of bacteriophage T4. Nature **227,** 680.

Laplaze, L., Benková, E., Casimiro, I., Maes, L., Vanneste, S., Swarup, R., Weijers, D., Calvo, V., Parizot, B., Herrera-Rodriguez, M.B., Offringa, R., Graham, N., Doumas, P., Friml, J., Bogusz, D., Beeckman, T., and Bennett, M. (2007). Cytokinins act directly on lateral root founder cells to inhibit root initiation. Plant Cell **19,** 3889-3900.

Lee, D.J., Kim, S., Ha, Y.M., and Kim, J. (2008). Phosphorylation of Arabidopsis response regulator 7 (ARR7) at the putative phospho-accepting site is required for ARR7 to act as a negative regulator of cytokinin signaling. Planta **227,** 577-587.

Lee, J.J., and Seo, S. (2015). PDE6D binds to the C-terminus of RPGR in a prenylation-dependent manner. EMBO (European Molecular Biology Organization) reports **16,** 1581-1582.

Leibfried, A., To, J.P.C., Busch, W., Stehling, S., Kehle, A., Demar, M., Kieber, J.J., and Lohmann, J.U. (2005). WUSCHEL controls meristem function by direct regulation of cytokinin-inducible response regulators. Nature **438,** 1172-1175.

Lerich, A., Langhans, M., Sturm, S., and Robinson, D.G. (2011). Is the 6 kDa tobacco etch viral protein a bona fide ERES marker? Journal of Experimental Botany **62,** 5013-5023.

Li, H., Xu, T., Lin, D., Wen, M., Xie, M., Duclercq, J., Bielach, A., Kim, J., Reddy, G.V., Zuo, J., Benková, E., Friml, J., Guo, H., and Yang, Z. (2013a). Cytokinin signaling regulates pavement cell morphogenesis in Arabidopsis. Cell Research **23,** 290.

Li, J.-F., Chung, H.S., Niu, Y., Bush, J., McCormack, M., and Sheen, J. (2013b). Comprehensive protein-based artificial microRNA screens for effective gene silencing in plants. Plant Cell **25,** 1507-1522.

Li, J., Nie, X., Tan, J.L.H., and Berger, F. (2013c). Integration of epigenetic and genetic controls of seed size by cytokinin in Arabidopsis. Proceedings of the National Academy of Sciences of the United States of America **110,** 15479-15484.

Li, W., Herrera-Estrella, L., and Tran, L.-S.P. (2016). The Yin-Yang of cytokinin homeostasis and drought acclimation/adaptation. Trends in Plant Science **21,** 548-550.

Li, X.G., Su, Y.H., Zhao, X.Y., Li, W., Gao, X.Q., and Zhang, X.S. (2010). Cytokinin overproduction-caused alteration of flower development is partially mediated by CUC2 and CUC3 in Arabidopsis. Gene **450,** 109-120.

Li, Y., and Qi, B. (2017). Progress toward understanding protein S-acylation: Prospective in plants. Frontiers in Plant Science **8,** Article 346.

Liebminger, E., Hüttner, S., Vavra, U., Fischl, R., Schoberer, J., Grass, J., Blaukopf, C., Seifert, G.J., Altmann, F., Mach, L., and Strasser, R. (2009). Class I α-mannosidases are required for N-glycan processing and root development in *Arabidopsis thaliana*. Plant Cell **21,** 3850-3867.

Liu, L., Cui, F., Li, Q., Yin, B., Zhang, H., Lin, B., Wu, Y., Xia, R., Tang, S., and Xie, Q. (2011). The endoplasmic reticulum-associated degradation is necessary for plant salt tolerance. Cell Research **21,** 957-969.

Liu, Y., and Li, J. (2014). Endoplasmic reticulum-mediated protein quality control in Arabidopsis. Frontiers in Plant Science **5,** Article 162.

Lomin, S.N., Yonekura-Sakakibara, K., Romanov, G.A., and Sakakibara, H. (2011). Ligand-binding properties and subcellular localization of maize cytokinin receptors. Journal of Experimental Botany **62,** 5149-5159.

Lomin, S.N., Krivosheev, D.M., Steklov, M.Y., Arkhipov, D.V., Osolodkin, D.I., Schmülling, T., and Romanov, G.A. (2015). Plant membrane assays with cytokinin receptors underpin the unique role of free cytokinin bases as biologically active ligands. Journal of Experimental Botany **66,** 1851-1863.

Mähönen, A.P., Bonke, M., Kauppinen, L., Riikonen, M., Benfey, P.N., and Helariutta, Y. (2000). A novel two-component hybrid molecule regulates vascular morphogenesis of the Arabidopsis root. Genes & Development **14,** 2938-2943.

Mähönen, A.P., Higuchi, M., Törmäkangas, K., Miyawaki, K., Pischke, M.S., Sussman, M.R., Helariutta, Y., and Kakimoto, T. (2006a). Cytokinins regulate a bidirectional phosphorelay network in Arabidopsis. Current Biology **16,** 1116-1122.

Mähönen, A.P., Bishopp, A., Higuchi, M., Nieminen, K.M., Kinoshita, K., Törmäkangas, K., Ikeda, Y., Oka, A., Kakimoto, T., and Helariutta, Y. (2006b). Cytokinin signaling and its inhibitor AHP6 regulate cell fate during vascular development. Science **311,** 94-98.

Malito, E., Coda, A., Bilyeu, K.D., Fraaije, M.W., and Mattevi, A. (2004). Structures of Michaelis and product complexes of plant cytokinin dehydrogenase: implications for flavoenzyme catalysis. Journal of Molecular Biology **341,** 1237-1249.

Mangeon, A., Junqueira, R.M., and Sachetto-Martins, G. (2010). Functional diversity of the plant glycine-rich proteins superfamily. Plant Signaling & Behavior **5,** 99-104.

Manolaridis, I., Kulkarni, K., Dodd, R.B., Ogasawara, S., Zhang, Z., Bineva, G., O'Reilly, N., Hanrahan, S.J., Thompson, A.J., and Cronin, N. (2013). Mechanism of farnesylated CAAX protein processing by the intramembrane protease Rce1. Nature **504,** 301.

Marín-de la Rosa, N., Pfeiffer, A., Hill, K., Locascio, A., Bhalerao, R.P., Miskolczi, P., Grønlund, A.L., Wanchoo-Kohli, A., Thomas, S.G., and Bennett, M.J. (2015). Genome wide binding site analysis reveals transcriptional coactivation of cytokinin-responsive genes by DELLA proteins. PLoS Genetics **11,** e1005337.

Marsch‐Martínez, N., Ramos‐Cruz, D., Irepan Reyes‐Olalde, J., Lozano‐Sotomayor, P., Zúñiga‐Mayo, V.M., and de Folter, S. (2012). The role of cytokinin during Arabidopsis gynoecia and fruit morphogenesis and patterning. Plant Journal **72,** 222-234.

Martin-Trillo, M., and Cubas, P. (2010). *TCP* genes: A family snapshot ten years later. Trends in Plant Science **15,** 31-39.

Maurer-Stroh, S., Washietl, S., and Eisenhaber, F. (2003). Protein prenyltransferases. Genome Biology **4,** 212.

McTaggart, S. (2006). Isoprenylated proteins. Cellular and Molecular Life Sciences **63,** 255-267.

Medicherla, B., Kostova, Z., Schaefer, A., and Wolf, D.H. (2004). A genomic screen identifies Dsk2p and Rad23p as essential components of ER-associated degradation. EMBO (European Molecular Biology Organization) reports **5,** 692-697.

Menges, M., Samland, A.K., Planchais, S., and Murray, J.A.H. (2006). The D-type cyclin CYCD3;1 is limiting for the G1-to-S-phase transition in Arabidopsis. Plant Cell **18,** 893-906.

Michaelson, D., Ali, W., Chiu, V.K., Bergo, M., Silletti, J., Wright, L., Young, S.G., and Philips, M. (2005). Postprenylation CAAX processing is required for proper localization of Ras but not Rho GTPases. Molecular Biology of the Cell **16,** 1606-1616.

Miller, C.O., Skoog, F., von Saltza, M.H., and Strong, F.M. (1955). Kinetin, a cell division factor from deoxyribonucleic acid. Journal of the American Chemical Society **77,** 1392-1392.

Miyawaki, K., Matsumoto-Kitano, M., and Kakimoto, T. (2004). Expression of cytokinin biosynthetic isopentenyltransferase genes in Arabidopsis: Tissue specificity and regulation by auxin, cytokinin, and nitrate. Plant Journal **37,** 128-138.

Miyawaki, K., Tarkowski, P., Matsumoto-Kitano, M., Kato, T., Sato, S., Tarkowska, D., Tabata, S., Sandberg, G., and Kakimoto, T. (2006). Roles of Arabidopsis ATP/ADP isopentenyltransferases and tRNA isopentenyltransferases in cytokinin biosynthesis. Proceedings of the National Academy of Sciences of the United States of America **103,** 16598-16603.

Mizuno, T. (1997). Compilation of all genes encoding two-component phosphotransfer signal transducers in the genome of *Escherichia coli*. DNA Research **4,** 161-168.

Mohorko, E., Glockshuber, R., and Aebi, M. (2011). Oligosaccharyltransferase: the central enzyme of N-linked protein glycosylation. Journal of inherited metabolic disease **34,** 869-878.

Mok, D.W., and Mok, M.C. (2001). Cytokinin metabolism and action. Annual Review of Plant Physiology and Plant Molecular Biology **52,** 89-118.

Moreira, S., Bishopp, A., Carvalho, H., and Campilho, A. (2013). AHP6 inhibits cytokinin signaling to regulate the orientation of pericycle cell division during lateral root initiation. PLoS ONE **8,** e56370.

Morris, R.O., Bilyeu, K.D., Laskey, J.G., and Cheikh, N.N. (1999). Isolation of a gene encoding a glycosylated cytokinin oxidase from maize. Biochemical and Biophysical Research Communications **255,** 328-333.

Motyka, V., Faiss, M., Strand, M., Kaminek, M., and Schmulling, T. (1996). Changes in cytokinin content and cytokinin oxidase activity in response to derepression of *ipt* gene transcription in transgenic tobacco calli and plants. Plant Physiology **112,** 1035-1043.

Motyka, V., Vankova, R., Capkova, V., Petrasek, J., Kaminek, M., and Schmülling, T. (2003). Cytokinin-induced upregulation of cytokinin oxidase activity in tobacco includes changes in enzyme glycosylation and secretion. Physiologia Plantarum **117,** 11-21.

Moubayidin, L., Di Mambro, R., and Sabatini, S. (2009). Cytokinin-auxin crosstalk. Trends in Plant Science **14,** 557-562.

Moubayidin, L., Perilli, S., Dello Ioio, R., Di Mambro, R., Costantino, P., and Sabatini, S. (2010). The rate of cell differentiation controls the Arabidopsis root meristem growth phase. Current Biology **20,** 1138-1143.

Moubayidin, L., Di Mambro, R., Sozzani, R., Pacifici, E., Salvi, E., Terpstra, I., Bao, D., van Dijken, A., Dello Ioio, R., Perilli, S., Ljung, K., Benfey, Philip N., Heidstra, R., Costantino, P., and Sabatini, S. (2013). Spatial coordination between stem cell activity and cell differentiation in the root meristem. Developmental Cell **26,** 405-415.

Müller, B., and Sheen, J. (2008). Cytokinin and auxin interaction in root stem-cell specification during early embryogenesis. Nature **453,** 1094-1097.

Mullis, K.B., and Faloona, F.A. (1987). Specific synthesis of DNA *in vitro* via a polymerase-catalyzed chain reaction. Methods in Enzymology **155,** 335-350.

Murashige, T., and Skoog, F. (1962). A revised medium for rapid growth and bioassays with tobacco tissue cultures. Physiologia Plantarum **15,** 473-497.

Mutasa-Göttgens, E., and Hedden, P. (2009). Gibberellin as a factor in floral regulatory networks. Journal of Experimental Botany **60,** 1979-1989.

Nakagawa, T., Kurose, T., Hino, T., Tanaka, K., Kawamukai, M., Niwa, Y., Toyooka, K., Matsuoka, K., Jinbo, T., and Kimura, T. (2007). Development of series of gateway binary vectors, pGWBs, for realizing efficient construction of fusion genes for plant transformation. Journal of Bioscience and Bioengineering **104,** 34-41.

Naseem, M., Philippi, N., Hussain, A., Wangorsch, G., Ahmed, N., and Dandekar, T. (2012). Integrated systems view on networking by hormones in Arabidopsis immunity reveals multiple crosstalk for cytokinin. Plant Cell **24,** 1793-1814.

Neuber, O., Jarosch, E., Volkwein, C., Walter, J., and Sommer, T. (2005). Ubx2 links the Cdc48 complex to ER-associated protein degradation. Nature Cell Biology **7,** 993.

Neumann, G., Massonneau, A., Martinoia, E., and Römheld, V. (1999). Physiological adaptations to phosphorus deficiency during proteoid root development in white lupin. Planta **208,** 373-382.

Nguyen, K.H., Ha, C.V., Nishiyama, R., Watanabe, Y., Leyva-González, M.A., Fujita, Y., Tran, U.T., Li, W., Tanaka, M., Seki, M., Schaller, G.E., Herrera-Estrella, L., and Tran, L.-S.P. (2016). Arabidopsis type B cytokinin response regulators ARR1, ARR10, and ARR12 negatively regulate plant responses to drought. Proceedings of the National Academy of Sciences of the United States of America **113,** 3090-3095.

Niemann, M.C., Weber, H., Hluska, T., Leonte, G., Anderson, S.M., Novak, O., Senes, A., and Werner, T. (2018). The cytokinin oxidase/dehydrogenase CKX1 is a membrane-bound protein requiring homooligomerization in the endoplasmic reticulum for its cellular activity. Plant Physiology **176,** 2024-2039.

Niemann, M.C.E., Bartrina, I., Ashikov, A., Weber, H., Novák, O., Spíchal, L., Strnad, M., Strasser, R., Bakker, H., Schmülling, T., and Werner, T. (2015). Arabidopsis ROCK1 transports UDP-GlcNAc/UDP-GalNAc and regulates ER protein quality control and cytokinin activity. Proceedings of the National Academy of Sciences of the United States of America **112,** 291-296.

Nikovics, K., Blein, T., Peaucelle, A., Ishida, T., Morin, H., Aida, M., and Laufs, P. (2006). The balance between the MIR164A and CUC2 genes controls leaf margin serration in Arabidopsis. Plant Cell **18,** 2929-2945.

Nishiyama, R., Watanabe, Y., Leyva-Gonzalez, M.A., Van Ha, C., Fujita, Y., Tanaka, M., Seki, M., Yamaguchi-Shinozaki, K., Shinozaki, K., Herrera-Estrella, L., and Tran, L.-S.P. (2013). Arabidopsis AHP2, AHP3, and AHP5 histidine phosphotransfer proteins function as redundant negative regulators of drought stress response. Proceedings of the National Academy of Sciences of the United States of America **110,** 4840-4845.

Nishiyama, R., Watanabe, Y., Fujita, Y., Le, D.T., Kojima, M., Werner, T., Vankova, R., Yamaguchi-Shinozaki, K., Shinozaki, K., Kakimoto, T., Sakakibara, H., Schmülling, T., and Tran, L.-S.P. (2011). Analysis of cytokinin mutants and regulation of cytokinin metabolic genes reveals important regulatory roles of cytokinins in drought, salt and abscisic acid responses, and abscisic acid biosynthesis. Plant Cell **23,** 2169-2183.

Niu, Q.-W., Lin, S.-S., Reyes, J.L., Chen, K.-C., Wu, H.-W., Yeh, S.-D., and Chua, N.-H. (2006). Expression of artificial microRNAs in transgenic *Arabidopsis thaliana* confers virus resistance. Nature Biotechnology **24,** 1420-1428.

O'Brien, J.A., and Benková, E. (2013). Cytokinin cross-talking during biotic and abiotic stress responses. Frontiers in Plant Science **4,** 451.

Oparka, K.J., Prior, D.A.M., Cruz, S.S., Padgett, H.S., and Beachy, R.N. (1997). Gating of epidermal plasmodesmata is restricted to the leading edge of expanding infection sites of tobacco mosaic virus (TMV). Plant Journal **12,** 781-789.

Ossowski, S., Schwab, R., and Weigel, D. (2008). Gene silencing in plants using artificial microRNAs and other small RNAs. Plant Journal **53,** 674-690.

Palatnik, J.F., Allen, E., Wu, X., Schommer, C., Schwab, R., Carrington, J.C., and Weigel, D. (2003). Control of leaf morphogenesis by microRNAs. Nature **425,** 257.

Parizotto, E.A., Dunoyer, P., Rahm, N., Himber, C., and Voinnet, O. (2004). *In vivo* investigation of the transcription, processing, endonucleolytic activity, and functional relevance of the spatial distribution of a plant miRNA. Genes & Development **18,** 2237-2242.

Perilli, S., Moubayidin, L., and Sabatini, S. (2010). The molecular basis of cytokinin function. Current Opinion in Plant Biology **13,** 21-26.

Pertry, I., Václavíková, K., Depuydt, S., Galuszka, P., Spíchal, L., Temmerman, W., Stes, E., Schmülling, T., Kakimoto, T., Van Montagu, M.C.E., Strnad, M., Holsters, M., Tarkowski, P., and Vereecke, D. (2009). Identification of *Rhodococcus fascians* cytokinins and their modus operandi to reshape the plant. Proceedings of the National Academy of Sciences of the United States of America **106,** 929-934.

Pickart, C.M. (2004). Back to the future with ubiquitin. Cell **116,** 181-190.

Pillitteri, L.J., Peterson, K.M., Horst, R.J., and Torii, K.U. (2011). Molecular profiling of stomatal meristemoids reveals new component of asymmetric cell division and commonalities among stem cell populations in Arabidopsis. Plant Cell **23,** 3260-3275.

Pryor, E.E., Horanyi, P.S., Clark, K.M., Fedoriw, N., Connelly, S.M., Koszelak-Rosenblum, M., Zhu, G., Malkowski, M.G., Wiener, M.C., and Dumont, M.E. (2013). Structure of the integral membrane protein CAAX protease Ste24p. Science **339,** 1600-1604.

Punwani, J.A., Hutchison, C.E., Schaller, G.E., and Kieber, J.J. (2010). The subcellular distribution of the Arabidopsis histidine phosphotransfer proteins is independent of cytokinin signaling. Plant Journal **62,** 473-482.

Quan, E.M., Kamiya, Y., Kamiya, D., Denic, V., Weibezahn, J., Kato, K., and Weissman, J.S. (2008). Defining the glycan destruction signal for endoplasmic reticulum-associated degradation. Molecular Cell **32,** 870-877.

Radakovic, Z.S., Anjam, M.S., Escobar, E., Chopra, D., Cabrera, J., Silva, A.C., Escobar, C., Sobczak, M., Grundler, F.M., and Siddique, S. (2018). Arabidopsis HIPP27 is a host susceptibility gene for the beet cyst nematode *Heterodera schachtii*. Molecular Plant Pathology **19,** 1917-1928.

Rashotte, A.M., Chae, H.S., Maxwell, B.B., and Kieber, J.J. (2005). The interaction of cytokinin with other signals. Physiologia Plantarum **123,** 184-194.

Rashotte, A.M., Mason, M.G., Hutchison, C.E., Ferreira, F.J., Schaller, G.E., and Kieber, J.J. (2006). A subset of Arabidopsis AP2 transcription factors mediates cytokinin responses in concert with a two-component pathway. Proceedings of the National Academy of Sciences of the United States of America **103,** 11081-11085.

Reid, D.E., Nadzieja, M., Novak, O., Heckmann, A.B., Sandal, N., and Stougaard, J. (2017). Cytokinin biosynthesis promotes cortical cell responses during nodule development. Plant Physiology **175,** 361-375.

Ren, B., Liang, Y., Deng, Y., Chen, Q., Zhang, J., Yang, X., and Zuo, J. (2009). Genome-wide comparative analysis of type-A *Arabidopsis response regulator* genes by overexpression studies reveals their diverse roles and regulatory mechanisms in cytokinin signaling. Cell Research **19,** 1178-1190.

Ren, J., Wen, L., Gao, X., Jin, C., Xue, Y., and Yao, X. (2008). CSS-Palm 2.0: An updated software for palmitoylation sites prediction. Protein Engineering, Design & Selection **21,** 639-644.

Riefler, M., Novak, O., Strnad, M., and Schmülling, T. (2006). Arabidopsis cytokinin receptor mutants reveal functions in shoot growth, leaf senescence, seed size, germination, root development, and cytokinin metabolism. Plant Cell **18,** 40-54.

Riou-Khamlichi, C., Huntley, R., Jacqmard, A., and Murray, J.A.H. (1999). Cytokinin activation of Arabidopsis cell division through a D-type cyclin. Science **283,** 1541-1544.

Rivero, R.M., Kojima, M., Gepstein, A., Sakakibara, H., Mittler, R., Gepstein, S., and Blumwald, E. (2007). Delayed leaf senescence induces extreme drought tolerance in a flowering plant. Proceedings of the National Academy of Sciences of the United States of America **104,** 19631-19636.

Romano, J.D., and Michaelis, S. (2001). Topological and mutational analysis of *Saccharomyces cerevisiae* Ste14p, founding member of the isoprenylcysteine carboxyl methyltransferase family. Molecular Biology of the Cell **12,** 1957-1971.

Romanov, G.A., Lomin, S.N., and Schmülling, T. (2018). Cytokinin signaling: from the ER or from the PM? That is the question! New Phytologist **218,** 41-53.

Romanov, G.A., Spíchal, L., Lomin, S.N., Strnad, M., and Schmülling, T. (2005). A live cell hormone-binding assay on transgenic bacteria expressing a eukaryotic receptor protein. Analytical Biochemistry **347,** 129-134.

Römisch, K. (2005). Endoplasmic reticulum-associated degradation. Annual Review of Cell and Developmental Biology **21,** 435-456.

Römisch, K. (2017). A case for Sec61 channel involvement in ERAD. Trends in Biochemical Sciences **42,** 171-179.

Rose, A.B., Elfersi, T., Parra, G., and Korf, I. (2008). Promoter-proximal introns in *Arabidopsis thaliana* are enriched in dispersed signals that elevate gene expression. Plant Cell **20,** 543-551.

Rose, M.D., Winston, F., and Hieter, P. (1990). Methods in yeast genetics. A laboratory course manual (Cold Spring Harbor). Cold Spring Harbor Laboratory Press, New York.

Rubino, J.T., and Franz, K.J. (2012). Coordination chemistry of copper proteins: How nature handles a toxic cargo for essential function. Journal of inorganic biochemistry **107,** 129-143.

Rupp, H.M., Frank, M., Werner, T., Strnad, M., and Schmülling, T. (1999). Increased steady state mRNA levels of the *STM* and *KNAT1* homeobox genes in cytokinin overproducing *Arabidopsis thaliana* indicate a role for cytokinins in the shoot apical meristem. Plant Journal **18,** 557-563.

Rutkevich, L.A., and Williams, D.B. (2011). Participation of lectin chaperones and thiol oxidoreductases in protein folding within the endoplasmic reticulum. Current Opinion in Cell Biology **23,** 157-166.

Sablok, G., Perez-Quintero, A.L., Hassan, M., Tatarinova, T.V., and Lopez, C. (2011). Artificial microRNAs (amiRNAs) engineering - On how microRNA-based silencing methods have affected current plant silencing research. Biochemical and Biophysical Research Communications **406,** 315-319.

Sachetto-Martins, G., Franco, L.O., and de Oliveira, D.E. (2000). Plant glycine-rich proteins: a family or just proteins with a common motif? Biochimica et Biophysica Acta (BBA)-Gene Structure and Expression **1492,** 1-14.

Sakai, H., Aoyama, T., and Oka, A. (2000). Arabidopsis ARR1 and ARR2 response regulators operate as transcriptional activators. Plant Journal **24,** 703-711.

Sakakibara, H. (2006). Cytokinins: Activity, biosynthesis, and translocation. Annual Review of Plant Biology **57,** 431-449.

Sakakibara, H., Kasahara, H., Ueda, N., Kojima, M., Takei, K., Hishiyama, S., Asami, T., Okada, K., Kamiya, Y., Yamaya, T., and Yamaguchi, S. (2005). *Agrobacterium*

tumefaciens increases cytokinin production in plastids by modifying the biosynthetic pathway in the host plant. Proceedings of the National Academy of Sciences of the United States of America **102,** 9972-9977.

Sambrook, J., and Russell, D. (2001). Molecular Cloning: A Laboratory Manual. 3rd edn: Cold Spring Harbor Laboratory Press, New York.

Schaller, G.E., Bishopp, A., and Kieber, J.J. (2015). The yin-yang of hormones: Cytokinin and auxin interactions in plant development. Plant Cell **27,** 44-63.

Schmülling, T., Werner, T., Riefler, M., Krupková, E., and Bartrina y Manns, I. (2003). Structure and function of cytokinin oxidase/dehydrogenase genes of maize, rice, Arabidopsis and other species. Journal of Plant Research **116,** 241-252.

Schwab, R., Ossowski, S., Riester, M., Warthmann, N., and Weigel, D. (2006). Highly specific gene silencing by artificial microRNAs in Arabidopsis. Plant Cell **18,** 1121-1133.

Schwarz, F., and Aebi, M. (2011). Mechanisms and principles of N-linked protein glycosylation. Current Opinion in Structural Biology **21,** 576-582.

Shani, E., Ben-Gera, H., Shleizer-Burko, S., Burko, Y., Weiss, D., and Ori, N. (2010). Cytokinin regulates compound leaf development in tomato. Plant Cell **22,** 3206-3217.

Siddique, S., Radakovic, Z.S., Carola, M., Chronis, D., Novák, O., Ramireddy, E., Holbein, J., Matera, C., Hütten, M., and Gutbrod, P. (2015). A parasitic nematode releases cytokinin that controls cell division and orchestrates feeding site formation in host plants. Proceedings of the National Academy of Sciences of the United States of America **112,** 12669-12674.

Sinensky, M. (2000). Functional aspects of polyisoprenoid protein substituents: roles in protein-protein interaction and trafficking. Biochimica et Biophysica Acta **1529,** 203-209.

Skoog, F., and Miller, C.O. (1957). Chemical regulation of growth and organ formation in plant tissue cultured *in vitro*. Symposia of the Society for Experimental Biology **11,** 118–131.

Smith, M.H., Ploegh, H.L., and Weissman, J.S. (2011). Road to ruin: Targeting proteins for degradation in the endoplasmic reticulum. Science **334,** 1086-1090.

Smith, P.e., Krohn, R.I., Hermanson, G., Mallia, A., Gartner, F., Provenzano, M., Fujimoto, E., Goeke, N., Olson, B., and Klenk, D. (1985). Measurement of protein using bicinchoninic acid. Analytical Biochemistry **150,** 76-85.

Sorek, N., Poraty, L., Sternberg, H., Bar, E., Lewinsohn, E., and Yalovsky, S. (2007). Activation status-coupled transient S acylation determines membrane partitioning of a plant Rho-related GTPase. Molecular and cellular biology **27,** 2144-2154.

Soyars, C.L., James, S.R., and Nimchuk, Z.L. (2016). Ready, aim, shoot: Stem cell regulation of the shoot apical meristem. Current Opinion in Plant Biology **29,** 163-168.

Sparkes, I.A., Runions, J., Kearns, A., and Hawes, C. (2006). Rapid, transient expression of fluorescent fusion proteins in tobacco plants and generation of stably transformed plants. Nature Protocols **1,** 2019-2025.

Spíchal, L., Rakova, N.Y., Riefler, M., Mizuno, T., Romanov, G.A., Strnad, M., and Schmülling, T. (2004). Two cytokinin receptors of *Arabidopsis thaliana*, CRE1/AHK4 and AHK3, differ in their ligand specificity in a bacterial assay. Plant and Cell Physiology **45,** 1299-1305.

Steiner, E., Efroni, I., Gopalraj, M., Saathoff, K., Tseng, T.S., Kieffer, M., Eshed, Y., Olszewski, N., and Weiss, D. (2012). The Arabidopsis O-linked N-acetylglucosamine transferase SPINDLY interacts with class I TCPs to facilitate cytokinin responses in leaves and flowers. Plant Cell **24,** 96-108.

Strasser, R. (2016). Plant protein glycosylation. Glycobiology **26,** 926-939.

Strasser, R. (2018). Protein quality control in the endoplasmic reticulum of plants. Annual Review of Plant Biology **69,** 147-172.

Sun, T.P. (2008). Gibberellin metabolism, perception and signaling pathways in Arabidopsis. Arabidopsis Book **6,** e0103.

Suzuki, N., Yamaguchi, Y., Koizumi, N., and Sano, H. (2002). Functional characterization of a heavy metal binding protein CdI19 from Arabidopsis. Plant Journal **32,** 165-173.

Suzuki, T., Miwa, K., Ishikawa, K., Yamada, H., Aiba, H., and Mizuno, T. (2001). The Arabidopsis sensor His-kinase, AHK4, can respond to cytokinins. Plant and Cell Physiology **42,** 107-113.

Takei, K., Yamaya, T., and Sakakibara, H. (2004). Arabidopsis *CYP735A1* and *CYP735A2* encode cytokinin hydroxylases that catalyze the biosynthesis of trans-Zeatin. Journal of Biological Chemistry **279,** 41866-41872.

Tamura, K., Dudley, J., Nei, M., and Kumar, S. (2007). MEGA4: Molecular Evolutionary Genetics Analysis (MEGA) software version 4.0. Molecular Biology and Evolution **24,** 1596-1599.

Tehseen, M., Cairns, N., Sherson, S., and Cobbett, C.S. (2010). Metallochaperone-like genes in *Arabidopsis thaliana*. Metallomics **2,** 556-564.

Tian, H., De Smet, I., and Ding, Z. (2014). Shaping a root system: Regulating lateral versus primary root growth. Trends in Plant Science **19,** 426-431.

Tirichine, L., Sandal, N., Madsen, L.H., Radutoiu, S., Albrektsen, A.S., Sato, S., Asamizu, E., Tabata, S., and Stougaard, J. (2007). A gain-of-function mutation in a cytokinin receptor triggers spontaneous root nodule organogenesis. Science **315,** 104-107.

Tissier, A.F., Marillonnet, S., Klimyuk, V., Patel, K., Torres, M.A., Murphy, G., and Jones, J.D. (1999). Multiple independent defective suppressor-mutator transposon insertions in Arabidopsis: a tool for functional genomics. Plant Cell **11,** 1841-1852.

To, J.P., and Kieber, J.J. (2008). Cytokinin signaling: Two-components and more. Trends in Plant Science **13,** 85-92.

To, J.P., Deruère, J., Maxwell, B.B., Morris, V.F., Hutchison, C.E., Ferreira, F.J., Schaller, G.E., and Kieber, J.J. (2007). Cytokinin regulates type-A Arabidopsis response regulator activity and protein stability via two-component phosphorelay. Plant Cell **19,** 3901-3914.

To, J.P.C., Haberer, G., Ferreira, F.J., Deruere, J., Mason, M.G., Schaller, G.E., Alonso, J.M., Ecker, J.R., and Kieber, J.J. (2004). Type-A Arabidopsis response regulators are partially redundant negative regulators of cytokinin signaling. Plant Cell **16,** 658-671.

Tran, L.-S.P., Urao, T., Qin, F., Maruyama, K., Kakimoto, T., Shinozaki, K., and Yamaguchi-Shinozaki, K. (2007a). Functional analysis of AHK1/ATHK1 and cytokinin receptor histidine kinases in response to abscisic acid, drought, and salt stress in Arabidopsis. Proceedings of the National Academy of Sciences of the United States of America **104,** 20623-20628.

Tran, L.S.P., Nakashima, K., Shinozaki, K., and Yamaguchi‐Shinozaki, K. (2007b). Plant gene networks in osmotic stress response: from genes to regulatory networks. In Methods in Enzymology (Elsevier), pp. 109-128.

Truskina, J., and Vernoux, T. (2018). The growth of a stable stationary structure: Coordinating cell behavior and patterning at the shoot apical meristem. Current Opinion in Plant Biology **41,** 83-88.

Turnbull, D., and Hemsley, P.A. (2017). Fats and function: Protein lipid modifications in plant cell signalling. Current Opinion in Plant Biology **40,** 63-70.

Ueguchi, C., Sato, S., Kato, T., and Tabata, S. (2001). The *AHK4* gene involved in the cytokinin-signaling pathway as a direct receptor molecule in *Arabidopsis thaliana*. Plant and Cell Physiology **42,** 751-755.

Uhde-Stone, C., Zinn, K.E., Ramirez-Yanez, M., Li, A., Vance, C.P., and Allan, D.L. (2003). Nylon filter arrays reveal differential gene expression in proteoid roots of white lupin in response to phosphorus deficiency. Plant Physiology **131,** 1064-1079.

Vandesompele, J., De Preter, K., Pattyn, F., Poppe, B., Van Roy, N., De Paepe, A., and Speleman, F. (2002). Accurate normalization of real-time quantitative RT-PCR data by geometric averaging of multiple internal control genes. Genome Biology **3,** research0034.

Vaseva-Gemisheva, I., Lee, D., and Karanov, E. (2005). Response of Pisum sativum cytokinin oxidase/dehydrogenase expression and specific activity to drought stress and herbicide treatments. Plant Growth Regulation **46,** 199-208.

Vatén, A., Soyars, C.L., Tarr, P.T., Nimchuk, Z.L., and Bergmann, D.C. (2018). Modulation of asymmetric division diversity through cytokinin and SPEECHLESS regulatory interactions in the Arabidopsis stomatal lineage. Developmental Cell **47,** 53-66.

Vembar, S.S., and Brodsky, J.L. (2008). One step at a time: Endoplasmic reticulum-associated degradation. Nature Reviews Molecular Cell Biology **9,** 944-957.

Vishwakarma, K., Upadhyay, N., Kumar, N., Yadav, G., Singh, J., Mishra, R.K., Kumar, V., Verma, R., Upadhyay, R.G., Pandey, M., and Sharma, S. (2017). Abscisic acid signaling and abiotic stress tolerance in plants: A review on current knowledge and future prospects. Frontiers in Plant Science **8,** Article 161.

Voinnet, O., Rivas, S., Mestre, P., and Baulcombe, D. (2003). An enhanced transient expression system in plants based on suppression of gene silencing by the p19 protein of tomato bushy stunt virus. Plant Journal **33,** 949-956.

Wang, H., Lee, M.M., and Schiefelbein, J.W. (2002). Regulation of the cell expansion gene RHD3 during Arabidopsis development. Plant Physiology **129,** 638-649.

Wang, J., Tian, C., Zhang, C., Cao, X., Zhang, T.-Q., Wang, J.-W., and Jiao, Y. (2017). Cytokinin signaling activates *WUSCHEL* expression during axillary meristem initiation. Plant Cell **29,** 1373-1387.

Wang, Y., Li, L., Ye, T., Zhao, S., Liu, Z., Feng, Y.Q., and Wu, Y. (2011). Cytokinin antagonizes ABA suppression to seed germination of Arabidopsis by downregulating ABI5 expression. Plant Journal **68,** 249-261.

Watt, M., and Evans, J.R. (1999). Proteoid roots. Physiology and development. Plant Physiology **121,** 317-323.

Weber, H., Bernhardt, A., Dieterle, M., Hano, P., Mutlu, A., Estelle, M., Genschik, P., and Hellmann, H. (2005). Arabidopsis AtCUL3a and AtCUL3b form complexes with members of the BTB/POZ-MATH protein family. Plant Physiology **137,** 83-93.

Weigel, D., and Glazebrook, J. (2002). Arabidopsis: A laboratory manual. Cold Spring Harbor Laboratory Press, New York.

Welinder, C., and Ekblad, L. (2011). Coomassie staining as loading control in Western blot analysis. Journal of Proteome Research **10,** 1416-1419.

Werner, S. (2016). Influence of cytokinin on organ size and developmental transitions in Arabidopsis thaliana. Dissertation. Institute of Biology/Applied Genetics Berlin, Freie Universität Berlin.

Werner, T., and Schmülling, T. (2009). Cytokinin action in plant development. Current Opinion in Plant Biology **12,** 527-538.

Werner, T., Motyka, V., Strnad, M., and Schmülling, T. (2001). Regulation of plant growth by cytokinin. Proceedings of the National Academy of Sciences of the United States of America **98,** 10487-10492.

Werner, T., Köllmer, I., Bartrina, I., Holst, K., and Schmülling, T. (2006). New insights into the biology of cytokinin degradation. Plant Biology **8,** 371-381.

Werner, T., Motyka, V., Laucou, V., Smets, R., Van Onckelen, H., and Schmülling, T. (2003). Cytokinin-deficient transgenic Arabidopsis plants show multiple developmental alterations indicating opposite functions of cytokinins in the regulation of shoot and root meristem activity. Plant Cell **15,** 2532-2550.

Werner, T., Nehnevajova, E., Köllmer, I., Novák, O., Strnad, M., Krämer, U., and Schmülling, T. (2010). Root-specific reduction of cytokinin causes enhanced root growth, drought tolerance, and leaf mineral enrichment in Arabidopsis and tobacco. Plant Cell **22,** 3905-3920.

Wernimont, A.K., Huffman, D.L., Lamb, A.L., O'Halloran, T.V., and Rosenzweig, A.C. (2000). Structural basis for copper transfer by the metallochaperone for the Menkes/Wilson disease proteins. Nature Structural and Molecular Biology **7,** 766.

Wijeyesakere, S.J., Rizvi, S.M., and Raghavan, M. (2013). Glycan-dependent and independent interactions contribute to cellular substrate recruitment by calreticulin. Journal of Biological Chemistry **288,** 35104-35116.

Winter-Vann, A.M., and Casey, P.J. (2005). Post-prenylation-processing enzymes as new targets in oncogenesis. Nature Reviews Cancer **5,** 405.

Wolf, D.H., and Stolz, A. (2012). The Cdc48 machine in endoplasmic reticulum associated protein degradation. Biochimica et Biophysica Acta (BBA)-Molecular Cell Research **1823,** 117-124.

Wright, L.P., and Philips, M.R. (2006). Thematic review series: lipid posttranslational modifications CAAX modification and membrane targeting of Ras. Journal of lipid research **47,** 883-891.

Wright, L.P., Mor, A., Ahearn, I.M., Casey, P.J., and Philips, M.R. (2009). Topology of mammalian isoprenylcysteine carboxyl methyltransferase determined in live cells with a fluorescent probe. Molecular and cellular biology **29,** 1826-1833.

Wu, X., and Rapoport, T.A. (2018). Mechanistic insights into ER-associated protein degradation. Current Opinion in Cell Biology **53,** 22-28.

Wulfetange, K., Lomin, S.N., Romanov, G.A., Stolz, A., Heyl, A., and Schmülling, T. (2011). The cytokinin receptors of Arabidopsis are located mainly to the endoplasmic reticulum. Plant Physiology **156,** 1808-1818.

Xiang, C., Han, P., Lutziger, I., Wang, K., and Oliver, D. (1999). A mini binary vector series for plant transformation. Plant Molecular Biology **40,** 711-717.

Yamada, H., Suzuki, T., Terada, K., Takei, K., Ishikawa, K., Miwa, K., Yamashino, T., and Mizuno, T. (2001). The Arabidopsis AHK4 histidine kinase is a cytokinin-binding receptor that transduces cytokinin signals across the membrane. Plant and Cell Physiology **42,** 1017-1023.

Yamaguchi, S. (2008). Gibberellin metabolism and its regulation. Annual Review of Plant Biology **59,** 225-251.

Yang, J., Kulkarni, K., Manolaridis, I., Zhang, Z., Dodd, R.B., Mas-Droux, C., and Barford, D. (2011). Mechanism of isoprenylcysteine carboxyl methylation from the crystal structure of the integral membrane methyltransferase ICMT. Molecular Cell **44,** 997-1004.

Yang, Z. (2008). Cell polarity signaling in Arabidopsis. Annual Review of Cell and Developmental Biology **24,** 551-575.

Yoshida, Y., and Tanaka, K. (2010). Lectin-like ERAD players in ER and cytosol. Biochimica et Biophysica Acta (BBA)-General Subjects **1800,** 172-180.

Young, S.G., Ambroziak, P., Kim, E., and Clarke, S. (2001). 7 Postisoprenylation protein processing: CXXX (CaaX) endoproteases and isoprenylcysteine carboxyl methyltransferase. The enzymes **21,** 155-213.

Yuan, C., Lazarowitz, S.G., and Citovsky, V. (2016). Identification of a functional plasmodesmal localization signal in a plant viral cell-to-cell-movement protein. mBio **7,** e02052-02015.

Zatloukal, M., Gemrotová, M., Doležal, K., Havlíček, L., Spíchal, L., and Strnad, M. (2008). Novel potent inhibitors of *A. thaliana* cytokinin oxidase/dehydrogenase. Bioorganic and Medicinal Chemistry **16,** 9268-9275.

Zeng, Y., Wagner, E.J., and Cullen, B.R. (2002). Both natural and designed micro RNAs can inhibit the expression of cognate mRNAs when expressed in Human cells. Molecular Cell **9,** 1327-1333.

Zhang, K., Novak, O., Wei, Z., Gou, M., Zhang, X., Yu, Y., Yang, H., Cai, Y., Strnad, M., and Liu, C.-J. (2014). Arabidopsis ABCG14 protein controls the acropetal translocation of root-synthesized cytokinins. Nature Communications **5,** Article 3274.

Zhang, W., Swarup, R., Bennett, M., Schaller, G.E., and Kieber, Joseph J. (2013). Cytokinin induces cell division in the quiescent center of the Arabidopsis root apical meristem. Current Biology **23,** 1979-1989.

Zhang, X., Feng, H., Feng, C., Xu, H., Huang, X., Wang, Q., Duan, X., Wang, X., Wei, G., and Huang, L. (2015). Isolation and characterisation of cDNA encoding a wheat heavy metal-associated isoprenylated protein involved in stress responses. Plant Biology **17,** 1176-1186.

Zhao, Z., Andersen, S.U., Ljung, K., Dolezal, K., Miotk, A., Schultheiss, S.J., and Lohmann, J.U. (2010). Hormonal control of the shoot stem-cell niche. Nature **465,** 1089-1092.

Zhu, Y., Liu, L., Shen, L., and Yu, H. (2016). NaKR1 regulates long-distance movement of FLOWERING LOCUS T in Arabidopsis. Nature Plants **2,** 16075.

Zimmermann, P., Hirsch-Hoffmann, M., Hennig, L., and Gruissem, W. (2004). GENEVESTIGATOR. Arabidopsis microarray database and analysis toolbox. Plant Physiology **136,** 2621-2632.

Zschiesche, W., Barth, O., Daniel, K., Böhme, S., Rausche, J., and Humbeck, K. (2015). The zinc-binding nuclear protein HIPP3 acts as an upstream regulator of the salicylate-dependent plant immunity pathway and of flowering time in *Arabidopsis thaliana*. New Phytologist **207,** 1084-1096.

Zubo, Y.O., Blakley, I.C., Yamburenko, M.V., Worthen, J.M., Street, I.H., Franco-Zorrilla, J.M., Zhang, W., Hill, K., Raines, T., and Solano, R. (2017). Cytokinin induces genome-wide binding of the type-B response regulator ARR10 to regulate growth and development in Arabidopsis. Proceedings of the National Academy of Sciences of the United States of America **114,** 5995-6004.

Zürcher, E., and Müller, B. (2016). Cytokinin synthesis, signaling, and function-advances and new insights. In International Review of Cell and Molecular Biology (Kwang, W. Jeon., eds) Academic Press, pp. 1-38.

Zürcher, E., Liu, J., di Donato, M., Geisler, M., and Müller, B. (2016). Plant development regulated by cytokinin sinks. Science **353,** 1027-1030.

Zürcher, E., Tavor-Deslex, D., Lituiev, D., Enkeli, K., Tarr, P.T., and Müller, B. (2013). A robust and sensitive synthetic sensor to monitor the transcriptional output of the cytokinin signaling network in planta. Plant Physiology **161,** 1066-1075.

Appendix

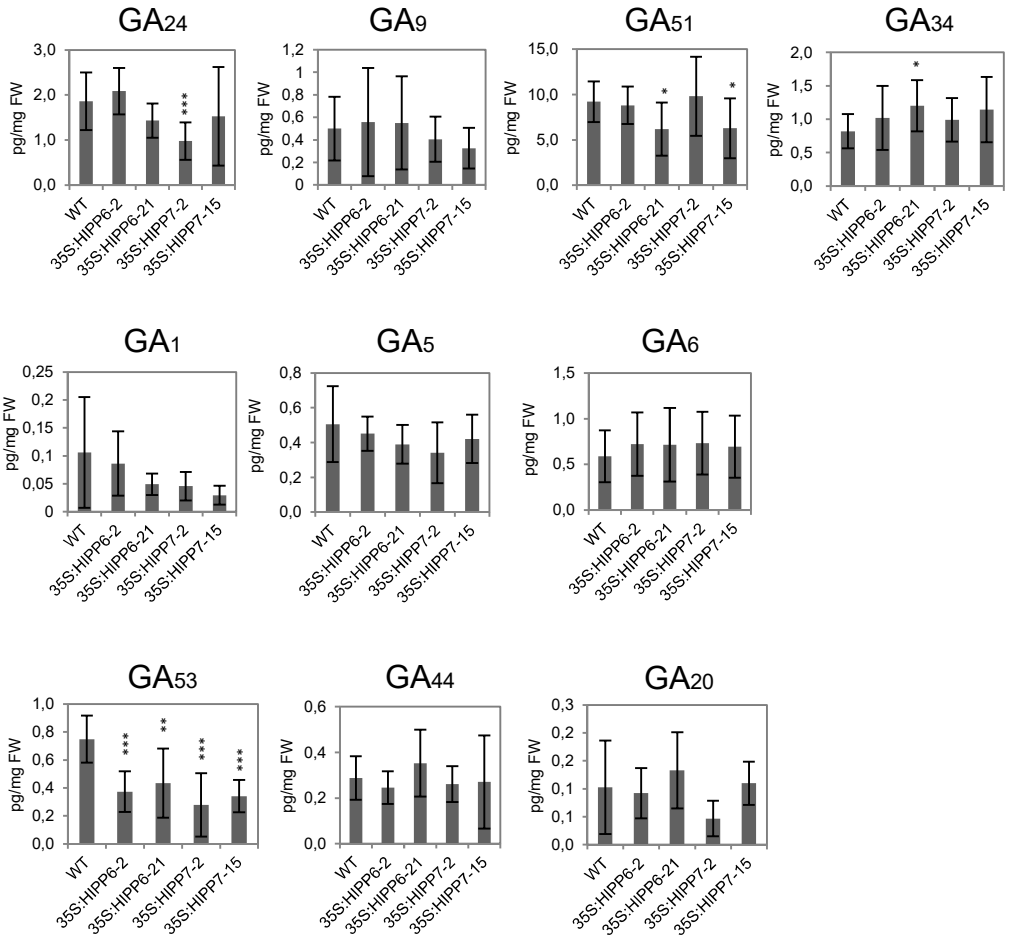

Figure A.1. Profiles of endogenous GA metabolites in HIPP-overexpressing Arabidopsis plants.
Contents of different GA metabolites were determined in rosettes of wild type (WT) and two independent homozygous lines expressing *35S:HIPP6* and *35S:HIPP7* 15 DAG. Data shown are means ± SD; $n = 3$. *$P < 0.05$, **$P < 0.01$, ***$P < 0.005$, calculated by Student's t test

Acknowledgements

First, I express my sincere gratitude to Prof. Dr. Tomáš Werner for giving me the opportunity to join this interesting project although I came from a completely different field. Thanks for his excellent supervision, guidance, and fruitful discussions. Thank you so much for your continuous support and deep encouragement during my doctoral study until the very end.

I also would like to thank my second supervisor Prof. Dr. Thomas Schmülling for his constant support, valuable suggestions, patient guidance and encouragement.

My deep thanks go to Dr. Henriette Weber. Thank you for all your advice, support and kindness during the past years. I enjoyed working with you. Thank you for your continuous help and for the great collaboration on the HIPP project.

Special thanks go to Dr. Michael Niemann for sharing his expertise to this project. Many thanks for your valuable comments and suggestions. I really appreciate your willingness to help.

I want to thank Dr. Ondřej Novák and Dr. Danuše Tarkowská (Laboratory of Growth Regulators, Centre of the Region Haná for Biotechnological and Agricultural Research, Palacký University and Institute of Experimental Botany ASCR, Olomouc, Czech Republic) for the successful collaboration.

Thanks also to Prof. Dr. Jianru Zuo, Prof. Dr. Joe Kieber and Dr. Bruno Müller for kindly providing seeds of mutant and transgenic plants that were valuable for this project.

Many thanks also to the Gardner team.

I would like to thank Dr. Isabel Bartrina and Dr. Sören Werner for reading and correcting this thesis, providing seeds as well as for your willingness to help.

Many thanks to the Master student Joshua Alcaniz Rolli for your kind help.

Thanks to all present and former colleagues, with whom I have shared an enjoyable and memorable time at the institute.

I am grateful to the DRS and the CSC for financing this work.

Finally, my deep and sincere gratitude goes to my family for their unflagging love and support. Thank you for believing in me, encouraging me, and supporting me, for your patience and for always being there for me.